Low-Cost Objective Measurement of Prehension Skills

Muhammad Awais Hafeez

Submitted in accordance with the requirements for the degree of

Doctor of Philosophy

The University of Leeds

School of Mechanical Engineering

Leeds

May 2023

Declaration

The candidate confirms that the work submitted is his own and that appropriate credit has been given where reference has been made to the work of others.

Abstract

This thesis aims to explore the feasibility of using low-cost, portable motion capture tools for the quantitative assessment of sequential 'reach-to-grasp' and repetitive 'finger-tapping' movements in neurologically intact and deficit populations, both in clinical and non-clinical settings. The research extends the capabilities of an existing optoelectronic postural sway assessment tool (PSAT) into a more general Boxed Infrared Gross Kinematic Assessment Tool (BIGKAT) to evaluate prehensile control of hand movements outside the laboratory environment. The contributions of this work include the validation of BIGKAT against a high-end motion capture system (Optotrak) for accuracy and precision in tracking kinematic data. BIGKAT was subsequently applied to kinematically resolve prehensile movements, where concurrent recordings with Optotrak demonstrate similar statistically significant results for five kinematic measures, two spatial measures (Maximum Grip Aperture – MGA, Peak Velocity – PV) and three temporal measures (Movement Time – MT, Time to MGA – TMGA, Time to PV – TPV). Regression analysis further establishes a strong relationship between BIGKAT and Optotrak, with nearly unity slope and low y-intercept values. Results showed reliable performance of BIGKAT and its ability to produce similar statistically significant results as Optotrak.

BIGKAT was also applied to quantitatively assess bradykinesia in Parkinson's patients during finger-tapping movements. The system demonstrated significant differences between PD patients and healthy controls in key kinematic measures, paving the way for potential clinical applications.

The study characterized kinematic differences in prehensile control in different sensory environments using a Virtual Reality head mounted display and finger tracking system (the Leap Motion), emphasizing the importance of sensory information during hand movements. This highlighted the role of hand vision and haptic feedback during initial and final phases of prehensile movement trajectory.

The research also explored marker-less pose estimation using deep learning tools, specifically DeepLabCut (DLC), for reach-to-grasp tracking. Despite challenges posed by COVID-19 limitations on data collection, the study showed promise in scaling reaching and grasping components but highlighted the need for diverse datasets to resolve kinematic differences accurately.

To facilitate the assessment of prehension activities, an Event Detection Tool (EDT) was developed, providing temporal measures for reaction time, reaching time, transport time, and movement time during object grasping and manipulation. Though initial pilot data was limited, the EDT holds potential for insights into disease progression and movement disorder severity.

Overall, this work contributes to the advancement of low-cost, portable solutions for quantitatively assessing upper-limb movements, demonstrating the potential for wider clinical use and guiding future research in the field of human movement analysis.

Acknowledgement

With boundless gratitude and profound appreciation, I attribute all acclamations and appreciations to Almighty ALLAH for His countless blessings upon me. This thesis stands as the culmination of four years of unwavering dedication and diligent effort, a journey in which I have been accompanied and uplifted by the gracious support of numerous individuals. It is with utmost pleasure and honour that I seize this moment to express my profound gratitude to each and every one of them.

To my esteemed supervisors, Dr. Raymond Holt, Dr. Rachel Coats, and Prof. Mark-Mon Williams, I extend my sincerest thanks for their invaluable advice, unwavering guidance, and unmatched knowledge. Without their constant encouragement, this thesis would never have come to fruition. Dr. Raymond Holt, in particular, exemplifies compassion and principle, offering both academic and personal support when needed. Additionally, I am indebted to Dr. Jack Brookes for his invaluable technical expertise in shaping experimental methods and meticulously critiquing my results.

I am immensely grateful to the University of Engineering and Technology (U.E.T), Lahore, for their generous financial support during my PhD studies. Moreover, the camaraderie and unwavering support of my friends, lab mates, and colleagues in the Perception Action Cognition Laboratory have been a constant source of strength throughout my research journey. Their assistance and camaraderie, both within the lab and during social interactions, have made this academic pursuit all the more meaningful.

My heartfelt appreciation extends to my late parents, whose profound teachings have shaped my vision and instilled the values that truly matter in life. I also wish to acknowledge the immeasurable support and encouragement provided by my wife, Dr. Tayyaba Roshni, and my daughter, Elif Guleen, whose presence and unwavering belief in me have been pivotal to my academic achievements. To them, I dedicate this work, for it would not have been possible without their boundless love and steadfast support.

In conclusion, I offer my deepest sense of gratitude to all those who have played a role, big or small, in the realization of this thesis. Their collective contributions have not only enriched my academic journey but have also left an indelible mark on my life. May their kindness and support continue to inspire and uplift others, as it has done for me.

Table of Contents

List of Figures

List of Tables

Chapter 1

1.1 Introduction

People suffering from neurological diseases such as Parkinson disease (PD), stroke, Multiple Sclerosis (MS) and spinal cord injury exhibit loss of sensory and motor functions, in turn affecting individual functional abilities, fine and gross motor control, balance and performance of activities of daily living [1], [2]. Reaching-to-grasp (prehension) is a universal human skill underlying numerous activities of daily living. Prehension entails coordinated and controlled movement of the hand towards a target object in order to grasp it successfully [3], [4]. Proficiency requires visual feedback of target position, an adequate motor plan, coordination of the arm and hand movements, and the use of online feedback to correct trajectory errors when necessary. Such controlled and coordinated movement functionally depends on various factors like object intrinsic and extrinsic properties [5], affordances provided by the object [6], purpose of the action to be performed after grasping [7], and sensorimotor constraints, and is fundamental to motor development and acquiring an astonishing number of motor skills. As a source of interaction with the environment, early childhood is embarked upon with learning new motor skills, and at the same time, infants with limited fine motor and grasping skills are at high risk of autism [8]–[10]. Deficits in motor behaviour reduce quality of life with increased dependence and impair everyday functioning. Similarly, later adulthood shows a natural decline in motor performance [11], [12]. Standardised clinical assessment methods are used by neurologists to determine the severity of chronic diseases (such as PD or MS). These involve patients being instructed to perform certain tasks under the observation of a neurologist, who scores their performance. Changes in amplitude, speed, and rhythm regularity, for example, are observed in finger tapping for Parkinson's patients and then rated according to standardized rating scales, e.g., the Movement Disorder Society Unified Parkinson's Disease Rating Scale (MDS-UPDRS) which provides the guideline that an investigator should "rate what you see". Clinicians' visual interpretation is inherently subjective [13]–[15], making it difficult for the clinicians to access subtle changes in the movement visually.

Subjective evaluation may result in inaccurate diagnosis and rough quantification [15] and also assessment heavily relies on clinician's experience and his/her ability to detect mild impairments and progressive decline in motor functions [13]. Therefore, it is critical and of prime importance to the neurologists/researchers to understand how movements unfold such that they can model behaviours, measure individual or group differences, quantify the degree of impairment, or track changes across time or as a result of an intervention [1], [16], [17].

1.2 Motivation

Commercially available optical motion capture systems can accurately and precisely represent digital patterns of a captured movement, thus making it possible to digitally infer clinical assessments using rigorous mathematical analysis. With the widespread availability of low-cost and high-resolution video cameras, together with credit-card sized computers and emerging computational techniques, researchers can explore low-cost alternatives with which human upper-arm movement can be measured, analysed, and interpreted. Recent decades have witnessed the emergence of digital sensing and tracking technologies such as accelerometers, gyroscopes, smartphones/digitized tablets, virtual reality, as well as marker-based and marker-less computer vision techniques. These evolving technological developments offer promising ways for clinical assessments that can be configured in practice. Their significance lies also in reducing cost, enhancing portability to assess movements in naturalistic settings, enabling measurements of activities of daily living (ADL) and offers flexibility in terms of assessment practices being followed in clinics. So, digitally presenting the patterns of reach-to-grasp movement and its components as a quantifiable object could supplement the observational approaches used by neurologists. This further opens the broader scope of investigation whether these sensing technologies could be used for tracking and representing complex movement trajectories as well as clinical assessment of symptomatic movement abnormalities and patterns and incorporated into clinical protocols for successful and timely intervention.

High-end optoelectronic motion capture systems available in laboratories are somewhat not applicable in clinical practice in terms of their practicalities and motor assessment possibilities [18]. These systems (e.g. Optotrak, Vicon, Qualisys, Xsens, just to name a few) are treated as gold-standard to accurately and reliably evaluate the spatiotemporal characteristics of human movement and to validate new technologies as well [19], [20]. Unfortunately, the gold-standard necessitates expensive 3D motion capture systems, and an expert is required to calibrate, collect, and interpret the data to address a multitude of neurological and gait disorders, hence, limiting its clinical use due to high costs of running tests and delays in the availability of results [21], [22]. All of which do not occur with other clinical tests for example neurologist while rating the performance of time-based tests such as repetitively tapping index finger against thumb or touching their nose with their finger or reach-to-grasp-to-transport hand movements, do not necessarily need to implement protocols required for motion capture systems.

Past decades have seen dramatic advancement in technology in both hardware and software domains making it possible for data to be accurately acquired, processed rapidly and efficiently, and then evaluated using modelling, statistical analysis, and artificial intelligence techniques. Therefore, it is imperative that technological advancements in the healthcare sector be incorporated by addressing

the aforementioned issues. However, there are several concerns that need to be addressed when understanding these technologies and their clinical significance. It is not enough to just look at the performance characteristics of these technologies, such as their accuracy and reliability, as these do not necessarily align with the clinical needs of a particular scenario. For example, a person with Parkinson's disease may require a different type of movement tracking than someone who is simply trying to track their daily steps. The goal is to understand the complex relationship between the technical aspects of body tracking and clinical needs, in order to fully appreciate their clinical significance. Literature indicates various instrumentation and computational techniques employed for investigating movement abnormalities for neurological deficit individuals, but those measurements need to be validated against high-end marker-based motion capture systems.

The development of digital sensing and tracking technologies such as accelerometers, gyroscopes, smartphones/digitized tablets, and virtual reality has made it possible to quantify human arm movement and interpret the data using mathematical analysis. These technologies offer low-cost alternatives to expensive 3D motion capture systems and provide flexibility in assessing movements in naturalistic settings. However, it is important to understand that the performance characteristics of these technologies and to understand the complex relationship between the technical aspects of body tracking and clinical needs. High-end optoelectronic motion capture systems available in laboratories are still considered the gold standard for accurately and reliably evaluating the spatiotemporal characteristics of human movement, but their high cost and need for expertise limit their clinical use. The goal is to explore technological advancements (both in terms of low-cost hardware and open-source software) and their potential role in studying sequential and repetitive human arm movement by extracting objective kinematic measures while addressing concerns and validating measurements against high-end motion capture systems.

1.3 Aims and Objectives

1.3.1 Aim

The aim of this thesis is to investigate the feasibility of using low-cost portable motion capture tools to take objective kinematic measurements of hand movements outside the laboratory environment to facilitate diagnosis and evaluation of motor impairments.

To do this, the research presented here focuses on three promising areas of low-cost motion capture (optoelectronic markers, hand-tracking systems developed for virtual reality and machine vision) and considers their use for capturing kinematics in two common tasks associated with studying motor control (sequential “reach-to-grasp" movements and repetitive “finger tapping” movements).

1.3.2 Objectives

The project's objectives are shown below, and they describe the steps that must be performed to accomplish the aim. The starting point for this enquiry will be an optoelectronic motion capture system previously developed at the University of Leeds called the Postural Sway Assessment Tool (PSAT). PSAT is an optical motion capture system and uses two infra-red diodes (IRED) to measure postural sway (presented in detail in Chapter 3 section 3.2)

1) Evaluate the suitability of the PSAT optoelectronic marker tracking system for use in measuring hand kinematics by:

1.1 Extending the existing PSAT system into a Boxed Infrared Gross Kinematic Assessment Tool (BIGKAT) capable of capturing and analysing kinematic data related to hand and arm movements;

1.2 Benchmarking the new BIGKAT system against an existing gold standard for motion capture (Optotrak) to determine the working volume in which BIGKAT provides an acceptable level of precision and accuracy; and

1.3 Validating the new BIGKAT system by comparing it with an existing gold standard for motion capture (Optotrak) when measuring reach-to-grasp and finger-tapping activities.

2) Investigate three alternatives to opto-electronic marker tracking for quantifying prehension actions:

2.1 Leap Motion: hand tracking technology used to perform prehension tasks in virtual reality.

2.2 DeepLabCut: a machine learning algorithm for marker-less motion tracking from recorded video by using sample videos as a training set; and

2.3 An Event Detection Kit designed and developed as part of this thesis that detects the timing of different phases of prehension activities based on an object being grasped and moved.

1.5 Summary and Structure of the report

The contents of the thesis are organized as follows and are outlined in Figure 1:

Chapter 1 introduces the background and the motivations regarding the project. The aims and objectives are defined, and the contributions of the thesis are presented.

Chapter 2 presents the literature background of the technologies being used to study sequential (reach-to-grasp) and repetitive (finger tapping) movements in laboratory and non-laboratory settings.

And presents the need of developing low-cost, portable, and easy-to-use optical motion capture system.

Chapter 3 introduces the Postural Sway Assessment Tool (PSAT) developed in prior research at the University of Leeds and discusses its development into BIGKAT (the Boxed Infrared Gross Kinematic Assessment Tool), a system capable of tracking reach-to-grasp movements. The spatial and temporal resolution and effective workspace of the BIGKAT system are evaluated.

Chapter 4 benchmarks BIGKAT performance against Optotrak motion capture system during prehension tasks to determine the relationship between spatiotemporal measures obtained from both devices.

Chapter 5 compares BIGKAT performance against Optotrak motion capture system during finger tapping (FT) task, a clinical exam to rate severity of bradykinesia, to investigate BIGKAT's applicability in clinical settings.

Chapter 6 explores the potential of integrating Leap motion and virtual reality to determine the effect of absences of sensory feedback on prehension skills performed in virtual environments with different sensing modalities.

C**hapter 7** focuses on training a deep-learning based neural network model consisting of reach-to-grasp videos obtained from BIGKAT without the use of optoelectronic markers to evaluate its potential usage in analysing unseen and marker-less reach-to-grasp videos.

Chapter 8 introduces a novel kit, Event Detection Kit (EDT), for the temporal assessment of sequential reach-to-grasp-to-transport movements to investigate whether we even need a marker-based tracking system for diagnostic purposes.

Chapter 9 summarizes the work and presents the conclusions obtained from this study. Furthermore, future work and challenges are also highlighted.

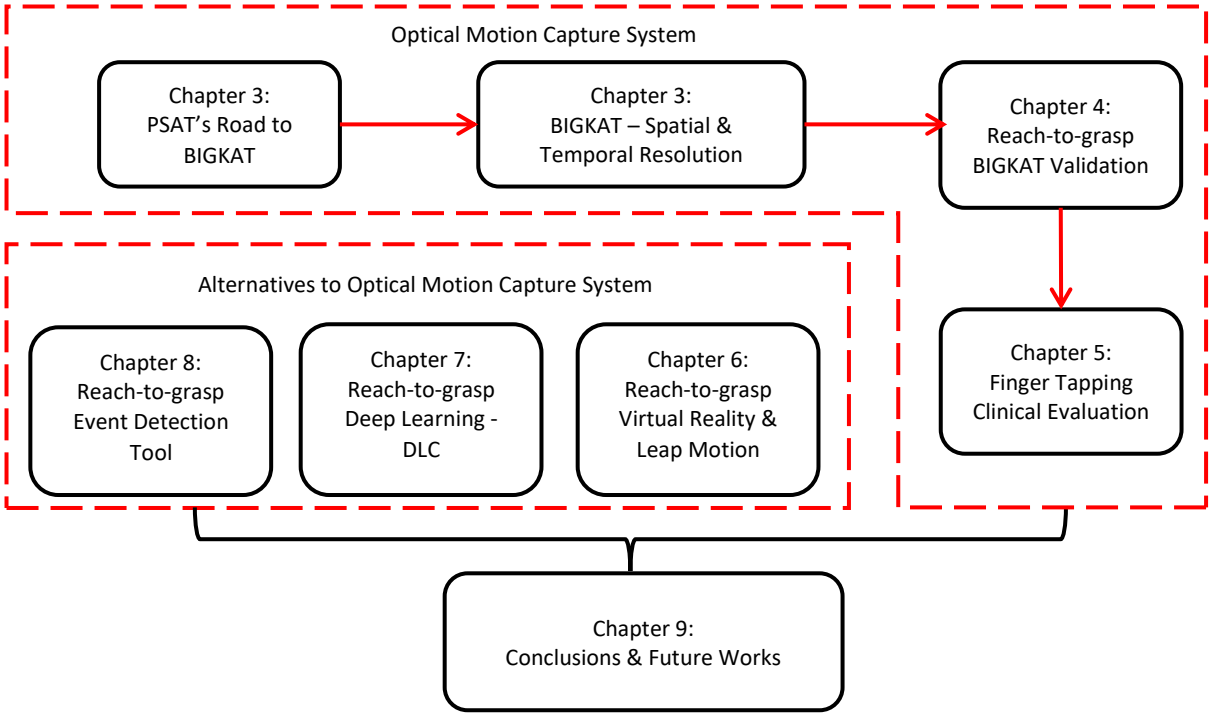

Figure 1: Structure of the thesis: Extending existing PSAT system into BIGKAT system, Validating BIGKAT's reach-to-grasp kinematic measures against research-grade Optotrak, and kinematic analysis of Finger Tapping movement (conventional clinical examination) performed by PD patients. Alternatives low-cost, portable technologies were investigated for detailed kinematic analysis of reach-to-grasp movements. Chapter 9 draws conclusions, discuss their potential usages and limitations, and recommends future works.

Chapter 2: Literature Review

This chapter evaluates the viability and advantages of studying reach-to-grasp movements, as it is a fundamental human ability that underpins many daily actions, with a low-cost, portable, and user-friendly optical motion capture system that may be utilised for body monitoring and analysis to infer specific neurological illness state. Prehension (or reach-to-grasp movement) is the process of moving the hand in a coordinated and controlled manner toward a target object in order to successfully grasp it. Prehension acts as a source of interaction with the environment and early childhood is embarked upon with learning new motor skills, and at the same time, infants with limited fine and grasping skills are at high risk of motor deficits in adulthood [8], [9]. Deficits in motor behaviours reduce quality of life with increased dependence and impairs everyday functioning. Similarly, later adulthood experience natural decline in motor performance [2]. Hence, focus of this thesis is on evaluating the spatio-temporal characteristics of prehensile skills exhibited by healthy and neurological deficit populations (Parkinson's disease and Multiple Sclerosis) using available technologies.

Observing prehensile act display coordination between its constituent components, reaching and transport component, to form a new complex in which transport and grasp component are constrained spatiotemporally. Speed and accuracy of prehensile movement varies with respect to the task in hand (relates to the object and purpose of the movement) [3] and sensorimotor constraints (related to the person performing the task) [23] This chapter highlights and review the technology being used to study prehensile skills and advancements being made in technologies that can potentially be used to study prehensile skills.

2.1 The Importance of Motor Skills in the Assessment of Parkinson's Disease and Multiple Sclerosis.

From infancy through old age, ageing is seen as a multidimensional process causing social, physical, cognitive and emotional changes to occur, and fortunately, most humans develop at similar rates [24]–[27]. Analysing and quantifying such predictable processes helps us to understand the framework behind how different developmental stages are linked together and how developmental changes across time are associated with enhancing capabilities and acquiring new skills which are non-existent at birth [28]. Throughout the life span, the central nervous system (CNS) plays an important role in controlling movements by processing sensory information about both the environment and limb positions, while utilizing this information to plan and execute single, and/or multi-joints movements successfully [29], [30]. Such remarkable control over movements start developing in the early months of life e.g. infants can focus on small objects and reach out to grasp them within six-to-twelve months and by three years of age they have developed enough control over grip that they can use lines to represent object boundaries [31], [32].

The ability of the CNS to learn motor behaviours is remarkable but unfortunately such motor behaviours are prone to impairment due to neural deficits [33], [34], inaccurate and noisy sensory information [35], [36], aging [37], [38], and motor dysfunction [39], [40]. Human daily activities which determine quality of life demand the display of complex motor skills over a variety of tasks. Motor skills are related to the body movements involving small or large sets of muscles acting on bony structure to carry out goal-directed actions and these skills are broadly classified in literature as fine motor skills and gross motor skills [41]. Actions such as crawling, running, walking involves maintaining postural stability with coordinated movement of extremities and are classified as gross motor abilities, whereas actions involving dexterous movements are classified as fine motor skills such as reaching movements, putting a key into hole [42], [43]. Fine and gross motor skills both work in coordination and impairment of one influences the other [44]. So, a better understanding of such skills requires assessment and quantification of movements made in achieving a specific control action like reaching for and grasping an object, and the underlying mechanisms for different control strategies involved in a successful movement or one at risk of movement problem. Quantitatively analysing such adaptive processes of growth, maintenance and regulation of loss provide insightful details on motor control development trajectory and/or identifying one at a risk of movement problem [33], [45], [46].

Degradation of motor skills occur in adulthood as a result of physical changes caused by neurodegenerative diseases like Parkinson's disease (PD), dementia, multiple sclerosis (MS) [2]. These age-dependent disorders (degenerative nerve diseases) progressively affect activities of daily living (ADL) involving fine and gross motor movements, limiting functional independence and quality of life. Furthermore, these are chronic neurodegenerative diseases that currently have no cure, but there are treatments available that can help manage symptoms and slow down the degenerative process to some extent. In Parkinson's disease, for example, medication such as levodopa and dopamine agonists can help control the motor symptoms, such as tremors, stiffness, and slowness of movement. However, these treatments do not slow down the underlying degenerative process of the disease. While there is currently no cure for Parkinson's disease or multiple sclerosis, ongoing research is focused on developing new therapies that can slow down or halt the degenerative process of these diseases.

In clinics, the measurement of motor dysfunction often relies on several qualitative assessment tools developed to determine motor performance across a range of activities [43], [45], [47]. Each tool has its own benefits and limitations and provides different outcome measures, but they have particularly been developed to maintain the independence and quality of life of individuals suffering from neurological disorders. For this purpose, several questionnaire-based assessments have been developed for assessing fine and gross motor control across different sets of activities in clinical

populations [48], [49], by helping neurologists identifying motor control deficits in children [50], [51]. Similarly, numerous outcome measures have been developed to clinically diagnose and evaluate upper limb dysfunction in older adults suffering from neurological disorders. For example, one well documented clinical rating scale defined by the Movement Disorder Society (MDS) is the Unified Parkinson's Diseases Rating Scale (MDS-UPDRS) used to rate bradykinesia severity by visually examining motor and non-motor symptoms [14]. Such qualitative forms of assessment depend on a clinician's experience and his/her ability to detect subtle changes and therefore suffer from considerable inter-rater variability [15], [52]. These tools are limited in their ability to investigate underlying movement components and how they are organized spatially or temporally as they provide absolute and subjective measures and draw normative comparisons [44], [47].

Objective and systematic characterisation of posture(s) and quantifying sequential 'reach-to-grasp' and repetitive 'finger-tapping' movements have long been topics of interest within laboratory settings. These types of movements are often studied in the fields of biomechanics, neuroscience, and motor control, among others. Optoelectronic and wearable motion capture systems are two commonly used methods to study these movements. Optoelectronic systems use cameras to track the position and orientation of markers placed on the body or objects, while wearable systems use sensors attached to the body. Other methods used in laboratory settings to study movement include electromyography (EMG), force sensors, and eye tracking. Optoelectronic systems are more accurate but require a controlled environment and are more expensive, while wearable systems are more portable but may be less accurate and have limitations.

Specifically, these methods evaluate the spatiotemporal measures like position and velocity of limbs/joints involved in achieving specific actions by tracking the movement trajectories and therefore, interpret outcome measures such as successful reaching and grasping of an object. These methods have enunciated the patterns and outcome measures for a healthy control and have shown the ability to discriminate healthy control from people with neurologically deficits by characterising the particular forms of clinical movement disorders. Such methods are laboratory specific, expensive and require a great degree of technical support thereby undermining their use in clinical environments. Hence, potential exploration of objectively measuring sequential, repetitive, and simultaneous movements will not only contribute towards our fundamental understanding of movement patterns of a healthy human. Such methods also augment the observational approaches used by experts by providing them with kinematic measures aiding diagnostic assessments of movement abnormalities (e.g., bradykinesia) and treatment planning of clinical conditions such as Parkinson's disease, multiple sclerosis (MS), stroke, and cerebral palsy.

2.2 Motoric Assessment of PD and MS patients

Neurological conditions lead towards abnormal features of movements such as decreased movement magnitude, prolonged movement time, deteriorating a patient's motor abilities and dexterity needed for everyday tasks. For example, PD patients exhibit impairments in the organization of sequential 'reach-to-grasp' movement displaying slow movement speed during transport component and wider grip aperture during grasping phase, in a common everyday practice. Whilst motor deterioration exhibited by patients with neurological conditions such as MS, PD may significantly vary and produce condition-specific patterns. Hence, the ability to quantify, characterise and/or assess fine and gross motor movements provide a powerful tool for identifying adults and children with neurological and motoric development deficits and considered as important element for effective clinical intervention [25].

2.2.1 Parkinson's Disease

In 1817, James Parkinson first described Parkinson's diseases (PD) in his detailed study "An Essay on the Shaking Palsy" [53], this is the second most common neurodegenerative disorder and a leading cause of disability and death worldwide [54]. PD is growing exponentially worldwide and is estimated to have already affected more than 6 million individuals. At this growth rate the number of individuals with PD is likely to have doubled by 2040 [55], [56], as shown in Figure 2. Middle-aged and older adults are those predominantly affected by PD. A meta-analysis of the worldwide data conducted by Pringsheim et al. by age group, geographic location and sex; showed a rising prevalence of 1903 per 100,000 in individuals older than age 80, prevalence of 1601 per 100,000 in individuals from North America, Europe, and Australia, compared with 646 individuals 70 to 79 years old from Asia, and - prevalence of 41 in females and 134 per 100,000 in males for individuals 50 to 59 years old, respectively [57]. The average age for the onset of PD is late middle-age, so, early signs and symptoms are often misattributed to ageing or other movement disorders [58]. Predominant signs and symptoms emerge during older age and at present no cure exists. As the global population ages, the future burden will probably be higher and it is, therefore, crucial to facilitate clinical diagnosis by objectively measuring Parkinson's syndrome (PS), monitoring disease progression, and delivering personalized therapeutic strategies [59].

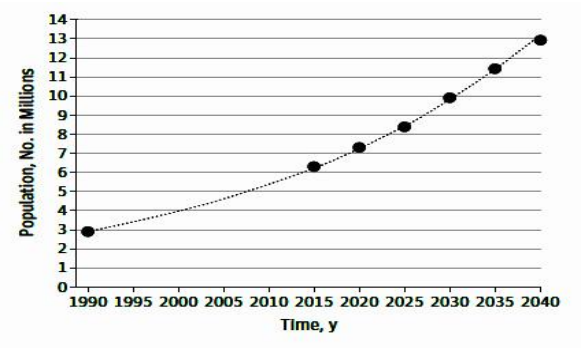

Figure 2: Estimated and Projected Number of Individuals with Parkinson Disease, 1990-2040. Sources: Global Burden of Disease Study (1990 and 2015) and projections based on published and public sources

PD is characterized by both motor and non-motor symptoms which affect individual functional abilities and cause people difficulties in performing daily life activities. PD consists of four characteristic movement disorders such as bradykinesia, rest tremor, muscular rigidity and postural instability (later in the course of disease). In addition, other early features of PD such as small and cramped handwriting (micrographia), reduced degree of facial expression (hypomimia) can be observed. These motor symptoms can vary between individuals and some PD patients with unilateral parkinsonism with severe dysfunction in mesocortical dopamine system more rapidly develop bilateral parkinsonism [60], [61], and the side initially affected remain more symptomatic. Bradykinesia is regarded as one of the leading cardinal symptoms of PD and is defined as the slowness of movement with decrements in speed and amplitude during repetitive performance [62]. Bradykinesia is the fundamental movement abnormality and is central for diagnosis and monitoring. Abnormalities of fine motor control evidenced as slowness of body movements are among the first signs of motor impairment in PD patients. PD patients lack the ability to organize sequential, simultaneous, and repetitive movement and take longer than when the same movements are performed in isolation. In clinics, bradykinesia is usually assessed by observing repetitive hand and leg movements such as finger and toe tapping, hand opening/closing over a certain time. These visual assessments are carried out by a physician, whose diagnostic accuracy clearly depends on his/her experience.

2.2.2 Multiple Sclerosis (MS)

MS is a chronic, progressive neurological disorder associated with reduce mobility and functional abilities with severe hand dexterity impairments in people with MS (PwMS). MS is growing worldwide and is estimated to have already affected 2.8 million people and global prevalence is 35.9 per 100,000 people as of 2020 [63]. Young adults between 20 and 40 years old get affected by MS with mean diagnostic age of 32 years [63]. It is a neurodegenerative disorder manifesting sensorimotor deterioration, impaired coordination, fatigue, tremor, and muscle weakness, hence, significantly impacting individuals' ability to perform activities of daily living (ADL) as shown in goal directions actions such as reaching-to-grasp. MS affects multiple functional systems including arm and hand

dysfunction and nearly 66% of PwMS have upper-limb motoric dysfunction [64]. Recent studies have reported that this deterioration of arm and hand functionality is increasingly recognized and reported by PwMS, even in the early stages of the disease. With the passage of time steady deterioration occurs and the disease enters a progressive phase, as reported in a study where 50% of 205 PwMS showed upper limb impairment and was significant in the group with progressive disease [65]. Likewise, 76% of 219 patients showed impaired manual dexterity measured using Nine-Hole Peg Test (9HPT) [66] i.e., a simple tasks like moving an object gets considerably compromised in PwMS.

2.3 Clinical Assessment of Movement Disorders

2.3.1 Bradykinesia – PD patients

In most cases, severity of bradykinesia is estimated by a qualified expert based on clinical rating scales defined by the Movement Disorder Society (MDS) sponsored Unified Parkinson's Disease Rating Scale (MDS-UPDRS) [67]. Part III of MDS-UPDRS, Motor Examination (Table 1), provides guidelines that the investigator should "rate what you see", therefore clinicians' visual interpretation is inherently subjective [52], [68], making it difficult for the clinicians to detect subtle changes in the movement visually [69]. To establish a diagnosis of PD, out of several diagnostic methods, a finger tapping task is widely used to assess fine motor bradykinesia by observing repeated tapping of the index finger on the thumb as quickly as possible and at maximal extent (distance between finger and thumb) [67].

Table 1: Movement Disorder Society revision of the Unified PD Rating Scale (MDS-UDPRS) Item 3.4 – Finger Tapping

Score	Description
0 – Normal	No Problem
1 – Slight	Any of the following a) Regular rhythm broken with 1-2 interruptions b) Slight slowing c) Amplitude decrement near the end of 10 taps
2 – Mild	Any of the following a) 3-5 interruptions b) Mild slowing c) Amplitude decreases midway
3 – Moderate	Any of the following a) More than 5 interruptions or at least one long freeze in the movement b) Moderate slowing c) The amplitude decrement starting after the 1st tap
4 – Severe	Cannot or can only barely perform the task because of slowing, interruptions or decrements.

Physicians visually analyse and rate motor performance with scores ranging from 0 to 4, where 0 corresponds to no symptoms, and 4 means severe bradykinesia, by observing decreasing speed,

amplitude decrement or rhythm losses (increased number of hesitations/freezes) as movements are continued. MDS-UPDRS scale has four components, with a total of 50 questions and requires the rater to consolidate his/her judgment into a single composite score. In contrast, the Modified Bradykinesia Rating Scale (MBRS) accesses each FT feature separately [52], [61] and rates it from 0 to 4 (Table 2). These scales inherently possess several limitations. Firstly, qualitative clinical assessment of bradykinesia and score assignment (0–4) with considerable inter-rater variability and subjective evaluation may result in inaccurate diagnosis and rough quantification [69]. Secondly, assessment heavily relies on the clinician's experience and his/her ability to detect mild impairments and progressive decline in motor functions in PD progression [68] and UPDRS has limited resolution as subtle motor signs can easily be missed [70]. Thirdly, it cannot be used as a monitoring tool as it needs to be scored by an expert, which requires regular visits to a neurologist, making it difficult for PD patients to use it at home. The need for low-cost, portable, easy-to-use, and quantitative assessment tool is critical in overcoming these potential limitations and the associated disadvantages of subjective evaluation.

Table 2: The Modified Bradykinesia Rating Scale (MBRS)

Score	Speed	Amplitude	Rhythm
0	Normal	Normal	Regular, no arrests or pauses in the ongoing movement.
1	Mild slowing	Mild reduction in amplitude in later performance, most movements close to normal	Mild impairment, up to two brief arrests in the 10s; none lasting > 1 s
2	Moderate slowing	Moderate, reduction in amplitude visible early in performance but continues to maintain 50% through most of the tasks.	Moderate, 3 – 4 arrests in 10 s; 1 or 2 lasting > 1 s
3	Severe slowing	Severe, less than 50% amplitude through most of the task	Severe, 5 or more arrests/10 seconds; more than 2 lasting > 1s
4	Can barely perform the task	Can barely perform the task	Can barely perform the task

2.3.2 Clinical assessment of PwMS

Performance based evaluations provide qualitative and quantitative measures based on perceived and actual performance, respectively. Participants complete perceived performance questionnaires (ABILHAND, AMSQ-SF) designed to examine difficulties while using their upper limbs during activities of daily living (ADL) [71]–[73]. These questionnaires can differentiate healthy controls from PwMS for example, but do not provide detailed kinematic analysis, thereby, making it difficult to interpret the subtle changes due to intervention or disease progression [74]. To evaluate upper limb performance quantitatively, clinicians use range of manual dexterity assessment tools like Nine-Hole Peg Test (NHPT), the Purdue Pegboard Test, Box and Block test, and the Action Research Arm Test (ARAT), each reporting Multiple Sclerosis (MS) disease state and are task specific. These tools are being used in clinical practice and PwMS research [47], [75]–[77]. Out of which, NHPT is taken as 'gold-standard'

and is the most widely used manual dexterity tool. NHPT provide timed base outcome measures by measuring the time taken by the participant to gasp test items (pegs) from the container, one by one, and inserted into the holes and then removing and placing pegs back to the container but NHPT cannot be used to measure severe upper extremity impairments [47].

One of the most common and widely used outcome measures in clinical examination is the expanded disability status scale (EDSS). It is a 20-point scale, ranging from 1 to 10, to assess disability in MS and to measure how functional movements are limited by MS [78]. Scoring is based on clinician's knowledge and expertise, and lower score by and large reflects a measurement of impairment rather than disability. Whereas high score predominately reflects disability to perform activities of daily living such as bulbar function (swallowing, chewing, and speaking) and upper limb function (reaching, grasping and manipulating objects) [79]. EDSS, in essence, is a form of quantified neurologic examination but it is known to have considerable inter and intra-rater variability [80], [81] and lacks cognition aspect of the disease, thus not a perfect tool for assessing disease progression. To overcome limitations associated with EDSS, an international task force developed a new outcome measure, the multiple sclerosis functional composite (MSFC), expanding clinical dimensions to include leg and arm function, cognition, and visual function. Three performance tests were finalized and included in MSFC to provide a composite z-score: NHPT for arm function, timed 25-foot walk test (TWT) for leg function and pseudo-auditory serial addition test (PASAT) for cognition function. TWT and NHPT performance is measured in seconds whereas PASAT is measured in the number of correct answers and the overall z-score is calculated for a single MSFC score result. Thus, MSFC provides a powerful tool to apply parametric statistics for the analysis, on the other hand, EDSS grades abnormalities on an ordinal scale. Despite this fact, EDSS is still in common use in clinical trials and neurologic examination as well.

Such standard tests do not provide fine movement details such as how sequential/repetitive/simultaneous movements are organized and how their spatiotemporal characteristics get affected by disease progression such as the wide range of symptoms manifested in MS. To determine the efficacy of such standardized scales requires large numbers of participants to participate in clinical trials to demonstrate the effects with acceptable levels of power [82]. Over the years, technological development in the field of motion capture systems and instrumentation techniques has furthered our ability to kinematically analyse and quantify motor impairment of arm function. The Next section discusses the technology-based systems being used in literature for MS research regarding upper limb function and in the context of clinical assessment of bradykinesia as well.

2.4 Quantitative Assessment of Movement Disorders

One of the key motivations for accurate and precise assessment of motor dysfunction is to augment the observational methods employed by experts during clinical assessment. Another key motivation for objectively assessing motor abilities is to investigate the intervention approaches, treatment effectiveness, and, making clinical trials shorter and cost effective by reducing the sample size and allowing quantitative and repeatable motor performance.

2.4.1 Bradykinesia

Bradykinesia diminishes an individual's ability to perform fine motor tasks and causes difficulties with repetitive movements, so, quantifying bradykinesia indicates the severity of PD experienced by an individual. Furthermore, quantitative information would provide neurologists with more useful information while differentiating between early and advanced PD symptoms, drug dose adjustment and/or as a screening between PD or other motor syndromes.

Okuno et al. measured single FT interval, average FT amplitude, and velocity using two 3-axis piezoelectric accelerometer and a pair of touch sensor. His findings showed kinematic variations as expected such that FT velocity and amplitude decreased with higher UPDRS score and similarly, irregularity between single FT interval for higher UPDRS score [83]. But, Dunnewold et al. calculated number of taps in 30s using two or three piezoresistive uniaxial accelerometer and found a low correlation with the UPDRS scale [84].

Quantitative assessment done by movement sensors (accelerometers, gyroscopes, magnetometers) reports significant differences between patients and healthy controls and found high correlation with UPDRS sub-score on FT task [83]–[87] but it remains to be seen whether they have clinical utility. Optical motion capture systems based on low-cost cameras and off-the-shelf components can provide comparable quantitative measures and can overcome the encumbrance, high cost and transport issues of commercially available optoelectronic systems. Literature suggests that expert neurologists prioritise progressive decrement in amplitude over changes in rhythm regularity or tapping frequency and pay less attention to speed while assigning a UPDRS score [88]. Thus, analysis of FT movement via low-cost optical motion capture system may produce more significant results than by movement sensors. As movement sensors are subject to errors and drift over time due to factors such as sensor noise, temperature changes and other environmental factors [89]–[91]. This can result in inaccuracies in the data collected by movement sensors. Only one study has reported the use of low-cost motion capture system using passive markers and differentiated parkinsonian subjects from healthy control by extracting average opening velocity and amplitude decrement from 3D positional FT data [90]. But this study suffers from many limitations such as, firstly, that it does not compare its findings with the

UPDRS FT score by experts, secondly, results are not validated against any research grade motion capture system and thirdly, this system can only work with two reflective markers.

In today's age of precision and personalized medicine, early and accurate diagnosis along with regular monitoring have increased the need for new, low-cost, portable and accessible technologies to facilitate exact and objective measurement of bradykinesia. The diagnostic ability of new methods in being able to correctly detect or exclude PD should be determined by comparing the results with the reference standard, UPDRS, and also with the objective measures obtained through high grade optoelectronic systems, so that, it can support in-clinic and at-home assessment throughout PD progression.

2.4.2 Quantitative assessment of MS

Laboratory based motion capture systems provide accurate, precise, and reliable tracking of kinematic landmarks involved in functional tasks such as 9HPT and ARAT involving upper limb mainly reaching, grasping and manipulate objects. Literature suggests the use of single inertial sensor on the wrist during the execution of ARAT clinical test and calculated time taken to complete the whole sequential movement and its sub-components (reaching, grasping, manipulating, release and return) [92]. Their proposed method was able to discriminate healthy individuals from MS group and was able to detect subtle changes differentiating impairment levels within MS patients as well. This study showed that reaching, manipulation and release phases of the movement were more compromised, thus, making it difficult for MS patients to perform activities of daily living. Despite these facts, this method only provides temporal measures whereas spatial measures such as grip profile (fingers opening/closing) during grasping phase could provide a useful insight into coordinated multi-joint movement and can reveal patients' specific deficits. For such kinematic measures, one needs to attach more than one inertial sensor on fingers and thumb or an instrumented glove, thereby, significantly impacting patient performance by adding additional weight. For example, 40 MS patients with EDSS score 0-7 wore a sensor engineered glove to measure repetitive finger opposition movement of thumb to index, medium, ring and little finger and were able to independently distinguish between MS and healthy controls [93]. Their proposed method showed low correlation between glove parameters and clinical variables (EDSS: $r = -0.39$, MSFC: $r = 0.47$, 9HPT: $r = -0.45$), suggesting that parameters calculated by sensor-engineered glove cannot be taken as a substitute for the clinical measures.

A similar study exploiting the use of a sensor-engineered glove to determine the finger impairments in older adults with MS found a significant relationship between finger motor performance and global disability [94]. They found that PwMS mostly show impaired bimanual coordination, increased movement time for complex tasks to perform accurate movements i.e., change in adopted strategy for slightly better accuracy and integrating sensory information to plan sequential movements, as was

also found in studies analysing kinematic performance during planar reaching task [95]–[99]. There is scientific evidence showing change in movement strategies [39], [100], adaptation to task constraints [37], [38], [101]–[103], increased variability during fine movements such as tracing, handwriting and drawing movements [46], [94], [104]–[106] and difficulties during multi-joint coordinated movement [107]–[111].

An electromyography (EMG) system in conjunction with a planar robotic manipulandum have also been used to record the activity of 15 upper body muscles while participants perform centre-out reaching movements in four different mechanical environments [97], [98]. Participants controlled a cursor on a computer screen by grasping and moving the handle of the planar robotic manipulandum in eight equidistant directions from a central target which lasted about 2 hours and output 2D kinematic data. They found, in accordance with previous studies [112], [113], that MS subjects moved slower and have distorted (less smooth and less accurate) movement trajectories and revealed different muscle activation patterns in MS subjects. Other studies have also analysed 2D planar reaching movements using a digitized tablet [113], tracing tasks using smartphone based [114], [115] and centre-out reaching movement using robotic manipulandum [95], [99], [116] and target-to-target pointing task as well [117]. 2D kinematic assessment revealed significant differences between able-bodied and MS subjects. Other than simple reaching movements, studies have also investigated manipulative task components such as reaching-to-grasp-to-pick-to-insert virtual pegs into holes using a commercial haptic display and extracted kinematic (smoothness, speed) and dynamic parameters (grip force) [112], [118], as shown in Figure 3. These studies presented the effectiveness and usefulness of using end-effectors as assessment tools to provide end-point kinematics and most studies have validated objectively quantified outcome measures with clinical standardized tests in observational studies but their usage in clinical practice is still to be known.

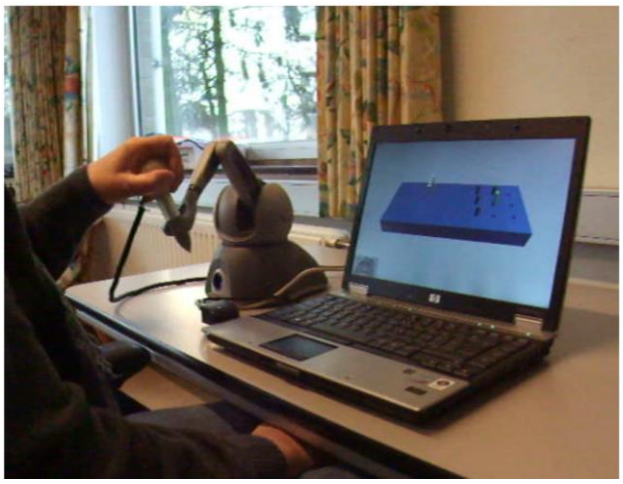

Figure 3: MS patients performing virtual peg insertion test. The setup is composed of haptic device, an instrumented handle and a virtual reality environment [112].

Other than 2D kinematic assessments techniques, literature presents 3D detailed kinematic analysis of lower limb during gait in PwMS to assess the gait deterioration and are well described (for a detailed review see [119]–[121]). While literature on kinematic analysis of changes in upper limb movement as a result of MS during goal-directed movement is scant. Despite the important role of upper limb during gait, few studies offer the potential usage of laboratory-based opto-electronic systems to track upper limb movement during gait but these have found out moderate relationship between upper and lower limb impairment [122]–[124]. Only small set of studies have used optical motion capture systems to study spatio-temporal characteristics of upper limb in MS patients [125]–[127], shown in Figure 4. Such setups provide good quality data but their use in clinical settings is limited due to the cost of acquiring commercial motion capture systems, the need for expertise to acquire and analyse data, the time required to setup the system and the large amount of dedicated space required.

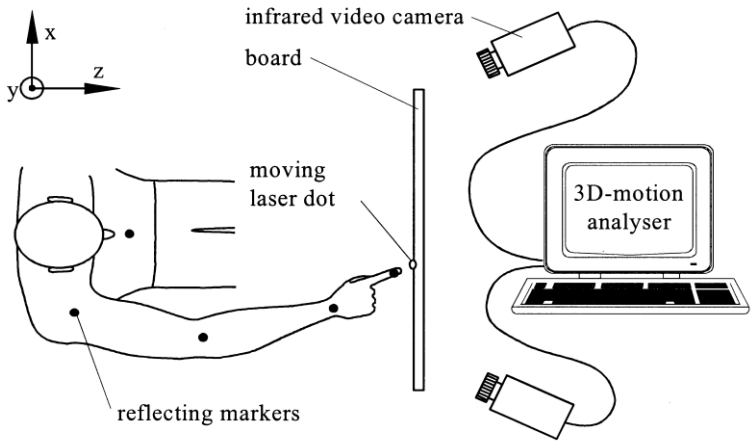

Figure 4: Schematic diagram of experimental setup using motion capture system to record markers movement [126].

An intriguing alternative shift to such expensive camera systems is the availability of much cheaper cameras such as Microsoft Kinect and Raspberry Pi no infra-red (NoIR) cameras. The Raspberry Pi NoIR cameras in particular are much cheaper and can record high resolution videos at 60 frames/second. By using infra-red filter and active markers, such cameras can only record marker movement irrespective of surrounding objects i.e., clinical paraphernalia and clutter. They can be controlled with a low-cost Raspberry Pi microcomputer and together with tacking algorithm it can provide three-dimensional data of kinematic landmarks i.e., markers attached to the body parts. It provides a far less expensive alternative to the elaborate optical motion capture setups. Only the most high-end motion capture systems are portable, whereas microcomputer-based systems can be very compact, making them suitable for easy deployment in a larger range of scenarios i.e., laboratory and non- laboratory settings.

In summary, a variety of sensing technologies are currently being used in laboratory settings to study upper limb motor dysfunction associated with MS. Almost every study in the literature presents quantitative assessment method for upper limb reaching movements using a single inertial sensor on the wrist [92], [128], [129], sensor-engineered glove [93], [94], EMG to study muscle activation patterns [65], robotic manipulandum for centre-out reaching task in different mechanical environments [97]–[99], [116], digitized tablets for copying and tracing tasks [113]–[115], goal directed reaching task in virtual environment [112], [118] and high-end optoelectronic system [122]–[125], [125], [130]. Although there are various ways that upper arm monitoring and analysis might be used to infer specific neurological illness states, however, the practical implementation of these assessments remains a profoundly exciting challenge. Studying reaching movements to grasp and manipulate objects can reveal underlying movement patterns for PwMS as reaching out to grab a cup of coffee is one example of the most frequent and basic activity—along with gripping and manipulating other everyday objects. It highlights the importance of studying prehension owing to its importance in activities of daily living.

2.5 Prehension

Prehension is a set of actions involving reaching for and grasping of objects and is treated as two separate, yet coordinated, components. The reaching action is the movement of a hand from its current location towards the object, and the grasping action is anticipating opening and closing of the fingers and thumb as the hand approaches the object to be grasped [131]. To execute these actions, the nervous system chooses particular movement patterns and these observed movement patterns are stereotypical and adapt against changing conditions and obstructions [6], [101]. The reaching movement involves proximal joints and muscle groups to guide the hand towards the point determined by the information available from the visual system. Similarly, grasping actions involve distal joints and muscle groups to increase and decrease intra digit aperture as perceived by the visual system [38].

Successful reaching and grasping requires information about the object distance from the body and the size of the object, respectively, and such information is available from the visual system. The visual system is used to extract intrinsic properties (Size, shape, colour) therefrom preparing and adjusting grasp component and similarly, to extract extrinsic properties (object distance and orientation) to guide hand towards target [131]. In the absence of sensory information, prehensile movements show systematic biases, signifying the importance of online sensory information to guide the hand until it makes contact with the object [132]–[134]. And in order for the grasping action to be completed successfully, information about fingers position and object contact points is sufficient [135]–[137]

2.5.1 Organization of prehensile movement

The visuo-motor link between the motor control and objects' attributes reflects the ability of humans to adapt hand movements according to the physical properties of the object to be grasped and the goal of the prehension task [5], [101]. Jeannerod kinematically analysed prehension movements, and proposed a visuo-motor channel hypothesis for transport and grasping components, and concluded that these two components are relatively independent, yet impose temporal constraints on each other [138] . In a prehension task, typically the hand moves from its current position towards the object and the index finger and thumb open up more than the width of the object during reaching and then close to grasp the object. The hand's velocity and intra-digit aperture occurs in a time duration called movement time (MT) and Jeannerod found that these two components are temporally coupled to each other as maximum grip aperture (MGA) occurs at 75% of MT which is also the beginning point of low-velocity final phase and he also found consistency in the duration of low velocity phase [131]. He found that MT and MGA remain more or less constant, irrespective of different object distances, but peak wrist velocity (PV) increases with object distance (extrinsic properties) and grip aperture changes with object size (intrinsic properties) [131], [138] and therefore, both reach and grasp components are different from each other and are independent.

Jakobson and Goodale also found that there is spatial coupling between the two components. They co-varied object size and object distance and recorded grip aperture and hand movements and found that object size does affect the transport component and similarly, the grasp component gets affected by object distance causing MGA to occur later in the movement [139]. Increasing object size shows an increase in PV magnitude and time to peak velocity (TPV), as large objects lower spatial accuracy demands while permitting a faster movement and the hand open up to a larger MGA. Similarly increasing object distance from the participant increases MGA magnitude and time to MGA [139], [140]. Different sized targets also produced uniquely shaped hand trajectories representing task-specific variations in the timing structure of reach-to-grasp [141]. These two prehensile components, reaching and grasping, seem to be coupled functionally and temporally.

The results of Van de kamp and Zaal & Bonger [142], [143] suggest that prehension must be treated as a composite behaviour not as an alternative approach proposed by Smeets and Brenner [144] in which they suggested prehension as two separate aiming movements being controlled by the tip of the thumb and finger. Van de kamp [143] observed that the effect of providing perturbation and changing the end position of one of the digits not only effects the digit's own kinematics, but also the kinematics of the other digit.

Figure 5 shows a stereotypical and replicable reach to grasp movement, which is described by tracking the position of key anatomical features over time taken by the subject and differentiated to provide a

speed profile and kinematic landmarks like peaks of wrist velocity and grip aperture with their time of occurrence as well. Figure 5a shows that the hand position starts from zero and reaches for a target of width 50mm placed at a distance of 450mm and Figure 5b&c shows a kinematic profile of hand velocity and grip size during hand transportation. These features allow quantification of reach-to-grasp movements and provide instantaneous snapshots of the hand kinematics at discrete points in time, enabling in-depth analysis by exploiting spatiotemporal characteristics. These kinematic features offered by the stereotypical nature of hand movements pave the way towards investigating the fundamental activities and exploring dimensions of motor control quantitatively. By far these features have been extensively investigated by the researchers and have brought useful insights into the strategies employed by the CNS in the control of skilled activities.

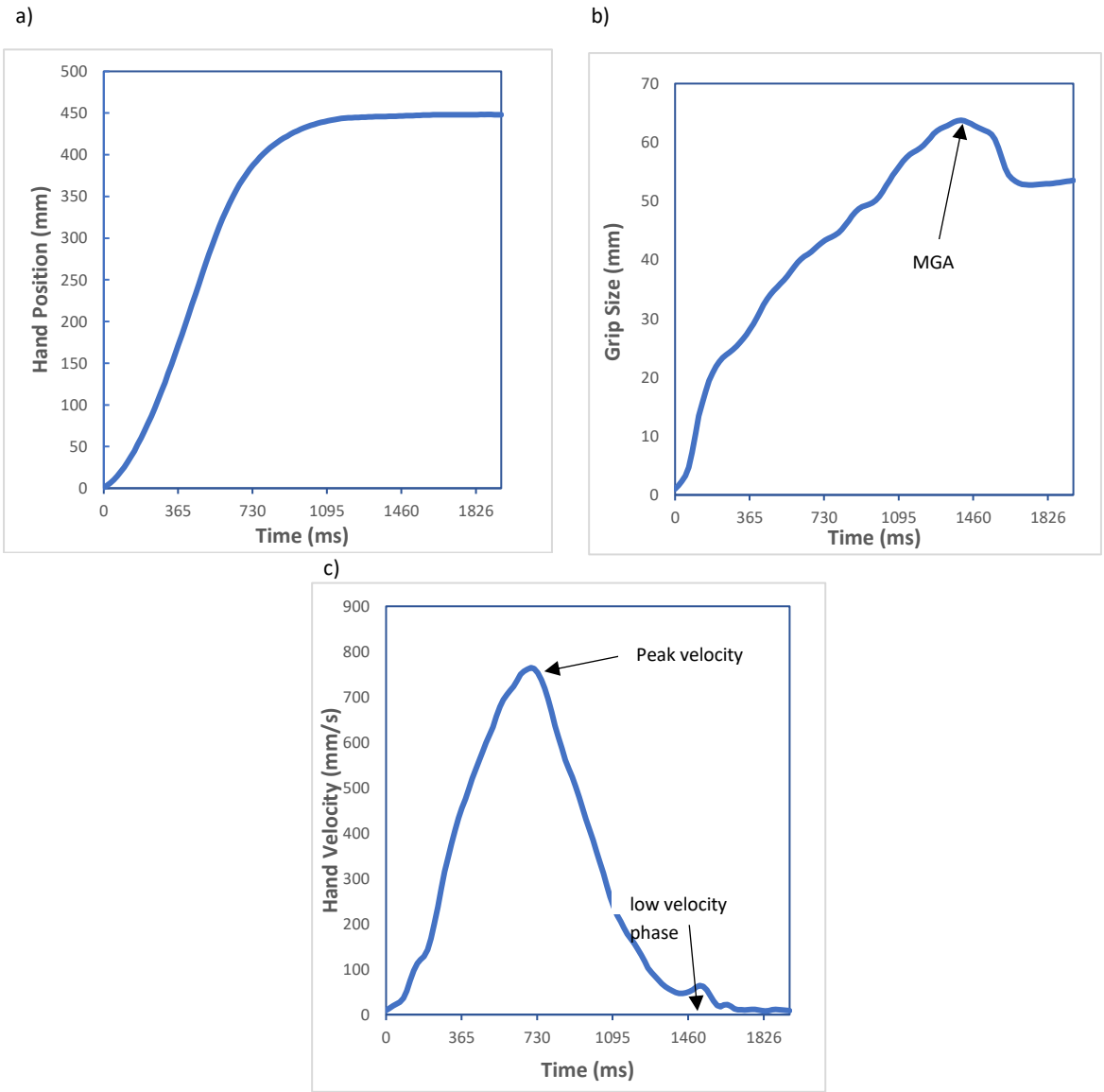

Figure 5: Kinematic hand profiles during reach-to-grasp movement. a) hand position from 0 to 450mm, b) Grip size as a function of task with maximum grip aperture greater than width of object (50mm), c) Hand velocity as it approaches the target with clear peak velocity.

2.5.2 Factors affecting prehensile movement

Reaching-to-grasp (prehension) is a universal human skill underlying numerous activities of daily living. Prehension entails coordinated and controlled movement of the hand towards a target object in order to grasp it successfully [3], [4]. Proficiency requires visual feedback of target position, an adequate motor plan, coordination of the arm and hand movements, and the use of online feedback to correct trajectory errors when necessary. Such controlled and coordinated movement functionally depends on various factors like object intrinsic and extrinsic properties [5], affordances provided by the object [6], the purpose of the action to be performed after grasping [7], and the person completing the movement.

Task constraints

Task constraints alter prehensile components quantitatively and may constrain temporal and/or spatial coordination between prehensile components e.g., Mon-Williams et al. investigated qualitative and quantitative aspects of prehension across various tasks (reach-to-grasp-to-lift objects with slow, normal and fast movements with and without touching the table) and found that spatial and temporal characteristics could be predicted from task constraints where movement duration can be predicted from the object properties (object distance, grasp surface and object size) [145]. But, such instructional constraints inflict coordinated and controlled prehension movement, given the speed/timing constraint of sensorimotor integration.

Since kinematics of reach-to-grasp movements are highly stereotypical in nature, though controlled relatively independently, they change lawfully as a function of the task and the properties of the object [5], [145]. Figure 6 shows the experimental setup determining how Spatial and temporal characteristics of prehensile movements varies with respect to the task constraints such that transport component get effected by the object distance causing PV to increase as well as causing PV to occur later in the movement; similarly, large grasp size lowers spatial accuracy demands while permitting a faster movement and hand opens up to a larger MGA and smaller grasping size demands higher precision during grasping phase [4], [139], [141].

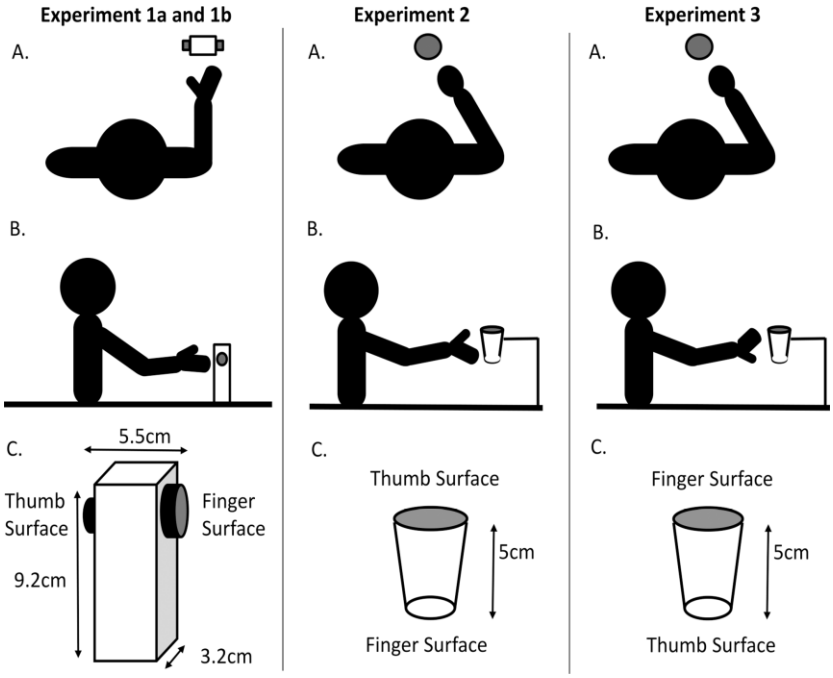

Figure 6: Three Experimental Setup determining the effect of task constraints on the duration of reach-to-grasp movements to objects with asymmetric contract surfaces (experiment 1), and when the object was grasped with the thumb on top and finger underneath in experiment 2 whist the opposite was the case for Experiment 3 [4].

In literature, several studies have analysed prehensile movement and its underlying control mechanisms by covarying object size and distance [140], [141], around obstacles [6], [101], the effect of grasping types [146], [147], perturbation studies when object location or size were changed at movement onset [148], [149], changes to target texture [150] and object orientation [151].

Sensorimotor constraints

Absence of sensory information causes prehensile movements to occur differently, and abnormal sensorimotor integration alter motor control which regulates one's functional independence thereby limiting his/her abilities to perform activities of daily living. PD patients lacks the ability of organizing sequential and simultaneous movement and took longer than movements performed in isolation [152]. Similarly, patients with degenerative cerebral disorders displays abnormalities in all components of prehensile movement (transport: increased path curvature, variable wrist velocity profiles, slower movement; Grasp: multiple peaks, increased grip aperture) and impaired coordination as well [17], [153], as shown in Figure 7. For example, Lu et al., investigated the role of attention during reach-to-grasp movement in 70 subjects (Controls: 24, PD:46) and found that PD patients were slow, rely on visual feedback and require focused attention [154]. According to the kinematic examination of grasping movements in PD, hand pre-shaping and the maximum grip aperture are delayed in comparison to age-matched controls, and PD patients start to close their hand much later than healthy controls [155], [156]. Additionally, compared to the actions of controls with neurologically healthy brains, the timing and amplitude of the maximal hand opening of PD patients are less responsive to

object size [157]. These traits are noteworthy because they may lead to improper treatment of the target objects.

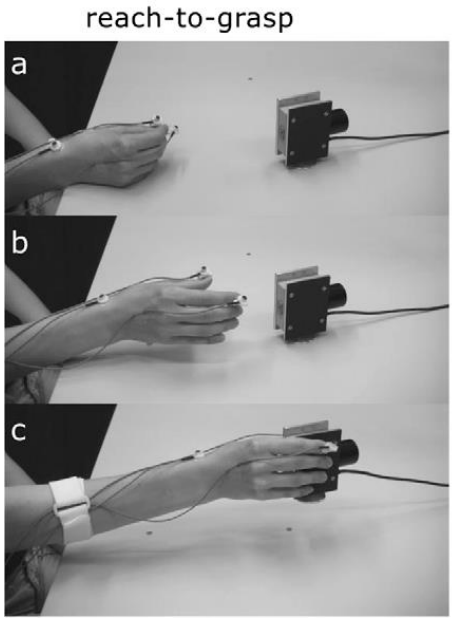

Figure 7: Illustration of the experimental task determining the impairments of prehension kinematics in patients with cerebellar degeneration [17].

Another significant source of feedback is the haptic information gained after grabbing an object. By gradually distorting the haptic feedback received when gripping visible target objects, Mon-Williams and Bingham investigated the haptic calibration of reach distance. The visual targets were produced using a mirror arrangement, and participants stretched out to grasp virtual cylinder targets placed at three different distances. The 'haptic' targets might then move gradually closer or farther to produce distorted haptic sensation at each of the multiple target positions. They found that when calibration (use of error to improve performance) is allowed, participants produced normal prehensile behaviour for virtual visible targets. Alterations are produced by the provision of feedback and are not cognitively invasive [135]. Consistent with this, Coats et al., investigated the presence of haptic feedback during grasping phase and explored the post adaptation effects by subtracting the results from the pre-adaptation trials to demonstrate calibration effects when participants were exposed to the distorted haptic feedback or otherwise. They found that distorted reach distance and grasp size information showed predictable shift in reaching distance and grip aperture size, respectively. Hence, participants calibrate reach and grasp components independently of one another when reaching for virtual targets under distorted visual and haptic feedback [3].

Reach-to-grasp motions can be challenging to perform successfully when sensory feedback is absent or poorly integrated with motor control. Studies investigated reach and the grasp components while movements were made in virtual environments (VEs) with the provision of haptic or visual feedback.

Characteristics of reach and grasp components were altered when compared to the movement made in a physical environment [158], [159] and showed the importance of eye-hand coordination and highlighted the need of online corrections as well.

These studies inform us that both prehensile components are controlled on the basis of sensory information and are not only tied to extrinsic and intrinsic object properties but also depend on affordances provided by the object, task constraints and sensorimotor constraints. More recently, it has been recognized that there is a third component to fully describe the action in this manner – viz., orientation of the hand [151]. Van Bergen et al. suggested that prehension is organised as a 'vector matching' task in which the object vector (defined by the grasping surfaces) and the grasp vector (formed between thumb and finger) are mapped onto each other. In this account, prehension involves moving the origin of the grasp vector towards the object vector (the transport component), altering the magnitude of the vector (the grasp component) and matching object vector orientation (the orientation component) [6], [151].

2.6 Biomechanics of Human Hand and Arm

The biomechanics of the human hand and arm play a crucial role in both fine motor movements (precise, intricate tasks) and gross motor movements (larger, more generalized movements). Following describe the biomechanics of the arm and hand in the context of these two types of movements:

2.6.1 Fine Motor Movements

Fine motor movements involve precise control and coordination of muscles to perform intricate tasks. The following biomechanical aspects contribute to fine motor control:

Hand Structure: The human hand is uniquely structured with opposable thumbs and a high degree of mobility in the fingers. The thumb's opposition allows for grasping objects and performing delicate manipulations.

Precision Grip: Fine motor tasks often require a precision grip, where the object is held between the fingertips and the pad of the thumb. This grip utilizes the muscles of the fingers and thumb to exert delicate forces and manipulate objects with accuracy.

Intrinsic Hand Muscles: The intrinsic muscles of the hand, located within the palm, provide precise control of finger movements. These muscles allow for fine adjustments in grip and finger motions, enabling tasks such as writing, typing, or playing musical instruments.

Fine Motor Control Centres: The brain's motor control centres, such as the primary motor cortex and cerebellum, regulate and coordinate the muscle activity needed for fine motor

movements. These regions receive sensory feedback and send commands to activate specific muscles with the required force and timing.

2.6.2 Gross Motor Movements

Gross motor movements involve larger muscle groups and coordinate actions to perform more generalized movements. The following biomechanical aspects are relevant to gross motor control:

Joint Mobility: The arm's joints, particularly the shoulder and elbow, provide a wide range of motion necessary for gross motor movements. The shoulder joint's ball-and-socket structure allows for movements in multiple planes, facilitating actions like throwing or swinging.

Muscle Power and Strength: Gross motor movements often require more force production and muscular strength. Larger muscles, such as the deltoids, pectoralis major, and triceps brachii, generate the necessary power for actions like lifting heavy objects, pushing, or pulling.

Coordination of Muscle Groups: Gross motor movements involve coordinated actions of multiple muscle groups working together. Agonist and antagonist muscles must work in harmony to produce smooth and controlled movements. For example, during a throwing motion, the muscles of the shoulder, elbow, and forearm work in sequence to generate and transfer force.

Proprioception and Balance: Gross motor movements rely on proprioceptive feedback, which helps maintain balance and coordinate movements. Proprioceptors located in muscles, tendons, and joints provide information about limb position, muscle length, and joint angles, allowing for adjustments in posture and movement control.

Energy Expenditure: Gross motor movements require greater energy expenditure compared to fine motor movements due to the involvement of larger muscle groups and increased force production.

Understanding the biomechanics of the human arm and hand in the context of fine and gross motor movements provides insights into the mechanics, muscle coordination, and control mechanisms involved in performing various tasks. This knowledge is valuable in fields such as rehabilitation, sports training, ergonomics, and the design of assistive technologies.

2.7 Motion Capture Systems

Motion capture systems, that track and record movement using sensors, are widely used in many diverse field such as medical [160], [161], entertainment [162], sports [163], animation [164] and virtual/augmented reality [165]. Motion capture system generally involve capturing human motion while performing tasks and then quantifying this performance [3], [160]. In terms of health services

such systems have the potential to improve patient care (by monitoring progress between medications), diagnose movement disorders (by quantifying finger tapping movement for Parkinson's disease (PD), kinematic analysis of reach-to-grasp movements for multiple sclerosis (MS) etc.) and how motion behaviour relates to disease formation (differentiating between different form of movement disorders: Ataxia/Parkinsonism/Essential tremor/Huntington disease) [160], [166], [167]. Thus, motion capture systems convey information about how someone or something moves by employing a large variety of sensors such as inertial sensors, potentiometer, magnetometers or an array of cameras while returning positional data (2D or 3D) and/or three dimensional orientation [1], [160], [168], [169].

Quantitative assessment tools are critical in overcoming potential limitations (stated in previous section) and the disadvantages associated with subjective evaluation. There are a number of sensing technologies currently being used in laboratory and non-laboratory settings capable of capturing the movements of the hands and they differ in terms of methodologies, movement analysis techniques, computer vision interpretation of 2D or 3D camera system, instrumentation and signal processing techniques. Based on the sensory technologies being used in these systems, they fall into the following categories: digitized tablets; wearable sensors; optical; computer vision; virtual reality; machine learning.

2.7.1 Digitized tablets

With the advancement of digitizing tables, it has become possible for researchers to quantify fine motor skills by recording hand end-point movement (x/y–coordinates) during handwriting, copying, tracing and self-paced drawing activities [170], [171]. Kinematic measures obtained through stylus position data evaluates handwriting and drawing quality. Culmer et al., developed a platform to investigate human motor control by measuring the end-point movement of the hand during tracing and copying tasks [45] as shown in Figure 8. This kinematic assessment tool (KAT) employs touch-sensitive screen of a tablet, records participants' response to stimuli at 120 Hz, and output two spatial metrics measuring path length and path accuracy by analysing positional data of handheld stylus through the trajectory length. They tested twelve healthy controls on copying and tracing task to compare the movement of preferred and non-preferred hand and found significant differences between task and hand. Since 2009, the KAT system, as part of the Born in Bradford (BiB) project, has mainly been used as an important tool to assess child's fine motor skill and to understand the factors related to child's educational and health development (www.borninbradford.nhs.uk). KAT has also been adapted by replacing the stylus with a joystick, incorporating shoulder and elbow joint movement, to investigate motoric deficits in children with cerebral palsy [172]. As for older adults, Smits et al. recorded pen tip trajectories during graphical tasks (tracing geometric figure and

handwriting) performed by PD patients and healthy controls using a graphic tablet and a modified digitizer pen [46]. This showed that Parkinson diseases (PD) patients were significantly slower than healthy controls due to bradykinesia and this was more evident in a writing task than tracing tasks.

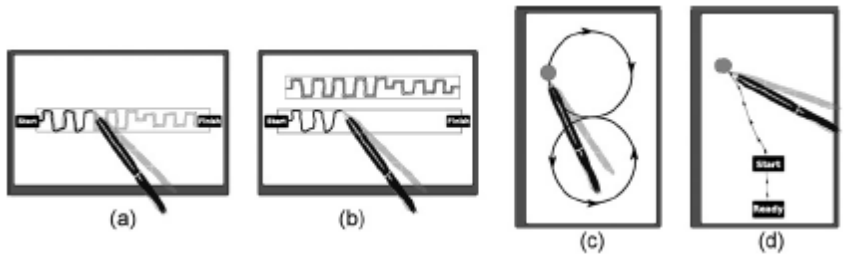

Figure 8: Four examples of trials implemented in Kinematic Assessment Tool (KAT). a) Handwriting tracing b) handwriting copying c) figure of 8 tracing d) jumping dot [45].

2.7.2 Wearable Sensors

Commonly used wearable sensors and devices that objectively measure and analyse movement include accelerometers, gyroscopes, and magnetometers, collectively referred to as inertial sensors. Inertial sensors capture movement by measuring and converting the reaction forces (acceleration) due to an acting muscular force into a proportional electrical signal which is then processed to extract different features, describing the severity of neurological disorder [173], [174]. A triaxial accelerometer based system used by Stamatakis et al. showed good predictive performance while extracting 18 different parameters describing finger-tapping and identifying most relevant features in the prediction of MDS-UPDRS score [85]. Gyroscopes, also known as angular rate sensors, measure angular velocity and are used to detect orientation changes of the object they are attached to. Wearable gyroscopes attached to both forearms measuring bradykinesia in two separate studies, where participants were instructed to perform 17 typical daily activities in 45-min protocol and for a period of 3–5hr during their daily activities, found significant correlation of $r = -0.83$ and $r = -0.73$ with MDS-UPDRS subscore, respectively [86]. Four performance indices derived from gyrosensor attached to the index finger only, showed significant differences between patients and controls and were also found to be statistically correlated with clinical score ($r = -0.73$ to -0.80) [87]. KAT system, shown in Figure 9, measured fine motor skills and to incorporate gross motor measurement it was adapted with accelerometer and gyroscope sensors (MTx, XSens, Netherlands) to investigate postural sway during fine motor tasks and in different viewing conditions [28].

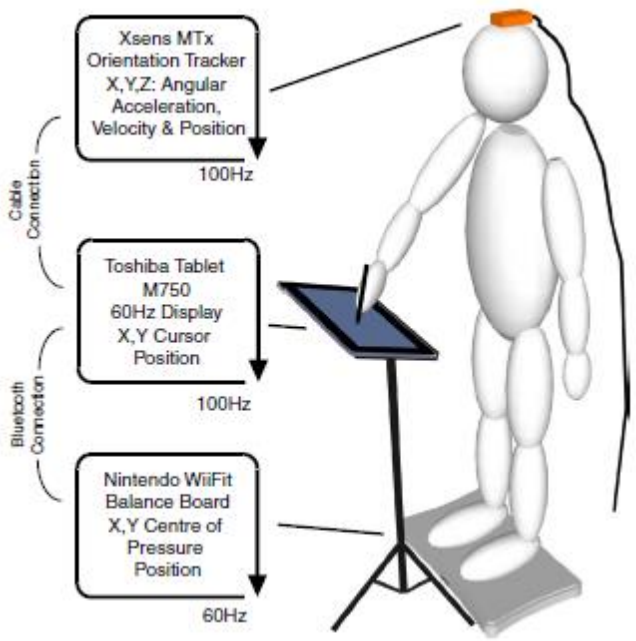

Figure 9: Schematic measuring head movement using Xsens tracker and centre of pressure measurement using Nintendo WiiFit balance board [175].

Combinations of accelerometers, magnetometers and gyroscopes have also been used to provide more reliable results by reconstructing hand and finger movement called PowerGlove system but require extensive anatomical calibration procedure determining a sensor-to-segment coordinate system for every patient [176]. It is not an optimal solution due to the sensor noises combined with a twofold integration to calculate the displacements, yielding inaccurate results and is not adaptable to different hand sizes [83], [89].

As these systems do not measure position and orientation explicitly, instead obtaining them by the integration of linear acceleration and angular velocity which leads to error accumulation over time as shown in Figure 10 [177]. Inertial systems are unable to directly measure the absolute position but relative displacement between parts of the same body as the actor must wear an exoskeleton or a glove made up of bend sensors or potentiometers measuring joint angles and extensions [178], [179]. Magnetometers are so sensitive that they easily pick up electromagnetic noise as well as the presence of ferrous objects in the tracking area which distorts measurement data and it is necessary to compensate when tracking large areas, therefore, so they must be calibrated before setting up every experiment [180], [181].

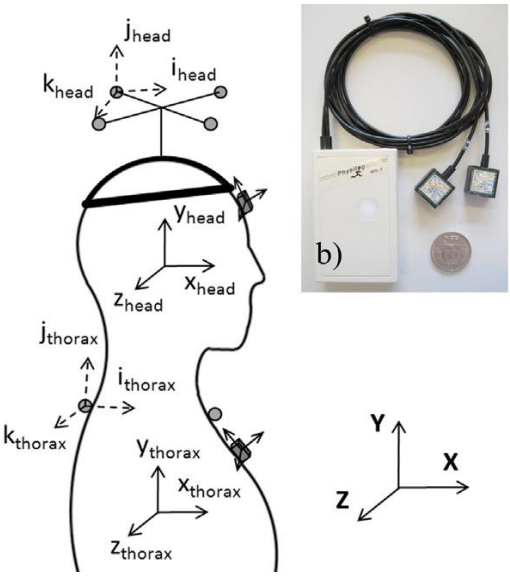

Figure 10: The wearable sensors (grey boxes, with their sensor frames) placed on the head and thorax with their anatomical segment frames (x,y,z) defined from the functional calibration and the reference frame (X,Y,Z) [177].

2.7.3 Computer vision

With recent advancements in computer vision systems, smartphone-based movement analysis techniques are being currently employed to extract information from images or videos. Wong et al. have used videos from an integrated smartphone camera to assess bradykinesia in Parkinson's patients. Randomly selected frames from these videos were used to train a model, the output of which was refined, segmented and then converted into an optical flow field to calculate the instantaneous speed at each point, in turn providing a metric of overall hand movement [182] as shown in Figure 11. This method discriminates between patients and healthy controls with an estimated test accuracy of 0.8 using Support Vector Machine and with an estimated test accuracy of 0.67 using Naïve Bayes model [183]. But this technique showed low correlation values between UPDRS score on a participant level, therefore each video had to be treated as an independent sample.

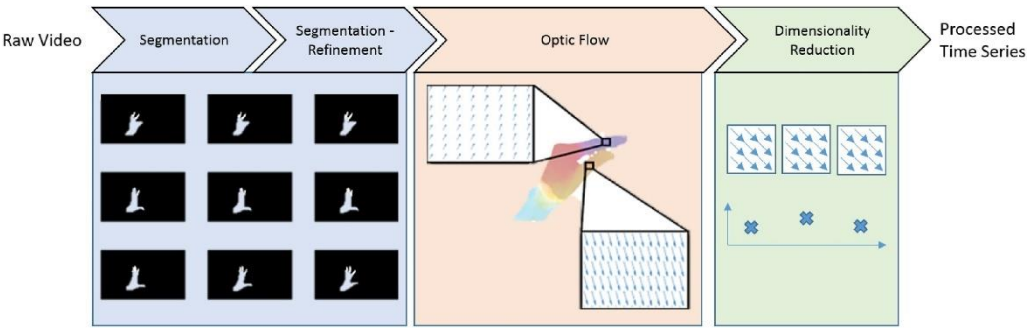

Figure 11: Data processing in which raw video is converted to an anonymous 1D time series. Raw video is first segmented using a convolutional neural network. The segmentation is refined using the grabcut method. Frame-by-frame movement of the hand is extracted using optical flow [182].

Another study extracting finger tapping information from the videos of 13 PD patients and 6 healthy controls discriminated between both groups with an accuracy of 95%, but it required inclusion of the

participants face such that face detection could be used to approximate hand position [184]. Williams et al. investigated bradykinesia by recording FT movement of 39 PD patients and 30 controls using a smartphone camera [52]. They used a deep learning tool, DeepLabCut, to track kinematic landmarks from the videos (frame-by-frame) by an already trained neural network from randomly selected 20 frames of the video itself, and output thumb and finger-tip pixel coordinates throughout the video as shown in Figure 12. Objective measures such as speed, amplitude and rhythm were extracted from normalized finger-thumb distance, and they found good correlation with clinical ratings done by 22 movement disorder neurologists. The computer vision methods described above inherently possess some limitations as they only use one camera which can only capture 2D movement, hence they lack an absolute measure of hand opening/closing and any hand rotation during movement would falsely alter an amplitude measurement [52].

Figure 12: Example video frames taken from smartphone video labelled by DeepLabCut for different kinematic landmarks [52].

2.7.4 Optical motion capture systems

Multi-camera systems are more accurate motion tracking systems with the ability of resolving movement in 3D. Optoelectronic systems are the most widely used motion capture systems within experimental settings, but they require a large space, heavy installation and an expert to operate it thus increasing its operational cost. Cameras detect the position of light emitters or reflectors (markers) placed on the hand (or other body part depending on the task). Passive systems (e.g., Vicon MX and Qualisys) use wireless reflective markers to bounce light back to cameras. Active systems (e.g., NDI Optotrak) use wired strobing light emitters. Whilst both types of system can be used to accurately measure whole-body movement, they are expensive, lack portability and require a degree of technical support thereby restricting them to laboratories [90], [91], [185]. Therefore, their use is limited to those participants who are able and willing to be tested in laboratory settings, meaning large scale assessment in clinical or educational settings are lacking. These optical motion capture systems are highly accurate and capable of tracking markers over wide ranges to sub-millimetre accuracy with high frequency sampling (Optotrak 3020: 3500Hz, accuracy 0.2mm; Vicon vintage: 2000Hz, accuracy 0.2mm; Qualisys Oqus 10,000 Hz, accuracy 0.6mm) [121], [163], [186], [187]. Studies using commercially available high end motion capture systems have demonstrated that spatiotemporal characteristics changes as a function of task constraints and can significantly discriminate patients

from healthy controls [3], [4], [38]. Depending on the intended application of use e.g., to study upper limb movement, it does not necessarily require large measurement volumes, which in turn permits simpler and cheaper solutions. Hence, a motion capture system based on low-cost cameras and off-the-shelf components that can provide comparable quantitative measures would help clinicians to overcome encumbrance, high cost and transport issues of commercially available optoelectronic systems which also require relatively large amounts of space.

Flatters et al. developed an optical motion capture system using off-the-shelf products from the Nintendo Wii platform, the WiiMote controller, particularly for postural sway measurement. The WiiMote controller contains a stereo pair of infrared cameras which can track up to four infrared emitting diodes (IREDs) at 60Hz, with an on-board data processing facility to resolve each IRED into 3D space using calibration techniques. The WiiMote controller is relatively low-cost and communicates with a computer wirelessly over Bluetooth. Figure 13 shows low-cost, portable, wireless motion capture system was developed to measure the head movements concurrently with data collection from the WiiFit Balance board which measured postural stability [41] and was also incorporated with the KAT to simultaneously measure fine and gross motor abilities [28]. These studies assess manual dexterity and postural control development throughout childhood and the system was deployed in schools to measure head, hand and postural control abilities in children in different age groups and suggested non-linear progression of the developmental progress from unskilled to skilled behaviour. In these studies, WiiMote controller was used to track one IRED mounted on the head strap and its positional data was validated against the angular data obtained through an accelerometer and gyroscope [41].

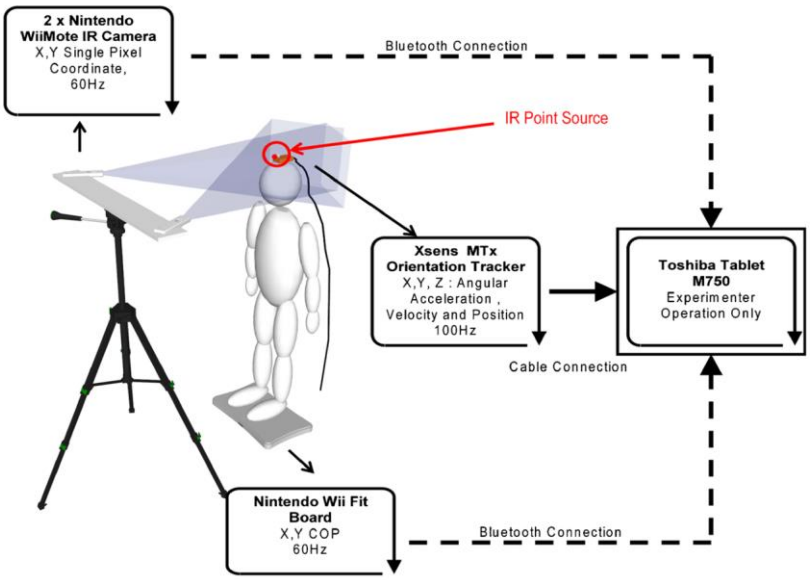

Figure 13: A three-dimensional motion capture system developed using a pair of Ninetendo Wii controllers and stereo triangulated to get the position of IR in three-dimensional space [41].

Only one study has reported the use of low-cost, portable motion capture system using passive markers as shown Figure 14 and differentiated parkinsonian subjects from healthy control by extracting average opening velocity and amplitude decrement from 3D positional FT data [90]. However, this study does not compare its findings with the UPDRS FT score by experts, and its results are not validated against any research grade motion capture system.

Figure 14: Motion capture system developed using commodity hardware being used for finger tapping movements made by PD patients [90].

The field of view (FOV) of any optical motion capture system determines its spatial accuracy and measurement resolution which in turn depends on the experimental setup, number of cameras, and the overlapping field of views determined by cameras position and orientation from each other [188]. Due to this inherent trade-off, motion capture systems can be optimized with respect to the intended application of use. Previously developed optical motion capture systems based on WiiMote-derived technology like the one mentioned-above required small measurement volume to measure head

movement with one IRED and in contrast, Hay et al. tested WiiMote for large measurement volume to determine the pose of a static object [189], WiiMote systems have been used in virtual reality (VR), augmented reality (AR), entertainment and gaming applications when operating over large volumes [188], [190], [191]. They have shown comparable performance to those obtained from expensive system using similar testing methods measuring static jitter of one IRED and the distance between two markers. But these studies do not discuss accuracy and precision of detected marker position if placed at the maximum range of WiiMote controller i.e., 5m, as accuracy and precision decreases by increasing the marker distance from the camera. One major drawback of using WiiMote controllers is they have to be placed relatively far away to cover larger tracking volumes due to the camera's narrow field of view (41^{o} horizontally and 31^{o} vertically) i.e. much space is required or increasing the number of synchronized cameras [192]. Also, camera images cannot be accessed directly, therefore, with on-board data processing facility it outputs real-time positional data of maximum of four IREDs with no provision of offline data processing.

To overcome the WiiMote's limitations, Immersive Cognition Research group at the University of Leeds developed a new low-cost, portable, easy-to-use optical motion capture system and is basically a continuation of postural sway assessment tool developed by Flatters et al [41]. Figure 15 shows the new optical motion capture system which was developed using off-the-shelf products from the Raspberry Pi platform, an infrared Raspberry Pi camera (the PiNoIR) provides large field of view of approximately 62.2^{o} horizontally and 48.8^{o} vertically [193] which can be easily connected to Raspberry Pi controller and programmed using python libraries to capture and record videos. Its sole purpose was to measure postural sway using two IREDs and referred as Postural Sway Assessment Tool (PSAT). PSAT comprises of two raspberry PiNoIR cameras, each connected to its own controller (Pi 3 Model B) and both controllers communicate with each other such that both cameras can record each IREDs' movement simultaneously. This thesis expands the existing work that had already been undertaken on the PSAT system. Next chapter 3 describes the PSAT system in detail and investigates it limitations and strength to study more complex movements such as reach-to-grasp movement with potential usage for laboratory and non-laboratory settings.

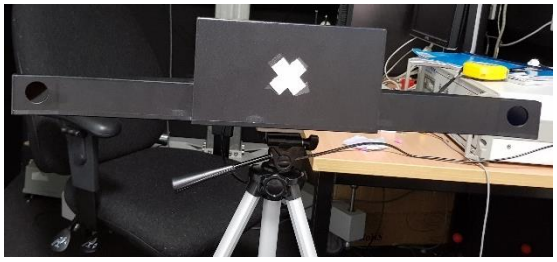

Figure 15: Postural Sway Assessment Tool (PSAT) developed using two PiNoIR cameras where each camera is controlled by Raspberry Pi microcomputer.

2.7.5 Machine learning – markerless human pose estimation

Optical motion capture systems generally involve markers (infra-red emitters or reflectors) to be attached on the participant's kinematic landmarks under study. It aids the analysis process by accurately tracking and triangulating markers in 3D space [121], [163]. Depending on the task and participant, markers introduce additional constraints, by restricting independent movement and can get occluded, forcing the participant to perform unnatural movements to keep the IREDs in view of the cameras. This can make it difficult to assess the underlying severity of movement disorders [3], [23], [163]. In contrast, marker-less motion capture systems track objects being moved in its FOV by detecting features like size, centroid etc. and then matching them to some predefined model, to obtain full tracking data [194], [195]. Both marker-based and marker-less motion capture system requires extensive programming to build software, and expertise in hardware design, as well [194], [196], [197]. With recent advances in new machine learning tools called deep neural networks, trained network automatically estimates important landmarks from images have been extracted from videos [198]–[200] and even cell phone videos [201]. Figure 16 shows the procedure of using DeepLabCut (DLC) toolbox to extract frames, labelling frames, training a deep neural network and then the trained network is used to extract the location of landmarks from unseen videos [200].

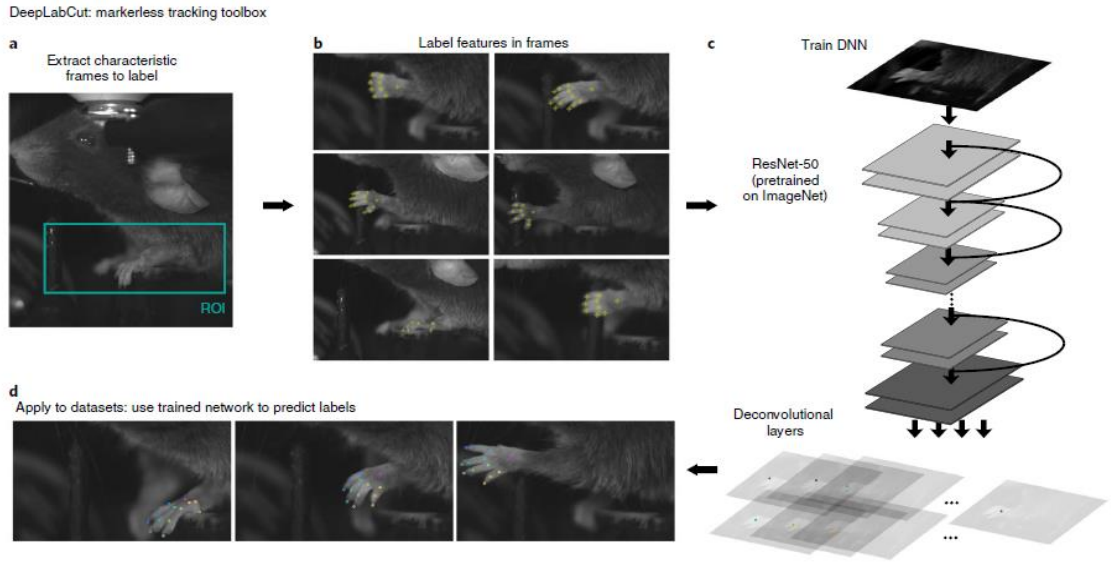

Figure 16: shows the workflow for using the DeepLabCut toolbox [200].

It can be seen that cameras are an integral part of such systems, and their frame rate determines the temporal resolution at which movement is recorded. Recent advances in machine learning has further reduced hardware barriers such that inexpensive smartphone camera can also be used for detailed movement analysis [201], but only provides 2D pixel coordinates. Literature reports deep learning tools being used for non-invasive, marker-less and quantitative behavioural output of key-point locations into 2D and 3D space by employing a single camera and multiple cameras, respectively [198],

[199], [202]. These tools (DeepLabcut – DLC; LEAP Estimates Animal Pose – LEAP; DeepPoseKit – DPK) are replacing conventional methods of quantifying movement using imaged-based methods captured in a highly controlled laboratory conditions [194]. These deep learning based motion capture tools are flexible, allowing users to identify, track and convert important landmarks over time into time series describing movement but differ in terms of inference speed and robustness (speed-accuracy trade-off) depending on the neural architecture being used [198], [203].

These three behavioural analysis toolboxes, DLC, LEAP and DPK are based on machine learning model called encoder-decoder model, allows researchers to automatically estimate subject posture–structural landmarks of the subject under study–enabling them to quantify behaviour, directly from images or videos [198], [203], [204]. Each toolbox has its own limitations and benefits, LEAP was designed for fast inference speed at the expense of accuracy using the SegNet architecture, while DLC and DPK were designed for accurate tracking with slow inference speed using the ResNet and Stacked DenseNet architectures, respectively [198], [205].

2.7.6 Virtual Reality

Virtual reality (VR) systems offer an opportunity to study human behaviour by presenting three-dimensional interactive stimuli, whose attributes are apparent through visual and auditory cues, in a computer-generated environment that allows researchers to conduct experiments outside laboratory settings. It incorporates mainly auditory and visual feedback of the objects but lacks other important sensory feedback like haptic and force feedback while interacting with the virtual environment. Moreover, VR systems know the precise location of the participant's position and of their hand in a simulated environment through VR headset and hand controller gripped by the participant, respectively, but it lacks the ability to precisely measure finger positions and forces generated during interaction with the virtual objects. Fortunately, modern VR systems allow other devices like the leap motion to capture real-time hand movements such as opening/closing of hand or intra-digit aperture and can also provide 3D positional data of each digit during the movement made. So, VR systems combined with other technologies enable researchers to better understand and analyse the processes of motor learning and decision-making [206], [207]. VR systems are being deployed widely in a number of applications e.g. medical training [208], [209] and neurorehabilitation, where user may need to reach and grasp objects of different sizes and shapes and, depending on the complexity of the device, its cost and availability, they are provided haptic feedback of object properties [210], [211]. Recent advances in virtual reality systems have enabled researchers to study human behaviour by presenting three-dimensional interactive stimuli but lack the sensory feedback important for reach-to-grasp movements like hand visual feedback during the reaching movement and haptic feedback while grasping object. Such reach-to-grasp movements are essential for

sensorimotor training in neurorehabilitation and allow researchers to evaluate the effect of sensory manipulation, perceptual modifications and error augmentation on such training using VR approaches.

VR has been used to kinematically analyse reach and grasp components with haptic feedback using wearable gloves [212] and without haptic feedback (visual feedback alone) [158]. These studies suggest that participants moved slower and showed longer relative deceleration times both during reaching and grasping as well as in pointing tasks [213] and took longer to complete a trial than in a physical environment. Specifically, previous studies suggest that the presence of intermittent or continuous haptic feedback in VEs improved grasping [132], [135], [159] but grasping was inaccurate in the absence of haptic feedback [214] and was more prominent such that the closure phase of reach-to-grasp movement was prolonged [158]. Though aperture scaling was preserved in both virtual and physical environments and MGA occurred at the same time but was much wider in VE when haptic feedback was present through haptic gloves [159], [212] than without haptic feedback [158]. So, wearing haptic gloves affected both reaching and grasping components by decreasing the reaching velocity and increasing the aperture size, respectively. The prehension literature [132], [215] also shows that absence of haptic or visual feedback effect existing spatiotemporal characteristics such that absence of visual feedback increases MGA and causes it to occur relatively earlier.

Another important benefit of using VR to study prehension is the fact that the third component of prehension (orientation) can be manipulated by rotating the object during the movement forcing participants to orient hand accordingly as well as forcing participants to make online corrections by perturbing the object position and above all can be used to design numerous experiments like affordances and illusions (shape/weight etc) which are difficult to realize in real world. Moreover, VR systems allow visual stimuli to be displayed in 3D stimulated environment and supports naturalistic interactions with virtual objects and can provide precise kinematic measures in response to displayed visual stimuli.

2.8 Summary

Advancements in hardware and software technologies have provided new opportunities for data acquisition, processing, and analysis in the field of human movement assessment. When it comes to studying movement abnormalities and assessing human arm movement, various technologies have emerged as promising tools. These include accelerometers, gyroscopes, smartphones, digitized tablets, and virtual reality systems [45], [90], [150], [173]–[175], [201], [213], [216]–[218]. These technologies offer advantages such as cost-effectiveness, portability, and the ability to assess

movements in real-world environments. They provide an alternative to expensive and specialized 3D motion capture systems, making movement analysis more accessible.

However, it is crucial to consider the performance characteristics and limitations of these technologies in relation to the specific clinical needs of each scenario. Different movement tracking requirements exist for different clinical conditions or research purposes. For example, monitoring daily steps for activity tracking may not require the same level of accuracy and precision as analysing movement abnormalities in individuals with neurological deficits

To fully understand the clinical significance of these technologies, it is necessary to establish a connection between the technical aspects of body tracking and the specific clinical needs. This involves validating the measurements obtained from these technologies against high-end marker-based motion capture systems, which are considered the gold standard for accurate and reliable evaluation of human movement [21], [48], [219].

By exploring and leveraging low-cost hardware, open-source software, and innovative computational techniques, researchers can extract objective kinematic measures from digital sensing and tracking technologies. However, it is important to validate and compare these measures against established motion capture systems to ensure their reliability and validity in clinical applications.

2.8.1 Key research areas

Literature highlights the significance of technological advancements in human movement analysis, particularly in the context of studying movement abnormalities and assessing human arm movements. It emphasizes the emergence of various technologies like accelerometers, gyroscopes, smartphones, and virtual reality systems as promising tools for movement assessment due to their cost-effectiveness, portability, and ability to assess movements in real-world settings. However, it also cautions the need to consider the performance characteristics and limitations of these technologies in relation to specific clinical needs.

While the literature covers the importance of validating measurements obtained from these technologies against high-end motion capture systems to ensure reliability and validity in clinical applications, it does not delve deeper into specific methodologies or approaches for conducting such validation. Additionally, it lacks a comprehensive discussion of the challenges associated with using low-cost systems, including potential trade-offs in accuracy and precision compared to high-end systems, and how these limitations might impact clinical decision-making.

Furthermore, the literature acknowledges the need for technological improvements, such as the development of low-cost motion capture systems and minimizing measurement errors, but it does not delve into current research efforts or the most promising directions in these areas.

The literature highlights the acceptability criteria for low-cost optical motion capture systems in the context of neurologists diagnosing or evaluating reach-to-grasp movements. However, it does not provide a comprehensive analysis of the existing low-cost systems available on the market or their performance against the stated criteria. A critical summary would benefit from more in-depth discussions on the state-of-the-art low-cost systems, their strengths and limitations, and any specific challenges in meeting the acceptability criteria for clinical applications.

In summary, the key knowledge/research gaps identified are:

1. Lack of detailed methodologies for validating measurements obtained from low-cost technologies against high-end motion capture systems.
2. Inadequate exploration of the challenges and trade-offs associated with using low-cost systems for clinical applications.
3. Limited discussion on current research efforts and advancements in technological improvements, such as low-cost, portable, and easy-to-use optical motion capture system for fine and gross motor measurements.
4. Absence of in-depth analysis and comparison of existing low-cost motion capture systems against the general acceptability criteria for clinical use.

Addressing these knowledge gaps would provide a more comprehensive understanding of the potential and limitations of low-cost optical motion capture systems in clinical settings and facilitate informed decision-making for neurologists and researchers.

In summary, while technological advancements have opened new avenues for studying human arm movement, it is essential to carefully consider the clinical needs, validate measurements, and establish a clear understanding of the relationship between the technical aspects of body tracking and clinical significance. The next section describes the general acceptability criteria for the development of motion capture system while incorporating advancement is sensing technologies. By addressing these concerns, we can fully harness the potential of these technologies to improve movement assessment, diagnosis, and treatment in healthcare.

2.9 Acceptability Criteria

When considering the acceptability criteria for low-cost optical motion capture systems in relation to neurologists diagnosing or evaluating the performance of reach-to-grasp movements, several factors should be taken into account. Here are some key criteria to consider:

Accuracy and Precision: The motion capture system should provide accurate and precise measurements of the reach-to-grasp movements. Neurologists rely on precise data to evaluate and diagnose motor impairments accurately. The system should have a low margin of error and provide reliable and consistent results.

Validity and Reliability: The system should have been validated and tested against established gold standard methods for motion analysis. It should demonstrate good reliability in repeated measurements and consistency across different sessions. Neurologists need to trust that the system's measurements are valid and reliable for clinical use.

Spatial and Temporal Resolution: The system should capture motion with sufficient spatial and temporal resolution. It should be capable of capturing fine details of hand and arm movements, including joint angles, velocities, and timing. Higher resolution allows for better assessment of motor control and coordination.

Ease of Use: A low-cost motion capture system should be user-friendly and easy to set up and operate. Neurologists may not have extensive technical expertise in motion capture technology, so the system should have intuitive software and straightforward calibration procedures. Ideally, the system should provide real-time feedback during data acquisition.

Portability: Portability is essential for practical clinical use. The system should be lightweight, compact, and easy to transport between different settings, such as clinics or research labs. It should not require a dedicated space or complex installation.

Affordability: As stated, the system should be low-cost, making it accessible to a wider range of clinics and research facilities. The overall cost should include not only the hardware but also any necessary software licenses or maintenance fees. The system should offer good value for the price, considering its performance and features.

Compatibility and Integration: The motion capture system should be compatible with standard software used by neurologists for analysing movement data. It should allow for data export in common file formats that can be easily imported into other analysis tools or integrated with existing clinical workflow.

Safety and Comfort: The system should not pose any safety risks or discomfort to patients during motion capture sessions. It should not restrict natural movement or cause any adverse effects. Any necessary markers or sensors should be non-invasive and easy to apply.

Data Management and Analysis: The system should provide efficient data management capabilities, including organization, storage, and retrieval of motion capture data. It should also offer basic analysis tools or integration with external analysis software commonly used by neurologists for further processing and interpretation of the data.

By considering these acceptability criteria, neurologists can make informed decisions when selecting a low-cost optical motion capture system for diagnosing and evaluating the performance of reach-to-grasp movements. It's important to note that while low-cost systems may have limitations compared to more expensive alternatives, they can still provide valuable insights and support clinical assessments when chosen appropriately.

Chapter 3: Low- cost, portable optical motion capture system

3.1 Introduction

This chapter explores the development of the existing Postural Sway Assessment Tool (PSAT) into a system capable of tracking prehension movements and benchmarking this system against an existing well-established system for optical motion capture (Optotrak). The PSAT is a low-cost, portable optical motion tracking system developed using off the shelf components, mainly Raspberry Pi products, housed in a 3D printed casing. The major goal of this chapter was to enhance PSAT's potentials by investigating its spatial and temporal resolution to characterise accuracy levels of PSAT's workspace needed for capturing and analysing sequential/repetitive/simultaneous movements. It is also important to assess its accuracy and precision by validating and comparing the kinematic data with laboratory based optical motion capture system, such as Optotrak, to determine if it is reliable and consistent. Hence, ensuring that its findings are based on reliable information, which is crucial for making accurate conclusions. Such a low-cost, portable, easy-to-use optical motion capture system could be taken outside laboratory settings to schools and clinics, where gross motor abilities associated with childhood development can be tracked and modelled without compromising data quality. The next section (3.2) describes PSAT development (hardware components and user interface) and its architecture for the processing of stereo images, as well as calibration procedures, that are necessary to ensure accurate and reliable measurement of postural sway in individuals. Section 3.3 explores the limitation of PSAT system and extends its capabilities firstly focussing on benchmarking accuracy and the decision to go with opto-markers instead of the off-the-shelf infra-red emitting diodes (IREDs); and secondly on adapting the software to deal with more than two markers and tracking in varying positions. Hence, extending existing PSAT system into a Boxed Infrared Gross Kinematic Assessment Tool (BIGKAT) to study coordinated and controlled upper limb movement. Two experiments (methods and results are reported in Sections 3.4 & 3.5, respectively) are performed to measure spatial and temporal resolution to characterize BIGKAT range that how far it can accurately resolve IRED position, and where in working volume movement should be made.

3.2 PSAT Development

Flatters et al., investigated performance of an expensive inertial sensor (Xsens) to measure the head movement concurrently with their Nintendo Wii based optical motion capture system, and found that the optical motion capture system was more capable of producing sensitive data to capture postural effects under different viewing condition [175], [218], [220]. Inspired by Flatters et al. work, an optoelectronic motion capture system was developed using Raspberry Pi products at the University of Leeds called the Postural Sway Assessment Tool (PSAT).

PSAT tracks the movement of two active infrared light emitting diodes (IREDs) by using two infrared (IR) cameras. Battery powered IREDs are mounted to a set of spectacles worn by the participant 1while attempting to stand still in front of the cameras, with both eyes either open or closed. Small swaying movements are picked up by IREDs and consequently captured by cameras at 60Hz as shown in Figure 17. Views from both cameras are then triangulated to produce the 3D movement trajectory of both IREDs to compute a simple measure of postural sway i.e., pathlength of each IRED and their mid-point. Larger pathlengths mean greater postural sway and Flatters et al., have showed that pathlength was greater when participants were instructed to close their eyes and stand still than when eyes were open [175], [220].

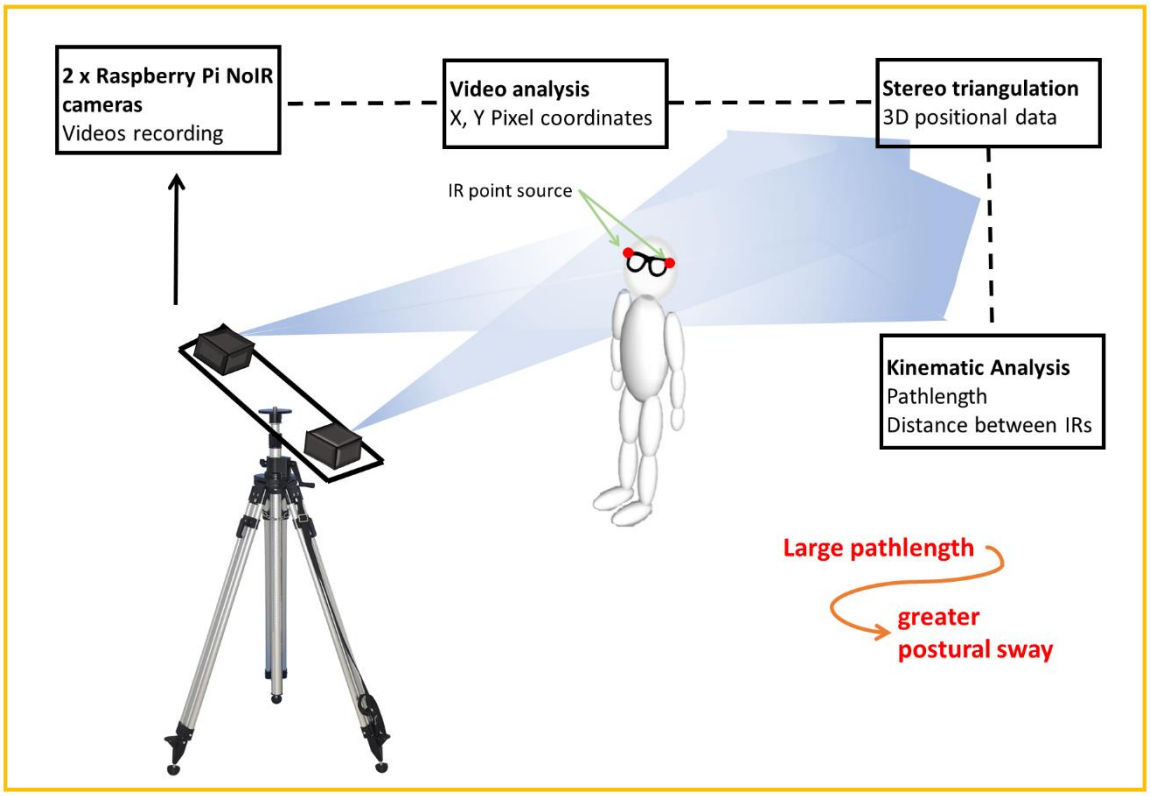

Figure 17: PSAT schematic. A three-dimensional motion capture system developed using Raspberry Pi products such as two PiNoIR cameras, two microcomputers and a LCD display. PSAT measures portual sway by triangulating IR source in 3D space and then measuring pathlength i.e., distance travelled by IR for the whole duration of movement while participants attempt to stand still.

3.2.1 Hardware Requirements

Cameras that are fast enough to record every aspect of the motion of interest and can work together is essential for the efficient recording and tracking of IREDs movement. In order to develop such a system, capable of resolving subtle changes in IRED position from the information coming from each pre-calibrated lens demands selection of a high-resolution infra-red camera capable of recording at high capture rate, and controllers with capabilities of processing and data communication at higher speeds. Also, controller holds main responsibilities of triggering cameras, recording, and storing

videos, and displaying real-time tracking of IREDs movement on graphic user interface. Low-cost Raspberry PiNoIR camera contains a Sony IMX219 8-megapixel sensor and has no infra-red filter giving the ability to see in the dark with infra-red lighting [221]. The camera lens needs to be protected by an infrared pass filter to block out visible light, which can be accomplished by film from a floppy disc drive, in order to function with custom bespoke IREDs as shown in Figure 18. PiNoIR cameras has high sensor resolution of 3280 x 2464 pixels and can be controlled programmatically to take still pictures along with full HD videos at different resolution and frequency. Because recording higher spatial resolution videos decreases the sampling frequency due to inherent camera properties, for example, PiNoIR can record full HD videos of resolution 1080p, 720p and 640 x 480 at sampling frequency of 90Hz, 60Hz and 30Hz respectively. Literature suggests that frequency of 60Hz is sufficient to fully capture human goal-directed movements [222]. PiNoIR provides the option of recording high resolution videos of 720p at 60Hz and are low-cost as well, therefore, PiNoIR camera satisfy our requirement.

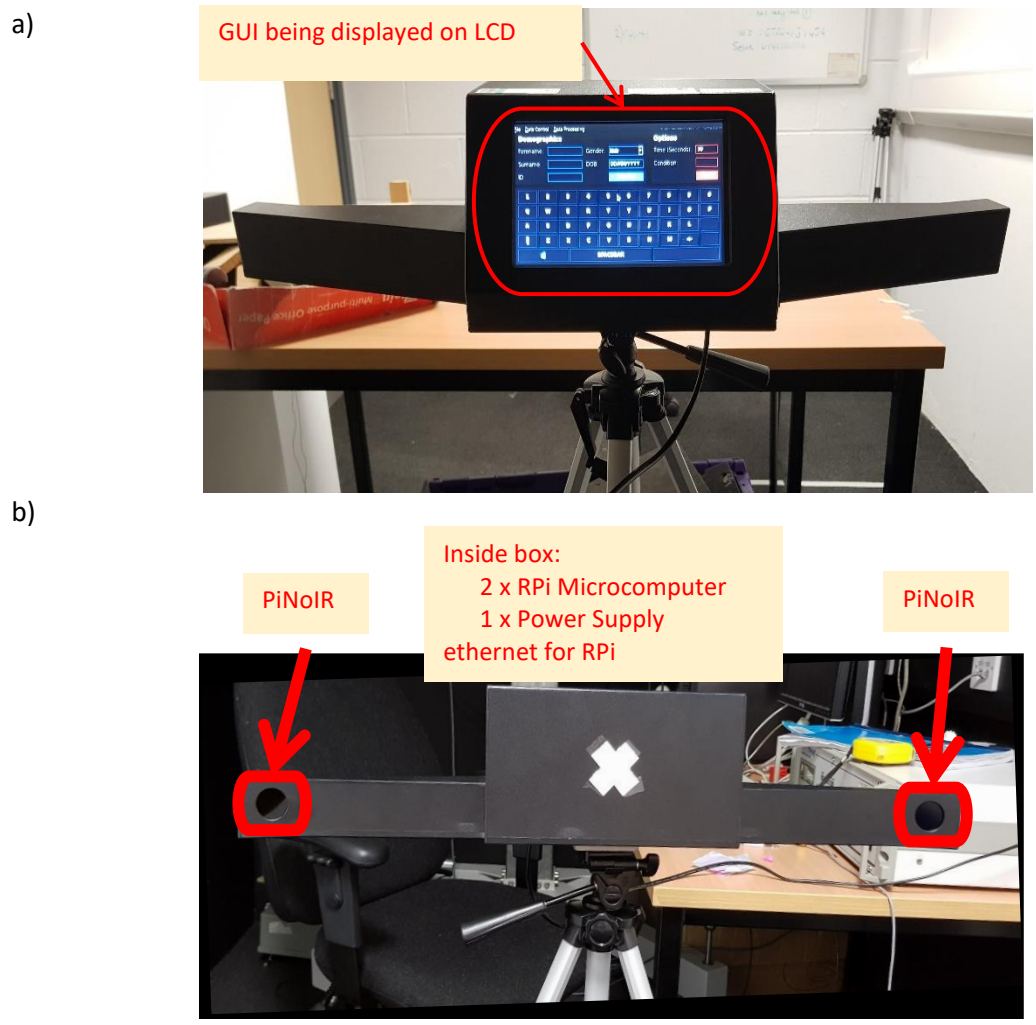

Figure 18: PSAT's front (a) and back (b) view showing two Raspberry PiNoIR cameras being connected to Raspberry Pi microcomputer contained in the box. Master Pi displays GUI on LCD, allowing user to insert participant information, experimental conditions and recording trials for a certain time duration.

For correct triangulation and 3D motion tracking, it is essential to use at least two cameras and should be controlled and programmed to record videos in synchronization [223], [224]. The secondary requirement is to select a low-cost controller to run the PSAT tracking software and to control cameras are a 64-bit computer running 64-bit windows or a low-cost 64-bit microcomputer such as Raspberry Pi (RPi) running on Raspbian [225]. For two cameras, two RPi microcomputers are required, one for each camera because a separate controller for each camera guaranteed that the camera port would not share bandwidth and RPi microcomputer has only one port to connect camera via serial interface (CSI) port.

The main method of interfacing with PSAT software is through a basic graphic user interface (GUI). Display interface is required to display GUI and to control PSAT. Raspberry Pi provides 7" LCD display which connects to the RPi board through dedicated display serial interface (DSI) connector. It is a plug and play device with a display resolution of 1920 x 1080 and 60Hz refresh rate [226]. It is a capacitive touch LCD and supports multiple finger touch allowing user to manage demographics information and choose settings for the recording and triangulation tasks. PSAT software provides three separate tabs (File, Data Control, Data Processing) in the top left corner of the GUI to control the functionality of the interface (for further details see section 3.2.3).

In essence, PSAT includes set of bespoke in-house IREDs, pair of PiNoIR cameras, touch screen display to display graphical user interface (GUI), data control and data processing software to be installed on RPi 3 Model B microcomputer.

3.2.2 General Architecture

Figure 19 shows general architecture of master-slave RPi controllers controlling attached Infrared cameras and communicating with each other over ethernet cable, so that, both cameras can work synchronously and as programmed. Slave RPi simply controls the right PiNoIR camera as instructed by the master RPi. After recording slave RPi transfer the captured data to master RPi and then master RPi saves the recordings from both cameras to USB drive attached to master RPi. Python libraries such as PyQt4, matplotlib, numpy were used to develop GUI enabling user over different PSAT features like collecting demographic information, time duration and destination folder to store captured movement. Master RPi displays GUI on touch screen display and controls the overall working of PSAT such as storing trial by trial movement data as per demographic information.

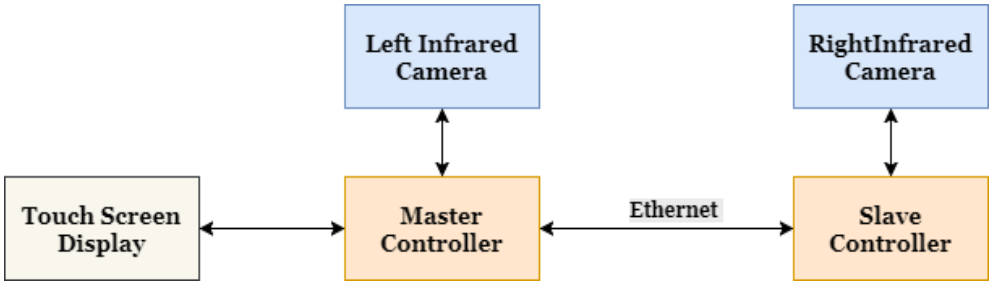

Figure 19: General architecture of PSAT master-slave controllers connected by Ethernet cable and collecting IRED information through cameras. User operate PSAT via GUI functionality being display on touch screen

In essence, PSAT records IREDs movement with both cameras working synchronously for the given time duration. Each video from master and slave RPi are processed using computer vision techniques to identify and detect IREDs. These IREDs points from both RPi are stereo triangulated to obtain the 3D position in space as per the calibration files. Together, this system can take still picture of resolution 3280 x 2464 and record HD videos of resolution 1080p, 720p and 640x480p at 30fps, 60fps and 90fps, respectively. PSAT was programmed to record 720p HD videos at 60 frames per second. Using PSAT for measuring postural sway, PSAT triangulates the position of two IREDs mounted to each leg of glasses worn by the participant and calculates the cumulative path length of each IRED and its midpoint.

3.2.3 User Interface and Backend Communication

Functionally PSAT is divided into two parts, PSAT GUI and PSAT backend, according to the functions they perform and user accessibility. Number of routines and subroutines are programmed using python libraries to execute different functions of GUI and backend and also the communication between them. Figure 20 shows an overview of the PSAT source code files. *'posturalCam_maser_NETWORK.py'* serves as backend communicating and transferring IREDs data between RPis and '*PSAT.py'* controls GUI along with some data analysis tasks. Running *'PSAT.py'* will launch PSAT software and it will detect automatically whether its running on windows or Raspbian. If *'PSAT.py'* is running on windows, then it will automatically load data analysis program or if running on Raspbianthen it will lead to data collection GUI. So, it acts as an entry point into the PSAT.

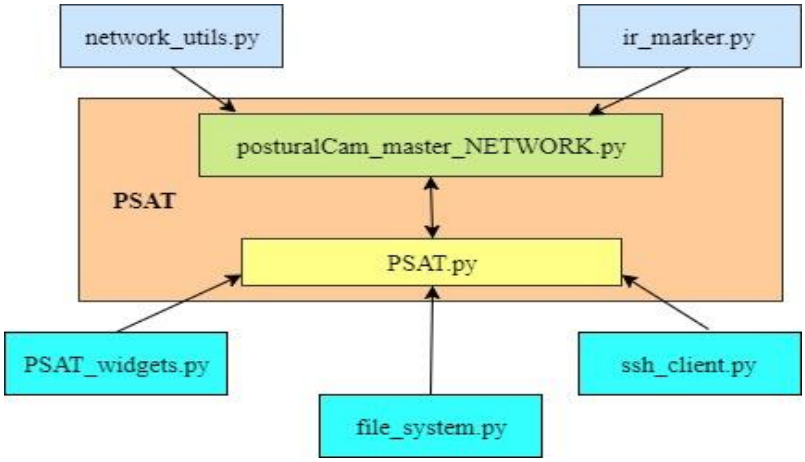

Figure 20: PSAT being functionally controlled by two main scripts. 'posturalCam_master_NETWORK.py' works in background controlling controllers and 'PSAT.py' display information on GUI and waits for user instructions and manage captured data.

Backend functionality such as controlling two cameras, establishing communication between the two RPis, calibrating cameras to extract extrinsic and intrinsic camera properties and performing data analysis are control and manage by *'posturalCam_master_Network.py'* file. This file contains number of functions and classes and is executed on boot on the server RPi and act as an entry point to the server RPi. This file is also accessed by master RPi as required. Important classes developed in this file are summarized as follows:

- Class named *'posturalCam'* is responsible for communication between two RPi's primarily over a TCP server and has methods for controlling the cameras to record videos synchronously. Firstly, TCP server will start on boot and will wait for the connection from master RPi to start receiving instructions after establishing connection. Subsequently, both cameras will start recording for a given time duration. After recording, master RPi will ask server to send over the timestamps files and will check timestamps for any dropped frames. Afterwards, it will ask for the recorded video file and will finally close the connection between the two RPis.
- *'posturalProc'* class contains large number of methods for different purposes. It processes a single video file from the master and server RPi by creating instances of the class and passing the location of the video file and the type of file. This class also contains methods for camera calibration to extract intrinsic (master and slave) and extrinsic (stereo) camera properties, which are required to process a video file it took. These methods are used for processing video file to obtain the 2D position of IREDs in an image.
- '*stereo_process*' class is much similar to 'posturalProc' class. It is responsible for running the stereo calibration file to triangulate the position of IREDs in both cameras to extract the 3D position of IREDs. It takes the 'posturalProc' instances as an argument and return as M X N X

3 array where M is the number of markers and N is the number of frames in a video. Following lines of code describe the working of 'posturalProc' and '*stereo_process*' classes

```
proc = psoturalProc (v_fname = 'testIR.h264' , kind = 'client')
proc2 = psoturalProc (v_fname = 'testIR_server.h264' , kind = 'server)

proc_all_markers = ir_marker.markers2numpy (proc.get_ir_markers ())
proc2_all_markers = ir_marker.markers2numpy (proc2.get_ir_markers ())

stereo = stereo_process (proc, proc2)
markers3d = stereo.triangulate_all_get_PL (proc_all_markers , proc2_all_markers)
```

First two lines process video files from client (master) and server camera by creating two instances of '*posturalProc*' classes and next two lines return dictionaries for each IRED which are then converted to a numpy array from the function in *'ir_marker'* script. Last two lines create a '*stereo_process*' instance to triangulate IRED positions obtained from '*posturalProc*' class and then triangulate those IRED positions and return them as M X N X 3 array. This whole process will leave all the files in the PSAT working directory on the master RPi to an appropriate location as managed by *'file_system.py'* and instructed by '*PSAT.py*' file.

'*PSAT.py*' is the entry point to PSAT and by far is the most complex script to create a GUI interface to the PSAT backend. It contains a *'MinWindow'* class to provide the vast majority of the GUI's functionality and relies on QT4 python bindings to execute the script as shown in Figure 21. GUI has three main windows to collect demographic information, data control and data processing and created by '*self.create_demographics_group'*, *'self.create_camera_group'* and *'self.create_processing_group'* methods. Custom made widgets were created in *'PSAT widgets.py*' file and are imported in *'PSAT.py*' file.

After uploading participant's list and inputting required information like participant ID, recording time and condition under which task has to be performed (Figure 21), new window (Figure 22) will appear as 'next' button is pressed. It further asks for under which control mode should PSAT record, for offline data analysis only 'Send Video' option is already marked and for on-board data analysis 'Process data' option is checked. To avoid delays during data collection and to speed up the process, it is recommended to only use 'Send Video' option.

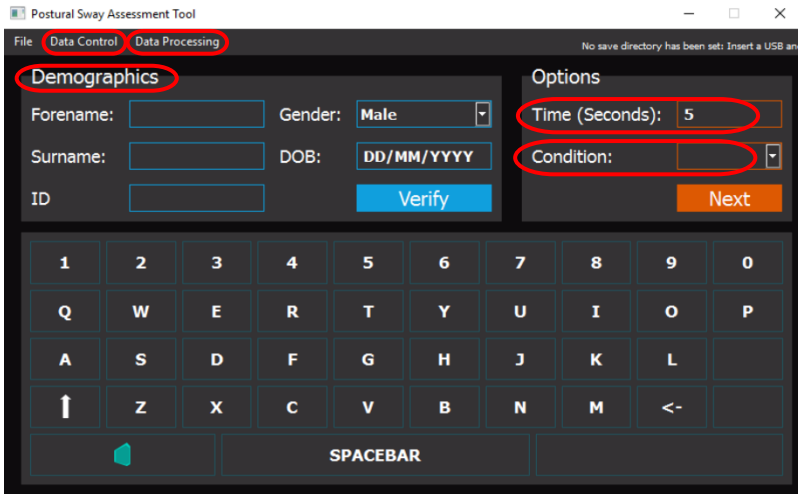

Figure 21: PSAT Graphical user interface (GUI)

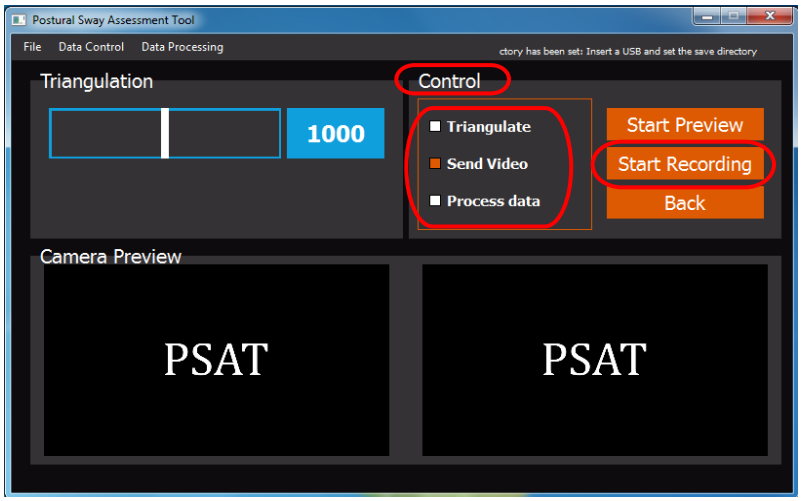

Figure 22: Different control modes for data collection. It provides option whether to just record video or to perform analysis as well.

While running PSAT.py on windows, data processing tab shows up on boot and asks user to select the folder containing recorded data via 'Data Control' tab. PSAT software will look for video files with .h264 within the folder and will automatically show every trial under participant ID and viewing conditions as shown in Figure 23**.** It provides options to user for selection of trials to process and even some or all of the trials of a participant by clicking the check button as shown in Figure 23. Pressing *'Process data'* button will start processing the selected videos from both cameras of a particular trial and will perform triangulation process to obtain the IRED position in 3D space. Console on the right hand side will provide a summary of the percentage of missing markers in each trial and time taken to process each trial.

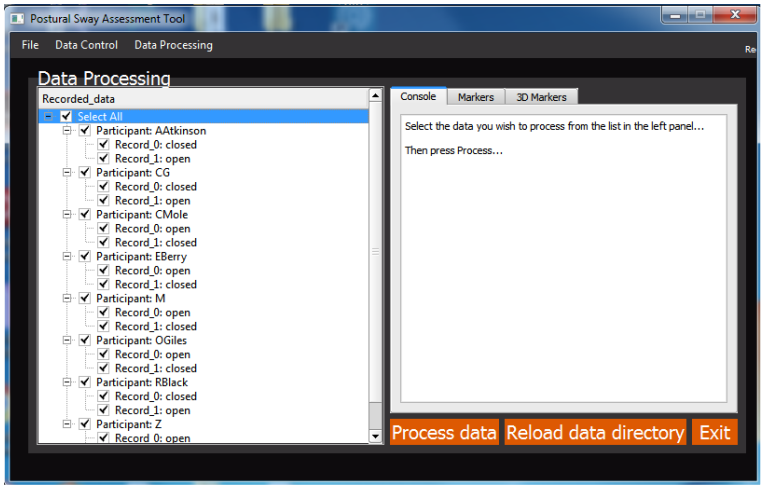

Figure 23: PSAT software running on desktop for offline processing of recorded videos.

PSAT calculates the 3D position of each marker in all trial videos of selected participant, filters the data points using zero-order low pass Butterworth filter with cut-off frequency 8Hz and perform analysis to output a summary file containing path length of each marker, its midpoint and midpoint mean displacement and contains many other files in each participant folder containing raw and filter data of each marker position, midpoint and distance between the markers. Filtered 3D marker position can be further analysed and provides an opportunity to record and analyse many other human movements like prehension, posture control while performing manual tasks etc. Figure 24 shows an output folder of a single trial before processing and after processing.

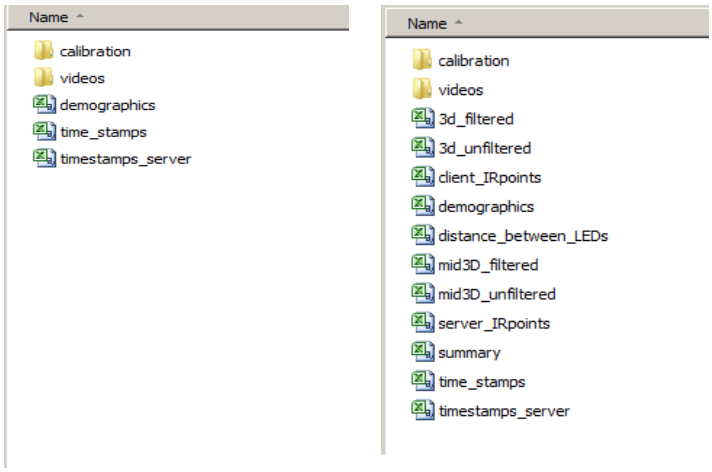

Figure 24: Participant folder containing participant's movement data

Data processing algorithm extracts 3D position of each marker and further processed to output path length of each marker and marker's midpoint and store on external USB. Data processing can also be done offline, after recording all trials, on a separate computer with an additional advantage of much time to record. Optical motion capture system based on off-the-shelf products requires calibration of each camera and both cameras together as a stereo-pair to compute intrinsic and extrinsic properties. Next section discusses adopted calibration procedure used to calibrate PSAT.

3.2.4 Calibration

After assembling all the hardware components together and uploading supported software and programs in to the PSAT, calibration procedure is required to calibrate each camera separately and then once again together and has to recalibrate if any one of the cameras dislocate itself from the assembly casing. So, before using PSAT for the first time or after fixing assembly support, calibration is necessary to accurately triangulate the 3D position of the IRED and movement followed by the IRED in space. The single camera calibrations aim to calibrate the focal length and distortion parameters of the cameras, while the stereo calibration seeks to establish the position of the cameras relative to each other. Both are critical for the successful operation of any optical motion capture system.

Camera calibration procedure is adopted as explained in PSAT development manual which Zhengyou [227] formulated to increase flexibility, robustness of calibration process, also at low cost. The viewing area that the cameras cover and the angles at which they are pointed determine the size of the image utilised for calibration. A calibration image must be large enough to be observed by multiple cameras simultaneously to accommodate a wide viewing angle and/or a broad viewing area. Finding correspondences across various levels of resolution is made possible by optimal calibration objects. The calibration item must be mounted to a movable planar surface so that the image can be moved within the field of view of the cameras while remaining flat. It is not necessary for all cameras to simultaneously see the calibration image or for the calibration image to be entirely visible by each camera [224]. It is more crucial for an extrinsic calibration to be successful that the cameras can be connected across shared images.

This is done by using calibration object, a hard-backed planar surface on which checkerboard pattern of 9 X 6 squares with each square of length 37.5mm is fixed after printing on A3 paper size as shown in Figure 25. Both master and client cameras of PSAT record video of calibration object in a range of different orientations and positions for 10s and subsequently save videos on USB connected with PSAT.

Figure 25: Calibration object presented to PSAT in different orientations and positions. Calibration procedure detecting intersection points.

Further calibration is done offline by running calibration script on each camera video separately (master & client) to generate an optical distortion model by identifying intersection point coordinates as shown in Figure 25, to calculate the disparities between anticipated and observed point location, resulting in correction of the images. Optical model generates a matrix of intrinsic camera properties containing focal point, principal point, and lens distortion. Similarly, stereo calibration was performed by selecting images at same timestamps from both cameras and then locating the corresponding intersection points of the grid. Difference in the detected position of the corresponding points between cameras is used to generate a matrix of extrinsic camera properties containing relative orientation and translation of the cameras. Together with intrinsic and extrinsic camera properties, pixel coordinates from both images can then be triangulated to determine the 3D position in space.

This whole procedure was repeated for five times, resulting in five versions of intrinsic and extrinsic camera properties which are then subsequently used to calculate average calibration values. Thus, accurately determining the triangulated position of markers depends on compensating optical distortion, and accurately determining relative position and orientation of camera, through intrinsic and extrinsic calibration technique.

PSAT's performance in terms of accuracy, precision and repeatability has not been validated against high-end optical motion capture systems or has not been through rigorous static and dynamic performance evaluation. Therefore, PSAT cannot be relied on to measure complex reach-to-grasp movement and even for quantifying simpler movements such as postural sway. The first focus of this chapter is on evaluating PSAT's performance by capturing and analysing static and dynamic movements against research-grade Optotrak 3020 (Optotrak NDI).

Most reported tests in the literature to measure spatial accuracy and precision of optical motion capture systems require two markers being connected to a rigid body and separated by a known distance [223], [228]. The system then tracks the markers for a given time duration and produces three-dimensional positional data to calculate the distance between markers which are then compared with the known input distance to determine spatial accuracy and frame to frame IRED positional variations to measure precision. Hence, to investigate the spatial accuracy and precision associated with PSAT tracking system, an experiment measuring postural sway was performed by tracking the position of two IREDs mounted on a pair of glasses and separated by a known distance, results of experiment are explained in detail in section 3.3. PSAT tracking algorithm can only detect two IREDs which does not meet the requirement of studying prehensile movements and it would produce inaccurate and imprecise 3D position as well if IREDs are presented in vertical direction i.e., if both IREDs have same y-coordinate value. So, it is necessary to extend the PSAT system into a Boxed

Infrared Gross Kinematic Assessment Tool (BIGKAT) by resolving PSAT's limitations to track and resolve more than two IREDs position and presented in any orientation (see next section).

3.3 BIGKAT Development

As stated in previous sections, PSAT capability to accurately measure postural sway has not been evaluated and has also not been validated against research-grade system to determine its limitations. In this section, PSAT was tested to measure postural sway in healthy adults while standing still and participants were instructed to close or open their eyes during recording. It has been shown that young healthy adults had developed more postural stability and can maintain posture for a long while. And it has also been shown that absence of feedback increases postural sway [175], [218], [220], since information isn't available to maintain posture and subsequently sway increases. So, it is expected to observe more postural sway during eye-close condition, even in healthy adults. If PSAT can successfully captures postural sway in healthy adults during still-stance under different viewing conditions, then there are high possibilities that such low-cost optical motion tracking system can be used to measure other gross motor performances. Only three healthy adults were recruited for this study as objective was to assess PSAT performance i.e., how accurately and precisely PSAT can pick up subtle head movements in comparison to Optotrak. If PSAT fails to perform well then it became important to identify the risks and limitations associated with PSAT hardware and/or marker detection and tracking software such as glare produced by bespoke IREDs and/or correct labelling of IREDs in consecutive frames of master and server videos.

Participants were instructed to wear glasses and stand still and were also instructed to alternatively open or close their eyes during recording. Bespoke IREDs were mounted on each side of the glasses and IREDs movement were recorded for thirty seconds. Offline data processing was performed to calculate the cumulative pathlength i.e., the distance travelled by each marker and its midpoint to quantify the postural sway. Distance between IREDs was also calculated for each trial and was averaged across all trials as IREDs were not removed during trials and this measure can be used to assess the calibration accuracy and precision of PSAT.

Figure 26 shows the cumulative path length of mid-point of bespoke IREDs under different viewing conditions and the mean distance between IREDs as calculated by PSAT. Cumulative path length of each marker, whether left or right shows higher value for eye-close condition than eyes-open condition as expected but data shows obscurity in a sense that mean path length of each IRED is in thousand meters and not equal as well. Figure 26a shows average cumulative mid-point path length of each trial during eyes-open and eyes-close condition and shows that data is corrupted with so much noise due to the glare that sway experience by one marker sway is larger than the other, which is

totally meaningless. IREDs mounted on glasses (rigid body) are at 127mm from each other, but mean distance calculated by PSAT shows a difference of more than 4mm.

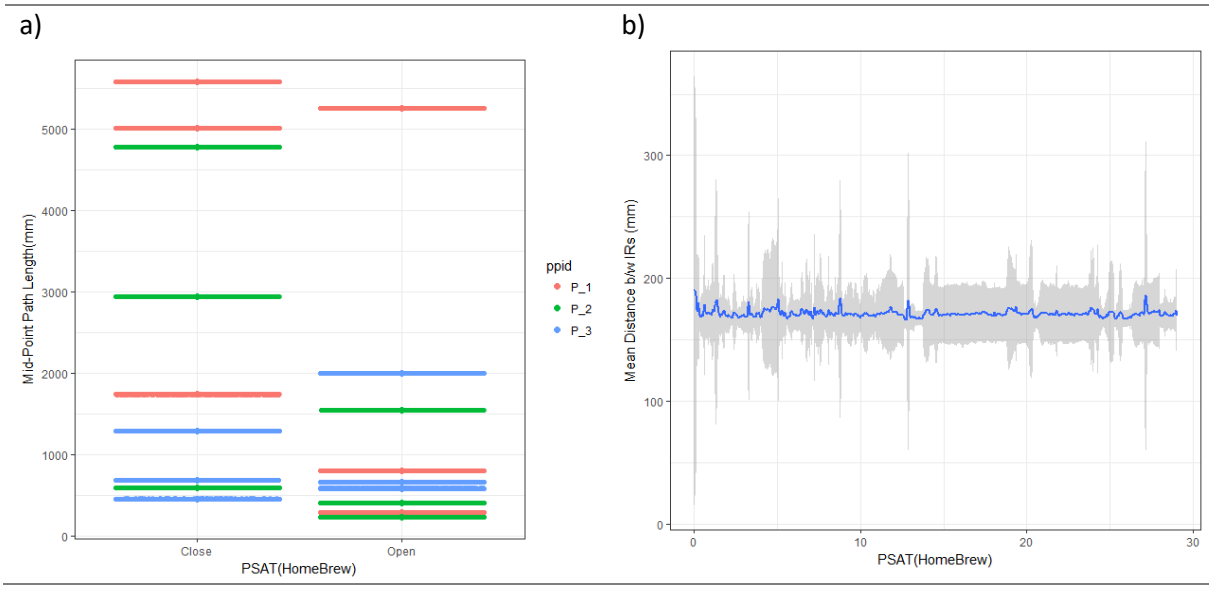

Figure 26: Path length and mean distance between IRs under different viewing conditions using only Homebrew markers with PSAT.

Initial experiments with PSAT to measure postural sway has shown large variations in calculated cumulative pathlength of both IREDs and its midpoint. Intuitively, both IREDS should produce similar pathlengths as they were mounted on the same rigid body, and both will experience the same amount of movement as participants sway. Similarly, distance between two IREDs is constant and known, and calculated average distance between IREDS by PSAT shows large variations showing poor accuracy. Table 3 shows that pathlength of one IRED is relatively much higher than the other IRED which may be due to the glare produced by IREDs or may be due to some serious issues in the tracking algorithm. Pathlength of both IREDs should be similar as they are mounted on a rigid body i.e., on a pair of glasses and experience same amount movement. For this specific reason, noise levels were measured for the positional data obtained by PSAT for both IREDs to determine the spatial accuracy and precision of a tracking algorithm and/or any hardware issues. It is measured by computing the standard deviation (SD) of measured position of a tracked object (static IRED) over time and is calculated in each dimension i.e., vector norm of SDs for each dimension (alike to the root mean square of the distance from mean position). Figure 27 shows high noise level in the tracked position of a bespoke IREDs mounted on a rigid body i.e., glasses and under different viewing conditions. It can be seen from the Figure 27a that the tracked IRED position (eyes open) moved considerably large in x and y direction likewise when eyes were closed. Figure 27b shows noise levels for the same trial obtained by Optotrak which suggests that PSAT performance in terms of accuracy and precision require further investigation before validating against laboratory-based optoelectronic motion capture system. IRED positional

data resolved by PSAT covers large spatial range for a static point source and, therefore, requires further investigation to determine the source of error.

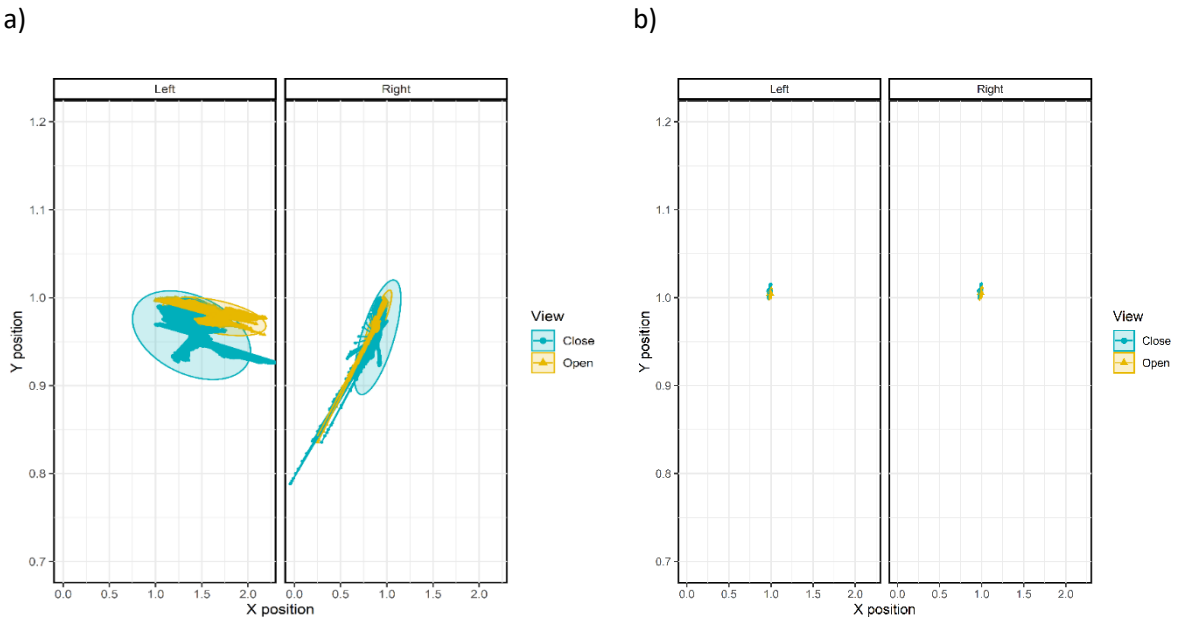

Figure 27: Noise levels in the resolved position of both IREDs (Left & Right) during different viewing conditions as obtained by PSAT and Optotrak. PSAT data shows large variations than Optotrak

Table 3: Correlation coefficient between cumulative path length and standard error for distance between IRs

	PL1(mm)	PL2(mm)	Correlation	Distance b/w IRs(mm)	Standard Error (mm)
Bespoke markers	283.078	1776.752	0.342	190.339	10.409
Opto-Markers	37.863	41.032	0.516	152.911	0.0135

Therefore, to determine whether this large spatial range occupied by IREDs is due to the glare issue or tracking algorithm, bespoke IREDs were replaced by the IREDs supplied with Optotrak and their positional data was collected by both PSAT and Optotrak simultaneously. For this specific purpose, two Optotrak IREDs were mounted on a rigid body at a known distance of 150mm and their position was recorded for 15s at 60Hz by both PSAT and Optotrak, simultaneously. Total of five trials were recorded and analysed with PSAT software to extract 3D positional data, distance between IREDs and cumulative pathlength of each IRED and their midpoint. Table 3 shows the cumulative pathlength and spacing between marker averaged across all trials. Replacing bespoke markers with opto-markers have tremendously reduced variations in the extracted 3D positional data across all trials. Figure 28 shows the result of the calculated distance between IREDs, cumulative pathlength of both left and right IRED and spatial range covered by IREDs as obtained by both PSAT and Optotrak for the same trial. It is evident from the Figure 28c that PSAT power of resolving IRED position increase by replacing bespoke IREDs with Optotrak IREDs. Because bespoke IREDs are too bright as shown in Figure 29c and

due to potential confoundment with glare results in inaccurate resolving of the centre point of an IRED.

Table 4: Mean cumulative path length and mean distance between IREDs calculated for all trials. All values are in mm.

		Left PL	Right PL	Distance between IREDs	SE
Test – Rigid body	**PSAT**	37.683	41.033	152.906	1.430e-3
	Optotrak	36.972	39.041	148.163	3.596e-4

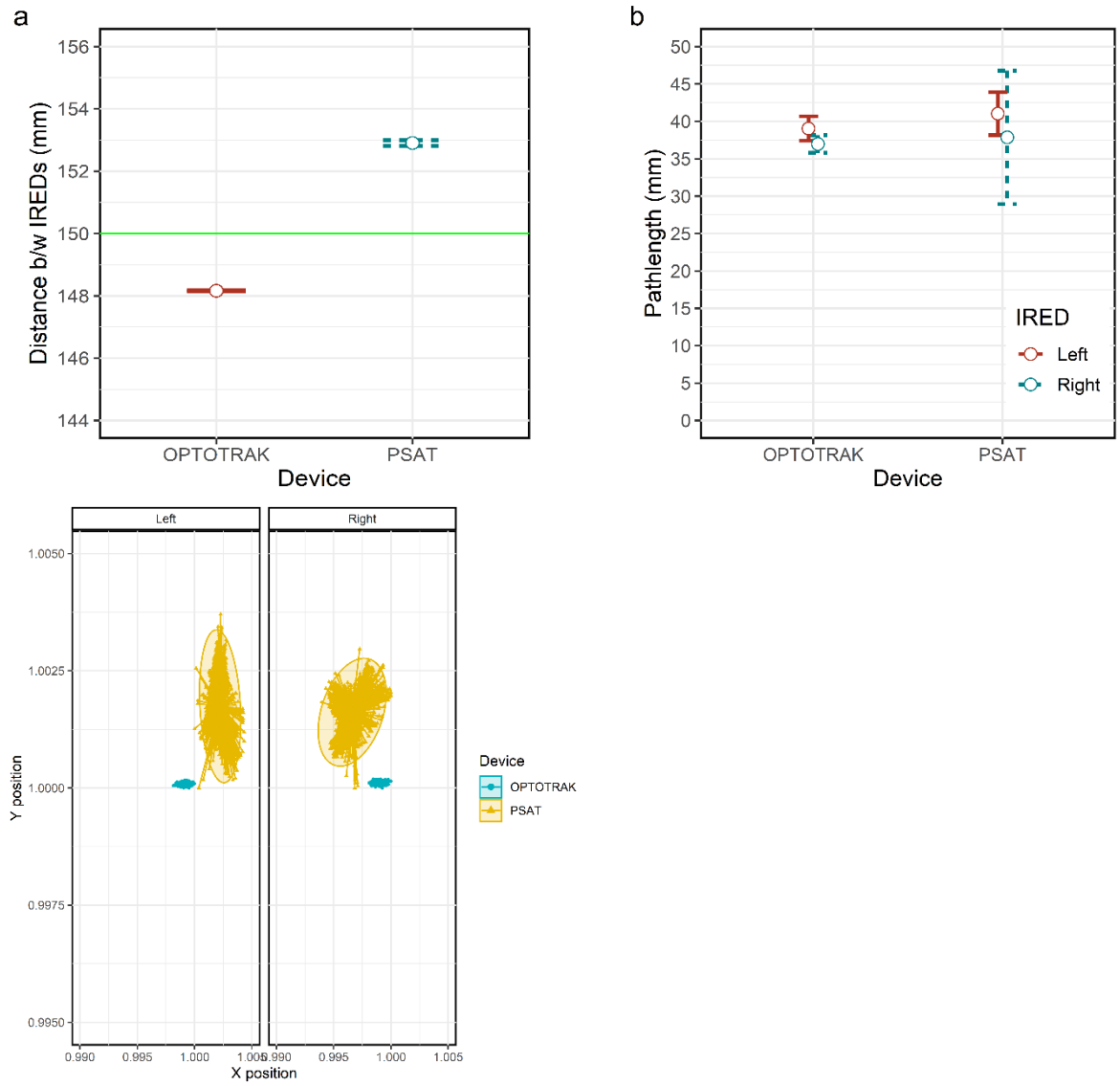

Figure 28: a) Distance between IREDs b) Cumulative path length as calculated by PSAT and Optotrak c) Noise levels for the extracted 3D position of the same trial by PSAT & Optotrak i.e., standard deviation of the measured position of the tracked marker

a) b)

Figure 29: Both Images are extracted from the recordings made by PSAT using a) bespoke markers b) opto-markers.

The PSAT data analysis software was particularly developed for processing postural sway videos i.e., it can only analyse videos with two IREDs. After careful and in-depth analysis of the algorithms it was pointed out that PSAT software would produce inaccurate results while analysing videos with more than two IREDs due to IRED labelling and tracking issues e.g., in a video containing 3 IREDs, two IREDs will be detected and labelled in a frame and may be mislabelled in next frame, hence, making it difficult to track as label jumps from one IRED to other IRED in subsequent frames. With this another issue arises if during movement IREDs become vertically aligned i.e., share the same y-value then PSAT software produce confounding results. In essence, PSAT software scan each frame horizontally for two white 'blobs' and label them horizontally as they appear, so, incorrect triangulation will be performed if IRED happens to switch positions in subsequent frames. Hence, PSAT's usage for studying tasks that require more than two IREDs gets limits and these two IREDs cannot be vertically aligned in any frame otherwise may result in inaccurate tracking due to label swapping. Both these issues were resolved by modifying the PSAT analysis software to track more than two IREDs, presented in any order and labelling IREDs in the first frame of both cameras by a scanning frame at an angle defined by the user according to the task as shown in Figure 30 and Figure 31. And then to make sure that labelled IREDs are tracked accurately throughout the video, distance between each IRED in two successive frames is calculated iteratively for whole video, and then based on minimum distance IREDs positional data is recorded in the respective label. So, tracking script including labelling and ordering any number of IREDs is updated to track IREDs in every frame based on labels assigned in the first frame and based on minimum distance in subsequent frames as shown in Figure 30. It works as follows starting from the first frame

- Get x and y values of makers
- Convert to polar coordinates
- Make a new frame by rotating the markers by an angle
- Convert back to Cartesian coordinates
- Label by new x position after rotation
- Remember the previous frame, and use this to inform labelling of markers

- Get the number of markers
- Generate all different permutations of markers
- Check each permutation
    - check closest marker based on visible marker in previous frame
    - compute distance between each marker in a frame
    - and find out the minimum total distance
- permutations which resulted in minimum total distance is selected

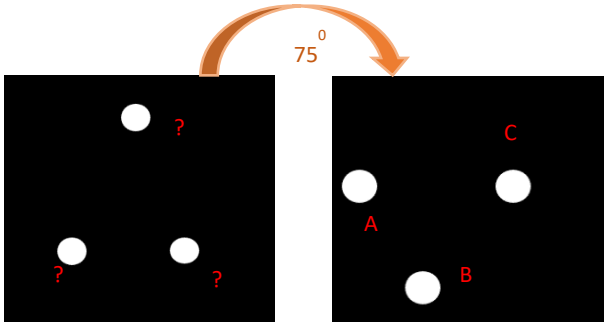

Figure 30: IREDs are labelled by making the first item the first by converting pixel coordinates into polar coordinated and then rotating at a given angle

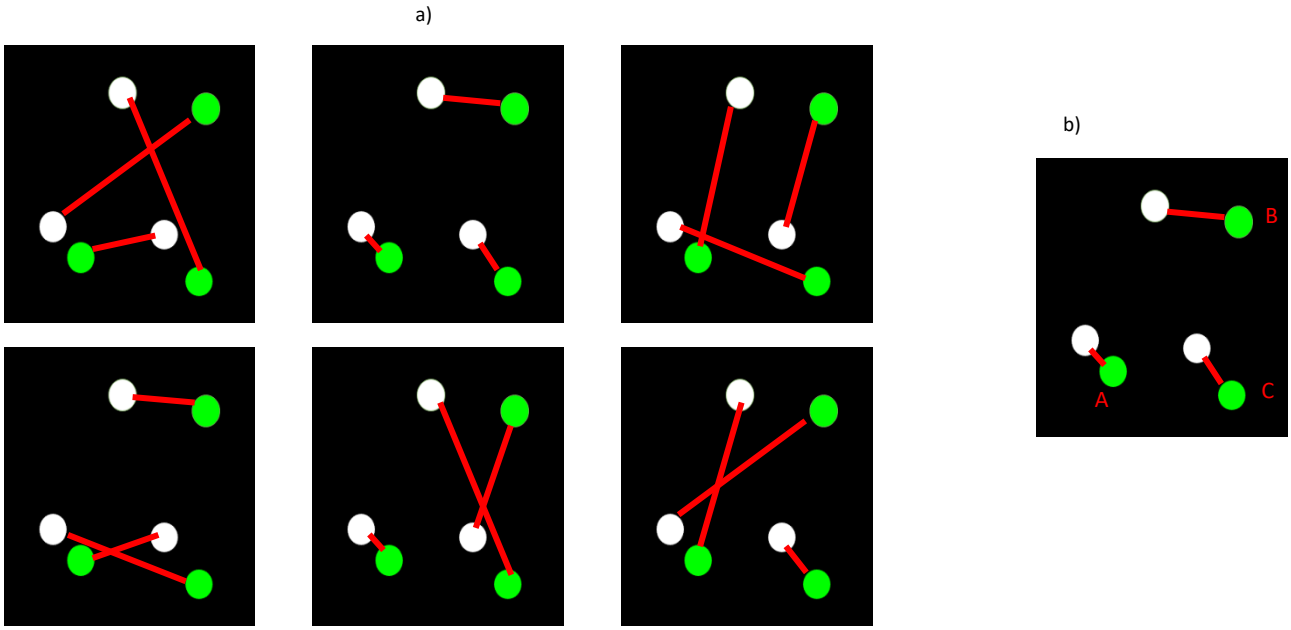

Figure 31: a) All different permutations of markers and red line shows distance between markers in two consecutive frames and the permutation which resulted in minimum total distance is selected as shown in b.

After resolving all the hardware and software related issues and incorporating relevant changes, PSAT was renamed to Boxed Infrared Gross Kinematic Assessment Tool (BIGKAT) to measure upper limb dexterity by providing objective kinematic measures of reach-to-grasp movements. Another main objective of this study was to determine spatial and temporal resolution of the system and how the spatial accuracy and precision changes across BIGKAT's workspace. For this purpose, it is necessary

to measure BIGKAT's spatial resolution to determine how spatial accuracy changes when IRED is placed at different location in its working volume. As accuracy of correctly detecting IRED position decreases when it is placed around the edges of the working volume because of inherent intrinsic camera properties. A novel method of measuring spatial resolution was devised to detect the position of an IRED using BIGKAT system and successively moving IRED at equidistant locations in its workspace. It was done for both horizontal and vertical planes such that BIGKAT's workspace can be sub-divided with respected to the reported spatial accuracy and precision values. Such information would help experimenter to know how far BIGKAT should be placed and where in BIGKAT workspace movement should be made, results of spatial resolution are presented in detail in section 3.4. Likewise, temporal resolution was tested by providing dynamic input in the form of simple harmonic motion to determine how fast BIGKAT can detect a moving IRED, thus, informing experimenter how accurately and precisely it can capture the temporal characteristic of a movement (see section 3.5 for further details).

3.4 Spatial and Temporal Resolution

Before using BIGKAT to collect data from participants, it is important to determine its spatial and temporal resolution along with validating its ability to resolve IRED position against an established research grade system such as Optotrak. As discussed in chapter 2, FOV determines the spatial accuracy and measurement resolution of any optical motion capture system which in turn depends on the intrinsic and extrinsic camera properties. In other words, how the accuracy and precision changes as a function of IRED position when placed at different locations in horizontal and vertical plane? Therefore, one main objective of this study was to sub-divide BIGKAT's FOV into smaller subsets with respect to the measured spatial accuracy and temporal resolution. Hence, two experiments were devised to track the static and dynamic movement of the IRED by BIGKAT and Optotrak, simultaneously.

Experiment 1 characterises BIGKAT's spatial accuracy and precision by tracking the position of a static IRED placed on a large grid presented both horizontally and vertically, within the overlapping field of view (FOV) of BIGKAT and Optotrak 3020. Both devices iteratively measured the 3D position of the IRED at every other grid corner point at the same time for a specific duration. Optotrak acted as a 'gold standard' to determine the mean absolute error (MAE) at each and every grid point, thereby, sub-setting FOV with respect to the computed MAE in both planes (horizontal & vertical). Also, to characterize BIGKAT range that how far it can accurately resolve IRED position, vertical resolution was also determined by successively increasing the BIGKAT distance from the grid. Basic purpose of experiment 1 was to provide us with tracking volumes based on different MAE levels (0~5mm, 5~10mm, 10~15mm) and large enough to conduct reach-to-grasp studies.

Experiment 2 determines the temporal resolution such that how precisely movement unfolds itself for the whole duration of measurement or in other words it determines the fastest changes that BIGKAT is able to track. For the exact same purpose, experiment 2 reconstructs dynamic movement presented in the form of simple harmonic motion by attaching two IREDs on either side of the pendulum. Similarly, as in experiment 1, both devices recorded IREDs movement, simultaneously, at five different locations within the overlapping FOV of BIGKAT and Optotrak.

3.4.1 Experiment 1: Spatial resolution

Accurate and precise tracking of marker movement in any system's workspace, and the resolving of markers into three-dimensional coordinates, is of critical importance to any optical motion capture system. A key factor determining the performance of any measurement system is therefore its spatial resolution, i.e., how accurately and precisely it can analyse its workspace [224], [229], [230]. So, to determine the spatial resolution of this system, we tested BIGKAT in its ability to reconstruct a grid of IRED markers visible in its FOV in comparison to the gold standard Optotrak system.

Method -Horizontal (XZ) Resolution

Two grids printed on A0 paper were placed side-by-side on the flat table (see Figure 32), with grid lines spaced by 36mm. BIGKAT was placed nearer to the grid because of its smaller FOV than Optotrak. The front edge of Optotrak was 1300mm from the near edge of the grid, and 2452mm from the origin (the top left grid point). The front edge of BIGKAT was 700mm from the nearest edge of the grid and 1852mm away from the origin as shown in Figure 33. This setup allowed us to make simultaneous measurements with BIGKAT and Optotrak, hence, a direct comparison of BIGKAT's performance against a commercially available accurate and precise optical motion capture system could be made.

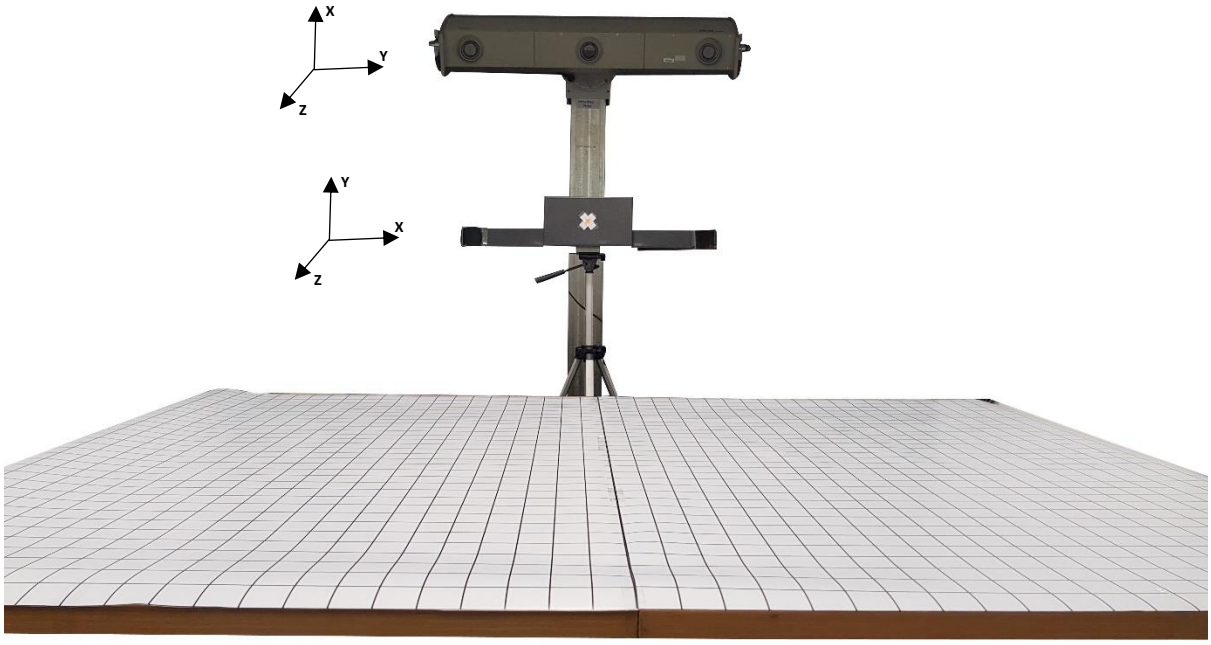

Figure 32: BIGKAT and Optotrak looking at the grid being presented horizontally.

The bottom left corner point of the grid visible in BIGKAT's FOV, as shown in Figure 33, was considered as an origin and its 3D coordinates were measured by both BIGKAT and Optotrak by placing an IRED on the origin for a duration of 6 seconds at 60Hz. The IRED was then moved along two grid points (in the X dimension for BIGKAT) and data collected for another 6s. This process continued until every second grid point (so a gap of 72mm between each) along the border and within the border denoted by the black dot in Figure 33was recorded by placing an IRED, where this change in IRED position was considered by BIGKAT as a change in the XZ-plane and a change in the YZ-plane by Optotrak. In essence, for BIGKAT change in IRED position along z-axis and x-axis corresponds to the columns and rows of the reconstructed grid. Similarly, for Optotrak change in IRED position along z-axis and y-axis corresponds to the columns and rows of the reconstructed grid. IRED position was measured at those grid corner points (266 points, 17 rows x 19 columns; not rectangular but trapezoidal) which were visible within the overlapping FOV of both devices. The visible grid was then reconstructed using the 3D positional data from both devices and It can be seen from the Figure 35that even though IRED points were visible, BIGKAT could not resolve first three columns (21 points) at the extreme left of the plane, therefore, corresponding three columns of the Optotrak's grid were cropped to match grid size observed via BIGKAT.

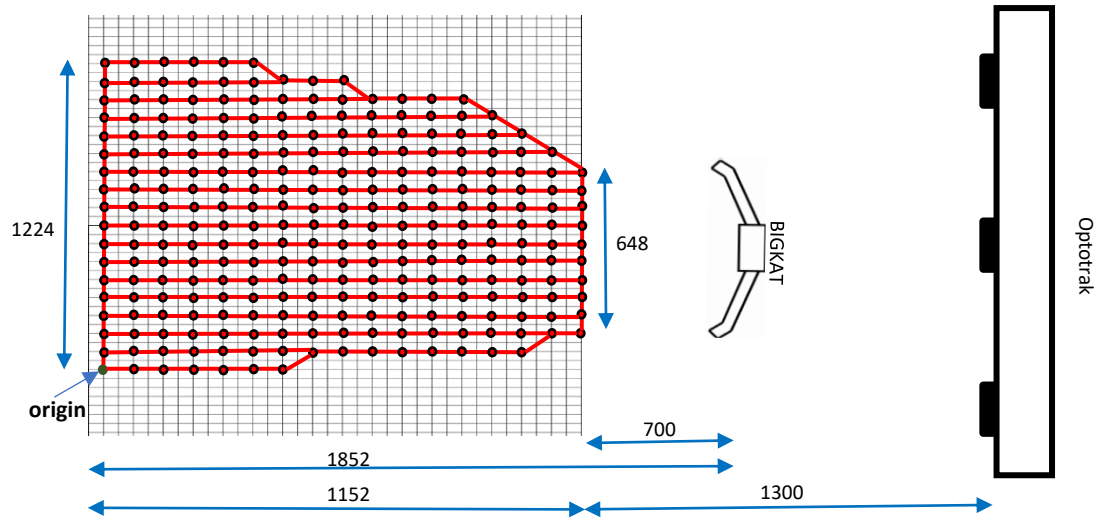

Figure 33: Spatial Resolution Experiment Setup. The red line shows the visible grid in BIGKAT's FOV. Each black dot refers to IRED position at every second grid point separated by 72mm within and along the border. (All values are in mm).

However, the 3D positional data of the reconstructed grids were different from each other, preventing measuring positional error between the two devices. To make a direct comparison between the grids as seen from both devices, coherent point drift (CPD) rigid registration method was then used to translate and rotate the observed BIGKAT grid onto the grid obtained by 'gold standard' Optotrak, resulting in characterizing the spatial accuracy and precision of BIGKAT.

Vertical (XY) Resolution:

As in horizontal resolution, vertical resolution was characterized by presenting grid in vertical plane of both BIGKAT and Optotrak and both devices recorded IRED position at every second grid corner point, simultaneously. Optotrak 3020 can accurately $(\pm 0.2mm)$ resolve IRED placed at a distance of 5m [187] and likewise to determine BIGKAT's range, vertical resolution was determined at multiple distances from the grid. Distance between the grid and Optotrak was kept constant (3 meters) because Optotrak's large FOV could capture the whole of the grid. BIGKAT's FOV is much smaller compared to Optotrak, so it was positioned at three different distances from the grid (700mm, 1400mm, and 2100mm), and the resolved visible grid was characterized for whole visible workspace in the same manner as for horizontal resolution. The IREDs' positions were recorded at those grid points which were visible through BIGKAT's lenses and data was collected for 6s at 60 Hz by both BIGKAT and Optotrak, simultaneously, at every second grid point, spaced by 72mm.

3.4.2 Data Analysis

One of the major considerations while calculating positional errors between BIGKAT reported IRED position and obtained from gold standard Optotrak is that both devices report IRED position in their own coordinate system. Therefore, one cannot simply find the MAE just by subtracting BIGKAT's IRED position from the Optotrak IRED position. Therefore, it is necessary to transform BIGKAT's coordinate

system onto the reference coordinate system (in this case Optotrak). Another major consideration is that coordinate axis of both devices differs from each other such as triangulated IRED position along X-axis of Optotrak corresponds to the BIGKAT's Y-axis and vice versa. There are several point set registration methods to overcome such limitations such as Iterative Closest Point (ICP), coherent point drift (CPD), Robust Point Mapping (RPM), and Gaussian Mixture Models (GMM). CPD is a powerful method to handle complex deformations, large data sets and non-rigid deformations, and a well-developed key component of computer vision, used to find spatial transformation by mapping BIGKAT grid to the Optotrak grid. Rigid registration method from CPD algorithm was used to register BIGKAT's positional data over Optotrak positional data [231], in order to make the direct comparison between the two i.e., transforming the BIGKAT positional data onto the Optotrak positional data while preserving the inherent information contained by the data.

One of the main objectives of this study was to characterize BIGKAT's workspace to conduct reach-to-grasp studies with sufficient accuracy and minimal distortion effects, therefore, it was needed to investigate how accuracy varies across workspace by dividing a whole visible grid (grid of IREDs viewed by BIGKAT and Optotrak) into smaller sets of grids and performing CPD to compute positional error for every possible combination of rows and columns. For example, for a grid (set) containing 3 columns (m, m-1, 1) and 2 rows (n, 1), a total number of 6 possible combinations (subsets: m x n, m x n-1, m-1 x n, m-1 x n-1, m-2 x n, m-2 x n-1) can be extracted. 3D coordinates of each subset of the grid from PSAT are transformed onto the Optotrak coordinate system which are then used to calculate mean absolute positional error for every subset. Using this approach, the position of a single IRED was calculated at successive locations throughout the workspace, whereas, for calculating positional errors (MAE) CPD rigid registration method is critical and has been performed for each subset of the whole grid. Figure34 shows the schematic of the whole characterisation process, where a subset of whole visible grid ($m\ rows \times n\ columns$) is selected and CPD applied repeatedly by removing a column from either side until left with a single column in the middle i.e. $m\ rows \times 1\ column$ and then computing the positional error at each sub-levels. Same procedure was adopted for the same visible grid by removing a row ($m - 1\ rows \times n\ columns$) and then performing CPD repeatedly by removing a row from the top and bottom until left with a single row ($1\ rows \times n\ columns$) in the middle. This whole procedure continued until left with a single column and a single row in the middle. In our case a subset of whole visible grid after performing first CPD has $17rows \times 9columns$, therefore, total of 153 sub-grids were transformed and analysed for positional errors. With this approach, it became possible to characterize how well BIGKAT grid fits onto the Optotrak grid and how much distance each BIGKAT's grid point is from the corresponding Optotrak's grid point.

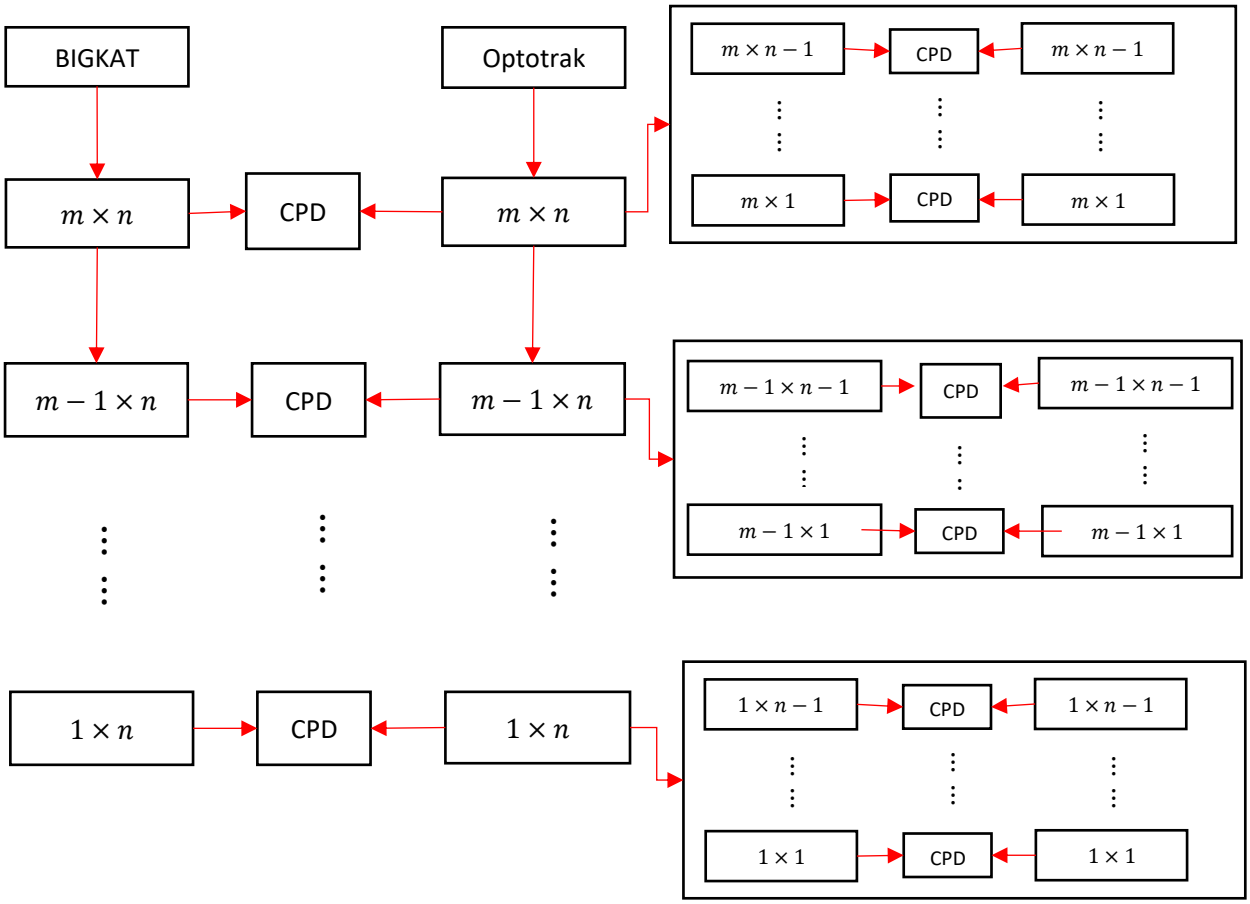

Figure34: Procedure of repeatedly applying coherent point drift method on several subsets of the observed grid until left with a single column and a row in the middle.

Above stated procedure would provide positional error as a combination of rows and columns but knowing how much positional error each row and column contributes towards overall error has two benefits; firstly it identifies parts of the workspace maximally/minimally affected by inherent camera distortion properties and therefore should be avoided/utilized during experimentation, secondly about error distribution by plotting an error histogram whether it produces a normal distribution with smaller standard deviation or it produces a left-skewed and flatter curve.

3.4.3 Results - Horizontal Resolution

Figure 35a & 17b show the reconstructed grids obtained from BIGKAT and Optotrak by calculating the mean 3D position of the IRED at each recorded position of the grid and it can be seen from the Figure 35a & 17b that both devices output IRED positions in their own coordinate frame which don't allow direct comparison thereof. This demonstrates the need for the CPD point set registration method to transform both sets of results onto a common coordinate system.

And Figure 35b shows that BIGKAT could not resolve first three columns (C1, C2, C3) even though these columns were visible via BIGKAT during data collection i.e., IREDs placed at the extreme left side of BIGKAT FOV was not detected as it was not visible in one of the cameras. Before applying CPD, both

Optotrak and BIGKAT grids should be of same size, hence, the first three columns of the Optotrak grid were removed. Figure 35c shows BIGKAT grid ('+') after performing CPD being overlaid on Optotrak grid (colour dots) i.e., BIGKAT grid undergoes spatial transformation with respect to the reference coordinate frame. Thus, enabling direct comparison by computing positional error at each grid point. As it can be seen from the post CPD grid (Figure 35c) that positional error increase significantly when the IRED is at the edges than at the middle of the FOV due to the inherent optical distortion.

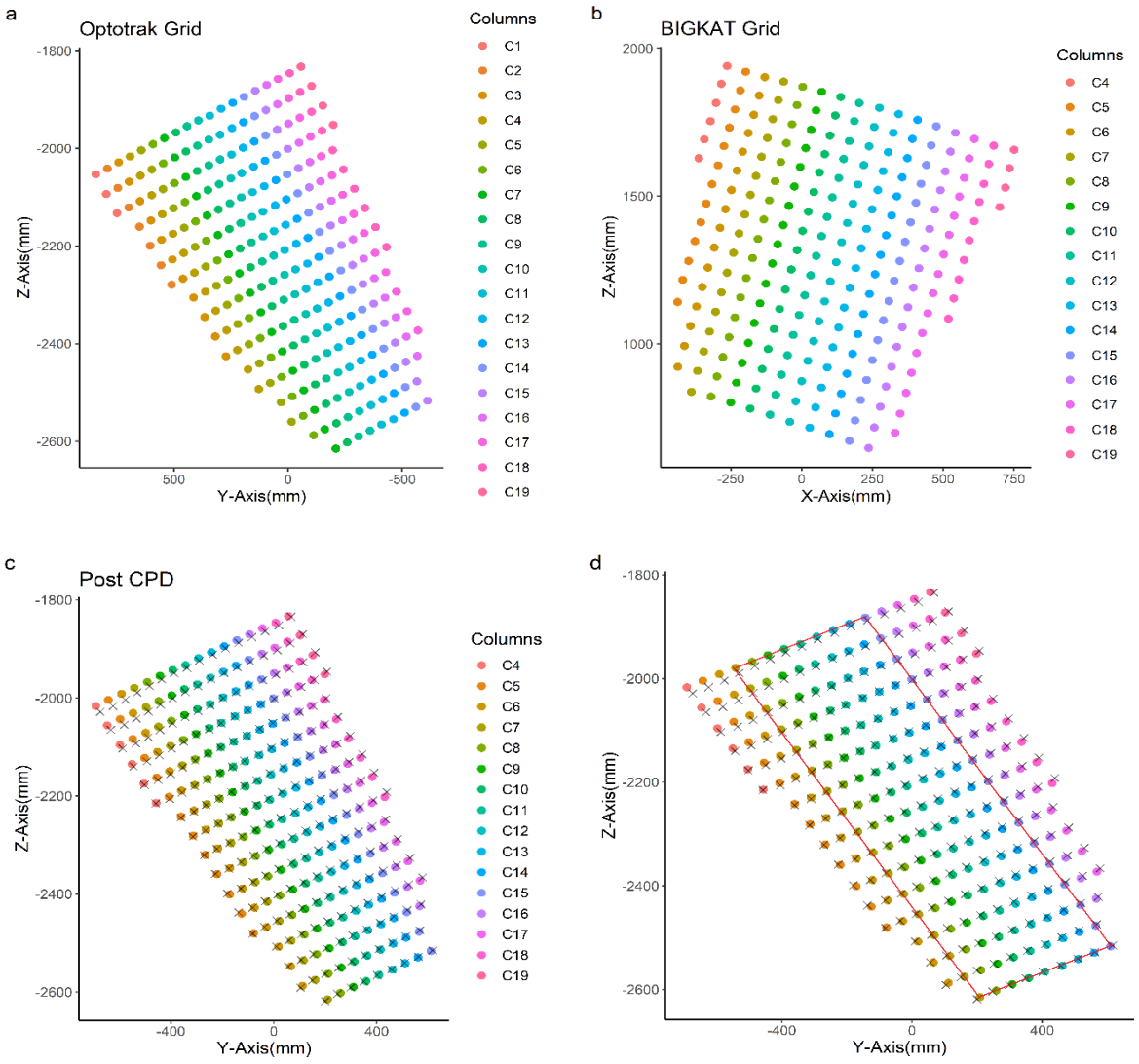

Figure 35a & b shows reconstructed grids as obtained from Optotrak and BIGKAT respectively c) coherent point drift (CPD) rigid registration of BIGKAT grid onto the Optotrak grid d) selected rectangular grid of 17x9 (rows x columns) from both devices after first CPD. Colour dots represents Optotrak grid point and '+' indicate BIGKAT grid points in figures c & d.

Figure 35d shows a subset of whole visible grid of size $17rows \times 9columns; 1224 \times 648mm^2$ selected after performing first CPD (enclosed within red border). The CPD rigid registration method was then applied repeatedly by removing columns from either side until left with a single column in the middle i.e., $17rows \times 1column; 1224 \times 72mm^2$. Likewise, rows were removed one-by-one and CPD performed for each subset of grid. Figure 36 shows the result from the above stated procedure

and grid of size $7rows \times 9columns$ (with an effective tracking area of $504 \times 648mm^2$) produced a maximum error up to 10mm and overall mean absolute error (MAE) of less than 5mm.

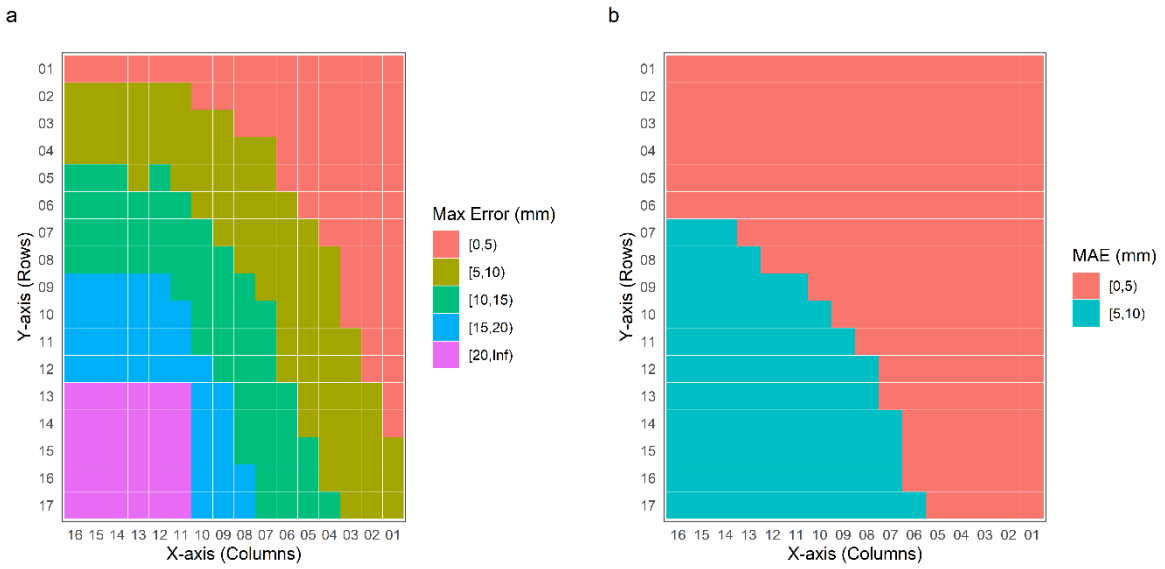

Figure 36:a) Maximum error b) Mean error of all the subsets of the rectangular grid 17x9 obtained from observed grid of size 17x16.

Figure 36 shows maximum error and MAE as a combination of rows and columns where each tile represents a grid size within BIGKAT's workspace, and it depicts how the error changes as the grid size changes i.e., if IRED is placed at the edges or in the middle of the workspace. It can be seen that if IRED is moved across the whole of workspace $(1224 \times 1152mm^2)$ then MAE error would lie in between 5 to 10 mm and maximum error of more than 20mm can be observed. On the other hand if movement is performed in the middle of the workspace covering an area of $504 \times 648mm^2$ to $72 \times 72mm^2$ would produce MAE between 0 to 5mm and maximum error ranging from 5 to 10mm. Figure 36 shows the error as a combination of rows and columns. It is also worth seeing how much error each row and column contribute towards overall error and how the error is distributed by looking at the error histogram.

Figure 37 shows the absolute error that each row and column have contributed, and it is higher at extremities than the rows and columns in the central workspace suggesting large effects of camera distortion at the edges whereas the central workspace shows less distortional affects. It suggests that movement should be performed within the central workspace, and it still needs to be determined how large the workspace should be and error distribution at different subsets of the visible workspace. Figure 38 shows density histogram of various grid sizes where MAE (shown by a blue dotted line) decreases with grid size and the density curve (shown by red line) follows a normal distribution with smaller standard deviation. Figure 38c&d whereas a large grid size produces a left-skewed and flatter curve Figure 38a&7b.

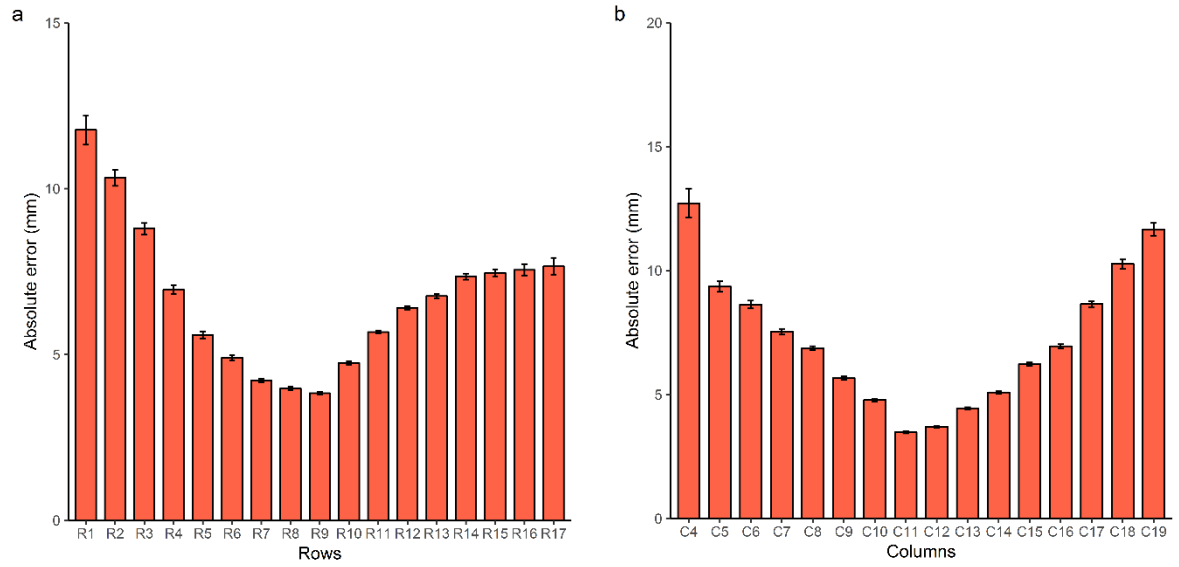

Figure 37 a) Row-wise &b) column-wise error contribution towards overall error

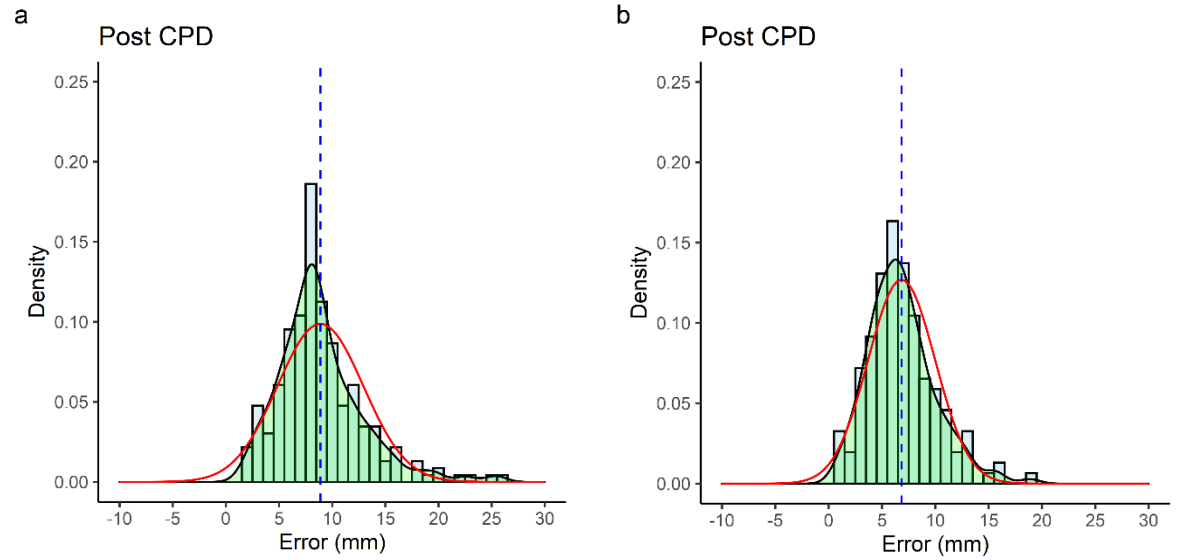

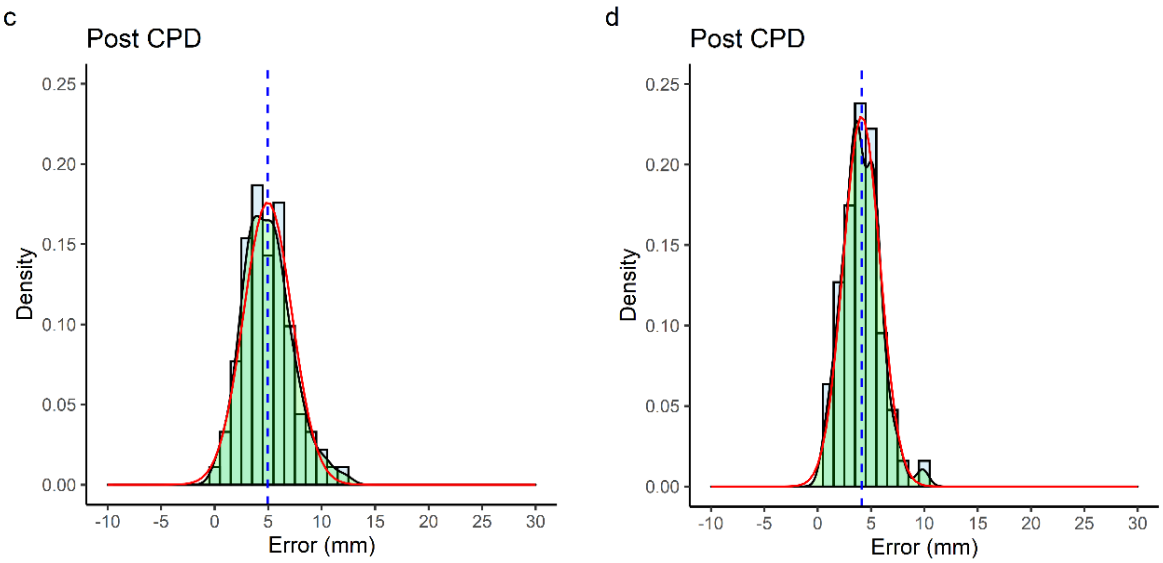

Figure 38: Density histogram of grid size a) 17x16 b) 17x9 c) 13x7 & d) 7x9 showing mean error (dotted line) reducing with size and shaded area (green) shows error density curve follows normal distribution (red line)

3.4.4 Precision

Sample-to-sample jitter (precision) was calculated by measuring the size of jumps that are made from frame-to-frame and for the whole duration of data collection (6s). This was measured by means of the root mean square (RMS) of the change in position values reported by BIGKAT and Optotrak, and is given by

$$RMS_m = \sqrt{\frac{1}{n}\sum_{i=1}^{n-1} \Delta x_i^2}$$

Where Δx_i is the difference between samples i and $i+1$ of the measured position x. Table 5 reports median sample-to-sample jitter calculated by measuring RMS level along each axis and for all grid points visible in BIGKAT's FOV. Lower RMS values indicate lower jitter artefacts and artefacts becomes more visible with large RMS values [232], [233]

Table 5: Median sample-to-sample jitter obtained from the raw data. Lower numbers indicate better resolution. All values are in mm.

Precision (Median Sample-to-sample jitter in mm)

Device	**x**	**y**	**z**
BIGKAT	9.752e-04	5.945e-04	6.559e-03
Optotrak	2.050e-5	3.069e-5	3.280e-5

Figure 39a & 21b shows a heatmap of measured sample-to-sample jitter along the x and z axes, respectively, for the whole observed grid, where each tile represents a grid size. It can be seen from the Figure 39a that the x axis shows reduced jitter artefacts (higher resolution) than along the z-axis

Figure 39b where depth values at the far end of workspace shows higher RMS level with some jitter artefacts in the middle.

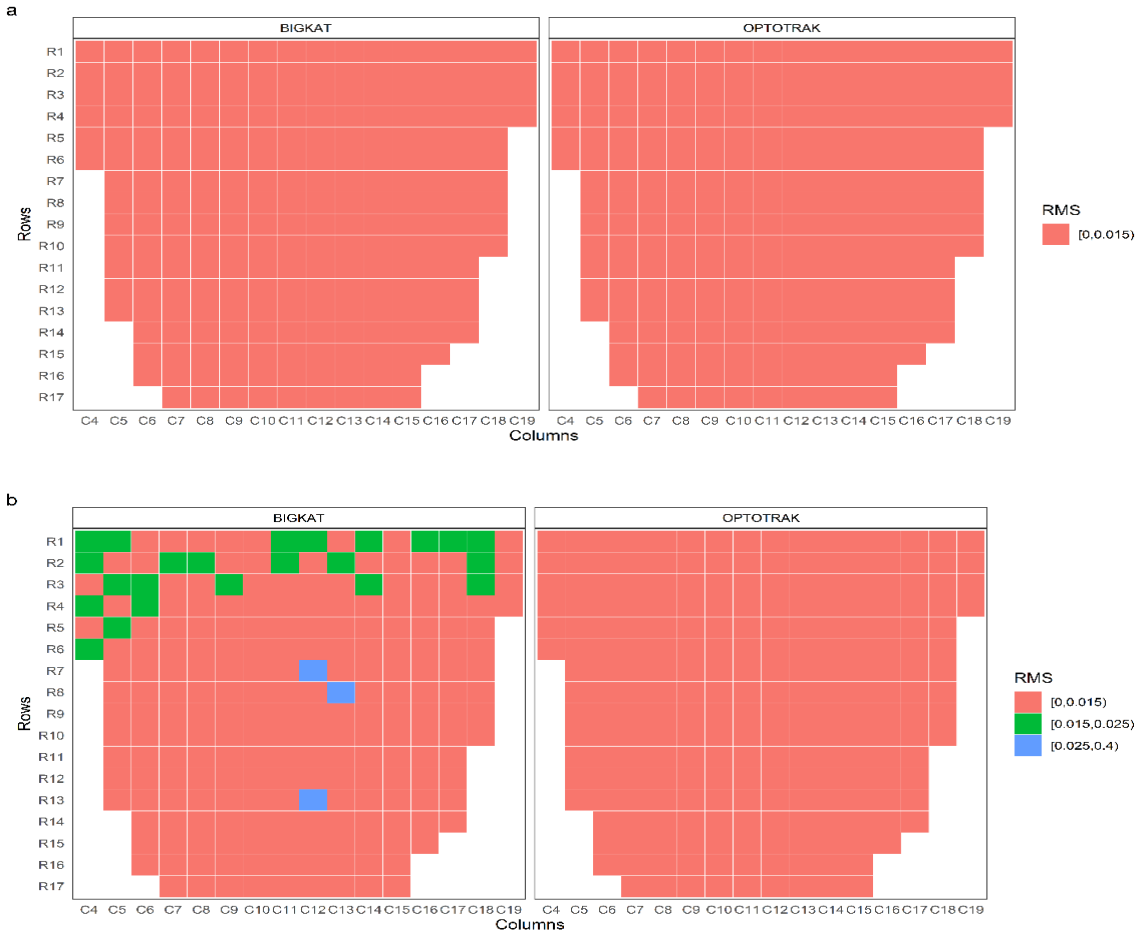

Figure 39: Root mean square level showing jitter effects at each grid point and along a) X-axis b) Z-axis

3.4.5 Vertical Resolution

Likewise for vertical resolution, IRED positional data was analysed for horizontal resolution by running CPD twice: first to select rectangular grid and then to characterize each subset of the rectangular grid. Three different observed grids at three different distances (700, 1400, & 2100mm) from BIGKAT were translated and rotated onto the corresponding Optotrak grid as shown in Figure 40, and then maximum error and MAE were calculated for each subset of the rectangular grid as shown in Figure 41. Observed grid size increases with increasing distance between grid and BIGKAT such as observed grid size increases from 6×12 at 700mm (Figure 40a) to 11×15 at 1400mm (Figure 40c) and then, to 16×17 at 2100mm (Figure 40e) and so as the selected rectangular grid size enclosed in red line shown in the corresponding Figure 41. These results suggest that with increasing distance, the effect of optical distortion on the resolved IRED position become more evident around the edges of the workspace than around the central workspace. Hence, resulting in reduced effective workplace for experimentation with BIGKAT at near and far ends (700mm and 2100mm). Observed grid size when

placed at 1400mm from BIGKAT produce large enough workspace to conduct reach-to-grasp movements.

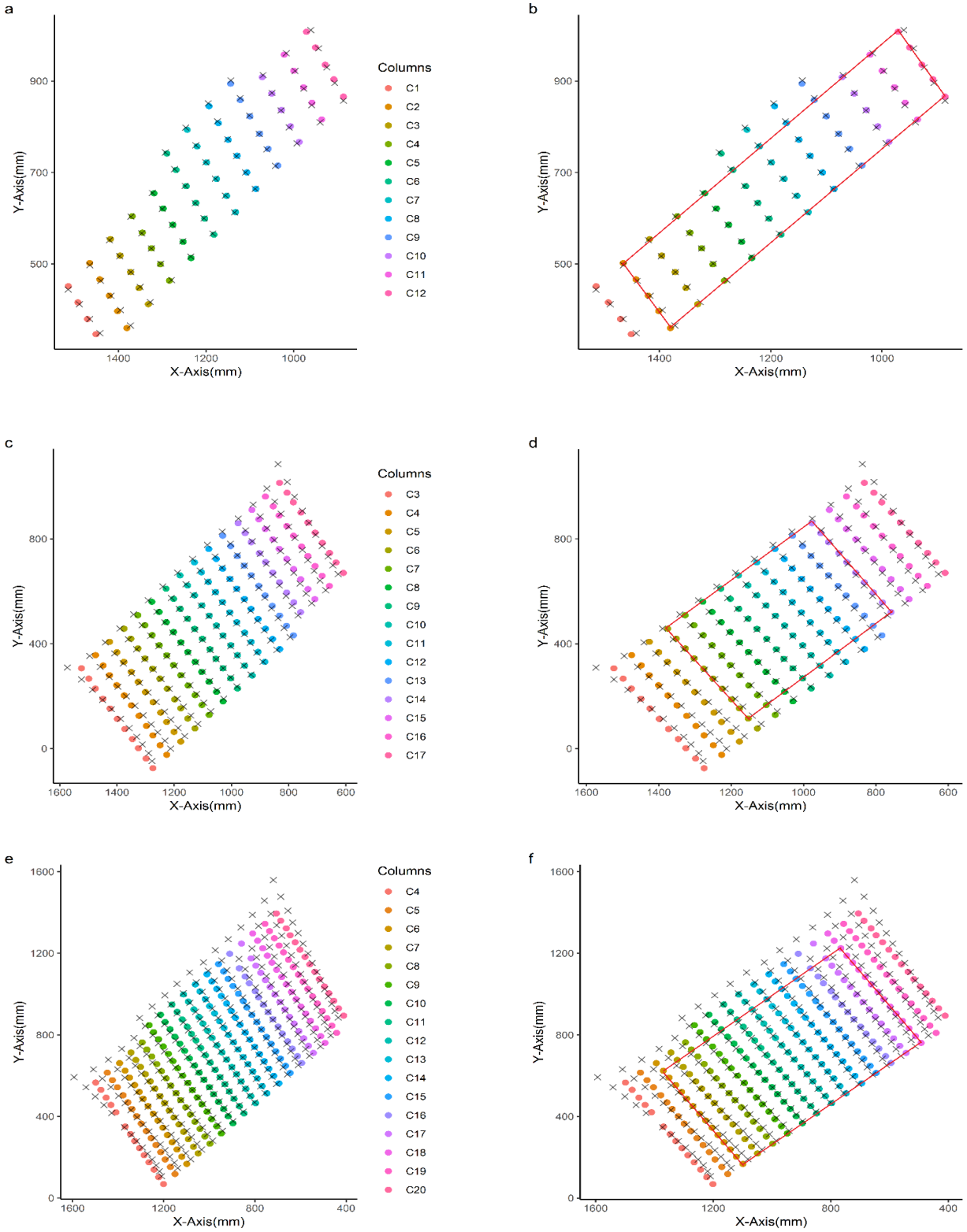

Figure 40: a,c & d shows BIGKAT grid rigidly registered onto the Optotrak grid obtained at three different distance from BIGKAT, where b, d & e shows the selected rectangular grid of size 5x11, 10x9 and 13x14 bounded by red line

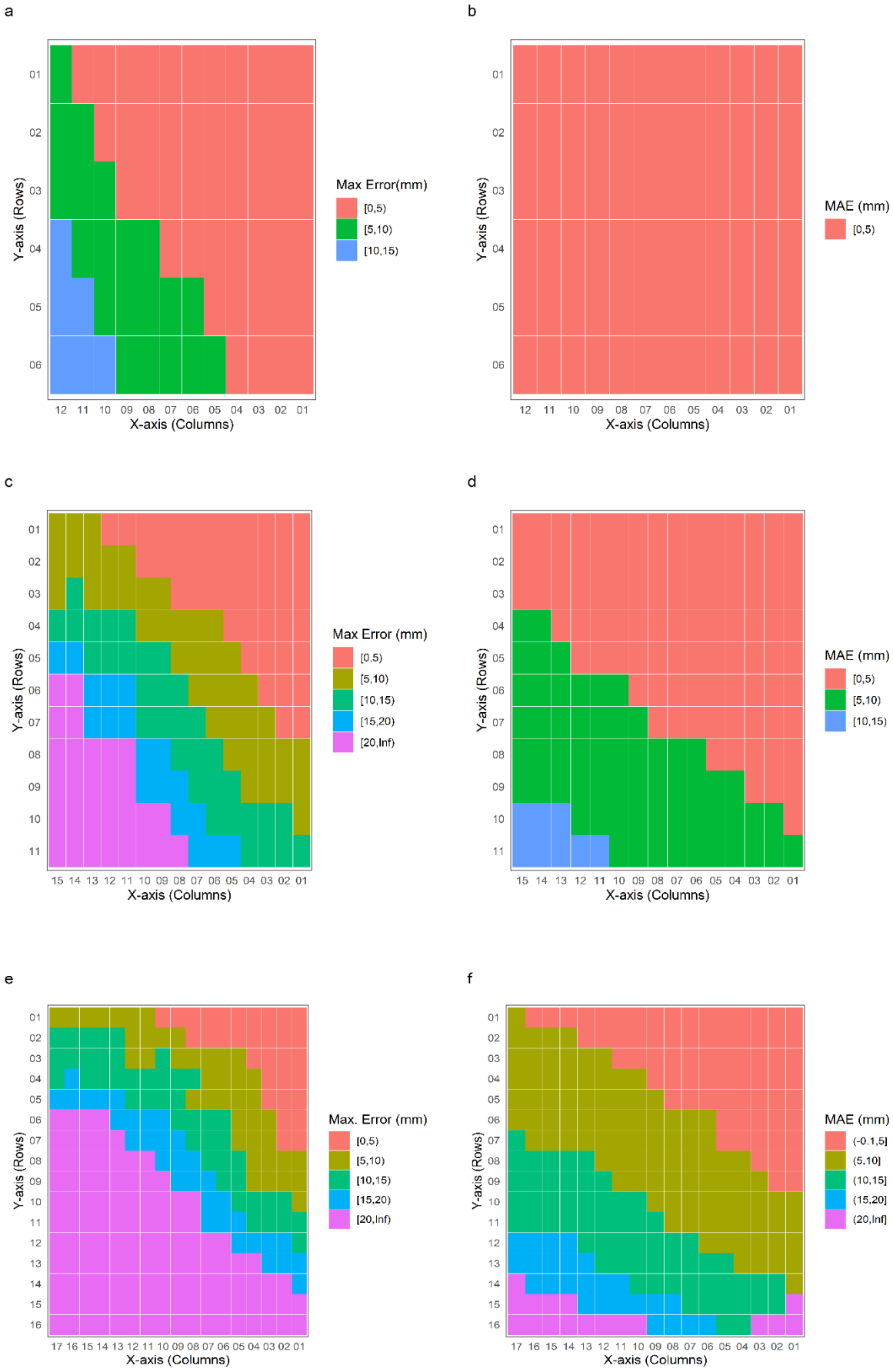

Figure 41: Maximum and mean error for observed grid and its subsets at 700mm (a, b), 1400mm (c, d) & 2100mm (e,f)

Figure 41 shows the maximum error and MAE as a combination of rows and columns where each tile represents a grid size and are colour shaded according to the amount of error present in each grid. So, to better understand the required optimal distance, density histograms (Figure 42) show that the mean error (blue dotted line) increases with increasing distance and produce flatter and left-skewed density curve (Figure 42a, 24c & 24e). Likewise decreasing grid size at the same distance (Figure 42b, 24d & 24f) reduces overall mean error and produces a narrow density curve which also follows a normal distribution (red line). Therefore, it seems that for effective utilization of BIGKAT's workspace (Figure 42b & 24d), the experimental setup should be installed at 700 to 1400 millimetres from BIGKAT, such that, at 1400mm IRED movement made within 504X576mm (see Figure 41d, grid size $7 \times 8; 504 \times 576mm^2$) in the YX-direction from the centre produces a maximum error of 11.37mm, but fortunately, the bimodal shape of density histogram (Figure 42d) shows the largest peak on the left of the mean error (< 5mm).

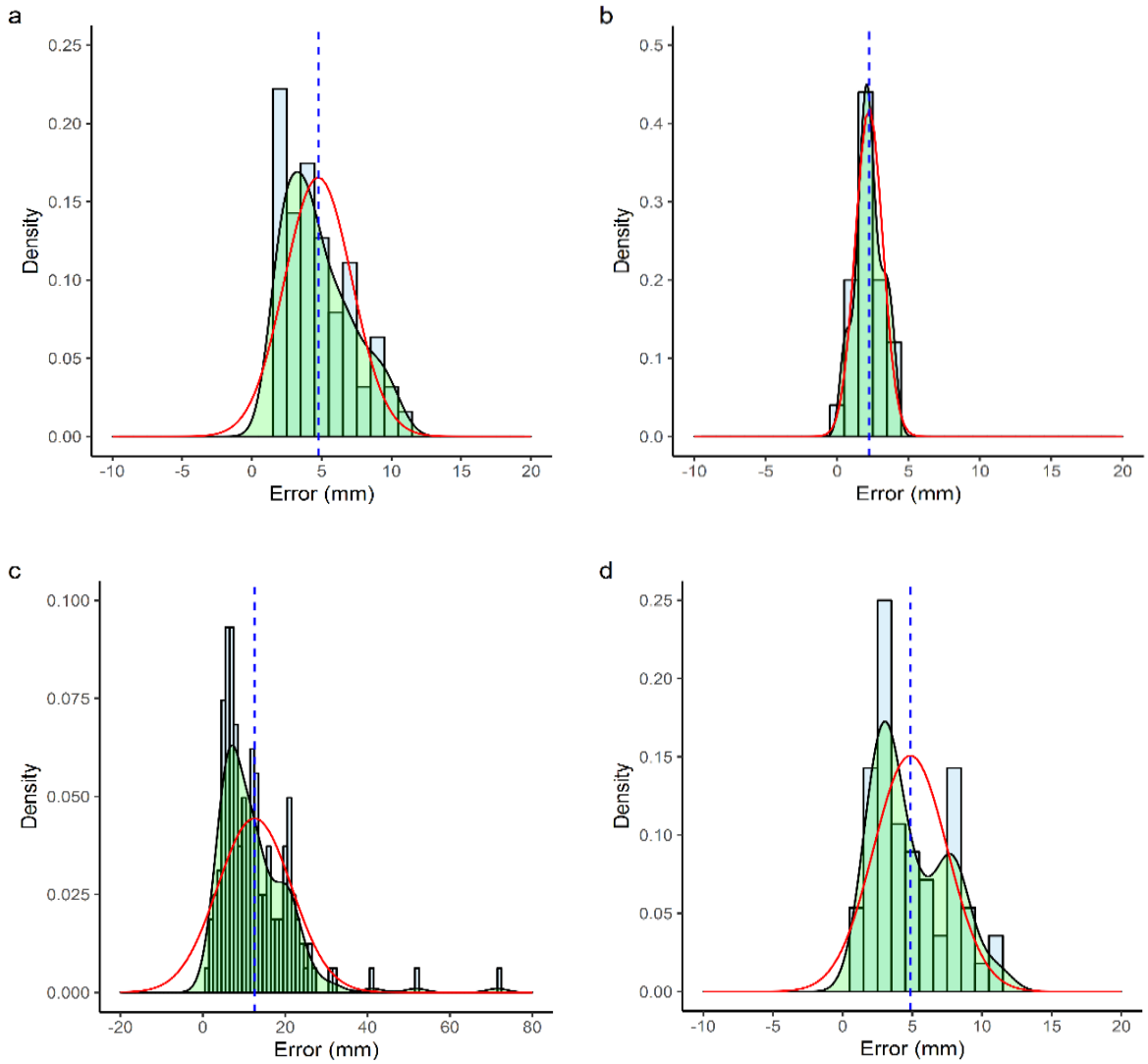

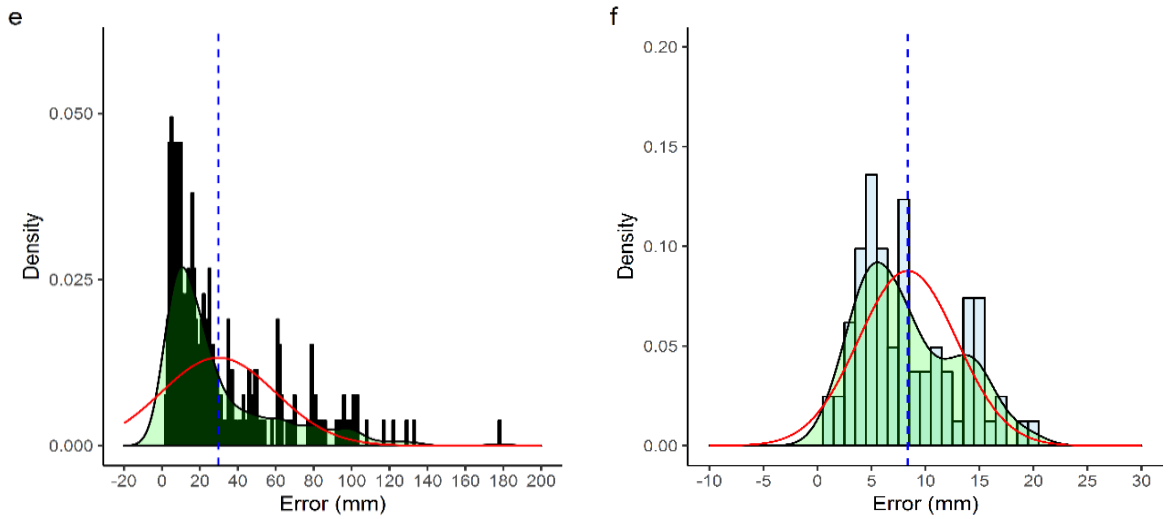

Figure 42: Density Histogram of grid size a) 6x12 b) 5x5 at 700mm, c) 11x15 d) 7x8 at 1400mm & e) 16x17 f) 9x9 at 2100mm.

Figure 43 shows the error contributed by each row and column and clearly shows large error exist at the extremities of the workspace same as in horizontal resolution but Figure 43e shows that at 2100mm the bottom rows (R6 to R13) contributes less than the top rows i.e., working in the lower half of the workspace should be preferred.

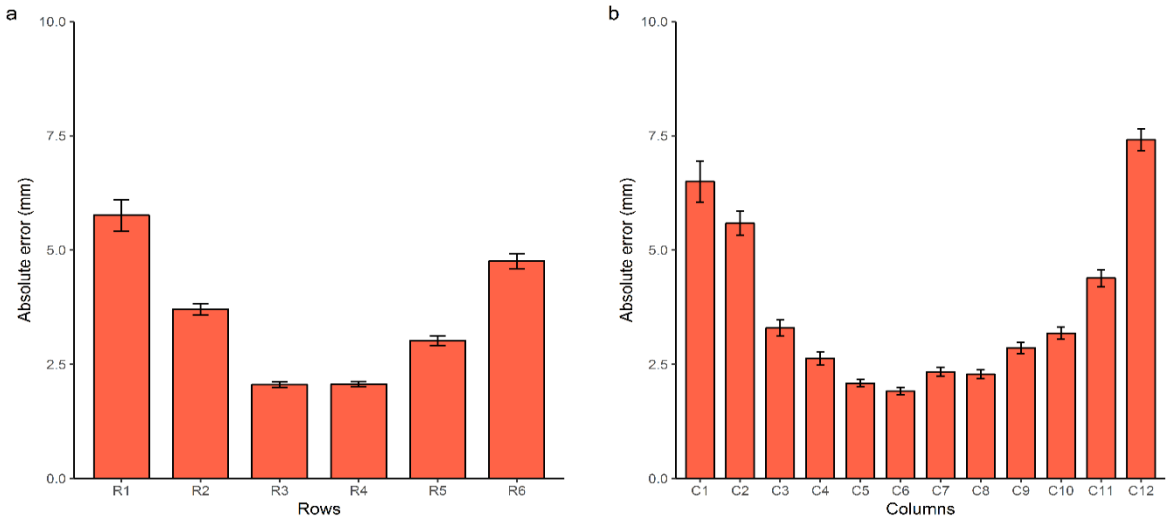

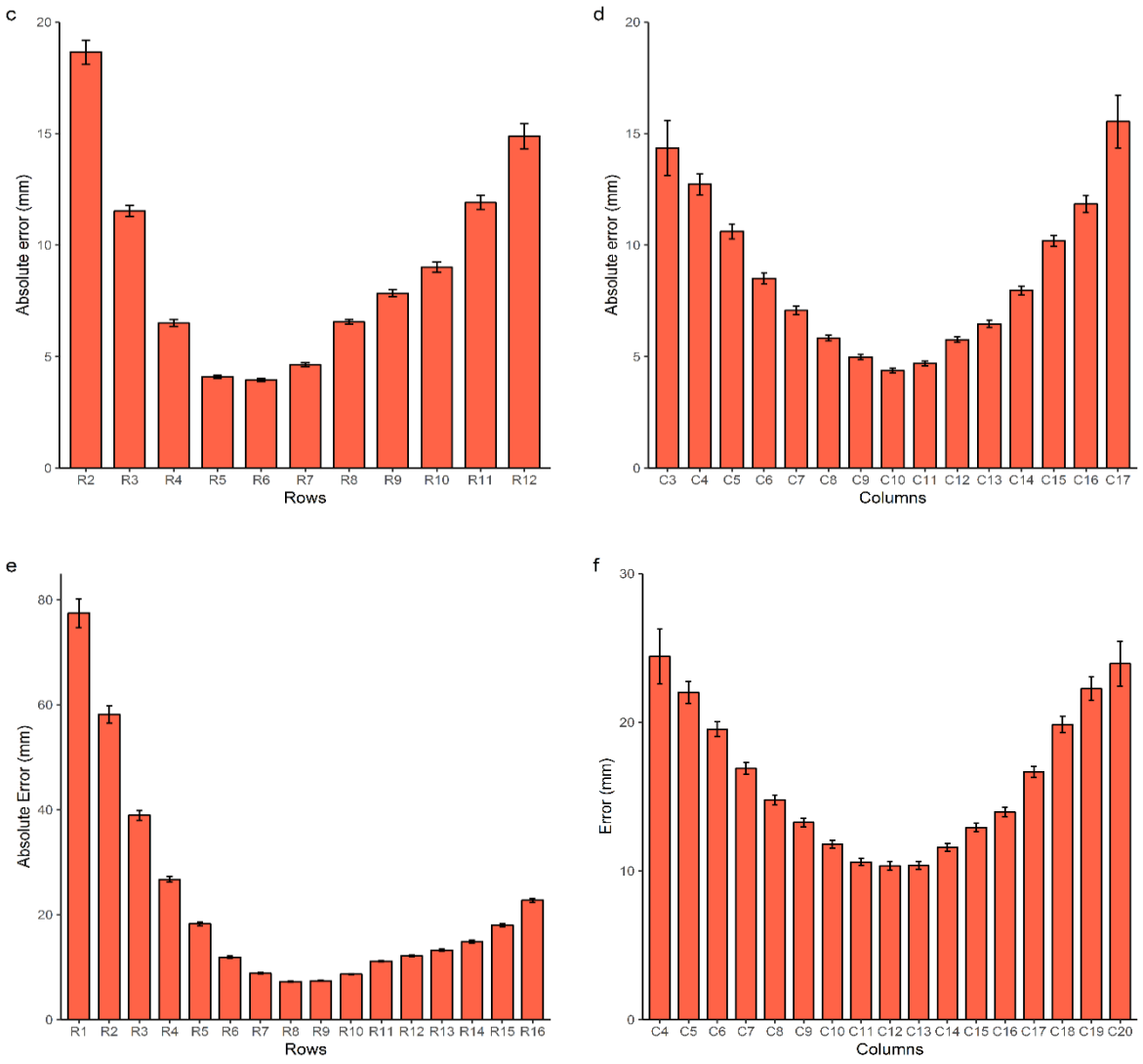

Figure 43: : (a,b),(c,d) & (e,f) shows row-wise & column-wise error contribution when grid was at 700, 1400, 2100mm from BIGKAT, respectively

Table 6 reports the median RMS values obtained with the same procedure as in horizontal resolution. Overall, it's evident from the Table 6 that Optotrak (gold standard) shows better resolution at each distance than BIGKAT, whereas BIGKAT also shows lower jitter artefacts than Optotrak at 700 & 1400mm but jitter artefacts become obvious at 2100mm, particularly in determining IRED depth (z-axis). RMS heatmaps at each distance and along each axis are shown in Appendix-A and reconstructed grids are shown in Appendix-B.

Table 6: Median sample-to-sample jitter. All values are in mm.

	BIGKAT			***Optotrak***		
Distance (mm)	**X**	**Y**	**Z**	**X**	**Y**	**Z**
700	5.444e-04	8.258e-04	2.213e-03	3.569e-04	1.596e-04	5.580e-04
1400	8.759e-04	7.009e-04	7.919e-03	3.234e-04	1.366e-04	7.016e-04
2100	2.927e-03	1.141e-03	2.915e-02	1.906e-04	1.034e-04	3.579e-04

3.5 Experiment 2: Temporal Resolution

Other than the spatial resolution it is also useful to measure temporal resolution as it determines the fastest change that we can track. As BIGKAT's main purpose is to measure and analyse reach-to-grasp movements (which involves gross and fine motor skills) it was tested by tracking two IREDs attached to a pendulum and determining how accurately BIGKAT can resolve the rate of change of IRED position.

3.5.1 Method

A pendulum of length 400mm with two IREDs, facing towards BIGKAT & Optotrak cameras, separated by 31mm were attached on either side of the pendulum ball. Using two IREDs helped to keep the pendulum balanced. Five trials were recorded at different locations of the workspace for 15s at 60Hz, and both devices simultaneously started recording when the pendulum was released from an initial angular displacement of 20°.

3.5.2 Results & Discussion

Figure 44 shows the decaying behaviour of the pendulum over time along the X-axis as tracked by both BIGKAT and Optotrak simultaneously. Mid-point of both IREDs was calculated and plotted for all trials as shown in Figure 44 and decaying behaviour was calculated by computing the change in IRED position between two subsequent frames, whereas difference in the time stamps of subsequent frames was measured to determine the frame rate (interval rate). Frame rate was then averaged to measure temporal resolution for the whole trial and all trials as well and produce a time difference of almost 16ms between two consecutive frames for both devices. The time-period and distance between IREDs was extracted from the temporal and 3D positional data resolved by BIGKAT & Optotrak and then was averaged over all trials as reported in Table 7 and shown in Figure 45. Equation 1 shows actual time period of a pendulum of length 400mm.

$$T = 2\pi\sqrt{l/g} = 2\pi\sqrt{0.4/9.81} = 1.269s \qquad 1$$

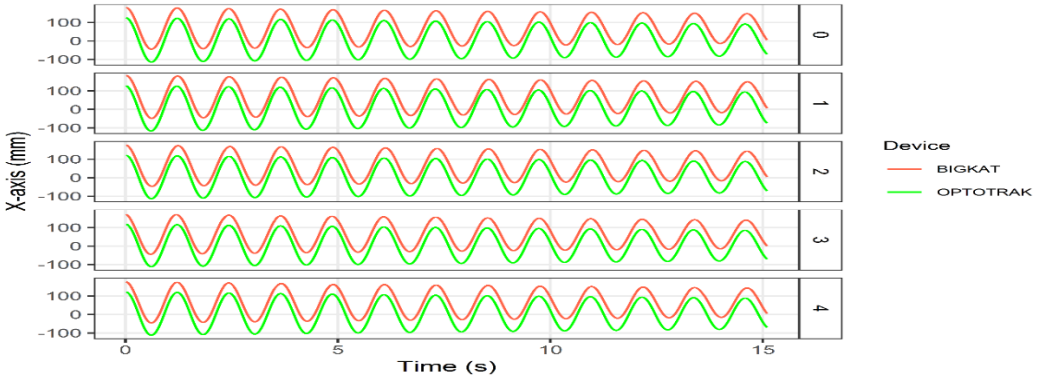

Figure 44: Pendulum oscillations shown for 5 trials of 15 seconds duration

Table 7: Time period and distance between IREDS calculated from BIGKAT and Optotrak's raw data for the 5 trials

		Trial 1	***Trial 2***	***Trial 3***	***Trial 4***	***Trial 5***
Time Period (s)	***BIGKAT***	1.214	1.274	1.219	1.219	1.219
	Optotrak	1.214	1.214	1.215	1.214	1.215
Distance b/w IREDs (mm)	***BIGKAT***	31.747	31.367	31.414	31.498	31.588
	Optotrak	30.428	30.451	30.390	30.404	30.445

As well as time-period, the distance between IREDs was also calculated and averaged across all trials to determine the absolute positional error by comparing with known input distance as shown in Figure 45. Such absolute measures obtained from the resolved IRED position in 3D space allows direct comparison of BIGKAT's performance against gold standard Optotrak. Results shown in Figure 45 suggests that both absolute measures (time-period and distance between markers) obtained by both devices output comparable measures and no significant variations were observed in BIGKAT temporal and spatial data. For the purpose of measuring detailed human motion, such as finger motion, Song et. al. measured the frame rate required for an optical motion capture system and found out that minimum frame rate is proportional to the ratio between the maximum speed of the motion and the minimum spacing between the markers [222]. They have shown that a frame rate of 20Hz is sufficient for tracking a marker moving at a speed of 1440mm/s and literature also shows that healthy subjects move with maximum wrist velocity ranging from 1200mm/s to 1600mm/s while reaching for grasping an object placed at the farthest distance of 400mm [234]–[237]. Hence, video recording of reach-to-grasp movement at 60Hz by BIGKAT might reveal significant differences, for this purpose chapter 4 investigates the use of BIGKAT for studying the effect of task constraints on reach-to-grasp movements.

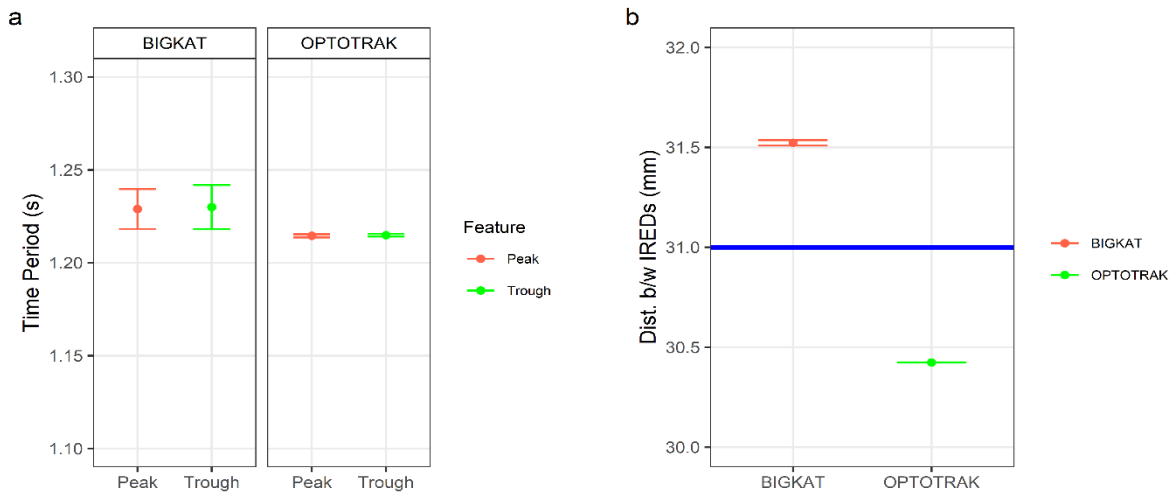

Figure 45: a) Mean Time period b) mean distance between IREDs across all trials as computed from BIGKAT and Optotrak's 3D positional data

3.6 Discussion

This Chapter investigated spatial accuracy and precision by tracking IRED position placed on a grid (printed on A0 paper) presented horizontally and vertically, within the overlapping FOV of BIGKAT and Optotrak 3020. Both devices recorded IRED position iteratively and simultaneously by moving IRED to every other grid corner point (spaced by 72mm) for 6s. Optotrak acted as a gold-standard to determine the absolute positional error between 3D position obtained from BIGKAT and Optotrak. With this approach, several subsets of tracking area, MAE less than 5mm, was found in the horizontal plane ranging from as large as $720 \times 648\ mm^2$ to $72 \times 72\ mm^2$ (centered around the middle FOV), which a user can select according to the experimental setup.

Also, to determine the range in which BIGKAT can accurately resolve IRED position, vertical resolution was determined at three different distance (700, 1400 & 2100mm) from BIGKAT which produced tracking area (MAE < 5mm) of $432 \times 864\ mm^2$ at $700\ mm$; $504 \times 576\ mm^2$ at $1400\ mm$, $360 \times 576\ mm^2$ at $2100\ mm$. These results suggests that tracking area significantly reduced as the distance from the BIGKAT increases and the movements should be carried out in the center of FOV within a distance of 700mm to 1400mm from BIGKAT. For example, BIGKAT at a distance of 1400mm can determine IRED position within the tracking area of $576 \times 504 mm^2$in vertical plane (XY) as shown in Figure 46and tracking area of $720 \times 648 mm^2$ in horizontal plane (XZ) as shown in Figure 36, with mean absolute error less than 5mm and median root mean square values less than 0.001mm and at temporal resolution of 16ms. Such a workspace is sufficient to carry out prehension studies because object intrinsic and extrinsic properties (object distance, object width and object height) determine needed workspace, in a sense that movements made in vertical direction (along y-axis) during transport component depends on object height; object width controlling grip apertures (along x-axis)

is always less than the maximum hand opening, similarly, movement amplitude manipulating transport component must be within participant's arm reach, and along the sagittal plane (z-axis) [234], [238], [239]. Considering object properties and the nature of experiment such as reach-to-grasp movement a tracking area of $576 \times 504mm^2$ in vertical plane (XY) meets standard requirements of prehension studies as presented in literature where object width is always less than the maximum hand opening of 45mm, and object height is smaller than 100mm. Likewise, literature shows that reaching distance in sagittal plane is always less than participant's arm length and its average value ranges from 600mm to 800mm for adults. In accordance with these requirements BIGKAT placed at a distance of 1400mm can accurately and precisely unfold movement details.

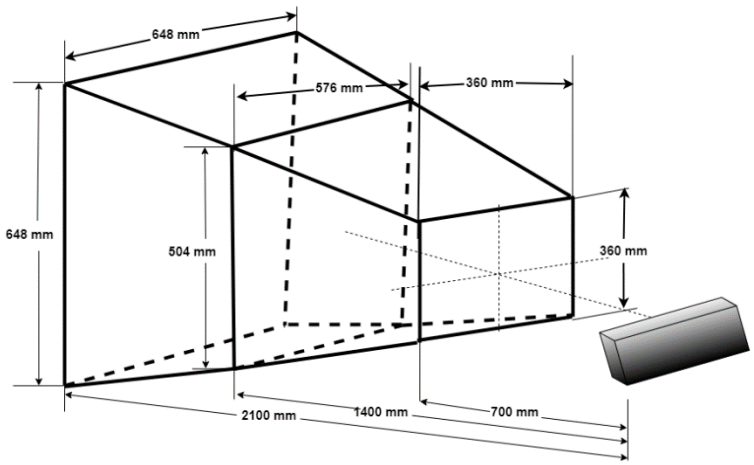

Figure 46: BIGKAT's field of view

The next chapter evaluates the use of BIGKAT as a tool to capture and analyse reach-to-grasp movements made by healthy adults to investigate its performance against Optotrak. As discussed earlier reach-to-grasp movements are affected by object size and location, so, finding the subtle differences between coordinated and controlled reach and grasp components by co-varying object size and location can strongly enhance our belief in low-cost, portable, easy-to-use optical motion capture system. Thus, encouraging its usability as an assessment tool in clinical routine.

Chapter 4: Performance Comparison of BIGKAT with an Optoelectronic Motion Capture System for Kinematic Analysis of Healthy Human Prehensile Movements.

4.1 Introduction

Having established the size of the workspace and temporal resolution afforded by BIGKAT, this chapter sets out to determine whether BIGKAT could be used within this workspace (XZ-plane $720 \times 648\ mm^2$; XY-plane $576 \times 504\ mm^2$, MAE error < 5mm) to measure reach-to-grasp movements when performed within a distance of 800mm to 1400mm from BIGKAT. Figure 47 shows the schematic of the adapted experimental procedure where participants sit in front of BIGKAT and the experiment involves reaching and grasping objects placed at three different distances from the start position, all within the sagittal plane. The two objects of different sizes are placed at distances of 250mm, 350mm, and 450mm from the start position and were covaried for different trials. From BIGKAT's perspective, the starting point is 1250mm away from BIGKAT and the farthest object (450mm) is also 800mm away from BIGKAT. Hence, the participant performs each reach-to-grasp movement within BIGKAT's workspace, which is defined as the area that can produce MAE of less than 5mm.

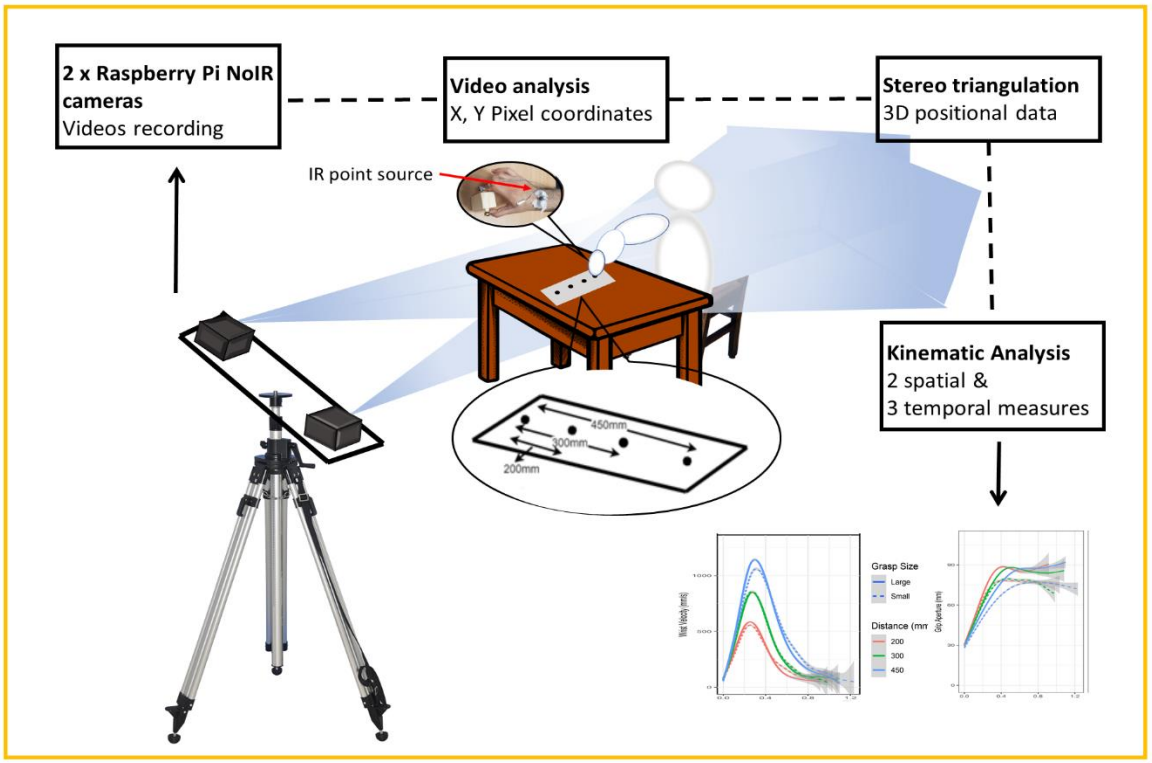

Figure 47: Experimental setup showing subset of workspace in which prehensile movements are performed.

In this study, BIGKAT's suitability as a capable motion capture system for measuring prehensile movements was assessed by quantitatively measuring, analysing, and comparing reach-to-grasp movements recorded by BIGKAT and Optotrak, simultaneously. Spatial and temporal characteristics of prehensile movements vary with respect to the task constraints, and, for the exact same purpose, measurements obtained from Optotrak acted as a 'gold standard' and were compared with measurements computed from BIGKAT. Therefore, the main objective of the study undertaken was to assess BIGKAT's performance by objectively measuring prehensile movements during reaching for and grasping objects in a controlled environment, and statistically analysing the relationship between the same kinematic measures obtained from both BIGKAT and Optotrak. We hypothesized that kinematic measures obtained from both devices would be linearly correlated to each other i.e., if Optotrak can determine statistically significant differences between kinematic measures due to task constraints then BIGKAT could do as well. To capture the coordinated structure of prehension movements, only healthy subjects were chosen since they can reproduce movements effectively, enabling us to test the repeatability and reproducibility of BIGKAT by analyzing prehensile kinematic measures between and within participants as well as correlating spatiotemporal characteristics with those measures obtained from Optotrak.

4.2 Method

Reach-to-grasp movement patterns are stereotypical in nature and change lawfully with task constraints and this chapter seeks to determine whether BIGKAT would show the same pattern and would provide the similar statistically significant results as gold standard Optotrak. To draw the performance comparison between the two devices, participants were instructed to reach for and grasp two different size objects placed at three different distances from the participant such that the farthest object would force participant to increase reach velocity and would take longer to reach and grasp than the nearest object.

4.2.1 Participants.

Nine unpaid participants aged 20-35 (mean = 26, All males) were recruited for the study. All participants were right-handed, gave their informed consent prior to participating and were naive as to the purpose of the experiment. None had any history of neurological deficit, and all had normal or corrected to normal vision. The study was approved by the ethics committee in the School of Psychology at the University of Leeds and was therefore performed in accordance with the ethical standards laid down in the Declaration of Helsinki.

4.2.2 Materials and procedure.

Each trial was prepared by placing a wooden object at one of the three distances and the participant prepared by holding the start position between the thumb and index finger which was defined by a moulded grip and was close to the table edge as shown in Figure 48. Participants were instructed to reach for and grasp an object that could be located at a distance of 200, 300 or 450mm from the hand position in the sagittal plane and can be reach with the simple extension of their right arm. Two wooden objects of same depth (D), width (W) and height (H) but different grasping surface size (determined by a wooden dowel glued on top of the object) were used as shown in Figure 49. Dowel size was characterized as large or small determined by its height and diameter, such that large dowel has a grasping size of (length= 63mm, diameter= 25mm) and a smaller dowel has a grasping size of (height= 53mm, diameter= 15mm). Participants were told to grip the object by its grasping surface with their thumb and index finger. Each participant performed 10 trials at each distance and object size combination, resulting in a total of 60 trials.

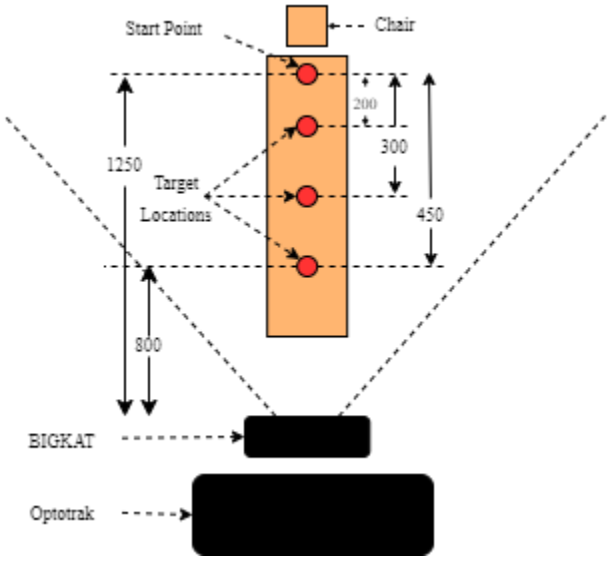

Figure 48: BIGKAT and Optotrak recording IRED movement, simultaneously, while participant sits on a chair and perform reaching movements to grasp objects, placed at three different target locations, in the sagittal plane with the simple extension of the arm. All values are in mm.

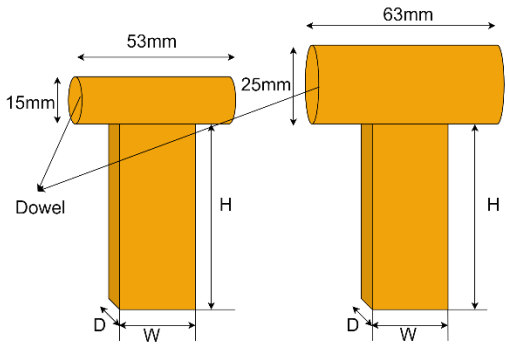

Figure 49: Two wooden objects having base of same dimension but differ by dowel size affixed on top of the base.

Data acquisition was completed by both Optotrak and BIGKAT and was initiated one second before the "go" in the experimenter's verbal start command "three, two, one, go" and the participant's task was to reach and grasp the object at the "go" signal. Reach responses were recorded by attaching an infra-red emitting diode (IRED) to each participant's wrist and measuring its positional change over time, similarly, grasping responses were recorded by attaching infra-red emitting diodes to the distal joint of the index finger and thumb and measuring the distance between them. Both Optotrak and BIGKAT recorded movements at 60Hz for 5 seconds. An R package was designed to extract and filter (2^{nd} order Butterworth, $f_c = 16Hz$) 3D positional data of each IRED and other relevant information like frame rate, data and time, user and system comments etc. from the binary files recorded by Optotrak (available on GitHub); '*read_ndi.R*' is the main script used to extract such information [240].

4.2.3 Data Analysis

A 2x3 repeated measures analysis of variance with factors grasp surface size (small, large) and object distance (200, 300 and 450mm) was used to evaluate the differences between BIGKAT and Optotrak for all calculated kinematics. Five dependent variables Movement time (MT), Maximum Grip Aperture (MGA), time to MGA (TMGA), Peak Velocity (PV) and time to PV (TPV) were extracted from the filtered 3D positional data from both devices. To determine the correlation between BIGKAT and Optotrak, linear regression analysis was also carried out between corresponding measures. All data analysis procedures were carried out in R.

Movement time is defined as the temporal difference between movement onset, which was set at the point when the wrist speed exceeds 50mm/s, and movement offset when wrist speed decreases below 50mm/s which determines the end of the trial. The distance between the thumb and index finger provides temporal changes in IRED position, in anticipation of the intended grasp size and are dependent on the shape of the object, thus maximum distance between the thumb and finger provides the maximum grip aperture (MGA) and its time of occurrence (TMGA). Similarly, hand transportation (trajectory of the hand) speed is influenced by the distance between the start point

and the object and is determined by tangential speed of the IRED attached to the wrist thus providing peak velocity (PV) and its time of occurrence (TPV).

4.3 Results

Figure 50 shows the trajectory profile of each IRED for the whole duration of each reach-to-grasp movement as captured by BIGKAT and Optotrak. The trajectory profile was averaged across all participants while reaching for objects places at three different distances and grasping objects of different grasp size. The movement trajectory obtained from BIGKAT follows the trajectory obtained from Optotrak, but it still needs investigating how well spatiotemporal characteristics correlates for both devices. For this purpose, two-way analysis of variance was carried out for each spatiotemporal measure to determine how well BIGKAT can extract important kinematic features (presented in detail in next section). It is evident from the Figure 50 that movement duration increases by increasing the distance between the object and start point, hence, participants move faster for the farthest object by increasing the wrist velocity thus causing TPV to occur later in the movement as shown in reaching movement profile (Figure 51a). Similarly, grip profile varies with grasp size such as smaller grabbing size requires greater precision during the gripping phase, while larger grasping size lowers spatial accuracy demands while allowing for a faster movement and wider MGA as shown in Figure 51b.

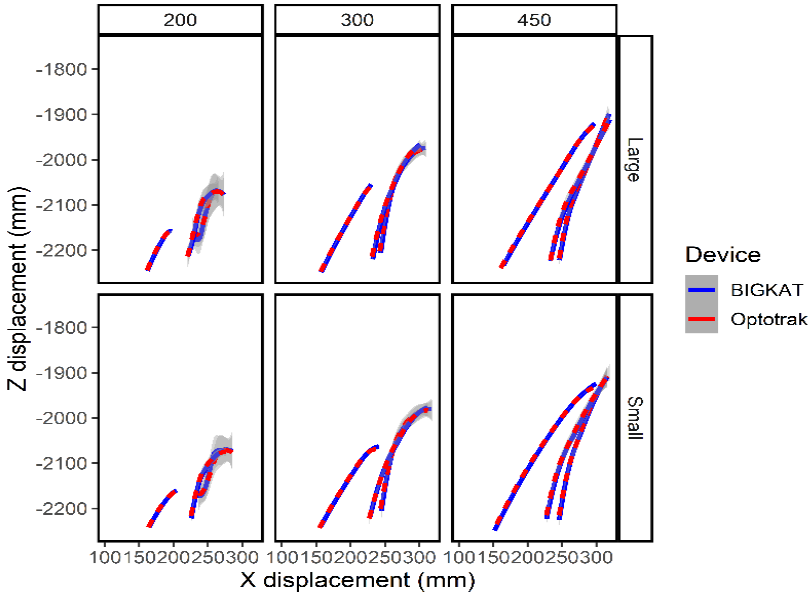

Figure 50: Movement trajectory averaged across all trials and particpants for objects of different grasp sizes placed at three different distances as captured by BIGKAT and Optotrak.

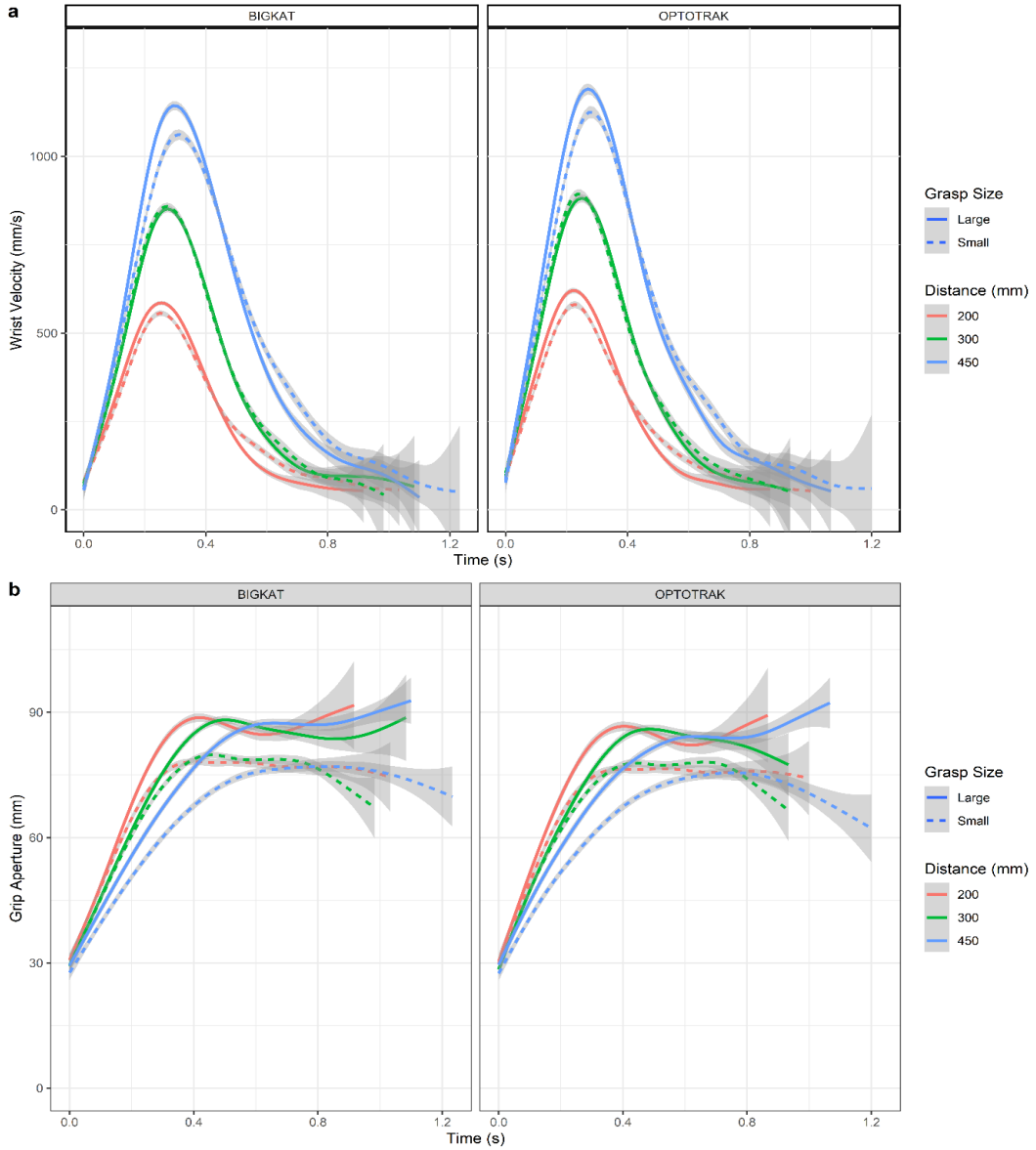

Figure 51: a) Mean wrist velocity b) Mean grip aperture averaged across all trials and factors extracted by BIGKAT and Optotrak

4.3.1 Movement time

Optotrak reported that movement duration increased as object distance increased ($F(2,16) = 45.168, p < 0.0001, \eta_G^2 = 0.276$) such that on average longer MT was obtained for further objects ($450mm$: $0.779 \pm 0.142s$) than for the nearer objects ($200mm$: $0.598 \pm 0.119s$; $300mm$: $0.661 \pm 0.122s$). Similarly, MT obtained from BIGKAT positional data showed a significant main effect of object distance ($F(2,16) = 48.022, p < 0.0001, \eta_G^2 = 0.301$), again with participants taking longer to reach farthest objects (450mm:($0.826 \pm 0.140s$) than those placed at 200mm ($0.639 \pm 0.114s$) and 300mm ($0.703 \pm 0.116s$). Post-hoc analysis (Tukey-HSD) on both the Optotrak and BIGKAT data revealed significant differences between the near and far objects and the middle and far objects, as shown in Figure 52a, but no significant difference was found between distances 200 and 300mm.

ANOVA analysis showed that MT was not significantly affected by grasping surface size: Optotrak $(F(1,8) = 1.348, p > 0.05, \eta_G^2 = 0.012)$ and BIGKAT $(F(1,8) = 1.539, p > 0.05, \eta_G^2 = 0.013)$ as shown in Figure 52b. It can be seen from the Table 8 that MT is slightly, but not significantly, higher for smaller grasping surface size $(small: Optotrak\ 0.693 \pm 0.136s, BIGKAT\ 0.736 \pm 0.132s)$ than large grasping surface size $(Large: Optotrak\ 0.666 \pm 0.120s, BIGKAT\ 0.709 \pm 0.115s)$. No significant interaction was found between distance and grasping size.

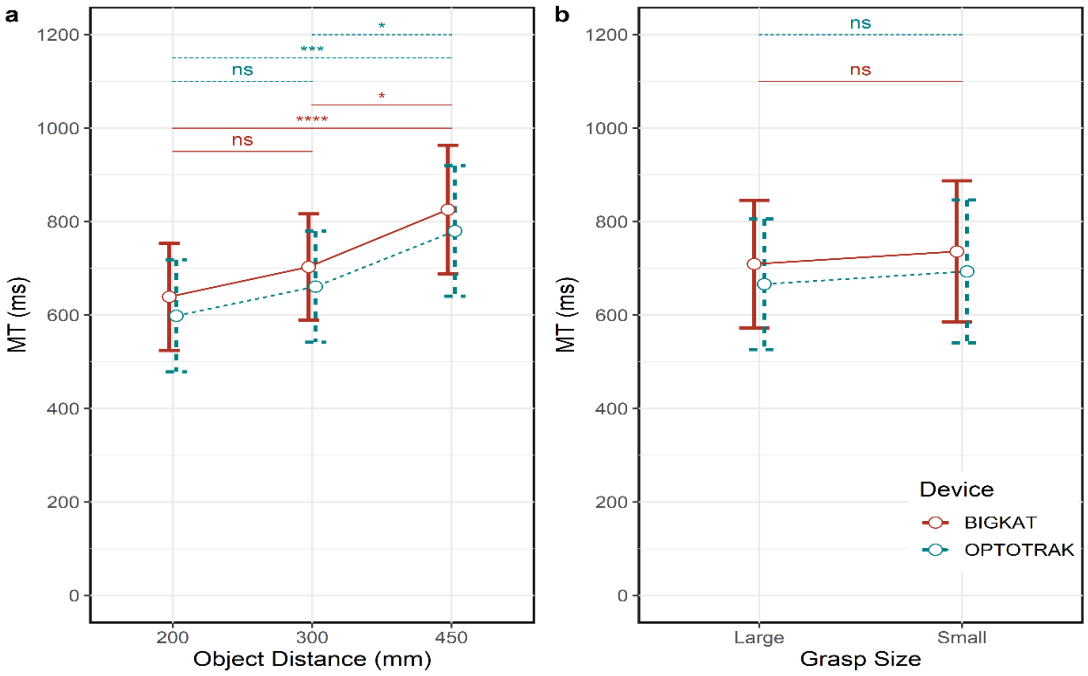

Figure 52: Both devices show similar significant results for MT a) object distance shows significant main effect and b) grasp surface size showing no effect on MT.

4.3.2 MGA and time to MGA

MGA was larger for the object with the larger grasp surfaces $(small: Optotrak\ 85.600 \pm 8.065mm; BIGKAT\ 86.198 \pm 7.681mm), (large: Optotrak\ 94.304 \pm 9.062mm; BIGKAT\ 95.216 \pm 8.713mm)$ as shown in Figure 53b and Table 1, and this significant main effect was captured by both Optotrak $(F(1,8) = 58.181, p < 0.001, \eta_G^2 = 0.220)$ and BIGKAT $(F(1,8) = 67.579, p < 0.001, \eta_G^2 = 0.247)$. Post-hoc analysis revealed large effect size (BIGKAT 1.955; Optotrak 1.872) between two grasp sizes. However, MGA was not significantly affected by object distance as reported by Optotrak $(F(2,16) = 0.765, p > 0.05, \eta_G^2 = 0.009)$ and BIGKAT $(F(2,16) = 0.185, p > 0.05, \eta_G^2 = 0.002)$ as shown in Figure 53a. No significant interaction was found between grasp size and object distance.

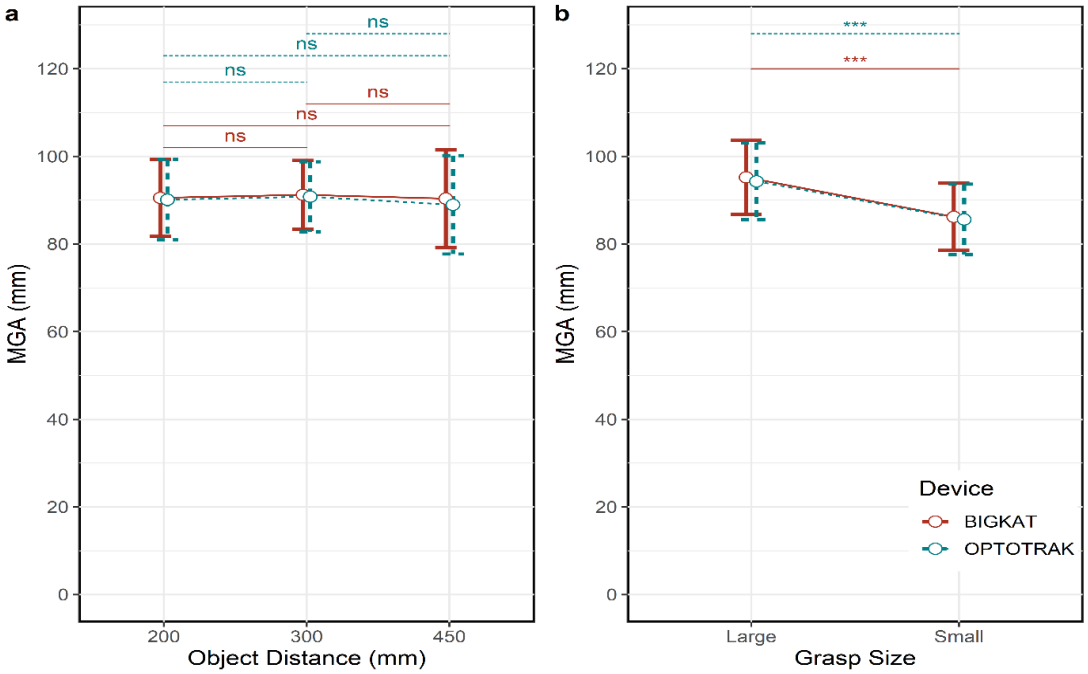

Figure 53: a) shows no significant effect of object distance for MGA b) grasp surface size significantly effected MGA as found by both low-cost and expensive optical motion capture system.

However, TMGA was found to be affected by object distance, causing it to occur later in the movement as distance increased: 450mm $(BIGKAT\ 0.669 \pm 0.149s; OPTOTRAK\ 0.636 \pm 0.147s)$, 300mm $(BIGKAT\ 0.532 \pm 0.120s; OPTOTRAK\ 0.514 \pm 0.124s)$, 200mm $(BIGKAT\ 0.487 \pm 0.134s; OPTOTRAK\ 0.469 \pm 0.134s)$. ANOVA showed significant main effect of object distance for both devices $(BIGKAT\ (F(2,16) = 57.315, p < 0.001, \eta_G^2 = 0.268)$ and $(Optotrak\ F(2,16) = 44.431, p < 0.001, \mu_G^2 = 0.233)$. Post-hoc analysis revealed significant differences between all distances except between 200mm and 300mm (Figure 54a) for both devices. A low sample size might be the reason for the lack of significant difference between the near and middle distances.

Time to MGA remained unaffected by different grasping surface sizes, where $(BIGKAT\ (F(1,8) = 0.008, p > 0.05, \eta_G^2 = 6.5e^{-5})$ and $(OPTOTRAK\ (F(1,8) = 0.067, p = 0.8, \eta_G^2 = 5.6e^{-4})$ showed no significant main effect. In fact, average time to MGA was almost equal for both grasping sizes, as shown in Figure 54b. No significant interactions were found between distance and grasping size.

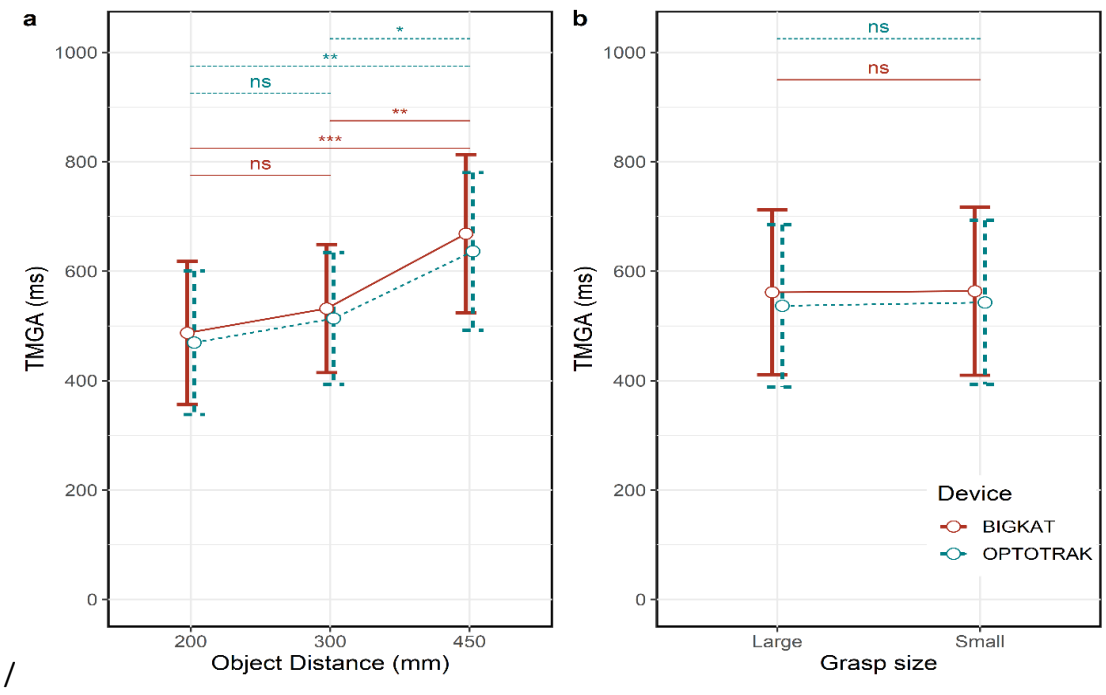

Figure 54: High end and low-cost optical motion capture system producing identical results for TMGA by a) object distance b) grasp size. Both plots show SD around mean.

4.3.3 Peak Velocity and time to Peak Velocity

Figure 55a shows that participants typically reached greater wrist velocities when moving to further targets but did not increase speed sufficiently to prevent longer movement durations. Object distance had a significant main effect on the reaching movement (Optotrak $(F(2,16) = 178.212, p < 0.0001, \eta_G^2 = 0.707)$ and BIGKAT $(F(2,16) = 133.207, p < 0.0001, \eta_G^2 = 0.733))$ such that peak velocity increased with increasing object distance: , 300mm: $BIGKAT\ 898.553 \pm 131.177 mm/s; OPTOTRAK\ 955.513 \pm 160.953 mm/s)$, 450mm: $BIGKAT\ 1176 \pm 198.188 mm/s; OPTOTRAK\ 1251.821 \pm 217.637 mm/s)$. Post-hoc analysis revealed significant differences between all object distances. Grasp surface size showed no effect on peak velocity as captured by Optotrak $(F(1,8) = 0.245, p > 0.05, \eta_G^2 = 1.59e^{-3})$ and BIGKAT $(F(1,8) = 0.0487, p = 0.83, \eta_G^2 = 2.83e^{-4})$ and shown in Figure 55b. No significant interactions were found between distance and grasping size.

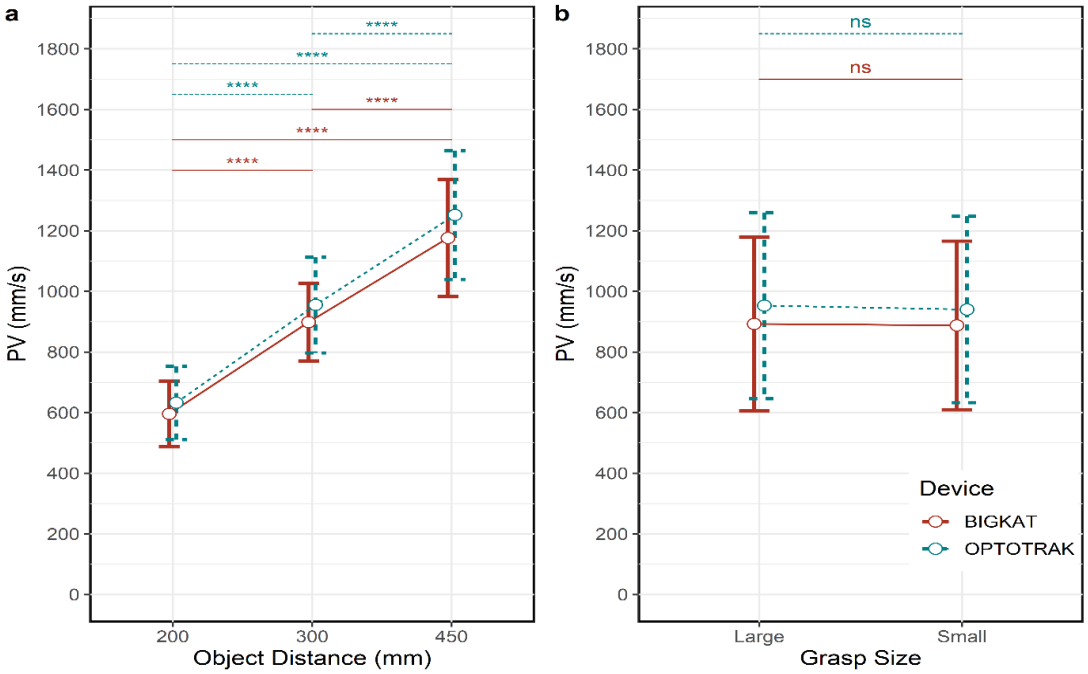

Figure 55a) object distance shows significant main effect for PV and b) grasp size shows no significant effect as computed by both devices. Both panels show SD around mean.

TPV was likewise influenced by object distance ($BIGKAT$: $F(2,16) = 28.837, p < 0.001, \eta_G^2 = 0.232$, Optotrak: $F(2,16) = 29.981, p < 0.001, \eta_G^2 = 0.187$), as shown in Figure 56a. TPV occurred later in the movement as distance increased: 200mm: ($BIGKAT$ $0.307 \pm 0.038s$; $OPTOTRAK$ $0.281 \pm 0.047s$), 300mm: ($BIGKAT$ $0.328 \pm 0.049s$; $OPTOTRAK$ $0.303 \pm 0.055s$), 450mm ($BIGKAT$ $0.372 \pm 0.063s$; $OPTOTRAK$ $0.341 \pm 0.058s$). TPV was not affected by the grasping surface size: Optotrak ($F(1,8) = 1.838, p > 0.05, \eta_G^2 = 0.016$) and BIGAKT ($F(1,8) = 2.397, p > 0.05, \eta_G^2 = 0.022$) as shown in Figure 56b. No significant interactions were found between distance and grasping size.

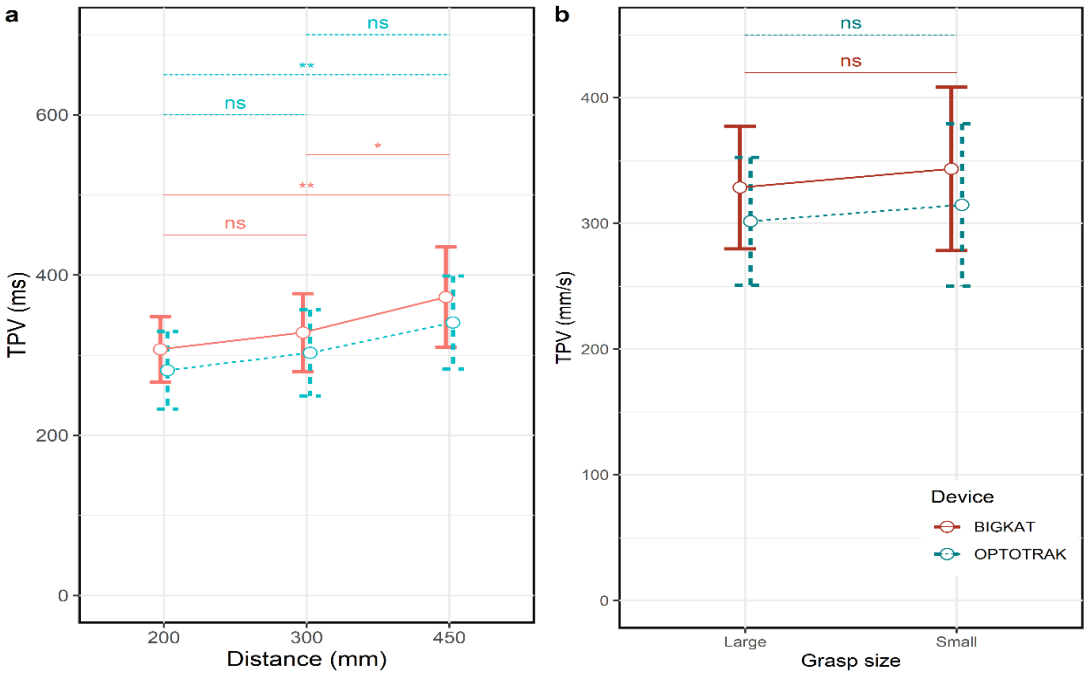

Figure 56: a) shows significant effect of object distance for TPV b) grasp surface size shows no significant effect for TPV as found by both low-cost and expensive optical motion capture system. Both plots shows SD around mean.

Table 8: Quantitative assessment of reach-to-grasp movements captured by BIGKAT and Optotrak, simultaneously. All values are presented with mean and SD summarized across all participants and trials.

Device	Grasp Size	Distance	MT (s)	MGA (mm)	TMGA (s)	PV (mm/s)	TPV (s)
BIGKAT	Small	200	0.66 ± 0.14	86.49 ± 6.62	0.49 ± 0.14	590.26 ± 121.54	0.32 ± 0.05
		300	0.70 ± 0.12	87.29 ± 6.06	0.52 ± 0.12	912.41 ± 135.85	0.33 ± 0.06
		450	0.84 ± 0.14	84.79 ± 10.35	0.67 ± 0.14	1160.93 ± 183.56	0.38 ± 0.07
	Large	200	0.62 ± 0.09	94.57 ± 9.19	0.48 ± 0.12	601.97 ± 98.52	0.30 ± 0.03
		300	0.70 ± 0.11	95.15 ± 7.66	0.54 ± 0.12	884.69 ± 126.50	0.33 ± 0.04
		450	0.81 ± 0.14	95.93 ± 9.28	0.66 ± 0.16	1191.35 ± 212.81	0.36 ± 0.05
Optotrak	Small	200	0.62 ± 0.14	86.13 ± 7.42	0.48 ± 0.15	620.91 ± 141.56	0.29 ± 0.06
		300	0.66 ± 0.12	87.03 ± 6.37	0.50 ± 0.12	968.24 ± 183.45	0.30 ± 0.06
		450	0.80 ± 0.14	83.63 ± 10.4	0.64 ± 0.14	1231.44 ± 204.09	0.35 ± 0.06
	Large	200	0.58 ± 0.09	94.09 ± 9.39	0.46 ± 0.12	644.44 ± 103.45	0.27 ± 0.03
		300	0.66 ± 0.12	94.56 ± 7.94	0.52 ± 0.13	942.78 ± 138.41	0.30 ± 0.05
		450	0.76 ± 0.14	94.25 ± 9.84	0.63 ± 0.16	1272.20 ± 231.18	0.33 ± 0.05

Spatial and temporal characteristics of prehensile movements vary with respect to the task constraints such that transport component are effected by the object distance causing PV to increase as well as causing PV to occur later in the movement; similarly, large grasp size lowers spatial accuracy demands while permitting a faster movement and hand opens up to a larger MGA and smaller grasping size demands higher precision during grasping phase [4], [139], [141], [145], [241]. For the exact same purpose, in this chapter object distance and grasp size were co-varied to observe prehensile behaviour from the positional data obtained from Optotrak which acted as 'gold standard' for the measurements obtained from BIGKAT. Analysis showed that BIGKAT can successfully reveal spatiotemporal characteristics of reach-to-grasp movements being manipulated by the task constraints and even when the movements are of small duration as well. Kinematic measures extracted from 3D positional data of BIGKAT were manipulated in the same manner as those extracted by Optotrak data. It still needs to be seen how these measures are related to Optotrak, hence, regression analysis was carried out and discussed in detail in the next section.

4.4 Linear Regression analysis

Simple linear regression was used to test the strength of relationship between BIGKAT and Optotrak kinematic measures at each level of object distance and grasping size. Regression analysis was carried out in R, first by averaging all the kinematic variables across all trials of every participant for each object distance and grasping size. Linear model function was used with 95% confidence region for the regression fit and visualized by adding a regression line onto the scatter plot provided by the 'ggplot' package. Linear model function provided the equation of the fitted line, co-efficient of determination (R-squared value) and p-value and were printed on top of each plot.

The principal goal of kinematically analysing reach-to-grasp movements was to assess BIGKAT's ability to characterise the constituent components of prehensile movements, performed in its workspace determined in chapter 3. Having established the fact within the previous section that BIGKAT can detect statistically significant differences between kinematic features of reach-to-grasp movement just as the 'gold standard' Optotrak, this section sets out to determine how those corresponding measures from two different devices are related to each other. Multiple linear regression analysis was performed between all of the retrieved kinematic variables (reach-to-grasp movements) across all trials, for each grip size, and for various object distances, for precisely the same reason.

Figure 57 shows the linear regression analysis for movement time during reach-to-grasp movements for different grasp size objects placed at different distances. Figure 57 depicts strong relationship between BIGKAT and Optotrak with nearly unity slope, low y-intercept values, large R-squared value with significant p-value. Linear model function provided the descriptive statistics about the residuals

of the model which was approximately zero. Absolute mean error was also calculated by subtracting the mean MT value of BIGKAT from Optotrak which was $40.5 \pm 8.5\ ms$, $42 \pm 10\ ms$ and $45.5 \pm 11\ ms$ when the object was at $200\ mm$, $300\ mm$ and $450\ mm$, respectively.

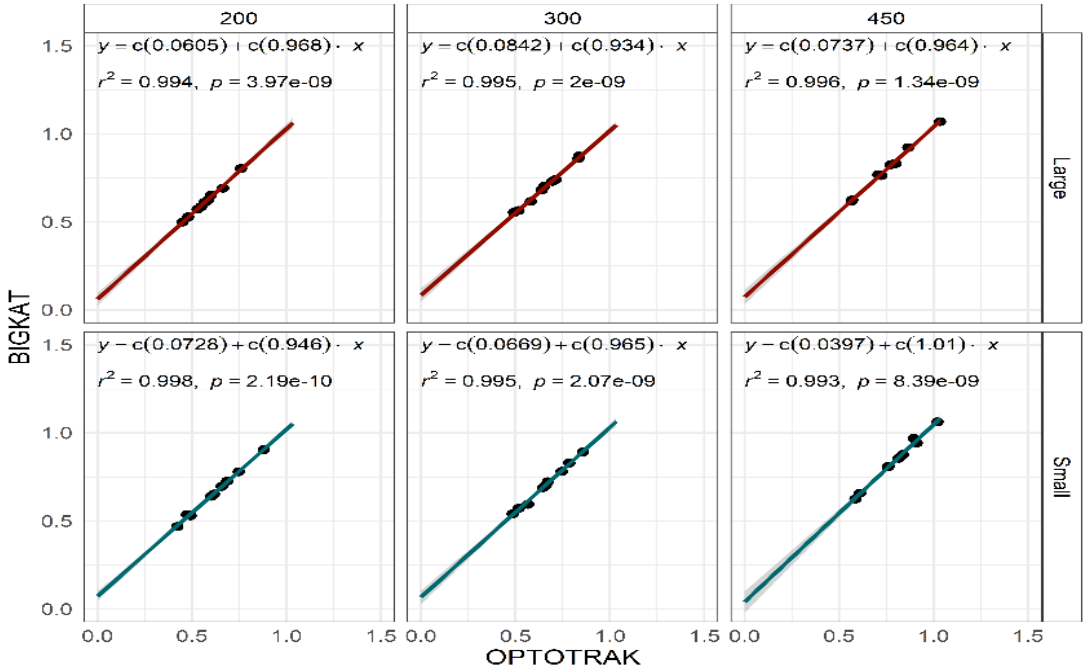

Figure 57: Regression analysis between Movement Time obtained through BIGKAT and Optotrak at each object distance and grasp surface size. Grey shade 95% confidence region.

Table 9: Absolute mean difference for all prehensile kinematic measures between Optotrak and BIGKAT

Distance (mm)	Grasp Size	Absolute mean difference				
		MT (s)	MGA (mm)	TMGA (s)	PV (mm/s)	TPV (s)
200		0.042 ± 0.007	0.711 ± 0.822	0.023 ± 0.010	42.465 ± 12.437	0.026 ± 0.010
300	**Large**	0.041 ± 0.011	0.892 ± 0.941	0.016 ± 0.008	58.084 ± 30.344	0.023 ± 0.011
450		0.046 ± 0.010	1.674 ± 1.336	0.035 ± 0.008	80.849 ± 93.672	0.031 ± 0.009
200		0.039 ± 0.010	0.979 ± 1.116	0.013 ± 0.009	30.651 ± 20.854	0.026 ± 0.012
300	**Small**	0.043 ± 0.009	0.818 ± 0.916	0.020 ± 0.009	55.836 ± 61.119	0.028 ± 0.006
450		0.045 ± 0.012	1.164 ± 0.697	0.029 ± 0.012	70.510 ± 109.792	0.032 ± 0.016

Regression analysis was also carried out on the kinematic data of the grasping component, as shown in Figure 58 and Figure 59. The results revealed a strong linear relationship between BIGKAT and Optotrak for the maximum opening of the hand (MGA) and the moment at which it occurred (TMGA), with a high R-squared value, a low p-value and an almost unity slope. Additionally, the absolute mean

MGA error was calculated. For large grip sizes, BIGKAT MGA values differ from Optotrak by $1.092 \pm 1.033\ mm$, whereas for small grasp sizes, it differs by $0.987 \pm 0.909\ mm$. The TMGA error shown (Table 9) that BIGKAT can detect the occurrence of MGA a little later than Optotrak; for objects positioned at 200mm, 300mm, and 450mm, respectively, the differences are $18 \pm 9.5\ ms$, $18 \pm 8.5\ ms$ and $32 \pm 10\ ms$.

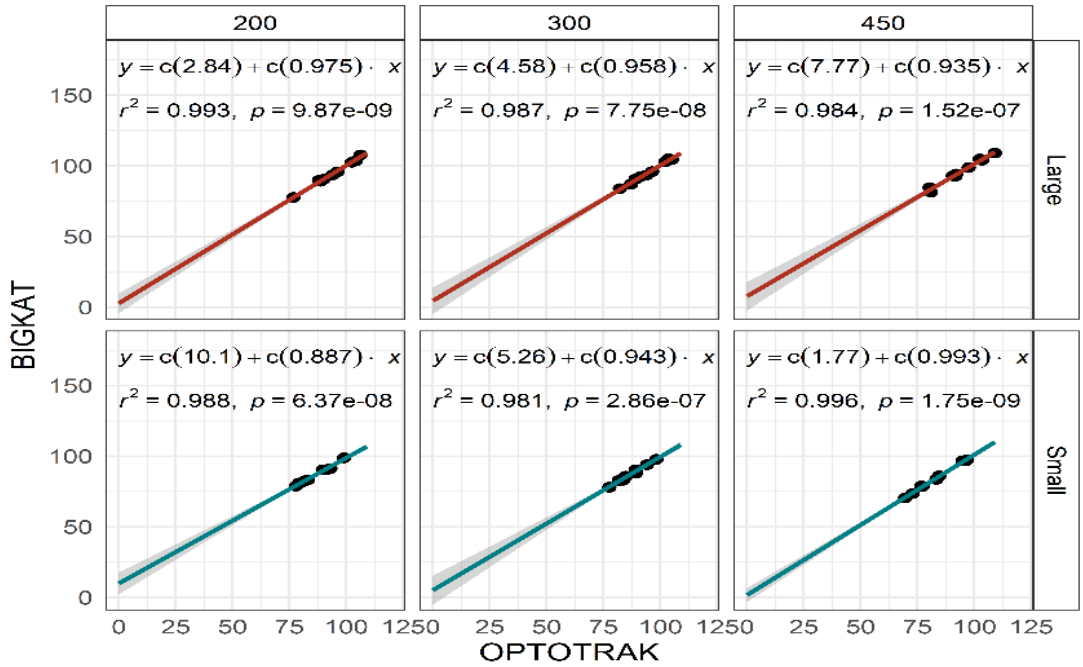

Figure 58: Regression analysis between MGA obtained through BIGKAT and Optotrak at each object distance and grasp surface size. Grey shade 95% confidence region.

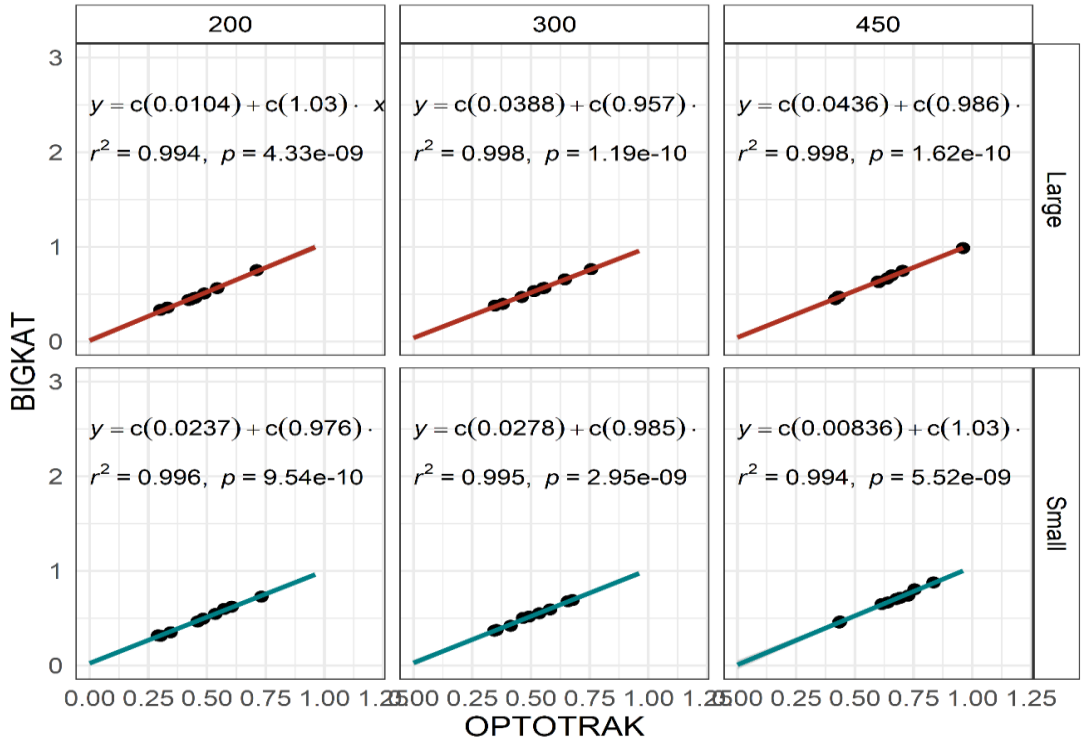

Figure 59: Regression analysis between TMGA obtained through BIGKAT and Optotrak at each object distance and grasp surface size. Grey shade 95% confidence region.

Likewise, kinematic measurements of reaching component, PV and TPV, from both devices were found to be linearly correlated at each level of object distance and grasping size as shown in Figure 60 and Figure 61. However, object placed at $450\ mm$ was recorded to have the lowest R-squared value (but significant p-value) among all kinematic variables and PV error was also larger ($75.679 \pm 101.732\ mm/s$) than the nearest objects ($200mm$: $36.558 \pm 16.645\ mm/s$, $300mm$: $56.96 \pm 45.731\ mm/s$), as shown in table.

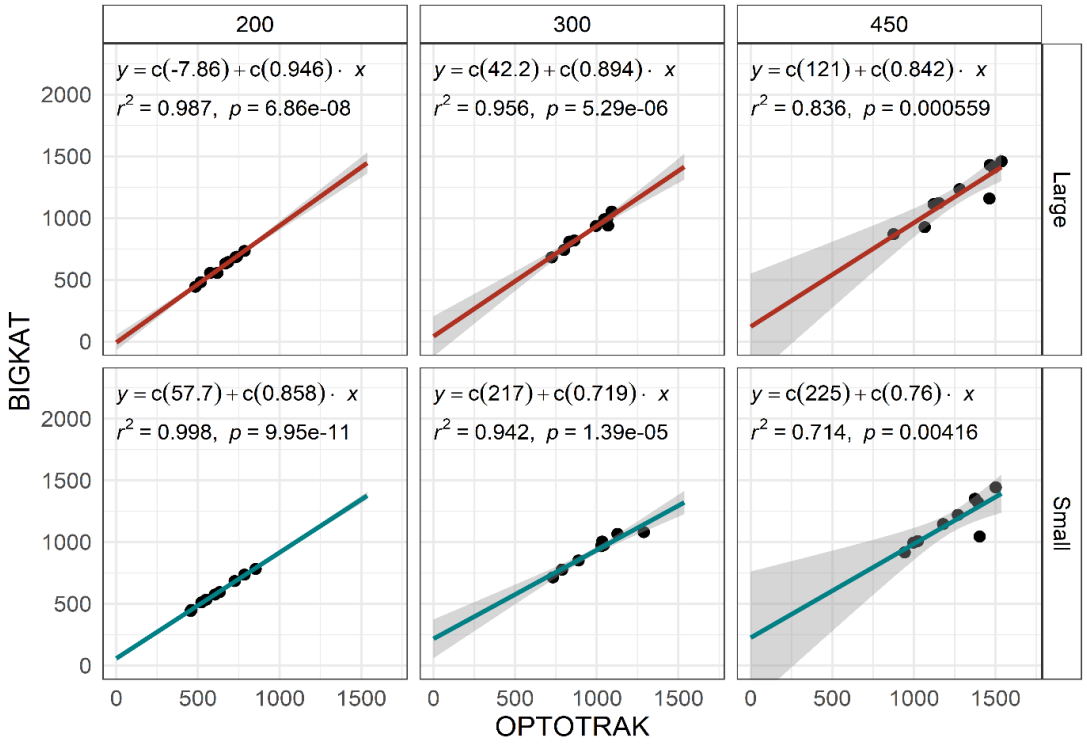

Figure 60: Regression analysis between PV obtained through BIGKAT and Optotrak at each object distance and grasp surface size. Grey shade 95% confidence region.

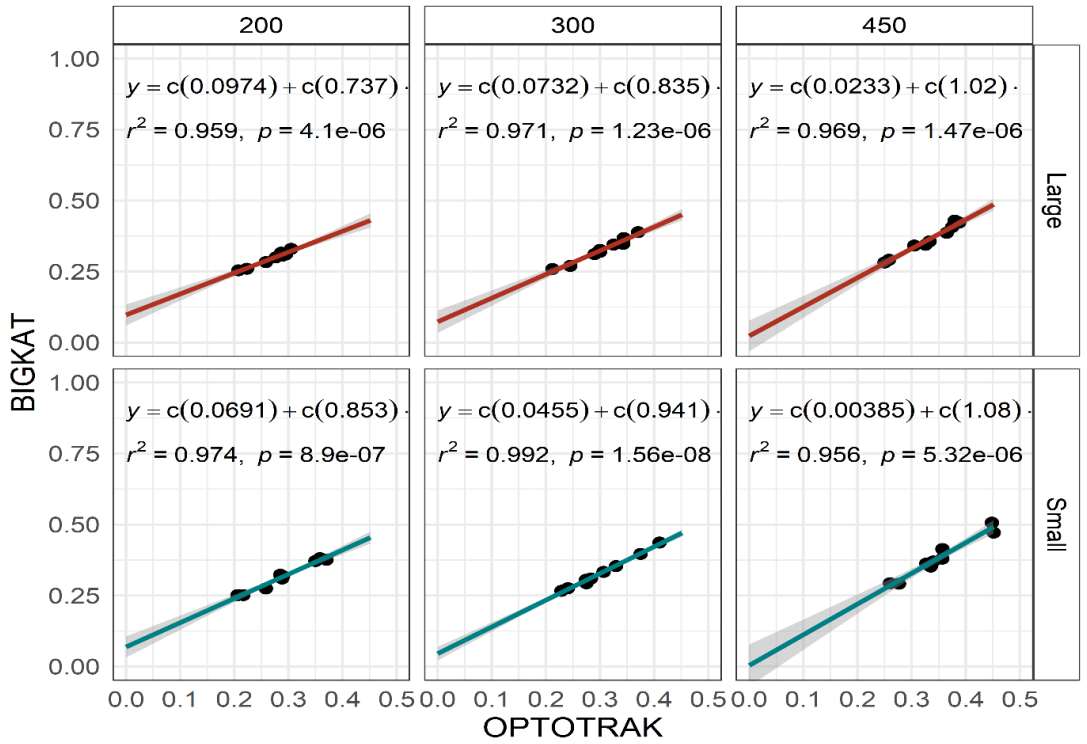

Figure 61: Regression analysis between TPV obtained through BIGKAT and Optotrak at each object distance and grasp surface size. Grey shade 95% confidence region.

Regression analysis between quantitative prehensile measures obtained through BIGKAT and Optotrak at each level of object distance and grasp surface size showed that spatiotemporal

characteristics extracted through 3D positional data of both optical motion capture systems are linearly correlated with a large coefficient of determination (R-squared), low y-intercept and almost unity slope. Results shows a linear relationship between both devices and it is evident that the kinematic measurements were strongly correlated except for one outlier present in PV measurement Figure 60, while making reaching movement towards object placed at 450mm. Regression results suggest that low-cost, portable, easy-to-use BIGKAT can capture comparable prehensile movement patterns to those recorded by the more expensive, laboratory-based Optotrak.

4.5 Discussion

The prehensile kinematic features extracted from 3D positional data showed that BIGKAT can successfully capture all spatiotemporal characteristics being manipulated by the task constraints in this study, leading to the equivalent findings in terms of the effects of task manipulations on kinematic measurements obtained via Optotrak. Linear regression analysis measuring relationships between both optoelectronic systems revealed highly correlated kinematic measures as shown in Figure 57 to Figure 61. BIGKAT kinematic measures are in good agreement with those obtained from Optotrak showing that the measured changes in reaching and grasping component due to the task constraints reflects BIGKAT potential of resolving coordinated and controlled movement successfully. Based on the evidence from statistical results, shown in Figure 52 to Figure 56, has strengthened our confidence that the portable, low-cost, and user-friendly BIGKAT may be used on a large scale to study and analyse reach-to-grasp movements in laboratory and non-laboratory contexts as a result of such tightly linked outputs from two distinct devices looking at the prehensile movement simultaneously.

In general, R-squared values of all measured kinematic variables were very high indicating a strong relationship between Optotrak and BIGKAT 3D positional data and produced small positional errors as well, see table 2. Spatiotemporal characteristics of reach-to-grasp movement was found to correspond well with the calculated value of the same movement by gold-standard, research-grade and expensive optical motion capture system, Optotrak. In other words, sequential movements recorded with BIGKAT can resolve IRED trajectory accurately, precisely and can produce comparable results as obtained by Optotrak. Thus, enabling researchers to quantitatively analyse upper arm reach-to-grasp movements and/or helping neurologists to keep track record of the treatment progress by providing them with objective measures.

For this study only healthy participants were recruited and movements from healthy subjects are less variable than those individuals suffering from neurological disorders who exhibit slower, progressive hesitation/halts, scaled in both the amplitude and time domains as movements are continued [17], [152]. It can be challenging to unfold the coordinated and controlled structure of sequential

movements of healthy individuals since they can reach objects quickly and change their grip aperture effectively. Furthermore, it has been demonstrated (see results) that BIGKAT was able to extract spatial and temporal measurements in accordance with Optotrak and that BIGKAT has delivered statistically significant outcomes that have previously been documented in literature. Literature also investigates the discriminative ability of motion capture system by kinematically analysing sequential/repetitive/simultaneous movements of neurologically disabled and healthy controls and to understand how such systems can be helpful to neurologist for diagnostic and to keep track record of improvement made during treatment. Hence, next chapter investigates BIGKAT's performance against gold standard Optotrak by simultaneously analysing spatiotemporal characteristics of repetitive finger tapping movement made by Parkinson's patients and healthy controls.

4.6 Conclusions

This study highlights the potential usage of the Boxed Infrared Kinematic Assessment Tool for studying reach-to-grasp movements in laboratory and clinical settings. The results of the investigation using BIGKAT are similar to those reported in the previous literature and were successfully validated against the research-grade optoelectronic system, Optotrak. The strong correlation between the two devices is evidence for of BIGKAT’s applicability and adaptability to effectively resolve upper limb movements performed within its workspace.

Chapter 5: Performance Comparison of BIGKAT with Optotrak for Kinematic Analysis of Repetitive Finger Tapping Movement of PD Patients and Healthy Controls.

5.1 Introduction

The prevalence of Parkinson's disease (PD) is rising on a global scale. PD, a chronic neurodegenerative ailment, is characterized by slow voluntary movement, which is the most significant functional disruption in patients [242]–[244]. Generally speaking, this syndrome is known as bradykinesia. The motor phenotypic spectrum also includes tremor and muscular rigidity [245]. Bradykinesia and other motor symptoms appear to be linked to a progressive loss of dopaminergic neurons in the substantia nigra, even if it has not been possible to pinpoint a single underlying pathophysiologic process that accounts for everything [59]. Bradykinesia is the condition's primary motor symptom, but there are currently no widespread, everyday applications for wearable sensors to monitor it [20]. To quantify the condition objectively, new technologies are urgently needed. Typically, clinicians employ established clinometric measures like the Unified Parkinson's Disease Rating Scale (MDS-UPDRS) to assess and quantify the motor clinical characteristics of Parkinson's disease (PD) [245]. However, subjectivity and inter-rater variability influence clinical assessments. As a result, the PD medical community is seeking for an easy, affordable, and impartial solution that can be deployed on large scale [246]. Chapter 4 demonstrated that BIGKAT is suitable for studying reach-to-grasp movements. This chapter expands this by assessing BIGKAT's ability to quantify measures related to Parkinson's bradykinesia using videos of finger tapping by healthy and clinical population.

One of the major aims of this study was to kinematically analyse the repetitive finger-tapping (FT) movements using BIGKAT and Optotrak. Hence, this chapter sets out to investigate BIGKAT's performance while kinematically analysing repetitive finger-tapping (FT) movements made by PD patients and healthy controls. It was accomplished by recording finger tapping (FT) movements and extracting features like rhythm, speed, and amplitude decrement from the 3D FT positional data obtained by a research-grade Optotrak system, which will serve as a gold-standard for our inexpensive, portable, user-friendly optical motion capture system. By conducting correlation and regression analyses between the quantitative measurements collected from the two devices, it seeks to compare BIGKAT performance against OPTOTRAK in a task other than prehension, thereby maximising its potential use in large-scale, routine clinical settings.

5.2 Method

The number of samples needed for such case control studies is based on the required level of confidence (95%), the proposed power of the study, prevalence rate and the assumed number of patients and controls in similar studies [247]. It was calculated with the following formula

$$n = z^2_{1-\alpha/2} * 0.25/d^2 \quad \text{i}$$

Where n is the number of samples, and for this study z is the confidence level of 95% (level of significance p-value of 5%) and d is the 22% margin of error (78% power of the study) is acceptable. Using equation i with these values the sample size is 19.843 which rounded up to 20. Finger tapping movement of 38 hands (including left and right) were obtained from 10 idiopathic Parkinson's disease patients and 9 healthy controls. All participants gave their written consent to participate in the study and was approved by the Health and Care Research Wales (HCRW), United Kingdom Health Research Authority. All patients were diagnosed with PD and were recruited from Leeds Teaching Hospitals NHS Trust, United Kingdom. Control subjects had no history of neurological disease or medical condition associated with movement impairment and were the companions of patients or university staff. Participants were instructed to repeatedly tap their index finger on the thumb as quickly and as wide as possible, while Optotrak and BIGKAT recorded FT movement, simultaneously. Infra-red emitting diodes (IRED) were attached on the distal phalanx of the thumb and index fingertip. Each participant performed FT movements eight times for a duration of 17s, four for each hand and each hand was tested separately and movements were recorded by the two optoelectronic devices at 60Hz.

5.3 Data Analysis

Data acquisition was completed by both Optotrak and BIGKAT and was initiated one second before the "go" in the experimenter's verbal start command "three, two, one, go" and the participant's task was to repeatedly tap their index finger on the thumb as quickly as possible and at maximal extent (distance between finger and thumb) at the "go" signal. Tapping response was recorded by attaching infra-red emitting diodes to the distal joint of the index finger and thumb and measuring the distance between them. An R script was designed to extract and filter (2nd order Butterworth, $f_c = 16Hz$) 3D data from the binary files recorded by Optotrak (available on GitHub) [240]. 3D positional coordinates were extracted from BIGKAT recordings using BIGKAT video analysis software. These 3D coordinates were then kinematically analysed to study movement patterns e.g., IRED velocity or distance between IREDs for the whole movement duration.

3D positional data produced by both devices were used to calculate the absolute distance between the thumb and finger using equation ii, and the tangential speed was calculated from the resulting time series. Trials were then cropped from movement onset, which was set at the point when the speed exceeds 50mm/s, and movement offset was determined when the speed decreases below 50mm/s. The resulting distance series, from both devices, were then aligned according to the movement onset.

$$S = abs\left(\sqrt{(a_x - b_x)^2 + \left(a_y - b_y\right)^2 + (a_z - b_z)^2}\right) \quad \text{ii}$$

Equation ii shows that distance series was calculated by subtracting the position of thumb and finger along each axis where a represent thumb and b represent finger. The resulting distance series was normalized across all trials and is transformed linearly using min-max normalisation. Using this method, all scaled data within the range (0,1) is obtained and calculated using equation iii.

$$S_{normalized} = \frac{x - x_{min}}{x_{max} - x_{min}} \quad \text{iii}$$

Figure shows the normalized distance between thumb and finger which was calculated by subtracting the current value from the minimum value and then dividing by the difference between the maximum and minimum distances.

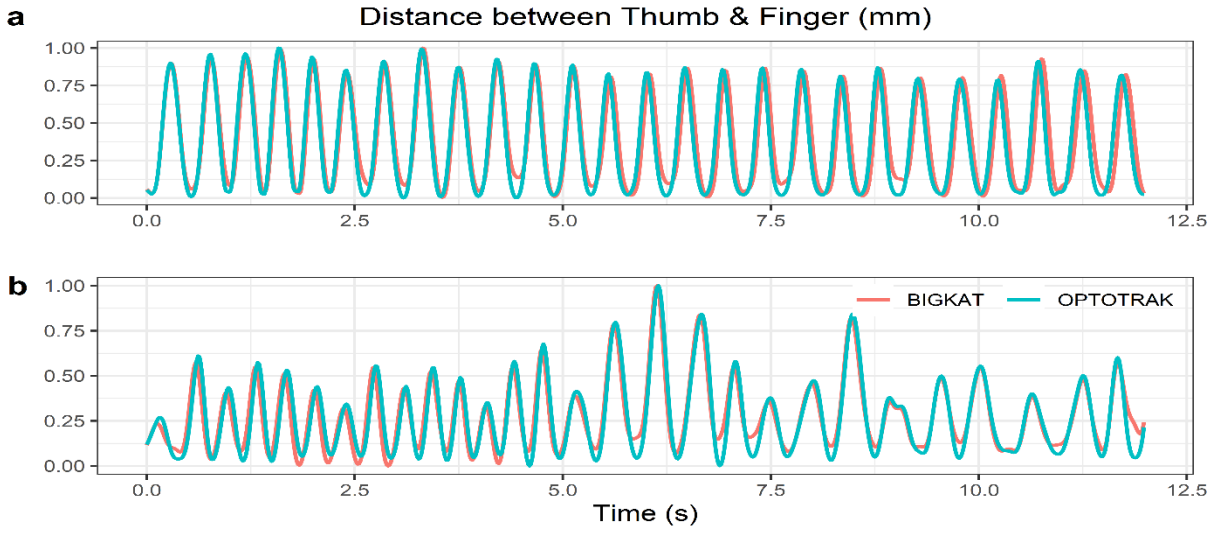

Figure 62 Normalized distance between thumb and finger as obtained from BIGKAT and Optotrak, simultaneously. a) Healthy Control b) PD patient

Three characteristics of the resulting fingertip to thumb tip distance time series were determined to reflect the speed, amplitude, and rhythm of clinical finger tapping as per MBRS and MDS-UPDRS scale. The average rate of change of the normalised distance between the tips of the fingers and thumb over time was measured as a measure of speed and calculated using equation iv and v.

$$V_i = \frac{S_i - s_{i-1}}{t_i - t_{i-1}} \quad \text{iv}$$

$$V_{ave} = \frac{1}{n-1}\sum_{1}^{n-1} V_i \quad \text{v}$$

Decrease in amplitude is expected as the movements are continued, and PD patients show large variability towards the end of the trial than healthy controls. For the exact same purpose, amplitude variance was calculated by dividing the normalized distance between thumb and fingertip times series for each trial into 1s windows to extract maximum and minimum amplitude values, which were then used to calculate the coefficient of variation within each window. To extract amplitude variations, a customized function was developed in R, pseudo-code shown below, which accept normalized distance and time series as input argument and output two arguments coefficient of variation within each window and standard of deviation of the peaks.

```
// Calculating the features of the amplitude
function [Output 1, Output 2] = Extract_Amplitude (Argument One, Argument Two)
// Inputs: Argument One: the input signal, Argument Two: the time index
// Outputs: Output 1: the Coefficient of Variation of the energy within each window, Output 2: the std of peaks
Subtracting the mean of argument one from argument one to remove the dc component
Find peaks and their occurrences from both input argument using 'findpeaks' function
Save all peak in 'peak' variable
Set energy list to 0
Set window length to 60 to make a one second window
For each window length
        OUTPUT difference in maximum and minimum value
        Store difference value in energy list
ENDFOR
Calculate the coefficient of variation of energy list
Store the result in output 1
Calculate peak differentiation
Calculate standard deviation in peak
Store the result in output 2
END
```

A third measure, rhythm regularity (differentiating regular rhythm from irregular rhythm) was calculated by taking the Fast Fourier Transform of each normalized distance. To find the distribution of frequencies inside each finger tap time series, and then evaluating the power of the dominant frequency peak added to the power of the frequencies 0.2 Hz each side of it. The Fast Fourier Transform of an irregular rhythm would produce a widely spread frequency distribution reduces the power of the dominant frequency band, whereas the Fast Fourier Transform of a more regular rhythm

will create a narrower frequency distribution subsequently increasing the power of dominant frequency as shown in Figure 63.

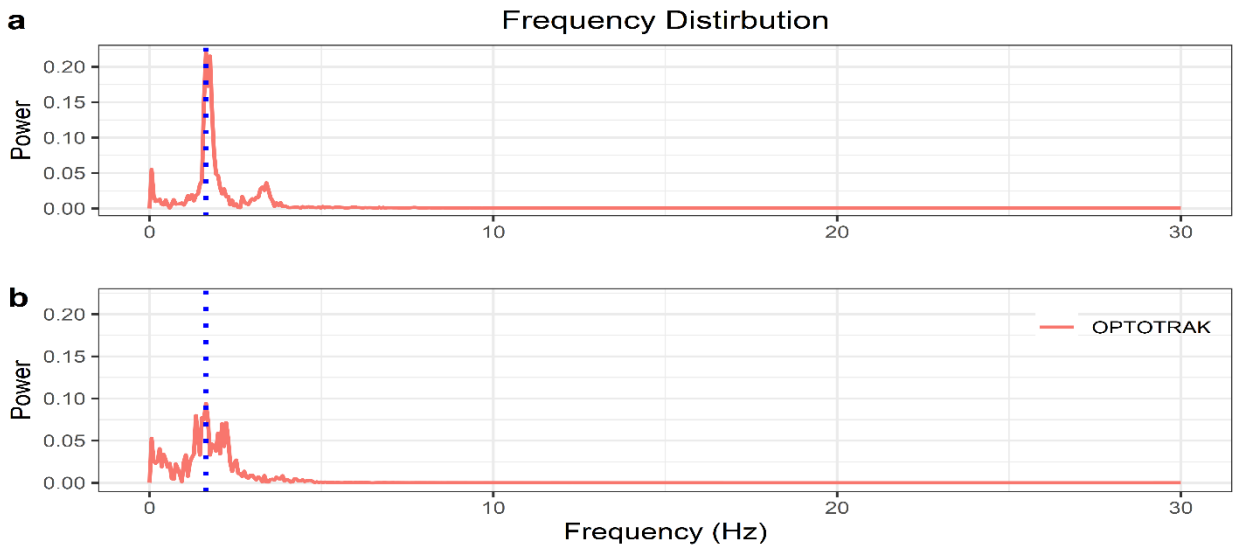

Figure 63 Fast Fourier Transform of the normalized distance between thumb and finger. Blue dotted line shows dominant frequency peak. a) Narrower frequency distribution by healthy control b) wider frequency distribution by PD

```
function [yf , f] = Dofft( Sig , Fs)
% Calculating the fast Fourier Transform of the signal
% Input:
%       Sig : the input signal
%       Fs : the sampling frequency
% Output:
%       yf : the FFT of the signal's envelope
%       f : the frequency index
        Store the length of signal    xlen <- length(Sig);
        Remove the dc component by subtracting the mean     Sig = Sig - mean(Sig);
        Calculate the next higher power of 2 to optimize fft    NFFT <- 2 ^ nextpow2(xlen);
        Compute the Discrete Fourier Transform   yf  <-  fft(Sig,NFFT) / xlen * 2;
        Take the absolute value for whole series   yf <- abs(yf(1 : NFFT/2+1));
        Find the frequency index for the whole sequence f <- Fs / 2 * linspace(0,1,NFFT/2+1);
END
```

Three finger tapping features were extracted from the 3D positional data obtained by both optical motion capture system (BIGKAT and Optotrak) to describe the characteristics of the movement pattern. The next section presents the statistical analysis adopted for the assessment of FT and is divided into two sub-sections. Firstly, quantitative measures were calculated from the positional data obtained by Optotrak. And then one-way analysis of variance was used to find statistically significant

differences between factor group (PD patients, healthy controls) for three FT features. Secondly, correlation and regression analysis were carried out between the quantitative measures computed from low-cost, portable BIGKAT and high-end, expensive Optotrak and therefore evaluating BIGKAT's potential usage in large scale, routine clinical settings.

5.4 Results

5.4.1 Quantitative assessment via Optotrak

One-way ANOVA showed a significant main effect of group ($F(1,1) = 1118.289, p < 0.001, \mu_G^2 = 0.465$) for amplitude variance as shown in Figure 64(a), suggesting larger amplitude variability among PD patients ($Left$: 0.200 ± 0.124; $Right$: 0217 ± 0.135) than healthy controls ($Left$; 0.190 ± 0.144; $Right$; 0.175 ± 0.122). Analysis of average speed showed a significant main effect of group ($F(1,1) = 1417, p < 0.001, \mu_G^2 = 0.981$), such that average speed of healthy controls was much higher ($Left$: $569.762 \pm 160.710 mm/s$; $Right$: $507.455 \pm 168.818 mm/s$) than PD patients ($Left$: $394.144 \pm 146.218 mm/s$; $Rigt$: $376.934 \pm 139.362 mm/s$) for both hands combined as shown in Figure 64(b). Factor group also showed a significant main effect for rhythm regularity ($F = 4150, p < 0.001, \mu_G^2 = 0.461$), such that rhythm (total power in the signal) was more regular for control ($Left$: $0.654 \pm 0.169 mm/Hz$; $Right$: $0.601 \pm 0.203 mm/Hz$) than PD patients ($Left$: $0.542 \pm 0.177 mm/Hz$; $Right$: $0.543 \pm 0.181 mm/Hz$). Post-hoc analysis showed a significant difference between both groups ($p < 0.0001$) as shown in Figure 64c.

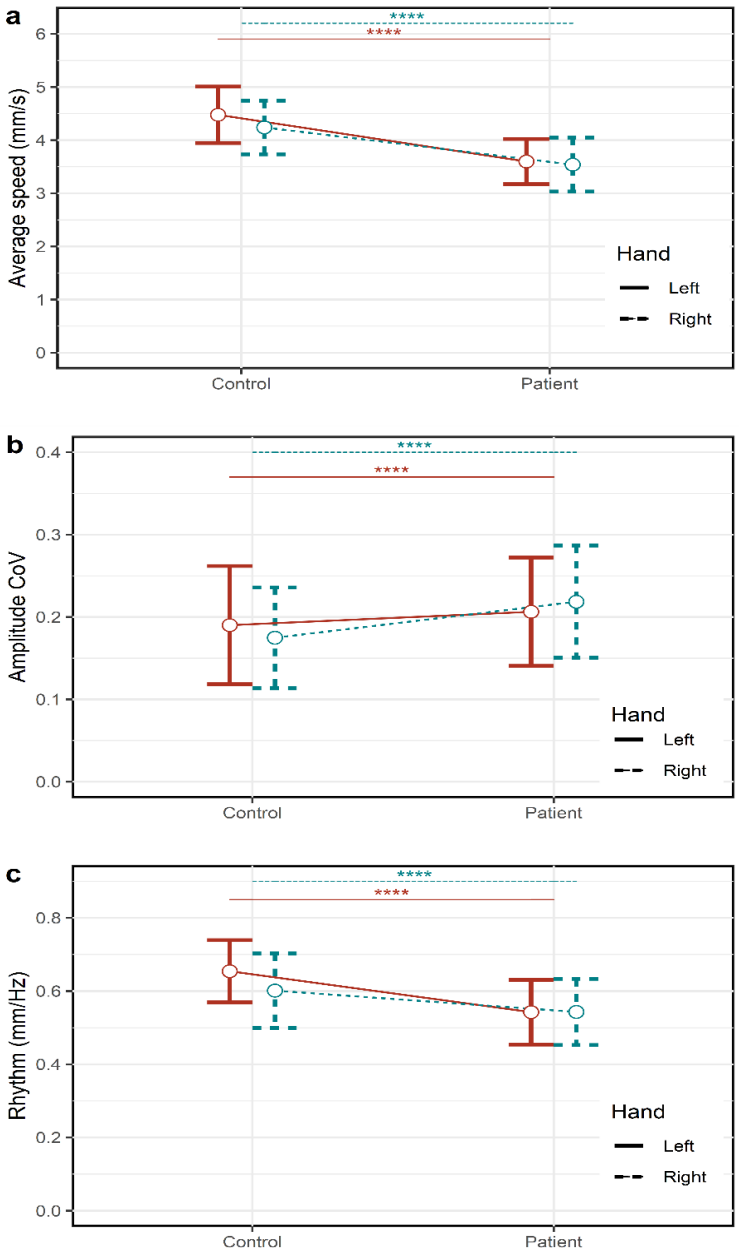

Figure 64 Kinematic features of finger tapping speed, amplitude and rhythm, computed from the 3D positional coordinates produced by Optotrak for both PD patient and Healthy controls and for each hand.

5.4.2 Correlation & Regression analysis with BIGKAT

The primary objective of this section was to compute correlation and regression analysis between the FT features measured by both optical motion capture systems, in-house BIGKAT and gold standard Optotrak. In line with the results obtained in the previous section, Optotrak has shown the ability to quantify repetitive FT movements of healthy control and PD patients, hence, significantly discriminating between the two based on amplitude variance, average speed, and rhythm regularity. Therefore, determining the strength of relationship between BIGKAT and Optotrak will shed light on the ability of BIGKAT to do the same. In a manner, can FT features extracted from 3D positional data of BIGKAT successfully capture repetitive FT movement? Therefore, rather than finding significant

differences between groups, this section sets out to determine the strength of relationship by performing regression analysis between the kinematic measures of BIGKAT and Optotrak.

A linear model function was used with 95% confidence region for the regression fit and visualized by adding a regression line onto the scatter plot provided by *'ggplot'* package. The linear model function provided the equation of the fitted line, co-efficient of determination (R-squared value) and p-value and were printed on top of each plot. Figure 65 shows regression analysis for the amplitude variance obtained through BIGKAT and Optotrak, healthy controls showed strong correlation with large R-squared value $(Right\ hand: r^2 = 0.923, p < 0.0001, Left\ hand: r^2 = 0.91, p < 0.0001)$ but PD patient showed low R-squared value $(Right\ hand: r^2 = 0.212, p < 0.005, Left\ hand: r^2 = 0.581, p < 0.0001)$ due to the outliers present in the PD data, as shown in Figure 65.

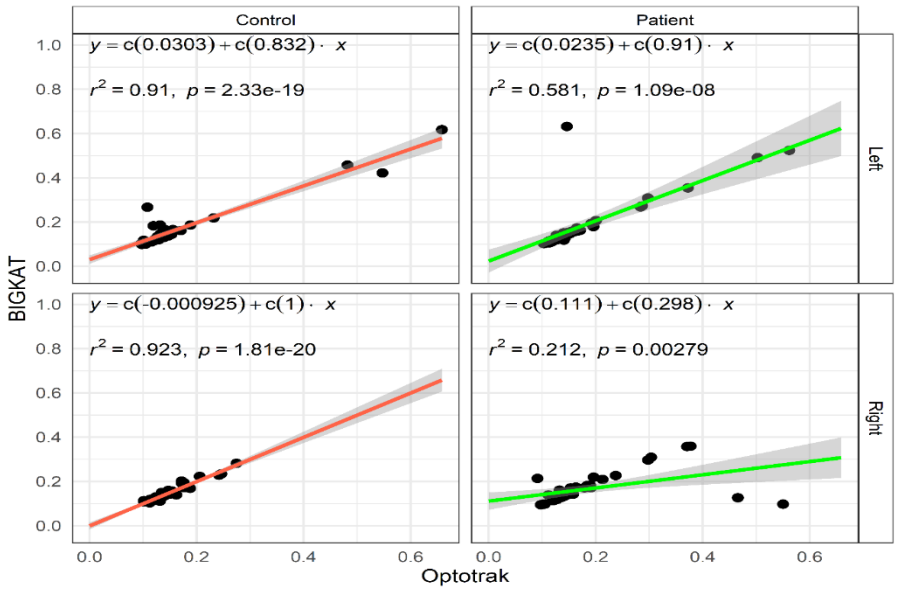

Figure 65: Correlation and regression analysis between BIGKAT and Optotrak for amplitude variance showing linear relationship

Similarly, correlation and regression analysis for average speed was determined as shown in Figure 66, which depicts a linear relationship between both devices at each level of hand and patient type. It depicts a strong relationship between BIGKAT and Optotrak with nearly unity slope, low y-intercept values, large R-squared value with significant p-value. Linear model function provided the descriptive statistics about the residuals of the model which were approximately zero. Large R-squared values, but significant p-value was obtained for both right $(Control: r^2 = 0.934, p < 0.0001, patient: r^2 = 0.906, p < 0.0001)$ and left hand $(Control: r^2 = 0.939, p < 0.0001, patient: r^2 = 0.904, p < 0.0001)$.

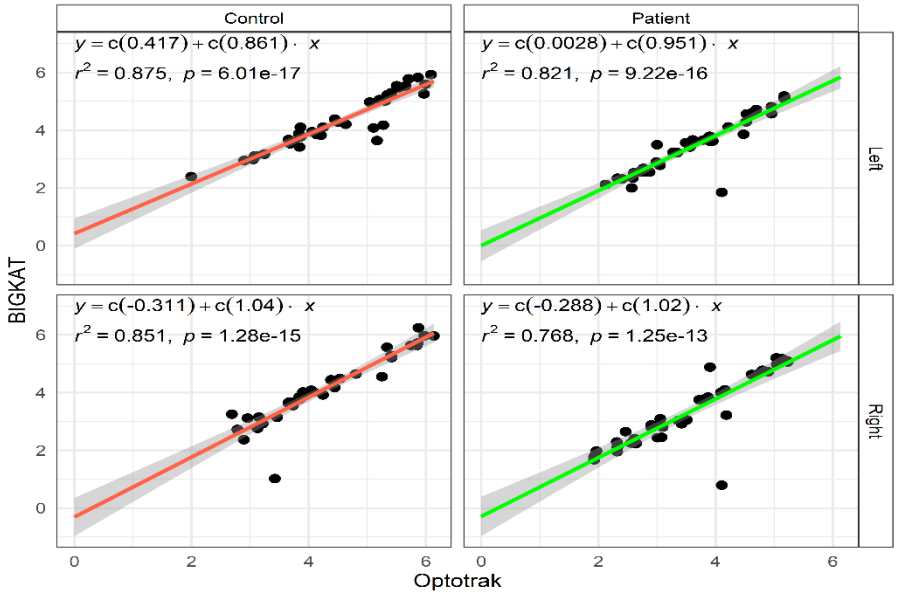

Figure 66 Correlation and regression analysis between BIGKAT and Optotrak for average speed showing linear relationship a) Full data b) variance considerably reduced after removing outliers

Likewise, correlation and regression analysis of rhythm variability from the 3D positional data (normalized thumb to finger distance) from both devices were highly correlated with each other for both right $(Control: r^2 = 0.822, p < 0.0001, patient: r^2 = 0.64, p < 0.0001)$ and left hand $(Control: r^2 = 0.759\ p < 0.0001, patient: r^2 = 0.784, p < 0.0001)$ as shown in Figure 67. Low r-squared values were due to the outliers which were identified and removed by measuring Cook's distance which was four times the average Cook's distance (explained in detail in the next section).

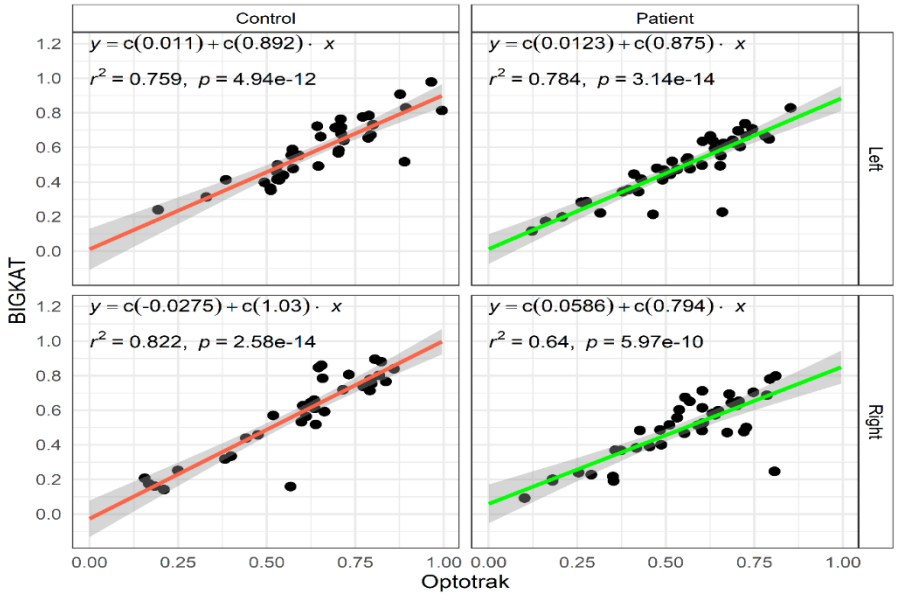

Figure 67: Correlation and regression analysis between BIGKAT and Optotrak for rhythm regularity showing linear relationship a) Full data b) variance considerably reduced after removing outliers

5.4.3 Detecting and Removing Outliers

Outliers were identified by measuring the Cook's distance which determines the influence of a data point by considering an observation's leverage and residuals values that may alter the outcome of regression. Leverage and residual values from each observation are combined to determine the Cook's distance, the more the leverage and residuals, the greater the Cook's distance. When the *ith* observation is taken out of a regression model, the Cook's distance measures how much the model changes. A typical guideline is to study any point that is greater than the threshold which is four times the average distance of all the points. Six observations were detected as outliers in the amplitude variance dataset as shown in Figure 68a, ten observations were detected in the average speed dataset as shown in Figure 68b and six observations were detected in rhythm regularity dataset as shown in Figure 68c. Some of the observations were repeated in all three datasets, so, a total of 14 trials were identified as outliers having Cook's distance higher than four times the mean Cook's distances of all other data points.

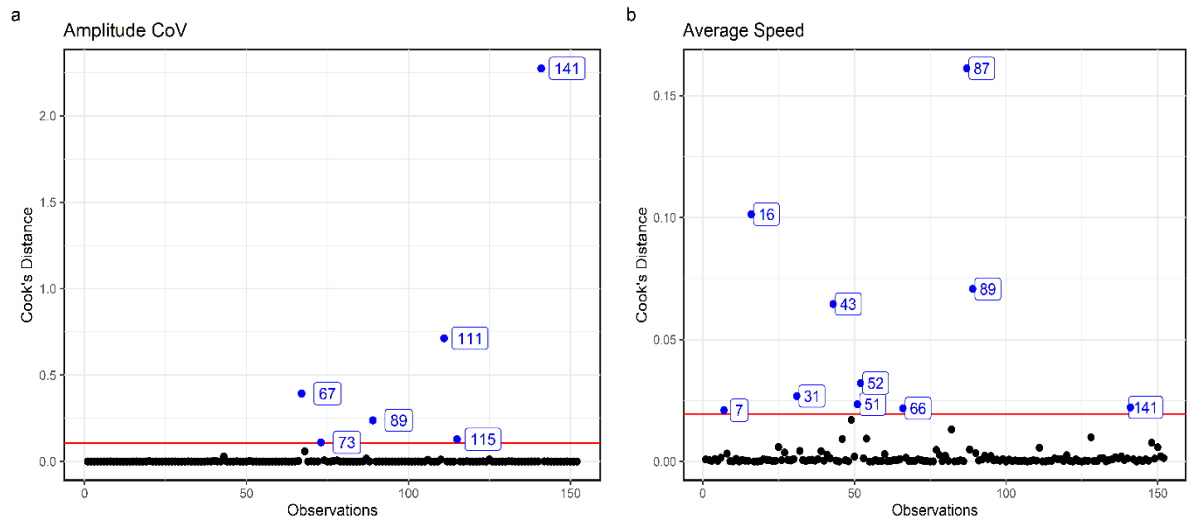

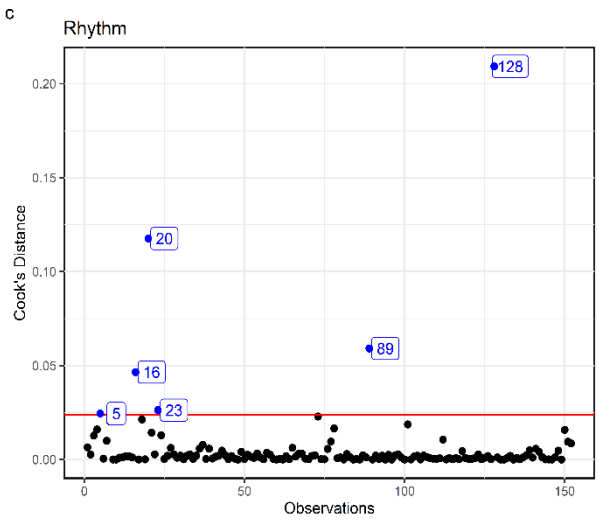

Figure 68: Red line show observations with the Cook's distance values exceeding the threshold are considered outliers and are shown for all three datasets; a) Amplitude variance b) Average speed, c) Rhythm regularity. Blue points show detected outliers and labels shows row number as they appear in data and it can be seen that observation number 89 appear in each dataset.

Figure 69 shows all fourteen trials that were detected as outliers, seven of which are from PD group and remaining seven from healthy controls. Each plot shows normalized distance between thumb and finger plotted over time to examine the underlying reasons of the low R-squared values in regression analysis. It is evident from the Figure 69 that all outliers can be categorized into three categories. In category-I, normalized distance values measured by BIGKAT are smaller when compared to Optotrak values, a total of 5 trials from Figure 69a to Figure 69e. Category-I trials are not useful and need to be excluded from the analysis. In category-II, trials lost synchronisation during recording even though both devices recorded FT movements simultaneously. A total of six trials (Figure 69f ~ 8k) out of 152 trials were out of synchronisation, it may be due to some delays in triggering time. In category-III, one of the devices started recording much earlier than the other device and again, it may be due to delays in triggering of one of the devices, 3 trials fall in this category as shown in Figure 69l to Figure 69n.

a)

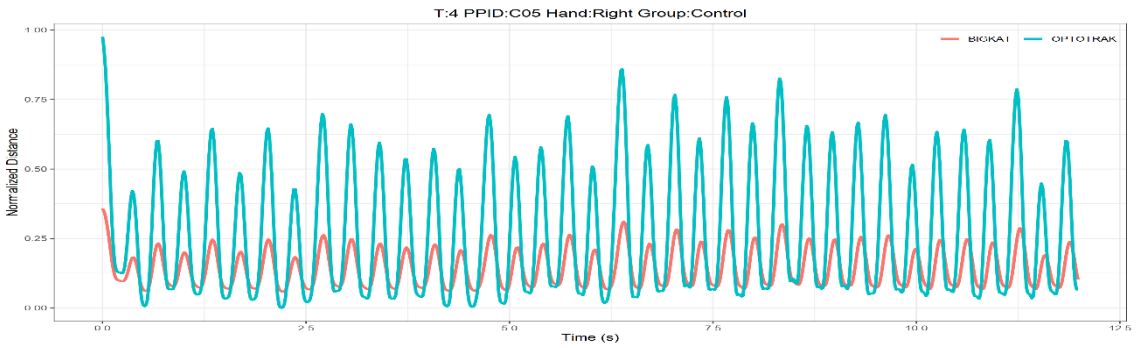

b)

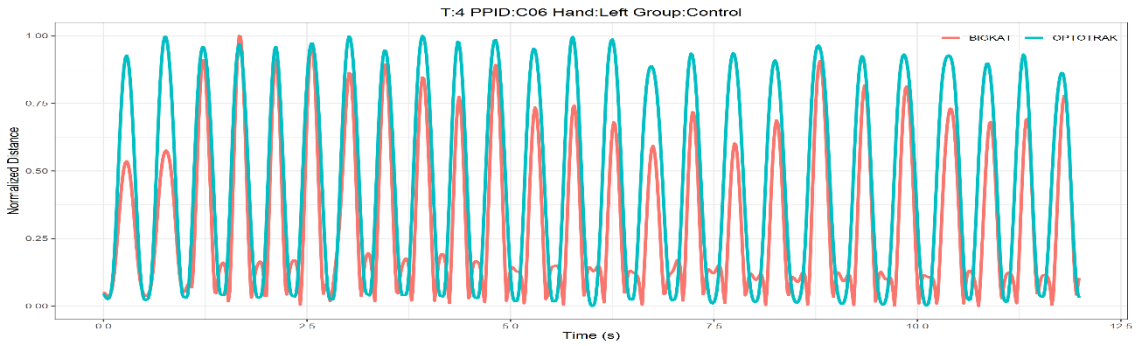
T:4 PPID:C06 Hand:Left Group:Control
BIOKAT
OPTOTRAK
Normalized Distance
Time (s)

c)

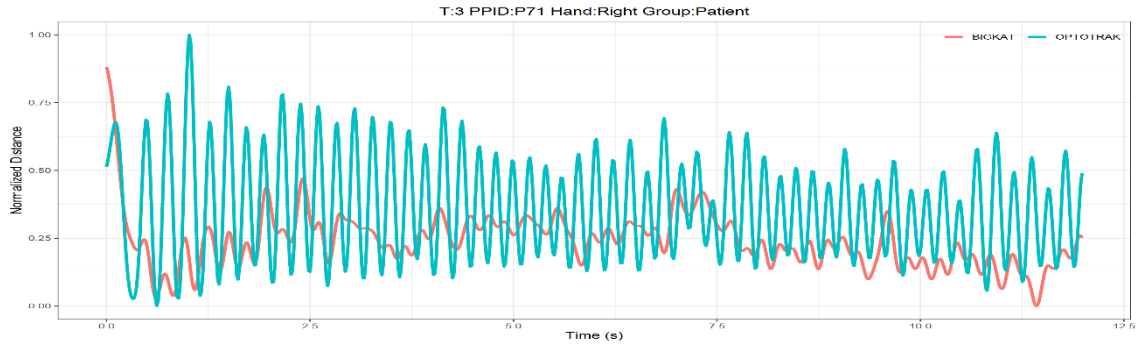
T:3 PPID:P71 Hand:Right Group:Patient
BIOKAT
OPTOTRAK
Normalized Distance
Time (s)

d)

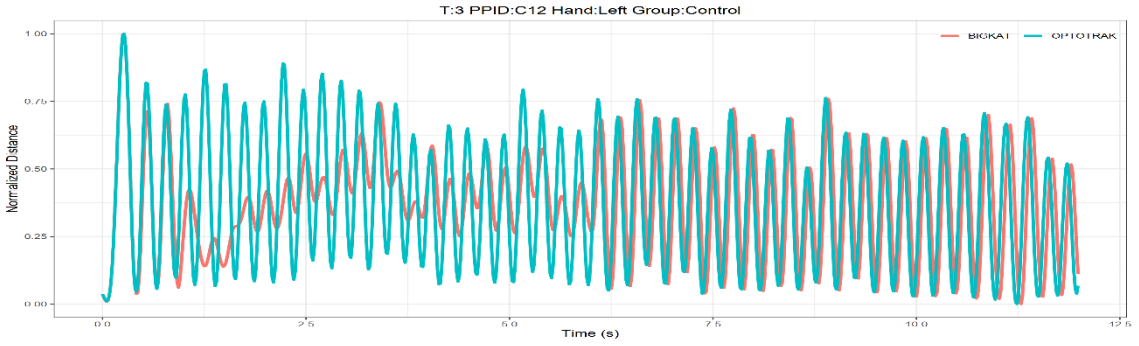
T:3 PPID:C12 Hand:Left Group:Control
BIOKAT
OPTOTRAK
Normalized Distance
Time (s)

e)

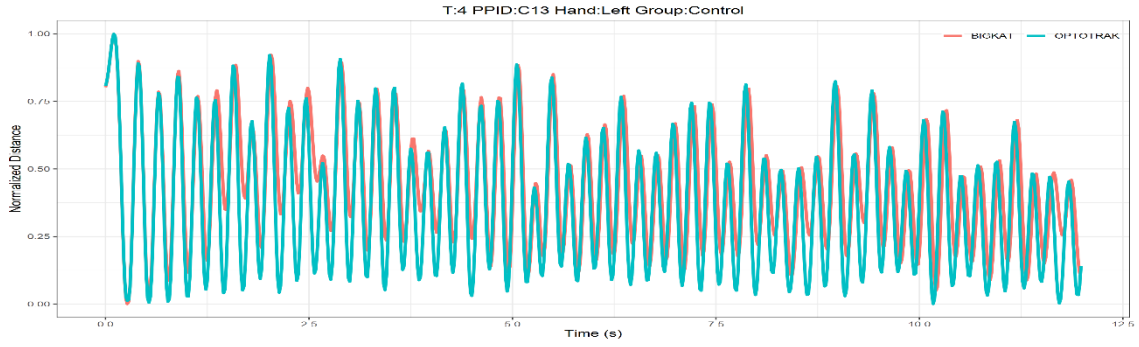
T:4 PPID:C13 Hand:Left Group:Control
BIOKAT
OPTOTRAK
Normalized Distance
Time (s)

f)

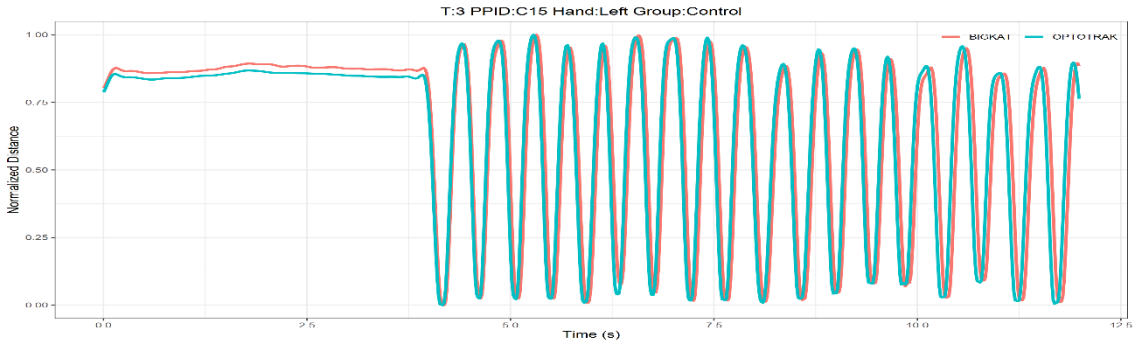
T:3 PPID:C15 Hand:Left Group:Control
BIOKAT
OPTOTRAK
Normalized Distance
1.00
0.75
0.50
0.25
0.00
0.0
2.5
5.0
7.5
10.0
12.5
Time (s)

g)

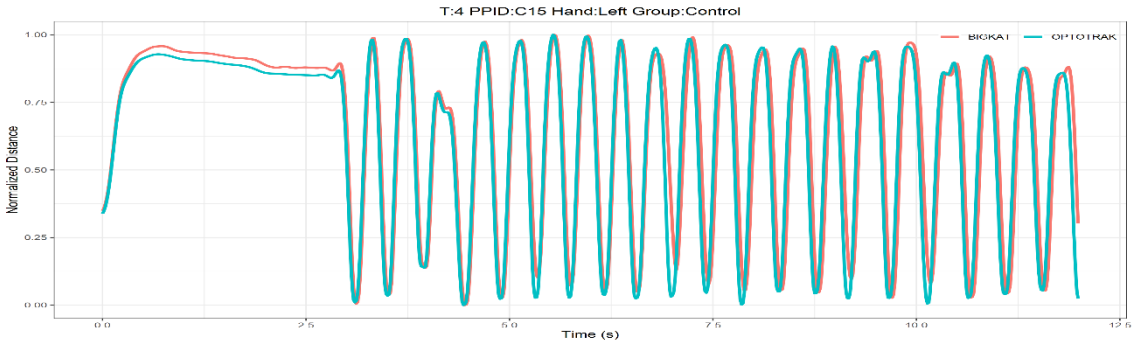
T:4 PPID:C15 Hand:Left Group:Control
BIOKAT
OPTOTRAK
Normalized Distance
1.00
0.75
0.50
0.25
0.00
0.0
2.5
5.0
7.5
10.0
12.5
Time (s)

h)

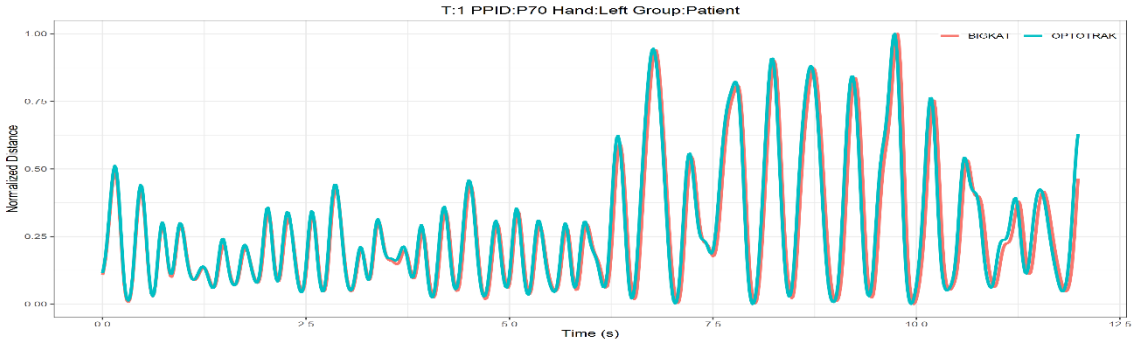
T:1 PPID:P70 Hand:Left Group:Patient
BIOKAT
OPTOTRAK
Normalized Distance
1.00
0.75
0.50
0.25
0.00
0.0
2.5
5.0
7.5
10.0
12.5
Time (s)

i)

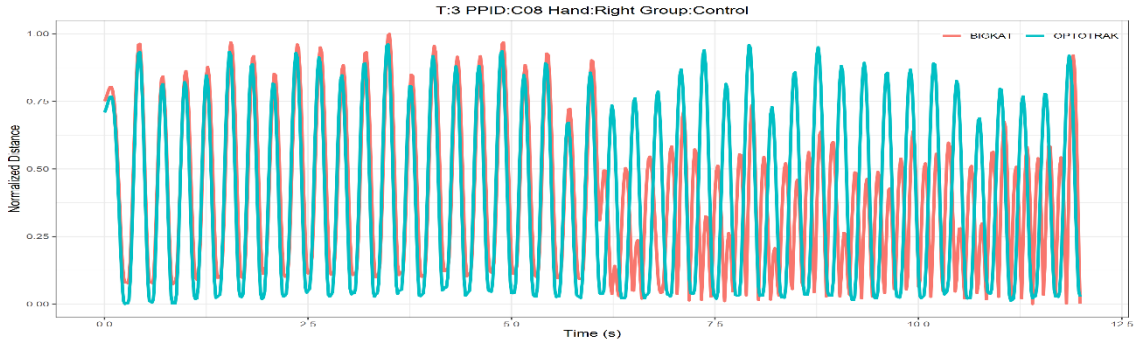
T:3 PPID:C08 Hand:Right Group:Control
BIOKAT
OPTOTRAK
Normalized Distance
1.00
0.75
0.50
0.25
0.00
0.0
2.5
5.0
7.5
10.0
12.5
Time (s)

j)

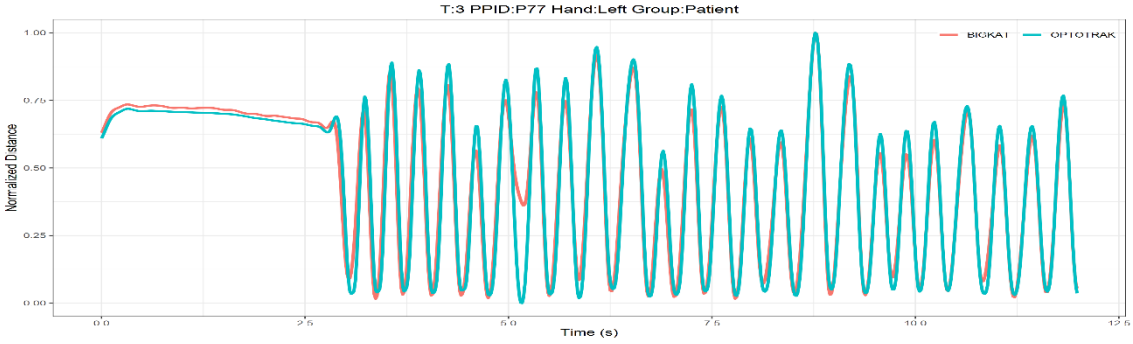
T:3 PPID:P77 Hand:Left Group:Patient
BIGKAT
OPTOTRAK
Normalized Distance
1.00
0.75
0.50
0.25
0.00
0.0
2.5
5.0
7.5
10.0
12.5
Time (s)

k)

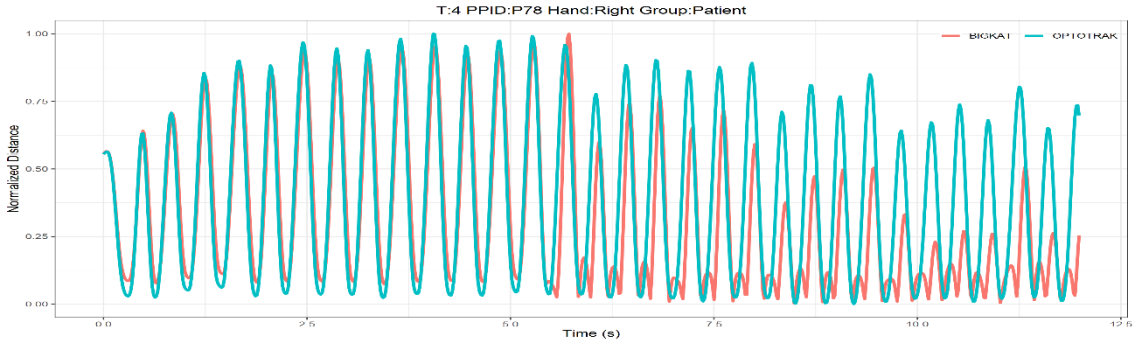
T:4 PPID:P78 Hand:Right Group:Patient
BIGKAT
OPTOTRAK
Normalized Distance
1.00
0.75
0.50
0.25
0.00
0.0
2.5
5.0
7.5
10.0
12.5
Time (s)

l)

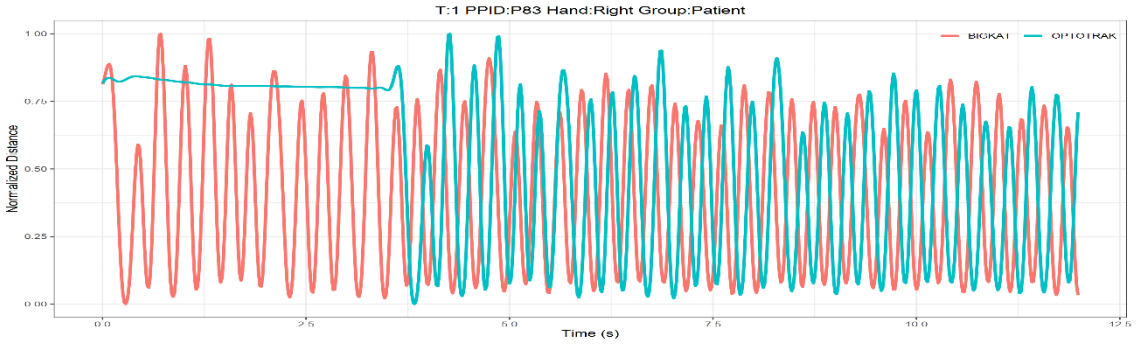
T:1 PPID:P83 Hand:Right Group:Patient
BIGKAT
OPTOTRAK
Normalized Distance
1.00
0.75
0.50
0.25
0.00
0.0
2.5
5.0
7.5
10.0
12.5
Time (s)

m)

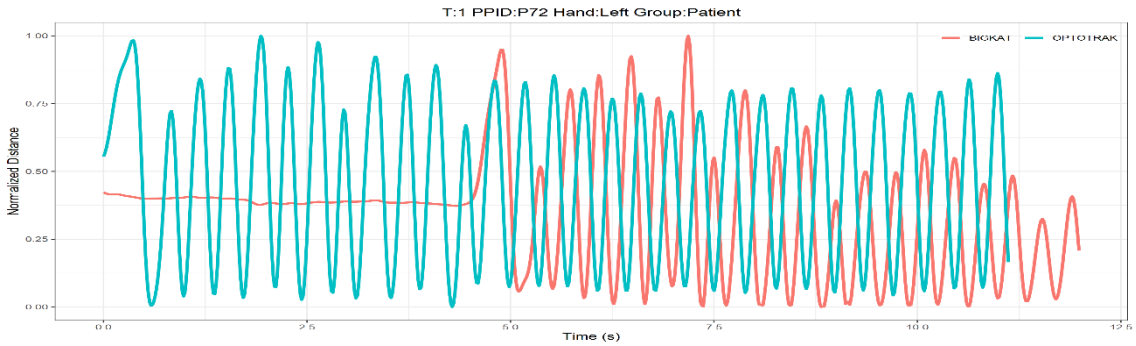
T:1 PPID:P72 Hand:Left Group:Patient
BIGKAT
OPTOTRAK
Normalized Distance
1.00
0.75
0.50
0.25
0.00
0.0
2.5
5.0
7.5
10.0
12.5
Time (s)

n)

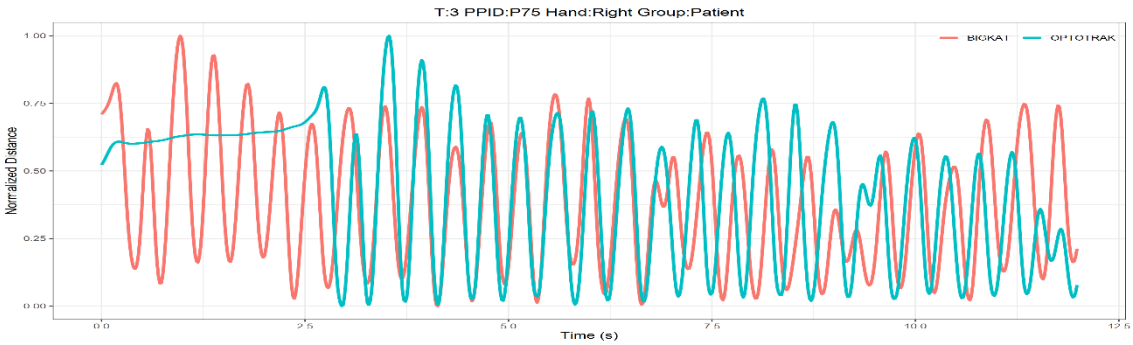

Figure 69: a to n shows all fourteen trials being detected as outliers. Each plot shows normalized distance between thumb and finger plotted over time for both BIGKAT and Optotrak. All outliers can be categorized into three categories: a - e) BIGKAT values are smaller than measured by Optotrak,f - k) trials lost synchronization during recording l -n) one of the two devices started recording earlier than other device.

Trials from category-II and III may still produce useful kinematic measures because normalized distance values are almost similar to Optotrak. This requires further investigation if FT measures obtained from BIGKAT produce statistically significant difference as obtained by Optotrak. For this purpose, category-I outliers (5 trials) were removed from the original dataset and quantitative analysis were carried out by running ANOVA for each FT measures to investigate if BIGKAT can discriminate between PD patients and healthy groups. Figure 70 shows the results for each FT measure and it is evident that BIGKAT can produce quantitively significant measures and can resolve FT movements efficiently as Optotrak.

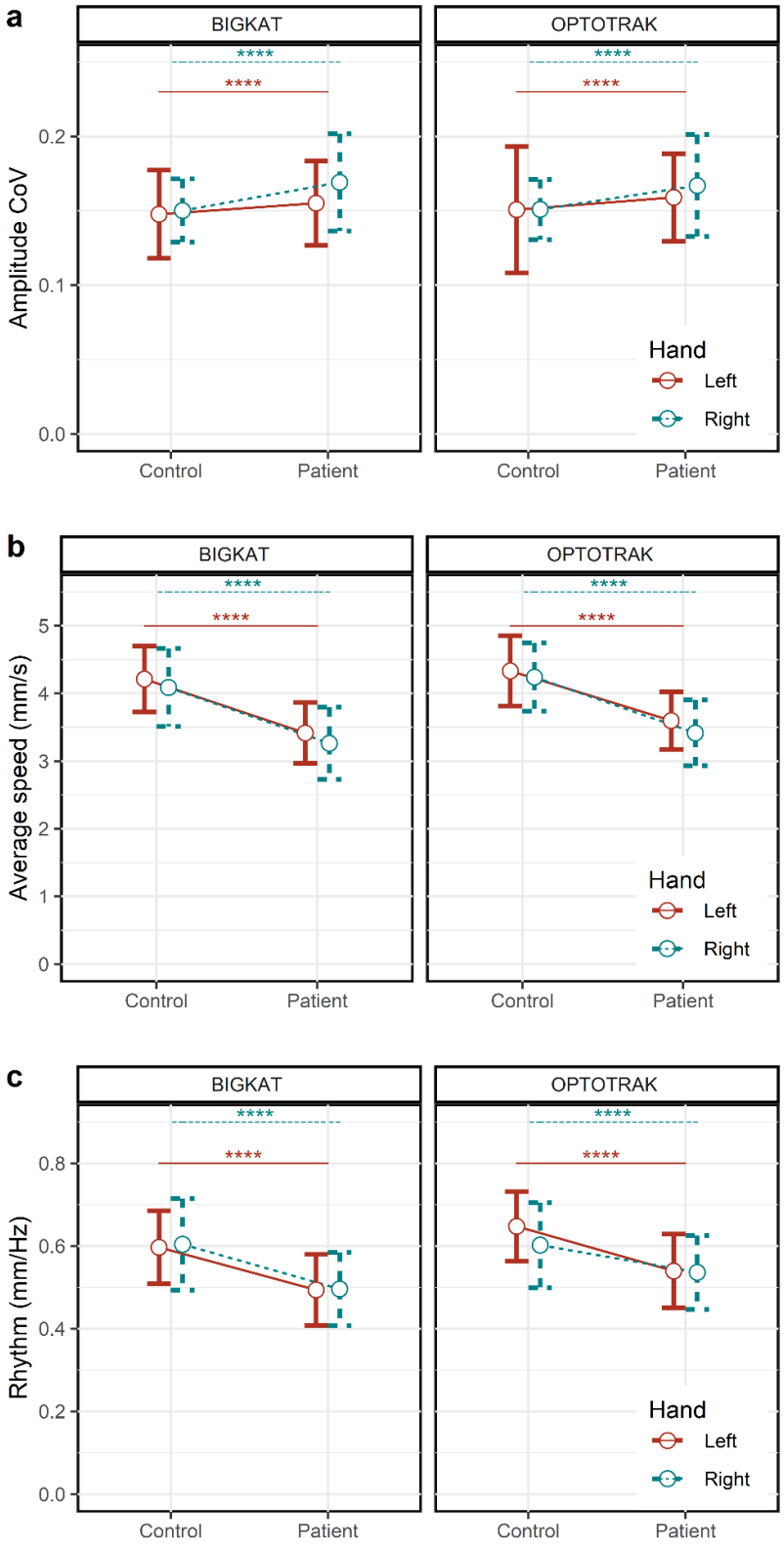

Figure 70: Objective FT measures extracted from BIGKAT and Optotrak recordings after removing outliers. BIGKAT detects statistically significant differences between PD patients and healthy controls in accordance with Optotrak measures.

5.5 Discussion

Quantitative assessment of bradykinesia in PD patients has seen a relatively large number of published studies over the last few years [52], [59], [68], [83], [85], [87], [89], [90], [184], [185], [219], [248]–[252]. They all were developed for the same purpose to objectively assess the severity of bradykinesia but differ in terms of introduced methodologies, movement analysis techniques, computer vision interpretation of 2D or 3d camera system, instrumentation, and signal processing techniques. Nevertheless, it remains to identify the suitable sensor system, best place on the body to obtain specific or global outcome measures and its acceptability for home based monitoring system. A systematic review analysing new methods for PD assessment published during 2005 – 2015 (848 studies) suggested that large number of studies were not available for clinical use and only 6% present of them could become available in near future [253].

The described motion capture system (BIGKAT) was successfully validated against Optotrak to determine spatiotemporal accuracy and had been used to study reach-to-grasp movements as well (see chapter 3). Therefore, in this chapter BIGKAT was deployed for the quantitative assessment of bradykinesia (FT movement) with the gold standard Optotrak system and simultaneous video recordings by Iphone for visual ratings by two neurological experts as well. The results proved that low-cost motion capture system BIGKAT is sufficient for computing the principal characteristics of bradykinesia and its potential usage in clinical settings.

We have shown that BIGKAT can track finger tapping by attaching IREDs at the distal end of finger and thumb of a PD patient in a conventional clinical examination, and kinematically analysing measures related to bradykinesia: average speed, amplitude variance and rhythm regularity. Expensive research grade optical motion capture system, Optotrak, found significant differences between patients and healthy controls for all three kinematic measures and for each hand [20], [232], [254]–[256]. Afterwards, linear regression analysis was carried out between the kinematic measures obtained from BIGKAT and gold-standard Optotrak, which revealed moderate R-squared value due to outliers present in the dataset. Upon further investigation, 14 outliers were identified and categorized in three categories depending on the source of error. Category-I outliers (5 trials) were excluded from further analysis of determining potential effect on the objective quantification of BIGKAT 3D positional data due to outliers. After removing outliers, BIGKAT determined statistically significant difference between the PD patients and healthy controls and for each hand as well. Hence, a strong relationship was found between the corresponding objective measures of finger tapping obtained from BIGKAT and Optotrak. Thus, BIGKAT measures exhibit convergent validity with Optotrak measures, and the results are statistically significant.

However, it is important to note that data should be checked for outliers before utilizing it for analysis using BIGKAT. The presence of outliers can affect the accuracy and reliability of the results. This requirement for outlier checking may pose a limitation on the use of BIGKAT by non-specialists who may not have the necessary expertise or knowledge to identify and handle outliers effectively.

In summary, the study highlights that BIGKAT has the potential to be used as a tool for studying human movement disorders, particularly in assessing prehension, bradykinesia, and postural instability. However, caution should be exercised in checking and addressing outliers in the data to ensure the accuracy and validity of the results. Non-specialists may require additional training and support to properly handle and interpret the data obtained from BIGKAT.

5.6 Conclusion

In this study, the Optotrak and BIGKAT 3D motion capture systems were used to objectively measure the finger tapping (FT) motion of PD patients and healthy controls. It was shown that these systems could distinguish between the two groups using the kinematic FT features average speed, amplitude variance, and rhythm irregularity. In contrast to visual ratings or timed instrumental tests, this enables researchers to independently analyse individual components by computing the primary features of FT movement in space and time. Furthermore, the FT features offered by the inexpensive BIGKAT had a linear correlation with the corresponding measurements produced by the research-grade Optotrak.

Chapter 6: Effect of absences of sensory feedback on prehension skills within Virtual Reality.

6.1 Introduction

The study undertaken in this chapter is part of a broader exploration into the potential of virtual reality (VR) as an alternative to optoelectronic systems like BIGKAT for measuring prehension movements. The aim of the thesis is to evaluate the suitability and effectiveness of VR technology in capturing and analysing prehensive performance. This chapter focuses on comparing prehensile performance in two virtual environments with different haptic feedback conditions, as well as comparing the performance in VR with real-world movements that provide both haptic and hand feedback. By examining the spatiotemporal characteristics, coordination between components, and the influence of feedback modalities on reaching and grasping kinematics, this study contributes to the broader investigation into the feasibility and applicability of VR as a tool for studying prehensive movements.

Virtual Reality (VR) has been used to kinematically analyse reach and grasp components with haptic feedback using wearable gloves [212] and without haptic feedback (visual feedback alone) [158]. These studies suggest that participants moved slower and showed longer relative deceleration times both during reaching and grasping as well as in pointing tasks [213] and took longer to complete a trial than in a physical environment. Specifically, previous studies suggest that the presence of intermittent or continuous haptic feedback in VEs improved grasping [132], [135], [159] but grasping was inaccurate in the absence of haptic feedback [214] and was more prominent such that the closure phase of reach-to-grasp movement was prolonged [158]. Though aperture scaling was preserved in both virtual and physical environments and MGA occurred at the same time but were much wider in VE when haptic feedback was present through haptic gloves [159], [212] than without haptic feedback [158]. So, wearing gloves affected both reaching and grasping components by decreasing the reaching velocity and increasing aperture size, respectively.

The study undertaken in this chapter differs from the previous studies in that it seeks to compare the prehensile performance in two VEs where in one haptic feedback was provided without gloves but through physical objects placed at predetermined positions (but with no vision of the hand) and the prehensile performance in another haptic free VE (hand vision alone) and then comparing VE performances with the real-world movements where both haptic and hand feedbacks are available. Prehension literature [132], [215] shows that the absence of haptic or visual feedback affects existing spatiotemporal characteristics such that the absence of visual feedback increases MGA and causes it to occur relatively earlier and so, this study aims to determine the phase specific differences in virtual reality and reality, as well as whether the coordination between the components is preserved while performing in VEs. We also sought to determine whether reaching kinematics were affected by the

absence or presence of hand feedback and similarly, if grasping kinematics were affected by the provision of haptic feedback in VE.

Since kinematics of reach-to-grasp movements are highly stereotypical in nature, though controlled relatively independently, they change lawfully as a function of the task and the properties of the object [5], [145]. As found in chapter 4, Spatial and temporal characteristics of prehensile movements vary with respect to the task constraints such that the transport component is effected by the object distance causing PV to increase as well as causing PV to occur later in the movement; similarly, large grasp size lowers spatial accuracy demands while permitting a faster movement and the hand opens up to a larger MGA and smaller grasping size demands higher precision during grasping phase [4], [139], [141]. However, the reach and the grasp components of reach-to-grasp movements made in virtual environments (VEs) with the provision of haptic or visual feedback may be altered compared to the movement made in a physical environment. Successful reaching and grasping requires information about the object distance from the body and the size of the object, respectively, and such information is available from the visual system. The Visual system is used to extract intrinsic properties (Size, shape, colour) therefrom preparing and adjusting grasp component and similarly, to extract extrinsic properties (object distance and orientation) to guide hand towards target. In the absence of sensory information, prehensile movements show systematic biases, signifying the importance of online sensory information to guide the hand until it makes contact with the object [132]–[134]. And in order for the grasping action to be completed successfully, information about fingers position and object contact points is sufficient [135]–[137].

Our goal was to systematically describe the temporal and spatial kinematic differences, when a participant was asked to reach and grasp objects of different widths placed at two different distances in a physical environment; when in an equivalent haptic free virtual environment; and also when in an equivalent haptic based virtual environment but without real-time hand feedback. Therefore, the general aim of this study was to understand how providing hand vision or haptics alternatively during reach-to-grasp movement in VR alter spatiotemporal characteristics and the trade-offs that experimenters should expect by comparing reach-to-grasp kinematics with those obtained from physical environments.

It was hypothesized that lower and earlier peak reaching velocity and longer deceleration and movement times would be observed in VEs. It was also hypothesized that wider grip apertures would be observed in VE without hand vision (haptic feedback available) than in VE with hand vision (without haptic feedback) and it will occur relatively earlier when haptic feedback is available. Moreover, it was also hypothesized that coordination between reaching and grasping kinematics made in VEs would not be different from the natural prehension movements. To test these hypotheses, two equivalent

VEs were created in the Unity game engine (Unity, 2018) (Steamvr, 2018) such that each environment was deprived of one of the two important sensory feedbacks required for successful reach-to-grasp movements. Spatiotemporal measures extracted from movements made in VEs would then be compared with measures obtained from physical environment to seek the underlying differences. In order to do so, experimental conditions must remain constant between physical and virtual environments such as object must be located at the same distance from the start point and must share the same object properties i.e., shape and size. Hence, virtual and real environments were calibrated and aligned using a HTC vive tracker to avoid any mismatch, thus, making sure that experimental setup does not move as participant moves his or her head while making movements in VEs. Similarly, a Leap Motion controller, which was designed for hand and finger tracking with an accuracy of 0.01mm, was used throughout the trial to provide real-time hand visual feedback, such as hand opening/closing. Leap motion controller allows virtual and real objects to co-exist and interact in real-time [257] and have been used in the field of neurorehabilitation as marker-less motion sensing to collect hand and wrist movement [258], [259].

Another important benefit of using VR to study prehension is the fact that the third component of prehension (orientation) can be manipulated by rotating the object during the movement forcing the participant to orient their hand accordingly as well as forcing participants to make online corrections by perturbing the object position and above all it can be used to design numerous experiments like affordances and illusions (shape/weight etc) which are difficult to realize in the real world. Moreover, VR systems allow visual stimuli to be displayed in a 3D simulated environment and supports naturalistic interactions with virtual objects but can only provide hand position, therefore, lacks the ability to provide of providing individual finger(s) position. So, to obtain precise and detailed kinematic measures in response to displayed visual stimuli, modern VR systems like HTC vive (used in this study) allows other devices like Leap motion to project real-time hand visual feedback (finger opening/closing) onto the VR display, and also allows Leap motion controller to be secured to the front of the headset as shown in Figure 71. Leap motion controller can be interfaces with HTC vive using the Leap motion software development kit (SDK) and Unity. Leap motion SDK provides a set of APIs which were used to project the real-time hand feedback onto the VR display. In this study, 3D positional data was recorded with an optical motion capture system (Optotrak, NDI Inc.) and BIGKAT couldn't be deployed because HTC base stations used infrared (IR) light to track the headset and controller which then interferes with BIGKAT's positional data. On the other hand, Optotrak actively communicates with its IR markers means that it cannot get confused by other sources of IR, whereas BIGKAT will just pick up all other IR sources in view.

Figure 71: Leap motion controller interfaced with HTC vive haedset to project real-time hand opening/closing.

6.2 Design

Conventional prehension studies are performed by manipulating two independent variables (object width and object distance) which in turn vary the spatiotemporal characteristics of prehensile movement. But, in this study, other than object width and object distance, sensory feedback (hand visual feedback and object haptics) was manipulated in two VEs. The experimental design is shown in Figure 72, where in one environment participant enjoys both visual and haptic feedback (termed as real) and VEs were alternatively deprived of sensory feedbacks and were accessible only by wearing VR headset. These VEs were termed as HV (hand vision feedback without haptic feedback) and Hap (Haptic feedback without hand vision). All blocks were then manipulated with objects of different widths (50 & 70mm) placed at two different distances of 200 & 400mm from the start position so that effect of absences of sensory feedback on existing spatiotemporal prehensile relationship can be understood.

	Hand Vision	No Hand Vision
Haptics	Real	Hap
No Haptics	HV	NA

	Object Width (mm)	
Distance(mm)	50	70
200	10 trials	10 trials
400	10 trials	10 trials

Figure 72- 2X2 experimental design where each environment consists of 40 trials. Environments were counter-balanced and in each environment object distance and width was covaried.

6.2.1 Unity Experimental Framework (UXF)

3D positional data was collected using research grade optical motion capture system (Optotrak) and data handling was performed via Unity Experimental Framework (UXF) developed by Brookes et al

[260]. With the C# programming language and Unity (3D graphics engine), which was primarily created for game designers, UXF offers a collection of tools for the development of human behaviour experiments. UXF allows behavioural researchers to generate a session-block-trial model for the task which presents stimuli and record trial-by-trial responses. In our study, the task itself was developed in Unity for two VEs (HV & Hap) and UXF handled several aspects of the experiment including participant information, trial conditions and stores 3D positional data for each trial in a separate folder [260].

To project real time hand movement onto the VR headset, a Leap motion controller was interfaced in Unity using a Software Development Kit (SDK) which was then manipulated for two VEs to provide hand visual feedback or otherwise. Likewise, within each environment (VE and real) dependent variables (object distance and width) were manipulated to record prehensile movements using Optotrak, so that, effect of absences of sensory feedback can be understood. Trials between different factors environment, object size and distance were counterbalanced using UXF framework. And UXF automatically creates a folder as per experimental conditions and stores 3D positional data of each IRED under participant ID. The "nuts and bolts" that keep an experiment created in Unity running are provided by UXF. Every data file is kept in a directory structure that is set up according to experiment, participant, and session numbers.

6.3 Method

Twenty unpaid participants of age 20-35 were recruited for this study. All participants were right-handed, gave their informed consent prior to participating and were naive as to the purpose of the experiment. None had any history of neurological deficit, and all had normal or corrected to normal vision. The study was approved by the ethics committee in the School of Psychology at the University of Leeds, and therefore performed in accordance with the ethical standards laid down in the Declaration of Helsinki.

Each trial was prepared by placing a wooden object at one of the two distances; and the participant prepared by holding the start position between the thumb and index finger which was defined by a moulded grip and was close to the edge as shown in Figure 73a&b. Participant can both visually see and haptically feel the start position in both VR blocks. Participants were instructed to reach for and grasp an object that could be located at a distance of 200 or 400mm from the hand start position in the sagittal plane and can be reach with the simple extension of the arm. Two wooden objects of the same depth (D) and height (H) but of different widths (50 and 70mm), determined by small sections of circular dowel affixed to the left and right side of the object but set back 15mm from the top of the object, were used in this study as shown in Figure 73c. the circular dowel acted as a grasping surface

(diameter 10mm) and participants were told to grasp the object by grasping surface. Each participant performed 10 trials at each movement amplitude and object size combination, resulting in a total of 40 trials per block type and overall, 120 trials for the whole experiment.

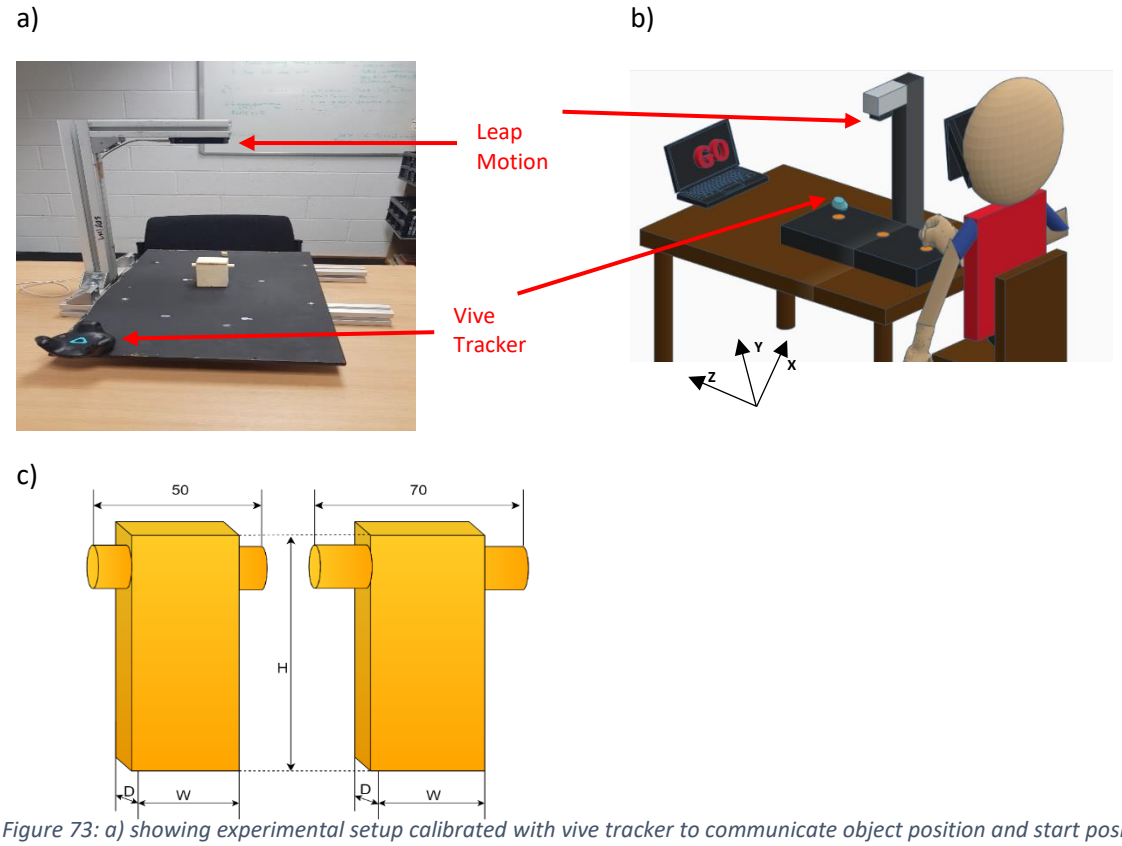

Figure 73: a) showing experimental setup calibrated with vive tracker to communicate object position and start position via Unity and Leap motion projecting hand opening/closing to HTC headset b) particpants wearing headset and holding start position at the start of each trial in VEs c) two wooden objects of same dimensions but differes in grasping surface size.

Kinematic data were recorded with a 3D optical motion capture system (Optotrak, NDI Inc.) for 4 seconds at 90 Hz. Data acquisition was initiated 1.5 seconds before the "go" command (displayed in VR and on LCD in real block) and the participant's task was to reach and grasp the object at the "go" and the "whistle" signal simultaneously. To record the reach responses infrared-emitting diodes (IREDs) were attached to the wrist and, similarly, to record the grasp responses two IREDs were attached to the distal joint of the index finger and thumb.

6.4 Data Analysis

Positional data was low-pass filtered with a 4th order Butterworth filter at a cut off frequency of 6 Hz. The onset of the movement was determined by identifying the time instant at which the rate of change of wrist position exceeds 50 mm/s, which indicated the start of the movement. The offset of the movement was determined when the wrist speed decreases below 50 mm/s, which indicated the end of the movement. Trials were then cropped to include only the segment of the movement between the onset and offset points. It was performed to isolate and focus on the reaching and grasping phase

of the trial. The temporal difference between the movement onset and offset is defined as the movement time (MT), which represents the duration of the trial in which the movement was made.

Tangential velocities during the reaching phase for all trials were obtained by the differentiation of the positional data of the wrist IRED. From velocity data, peak velocity (PV) and its time of occurrence (TPV) was determined for all trials. Similarly, during the grasping phase, aperture opening/closing was determined by measuring the distance between the thumb and index finger IREDs to calculate maximum grip aperture (MGA) and its time of occurrence (TMGA). To determine the temporal coordination difference between the two temporal parameters (Delay (TPV - TMGA); both normalized to MT) was calculated.

As reported in the introduction section, participants usually tend to increase grip aperture when no hand visual feedback is available due to the perceptual uncertainty ,thereby increasing safety margin to avoid hitting the object and under visuo-haptic guidance grip aperture is maximally optimized [214], [261]. Safety margin is defined as the difference between the MGA and the object width. It was calculated by taking the average across all participant and trials for all three environments. It would highlight that how safety margin varies with respect to the availability/unavailability of feedback type. To determine how grip aperture profile varies, index of curvature (IC), was estimated as the ratio of the endpoint trajectory length to the distance between initial and final position [262].

6.5 Results

6.5.1 Trajectories Comparison

To determine how the reach and grasp components relate in different block types, Pearson's correlation coefficients were calculated between real and VEs and then averaged across all participants and trials and are presented in Table 10. Movement trials were averaged across all participants and conditions to plot the finger, thumb and wrist trajectories as shown in Figure 74, which depicts invariant movement patterns in the horizontal XZ plane. Strong correlation and invariant movement patterns between wrist velocity and grip aperture profiles between all environments showed that participants used similar reach-to-grasp strategies, preserving the coordination between reaching and grasping components.

Table 10: Pearson correlation between each VR block with Real block grip aperture and wrist velocity profiles

Real vs VEs	Object Width	Distance	Grip aperture	Wrist Velocity
Real vs HV	5	20	0.95±0.05	0.92±0.14
		40	0.94±0.05	0.93±0.12
	7	20	0.97±0.04	0.93±0.10
		40	0.95±0.05	0.91±0.12
		Mean	**0.95±0.05**	**0.92±0.12**
Real vs Hap	5	20	0.95±0.06	0.87±0.15
		40	0.94±0.05	0.89±0.16
	7	20	0.97±0.04	0.89±0.13
		40	0.95±0.05	0.87±0.16

Mean	0.95±0.05	0.88±0.15

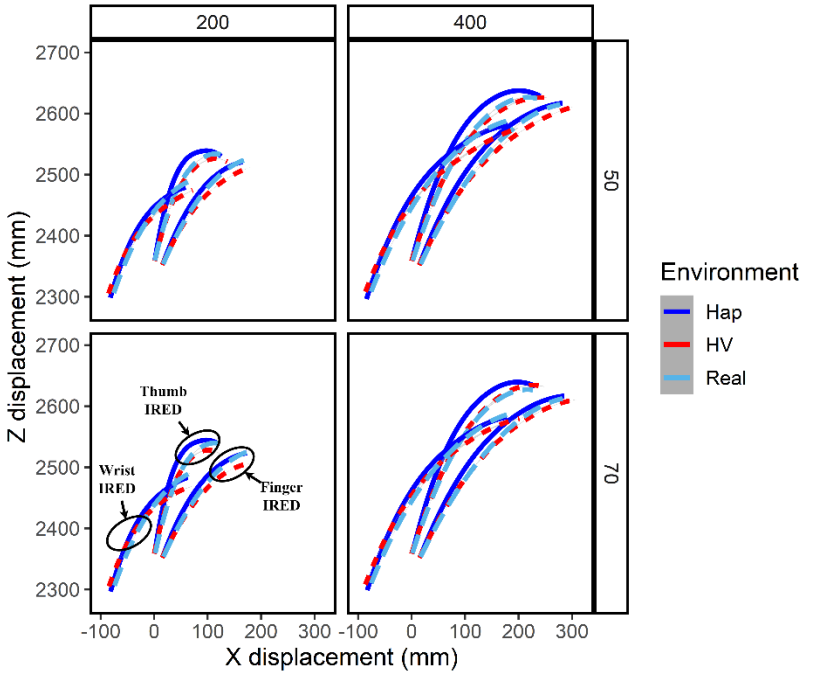

Figure 74: Trajectories of each IRED averaged across all trials and participants while reaching out for grasping an object of different sizes placed at two different distances in all three environments (physical & virtual).

The relationship between grip aperture profiles in real and VEs showed identical correlation (0.95 ± 0.05) irrespective of the availability of sensory feedback. The reaching component showed stronger correlation between real and HV (0.92 ± 0.12) than Hap (0.88 ± 0.15). To eliminate the effect of variation of movement time, time was normalized using min-max normalization to compare the corresponding reaching and grasping profiles. Figure 75a&b shows time normalized wrist velocity and grip aperture profiles, respectively, averaged across all conditions for real and VEs which clearly depicts invariant movement patterns but with varying values of MGA and PV and their time of occurrence.

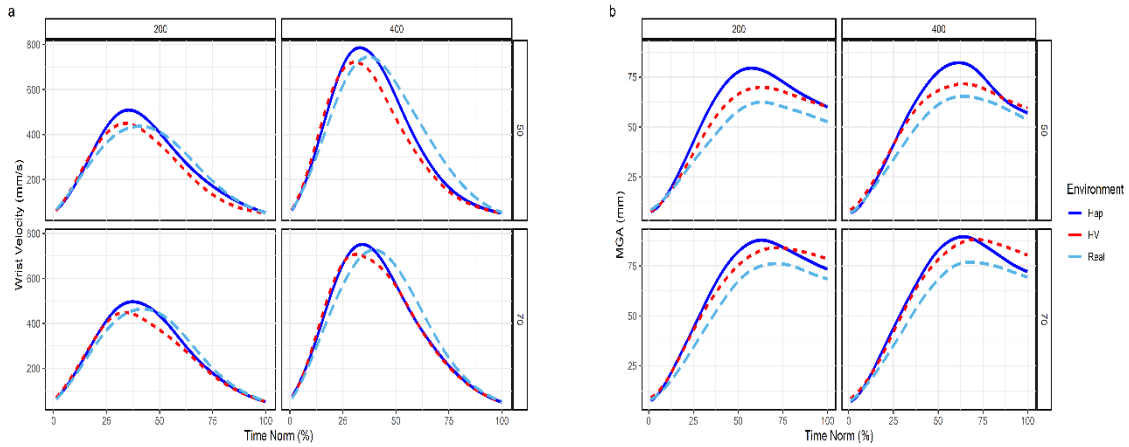

Figure 75: Normalized grip aperture and wrist velocity profiles across all trials and participants while reaching out for grasping an object of different sizes placed at two different distances in all three environments (physical & virtual).

6.5.2 Kinematics Comparison

6.5.2.1 Movement Time

A 3x2x2 repeated measures analysis of variance with factors Environment (Real, HV, Hap), object distance (200 & 400mm), object Width (50 &70mm) was used to evaluate the differences between real and VEs for all calculated kinematics.

Table 11 presents the spatiotemporal kinematics calculated for all conditions. Factor environment revealed a significant main effect for MT ($F_{(2,38)} = 31.43, p < 0.0001, \eta_G^2 = 0.522$) such that on average longer MT was observed in HV ($933.959 \pm 228.532ms$) than in Hap ($907.195 \pm 186.513ms$) and MT was lower in real environment ($733.478 \pm 147.737ms$) than in both VEs as shown in Figure 76. Post-hoc analysis showed significant differences between real and VEs ($Real\ vs\ HV: TukeyHSD: p < 0.0001, d = 1.21, Real\ vs\ Hap: HSD: p < 0.0001, d = 1.34$) and smaller significant difference between VEs ($HSD: p < 0.05, d = 0.15\ negligible\ effectsize$). Factor distance showed a main effect ($F_{(1,19)} = 139.71, p < 0.0001, \eta_G^2 = 0.562$) and on average participants took longer to reach-to-grasp farthest objects ($952.384 \pm 210.813ms$) than the nearest object ($762.359 \pm 157.399\ ms$). Post-hoc showed significant differences between MT for object placed at two distances ($HSD: p < 0.0001, d = 1.02$). There was a significant interaction between factors distances and environments ($F_{(2,38)} = 16.92, p < 0.0001, \eta_G^2 = 0.044$) and Post-hoc analysis showed significant effect of environments at each level of distance as shown in Figure 76, revealing significant differences between real and both VR blocks and no significant differences was found between VEs. No significant effect of object width was observed for MT.

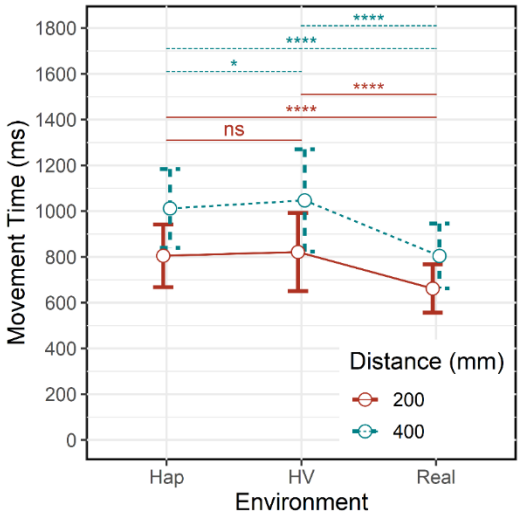

Figure 76: Effect of environment on movement time. It shows significant differences between real and VEs and negligible effect size within VR.

Table 11: Reach-to-grasp movement kinematics for all conditions across all participants and trials.

Environment		Distance	MT	MGA	TMGA	PV	TPV	IC	Delay	Safety Margin
Real	5	20	0.66	93.99	0.46	802.51	0.29	1.24	0.26	43.99
		40	0.81	94.43	0.6	1189.30	0.35	1.19	0.31	44.43
	7	20	0.66	106.45	0.48	809.42	0.29	1.22	0.28	36.45
		40	0.79	106.98	0.61	1204.70	0.34	1.18	0.34	36.98
HV	5	20	0.83	98.44	0.60	674.98	0.34	0.23	0.31	48.44
		40	1.04	99.29	0.78	1052.09	0.38	0.27	0.37	49.29
	7	20	0.81	112.44	0.60	683.39	0.33	0.22	0.32	42.45
		40	1.05	113.65	0.82	1049.56	0.39	0.24	0.40	43.65
Hap	5	20	0.81	108.84	0.51	689.83	0.32	1.29	0.23	58.84
		40	1.01	111.6	0.68	1082.34	0.37	1.21	0.30	61.66
	7	20	0.79	118.18	0.53	709.80	0.32	1.28	0.25	48.18
		40	1.00	119.99	0.68	1074.96	0.37	1.20	0.31	49.99

6.5.2.2 Max. Wrist Velocity

The ANOVA showed a significant main effect of Environment and distance for maximum wrist velocity $\left(F_{(2,38)} = 11.01, p < 0.0001, \eta_G^2 = 0.10\right)$ and $\left(F_{(1,19)} = 98.08, p < 0.0001, \eta_G^2 = 0.54\right)$, respectively. Post-hoc analysis of environment effect on wrist velocity showed significant differences between real and VEs $(Real\ vs. HV\ (HSD: p < 0.05, Cohen's\ d = 0.76),\ Real\ vs\ Hap\ (HSD: p < 0.05, Cohen's\ d = 0.8)$ as shown in Figure 77, which suggests that participants move slower in both VR environments $(HV: 865 \pm 197.75\, mm/s\, , Hap: 889.23 \pm 145.28\, mm/s)$ and were faster in the real environment $(1001.48 \pm 174.31\, mm/s)$. Similarly, it is evident from the Figure 77 that objects nearest to the starting point forced participants to reach at lower wrist velocity $(728.32 \pm 143.12\, mm/s)$ than the farthest object$(1108.83 \pm 201.78\, mm/s)$. Post-hoc $(HSD: p < 0.0001, Cohen's\ d = -1.75)$. No significant interaction between factors were found for wrist velocity and object width caused no such effect on wrist velocity.

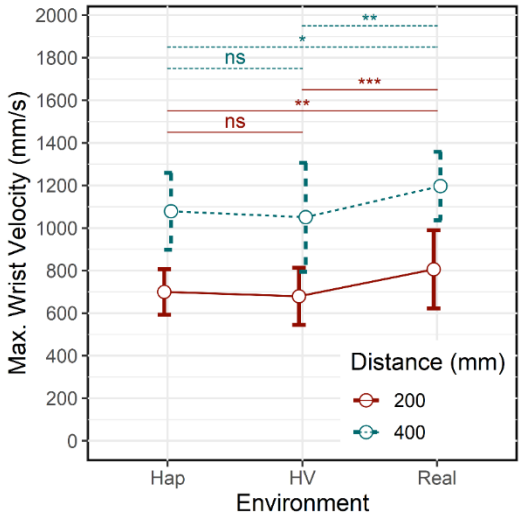

Figure 77: Effect of environment on Maximum wrist velocity

6.5.2.3 Time to Max. Wrist velocity

Factor environment showed a significant main effect $\left(F_{(2,38)} = 14.75, p < 0.0001, \eta_G^2 = 0.092\right)$ on time to maximum wrist velocity such that participants took longer to reach maximum wrist velocity in VR $(HV: 362.02 \pm 87.26\, mm/s\,, Hap: 345.02 \pm 66.19\, mm/s)$ than in real environment $(Real: 317.49 \pm 66.09\, mm/s)$. Post-hoc analysis revealed moderate effect size $(p < 0.0001, d = 0.65)$ between Real and HV, and between Real and Hap $(p < 0.05, d = 0.51)$, and between HV and Hap $(p > 0.0.05, d = 0.24)$ as shown in Figure 78. Factor distance also showed a main significant effect $\left(F_{(1,19)} = 69.02, p < 0.0001, \eta_G^2 = 0.15\right)$. Post-hoc analysis $(p < 0.0001, d = 0.67)$. Object width showed no significant effect.

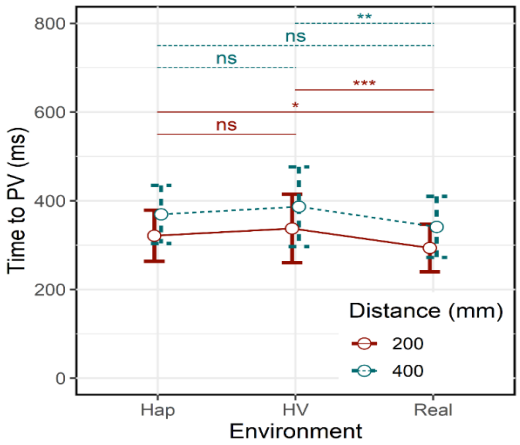

Figure 78: a) Effect of environment on Time to Maximum wrist velocity

6.5.2.4 Max. Grip Aperture

Analysis of MGA showed a significant main effect of all factors; environment $\left(F_{(2,38)} = 28.65, p < 0.0001, \eta_G^2 = 0.26\right)$, object width $\left(F_{(1,19)} = 188.82, p < 0.0001, \eta_G^2 = 0.26\right)$ and distance$\left(F_{(1,19)} = 5.80, p < 0.001, \eta_G^2 = 0.004\right)$. ANOVA showed significant interaction between object width and environment $\left(F_{(2,38)} = 7.19, p < 0.001, \eta_G^2 = 0.012\right)$ suggesting that grasping parameters were influenced by environment and differed by object width which confirms the fact that grip aperture was scaled accordingly and was preserved in both environments.

Large grip aperture was observed in Hap $(114.82 \pm 12.60\, mm)$ than HV $(106.50 \pm 16.61\, mm)$ but was lower in real $(100.50 \pm 10.98\, mm)$ than both VEs. Similarly, large safety margins were observed while grasping objects in Hap $(54.70 \pm 13.07\, mm)$ than HV $(46.42 \pm 15.24\, mm)$ but was lower in real $(40.54 \pm 9.72\, mm)$ than both VR suggesting wider grip apertures in VR. Post-hoc analysis between block types showed small effect size between Real and HV $(HSD: p < 0.001, Cohen's\ d = 0.43)$, large effect size between Real and Hap $(HSD: p < 0.0001, Cohen's\ d = 1.21)$ and moderate effect size between HV and Hap $(HSD: p < 0.0001, Cohen's\ d = 0.56)$ as shown in Figure 79.

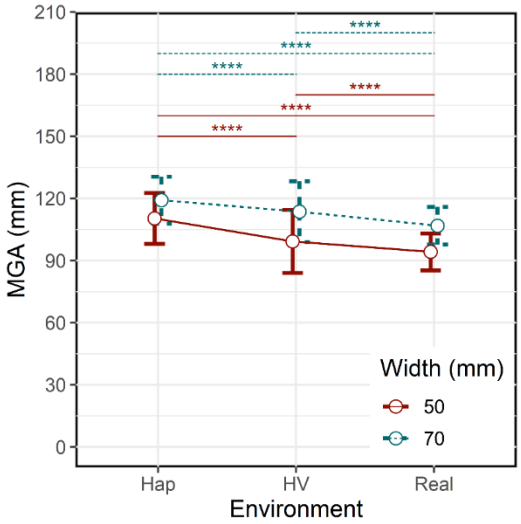

Figure 79: Effect of environment on Maximum Grip Aperture and revealed significant differences for MGA achieved in different sensory modalities.

As expected, post-hoc analysis revealed large effect size of object width ($HSD: p < 0.0001, Cohen's\ d = -0.88$) as shown in Figure 79 such that grip aperture was scaled with respect to the size such that for larger object MGA was wider ($113.22 \pm 12.94\ mm$) than smaller object ($101.25 \pm 14.09\ mm$). Safety margin was smaller ($43.22 \pm 12.94\ mm$) for objects with width larger than smaller object width ($51.25 \pm 14.09\ mm$). Furthermore, object distance showed an effect on MGA and post-hoc test showed minor significant difference ($p = 0.021$) with negligible effect size ($d = 0.096$). Post-hoc test for the significant interaction between object width and block type, showed significant differences between all block types at each level of distance and width as shown in Figure 80.

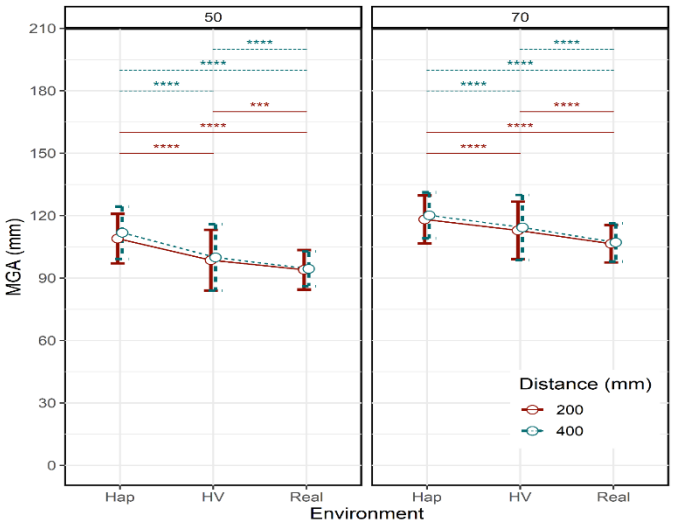

Figure 80: Effect of environment at each level of object width and distance on Maximum Grip Aperture

6.5.2.5 Time to Max. Grip Aperture

Likewise, ANOVA results showed that time to MGA was influenced by all the factors and significant interaction was observed between type of environment and distance. Factor environment had a significant effect $\left(F_{(2,38)} = 23.61, p < 0.0001, \eta_G^2 = 0.23\right)$ such that MGA occurred later in HV $(703 \pm 171\ ms)$ than Hap $(599.97 \pm 90\ ms)$ but achieved earlier in real $(539.03 \pm 93.92\ ms)$ than both VEs. Post-hoc analysis main significant differences between all block types$(p < 0.0001)$. Factor object distance revealed a significant main effect $\left(F_{(1,19)} = 126.51, p < 0.0001, \eta_G^2 = 0.31\right)$ that maximum aperture was achieved later for the farthest object $(695.87 \pm 133.74\ ms)$ than the nearest object $(532.08 \pm 103.04\ ms)$. Post-hoc test showed a large effect size $(p < 0.0001, d = 0.96)$. Object width also showed a minor significant effect $\left(F_{(1,19)} = 7.18, p < 0.05, \eta_G^2 = 0.003\right)$ and post-hoc test also showed a significant effect $(p < 0.05)$ but Cohen's effect size was negligible $(d = 0.09)$ which on average showed $(13.96\ ms)$ difference between large and small object widths. Significant interaction was also found between environment and distance$\left(F_{(2,38)} = 11.37, p < 0.001, \eta_G^2 = 0.013\right)$. Post hoc analysis showed a significant effect across each type of environment as shown in Figure 81.

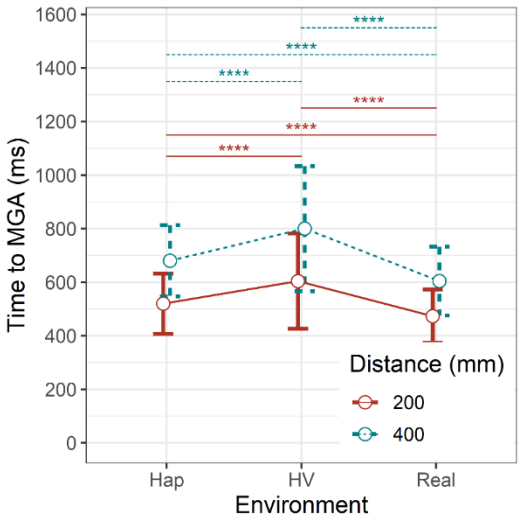

Figure 81: Effect of environment on Time to Maximum Grip Aperture and revealed significant differences.

6.5.2.6 Index of Curvature

ANOVA showed a significant effect of distance $\left(F_{(1,19)} = 126.51, p < 0.0001, \eta_G^2 = 0.31\right)$ on trajectory straightness such that objects placed at the farthest distance (1.19 ± 0.08) showed smaller index of curvature than the nearest ones (1.26 ± 0.10) whereas object width showed no such effects. Post-hoc analysis of distance for the index of curvature showed large effect size $(p < 0.0001, d = 0.69)$. Factor environment also showed a significant effect on index of curvature $\left(F_{(2,38)} = 23.61, p < 0.0001, \eta_G^2 = 0.23\right)$ and post-hoc analysis of type of environment showed significant differences between real and Hap $(p < 0.0001, d = 0.53)$, between HV and Hap $(p < 0.0001, d =$

$1.01)$ and smaller effect size between real and HV $(p < 0.0001, d = -0.31)$ suggesting effect on trajectory straightness with the unavailability of hand vision. ANOVA also revealed a significant interaction between distance and environment $\left(F_{(2,38)} = 11.38, p < 0.001, \eta_G^2 = 0.01\right)$ Post-hoc analysis of interaction between distance and bock type also showed no significant interaction when participants had access to hand vision but significant differences was observed when there was no hand vision available as shown in Figure 82.

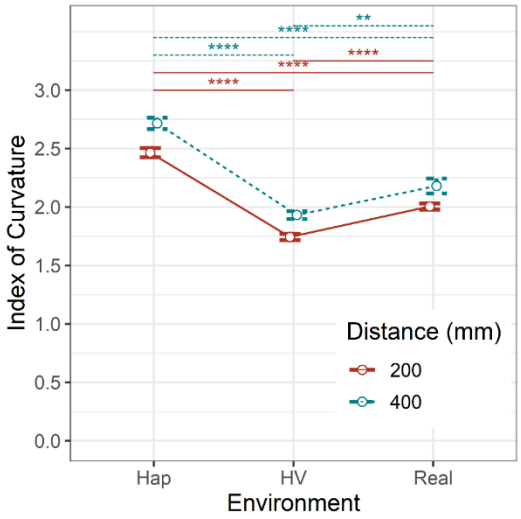

Figure 82: Effect of environment on Index of Curvature.

6.5.2.7 Delay (TPV - TMGA)

To determine the temporal coordination between reaching and grasping components, ANOVA was carried out for the difference between the TPV and TMGA. Factor environment showed significant differences $\left(F_{(2,38)} = 18.25, p < 0.0001, \eta_G^2 = 0.21\right)$ on temporal coordination showing higher delay for the movement performed in HV (0.35 ± 0.08) than Hap (0.27 ± 0.05) and real (0.29 ± 0.06), respectively, as shown in Figure 83. Post-hoc test showed moderate effect size $(p < 0.0001, 0.27)$ for HV. On running ANOVA on factor distance showed main significant effect $\left(F_{(1,19)} = 59.65, p < 0.0001, \eta_G^2 = 0.19\right)$ such that it was smaller for nearest objects (0.28 ± 0.07) and higher for object placed at farthest distance (0.34 ± 0.06). Post-hoc test revealed moderate effect size $(p < 0.0001, 0.63)$. Similarly, object width also showed significant effect on temporal coordination $\left(F_{(2,38)} = 11.46, p < 0.001, \eta_G^2 = 0.02\right)$ such that it was smaller for smaller object (0.29 ± 0.06) than for large object size (0.32 ± 0.06) but post-hoc test revealed negligible effect size. No interaction was found between all the factors.

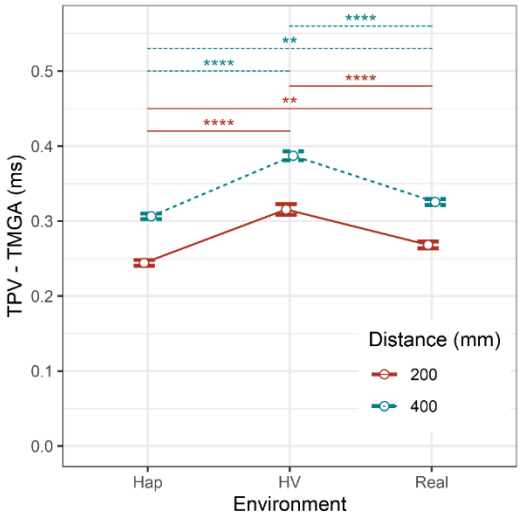

Figure 83: Effect of environment on the temporal coordination and shows significant effect.

6.6 Discussion

VR systems offer opportunities for the development of novel strategies that can stimulate different sensory systems in difficult to reach populations which in turn support treatment, enhance real-world functional improvements, and speed up the recovery process. However, investigation is still required to determine whether the reach-to-grasp movements produced in virtual environments are kinematically similar to real-world movements.

So, the goal of our study was to compare prehensile performance in two VEs with the provision of alternative sensory feedback and then comparing prehensile performance performed in real world environment where all sensory feedbacks were available. We found that kinematics of the reach component was strongly affected by the visibility of the hand in VEs such that the reaching in 'HV' environment was highly correlated with real environment than' Hap'. Similarly, grasping profiles produced in VEs was compared with grasping produced in real environment which showed strong correlation values indicating that grip aperture gets scaled according to the object size. Upon further investigation by plotting the profiles of reaching and grasping component over normalized time, it was found that shows movement made in real and VEs clearly depicts invariant movement patterns but with varying values of MGA and PV and their time of occurrence as shown in Figure 75a&b and grasping kinematic landmarks (MGA, TMGA) showed significant differences among environment as shown in Figure 80 & Figure 81. It suggests that even if the absolute landmarks changed in different environments, the correlations between conditions held, such that differences were preserved and strong correlation between wrist velocity and grip aperture profiles across environments showed that participants used similar reach-to-grasp actions, preserving the coordination between reaching and grasping components.

We compared reaching and grasping kinematics to two objects in real and virtual environments and were interested in determining whether the kinematics of reach-to-grasp movements produced in the absence of haptic or visual feedback are comparable to real-world movements. As reported in the previous literature, we also found that participants move slower in VR with longer movement and deceleration times [158], [212]. We found significant differences between Real and VEs regarding MT but within VEs post-hoc test showed significant difference for farthest object as shown in Figure 76 and cohen's d value was negligible between VEs suggesting that in VR absence of haptic or visual feedback doesn't affect MT but it's always greater than real-world prehensile movement.

Like MT, participants moved slower in VEs achieving maximum wrist velocity relatively later in the movement showing significant differences to the real-world prehensile movement as shown in Figure 77 but within VEs no significant differences were found for PV. To access the role of haptics or hand vision on wrist velocity, cohen's d analysis showed a small effect size between real and VEs suggesting that absence of sensory feedback in VR didn't affect maximum wrist velocity but VR itself is responsible for slowness of movement making participants more cautious while reaching towards the object. Moreover, cohen's d value showed moderate effect size for TPV while comparing 'HV' VE with real environment and small effect size was observed in 'Hap' VE with real environment. Whereas, within VEs small effect size was found with no significant difference between the occurrence of PV in HV and Hap. These results indicate that in VR absence of sensory information does not affect the reaching component (PV & TPV) but VR itself is responsible when kinematics of reaching component was compared with real environment causing participant to achieve PV later in the movement and with lower speed.

Aside from the decrease in speed and prolonged movement time, participants in VEs scaled grip aperture according to the object size. However, in VE without hand vision (hap) maximum grip aperture was observed to have a large effect size (more than 1 SD) and large safety margin compared to movements made in real environments as shown in Figure 80. Post-hoc (Tukey-HSD) showed a moderate effect size within VR indicating the importance of being able to see the hand as well as the object size while grasping. Large grip aperture may also be due to the increased perceptual uncertainty (under no visual guidance) to avoid knocking down the target by increasing the safety margin thus making participants more cautious while reaching. Hence it is safe to say that in the absence of haptic feedback under visual guidance, grasping an object turn out to be an aperture matching task. In VR, TMGA occurred later in the movement and showed large effect size when haptic feedback (visual guidance alone) was not available than in VR block with no visual guidance forcing participant to achieve wider grip aperture earlier on.

Reach-to-grasp movement kinematics, reported in our study show that under visual or haptic guidance, are somewhat similar but also exhibit critical differences, and in combined visuo-haptic guidance, movement becomes optimized by reducing the grip aperture and by speeding up the reach component [261], [263]. Kinematic similarities between HV and Hap might suggest that vision is as good as haptics to successfully reach-to-grasp the target. But in Hap (No hand vision + haptics) MGA and PV occur relatively earlier along movement trajectory suggesting hand pre-shaping was initiated earlier, so, participants have more time during the closure phase to enclose the object within digits more slowly, and with wider grip apertures to avoid accidental collision with the object than in HV (hand vision + No haptics) [261], [264]. But when reach-to-grasp movements benefit from both visuo-haptic information, grip opened less and executed in shorter amount of time than in VR conditions [210].

6.7 Conclusion

Characterising kinematic differences produced in three different environments (based on available sensory information) can help understand what trade-offs have to be taken care of while using VR approaches to study prehension skills, to guide future clinical inquiry and upper limb rehabilitation that is transferable into real-world functional independence. This study shows that reach and grasp components were strongly correlated in both environments and showed properly coordinated reaching and grasping kinematic profiles. Instead of similarities, we also found significant differences in kinematic landmarks demonstrating key role of hand vision and haptic feedback during initial and final phase of movement trajectory.

In conclusion, these findings suggest that in the absence of sensory information, prehensile movement show systematic biases, signifying the importance of online sensory information to guide the hand until it makes contact with the object [132]–[134]. And in order for the grasping action to be completed successfully, information about fingers position and object contact points is sufficient [135]–[137].

In a nutshell, it seems both sensory modalities play their role at different times of the movement trajectory such that initial phase of the movement is dominated by the perceived haptic information of the object shape and location and then guided by visual feedback in the final phase. Thus, visuo-haptic information would be integrated to plan and execute the prehensile actions. And we found that movement patterns are strongly correlated in both real and VEs with or without visual and haptic feedback. And it was observed that prehensile movements made in VEs did produce statistically significant kinematic measures as was observed in real environment presenting appropriate visuo-motor scaling towards different object sizes and distances. But these measures were scaled and occurred at different time instants i.e., kinematically similar to real-world movements. Such that grip

aperture was scaled according to the object size and MGA values were larger in VEs (MGA: Hap > HV) than real environment, suggesting the importance of hand visual information while grasping in VR. And reaching component was not statistically significant within VEs i.e., irrespective of available feedback but was statistically significant when compared with real-world movement. Such that participants moved with slower reaching velocity perhaps due to lack of perceptual uncertainty (availability or unavailability of hand visual feedback) and achieved TPV later in the movement. It suggests that VR is sole responsible for the effects captured in reaching component and experimenter must account for these potential differences. And it also suggests that hand visual feedback is important to guid the hand and make necessary online corrections while grasping in VR. So, VR can be used to study prehensile movements as alternative to optical motion capture system.

Chapter 7: Training and Validation of a Deep Neural Network Model, DeepLabCut, for Marker-less tracking of Kinematic Landmarks during reach-to-grasp movements.

7.1 Introduction

This chapter sets out to investigate a marker-less motion capture system trained on a deep neural-network called DeepLabCut (DLC). DLC requires a set of images, extracted from a video, being labelled for important landmarks by a user to track the position of the defined landmarks throughout the video and important kinematic measures are extracted. In other words, labelled images act as input for DLC to get trained on and trained model is then used for further analysis of unseen videos. Hence, cameras are necessary to capture videos in a highly controlled environment to extract the set of training images. DLC is being widely used to study animal behaviour and only one paper presents the usage of DLC to characterise finger tapping (FT) movement made by Parkinson patients [201]. This study recorded FT movements using iPhone camera (single camera) to record videos, therefore, DLC provides 2D pixel coordinates of labelled landmarks to look at the trajectories and to extract the important kinematic features. In this study, author had to instruct participants to keep tapping fingers in a plane without moving hand away or nearer to the iPhone camera. But literature suggest using two or more cameras to record videos synchronously and then stereo triangulated to extract the 3D position of the marker in space. Hence, this chapter deploys BIGKAT for recording reach-to-grasp movements without attaching infrared emitting diodes (IREDs) via stereo calibrated cameras. Images from these videos are labelled and used to train a separate DLC network for each camera, which then can be used to find and track the labels in unseen videos, hence, providing 2D pixel coordinates for each labelled body part. These pixels coordinated are triangulated using intrinsic and extrinsic camera properties to determine the depth of each label i.e., 3D positional data. DLC has been used to study animal behaviour and it would be the first time DLC would be trained on prehension videos.

One of the major objectives is to evaluate DeepLabCut's suitability for studying prehensile tasks by training a deep neural network model, provided by DeepLabCut, to investigate prehensile movement recorded by BIGKAT cameras. Hence, the focus is to determine whether is possible to train a DLC model that can reliably and efficiently extract important kinematic landmarks of reach-to-grasp videos and can be generalized to new unseen videos. For this specific reason, the model should be trained on a diverse training dataset such as varying task constraints, lightning conditions, and background environment. This chapter also sought to measure spatial accuracy of the trained model by analysing the noise levels which can be measured by the standard deviation of the position of a static marker over time and the cumulative distance travelled by a static marker [265], [266]. For this reason, other

than kinematic landmarks of the participant's hand (wrist, thumb, and forefinger) during reach-to-grasp movement, the object to be grasped was also tracked to measure spatial accuracy.

To evaluate the performance of the trained model, DLC provides a function to evaluate trained network performance which measures its prediction accuracy proportional to the average root mean square error. Therefore, it is necessary to understand how large a training data set is required by DLC for accurate and precise extraction of 3D positional data. For this reason, the whole labelling and training process was divided into different batches of successively training the network by varying the training dataset. For example, how the trained model performs when trained on images from one participant and five participants and then on ten participants i.e., by systematically increasing the diversity of the training dataset. Due to COVID-19 pandemic, this study managed to collect reach-to-grasp videos from 8 participants before data collection had to be paused owing to the lockdown imposed. Hence, we managed to only train two DLC models; first DLC model was trained on the set of images obtained from some of the reach-to-grasp videos of one participant only and was then used to analyse the remaining videos from the same participant and of two other participants as well. Similarly, the second model was trained on set of images from five participants which was then tested for unseen videos from same and new participants (for further details see section 8.3.2).

The ultimate goal of this study was to evaluate the potential for DLC to be used as a part of the BIGKAT toolbox, such that reach-to-grasp videos from BIGKAT can be analysed with a well-trained DLC network, and furthermore, DLC allows tracking of kinematic landmarks without the use of powered markers, which are a significant limit to the existing BIGKAT setup. Such a system requires synchronized and calibrated cameras, recording movement as it happens, and well-trained and accurate video analyser, a deep-learning toolkit. Fortunately, the BIGKAT system, used for studying reach-to-grasp movements in previous chapters, offers a pair of synchronized and calibrated cameras and we are left with a task to train a neural network model using deep-learning architecture. Figure 84 shows the schematic of the overall operational sequence opted for each model being trained on the training dataset obtained from one participant or five participants.

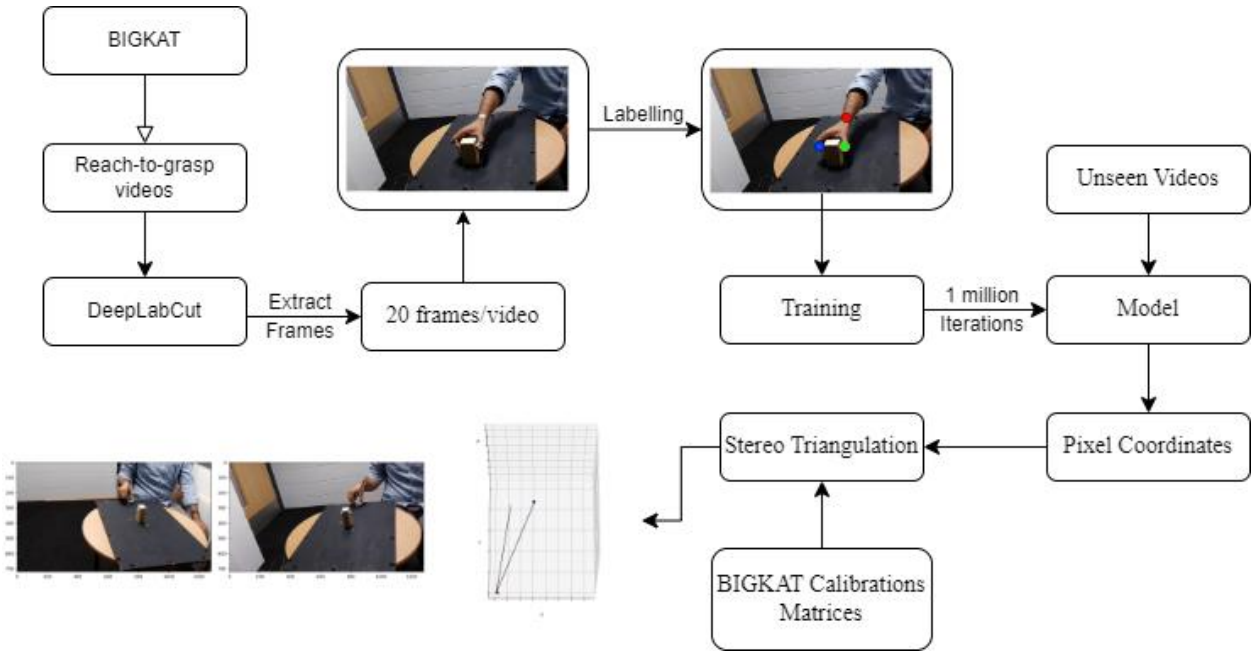

Figure 84: Schematic of the overall operational sequence of using BIGKAT and DLC, where BIGKAT record videos which are used to train the DLC model and then to analyse the unseen videos. Extracted 2D pixel coordinates are then stereo triangulated using BIGKAT calibration intrinsic and extrinsic properties to reconstruct the 3D positional data.

Hence, our aim was to train an accurate and precise DLC network capable of resolving prehensile videos (obtained from BIGKAT) into reliable kinematic measures, so that, DLC network can be utilized as a video analyser tool for BIGKAT. Unfortunately, due to the COVID-19 pandemic, instead of validating kinematic measures obtained from DLC against research-grade Optotrak and/or low-cost BIGKAT, this study just relied on observing spatiotemporal characteristics as they reveal the coordinated and controlled structure of prehensile movement and change lawfully by task constraints as was observed in chapter 4 & 6 and as presented in the literature.

7.2 DLC overview

DLC utilizes a feature detector algorithm from a previously published model called DeeperCut [267]. Like the DeeperCut model, DLC is built on a state-of-the-art deep-learning model using residual networks. It uses transfer learning, by initializing DLC with weights pre-trained on ImageNet, a massive object recognition database [268]. This reduces the size of training dataset needed to train the network, in turn increasing the inference speed and achieving good generalization to novel and multiple individuals in a dynamic changing environment i.e. human-level accuracy [200], [269]. DLC trained for 3D marker-less pose estimation across species with 100 and 500 labelled frames achieves less than 5 and 2.7 pixel error on 800 x 800 pixel frames, respectively [202].

DLC was mainly developed for animal species behavioural analysis and it offers many advantages over several human pose-estimation algorithms including DeeperCut, DeepPose, OpenPose, ArtTrack and OpenPose-Plus as well [267], [270]–[272]. Two main advantages of DLC is that it can learn to robustly

extract additional body parts not contained in the pre-trained network for analysing unseen prehensile videos and secondly, it allows for 3D pose estimation via views from multiple cameras, by training a separate network for each camera or one network across all views from multiple cameras and then resolving 3D coordinates using calibration techniques [202].

The DLC workflow is shown in Figure 85, where the user starts by opening a python session within a Docker, importing DLC and then creating a new project with some initial videos required for the training dataset. The new project folder will contain four subfolders and one configuration file 'config.yaml', in which the user specify training parameters such as how many landmarks to be tracked in successive frames and name of each body part; cropping parameters to crop frames; how many frames to be extracted from each training video and the extraction method (manual or k-Means clustering); path for the videos that the network would be trained on; and an over-connected skeleton defined by the links between body parts such that body parts should be connected by at least one path or redundant multiple paths to overcome occlusion. After setting-up 'config.yaml', the next step is to extract frames from all the videos mentioned in the 'config.yaml' file using the 'extract_frames' function which can extract frames automatically or manually in a graphical user interface (GUI). It is suggested by DLC authors to extract frames automatically in cases when the participant is not moving much between trials. This is the case in reach-to-grasp tasks, where reach and grasp movements are fast, but the participant is not moving. In such a case, videos are downsampled and frames are selected from different clusters based on k-means vector quantization, where each frame is treated as vector.

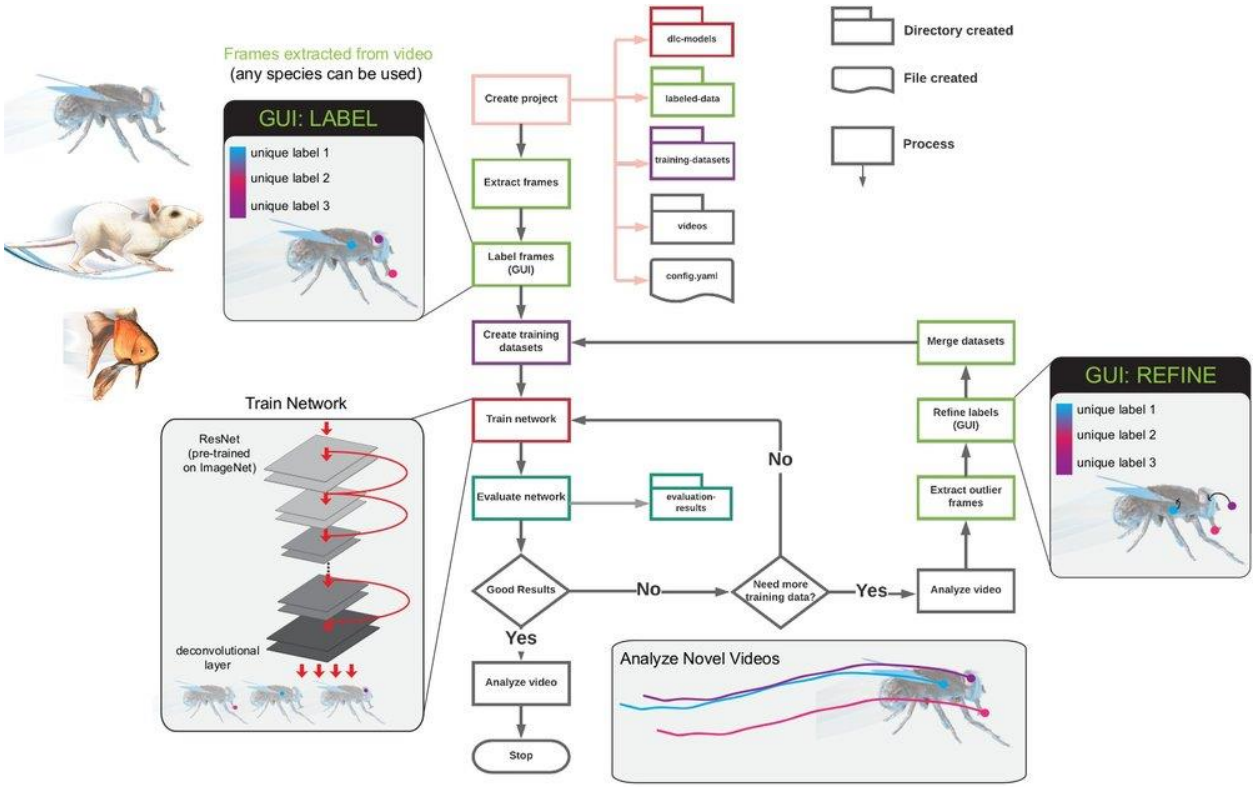

Figure 85: DeepLabCut workflow, directory and file structure. Shows all the necessary steps to train a network as depicted in [202].

Function 'label_frames' allows the user to manually annotate the body parts visible in the extracted frames using the GUI. After labelling all the frames from one of the videos, a labelled data set corresponding to the particular video is created in a hierarchal data format (HDF). The toolbox provides a function 'create_training_dataset', which combines the labelled datasets from all the videos and then splits the dataset into training (95%) and testing datasets (5%) for training the network and for evaluating the network after training, respectively.

Now the user can train the ResNet architecture of DLC with the trained dataset by calling a function called 'train_network', which will download the pretrained networks and starts training the residual network with either 50 or 101 layers (ResNets) for 1,030,000 training iterations. The 'evaluate_network' function evaluates the performance of the trained network by calculating the Euclidian error (mean absolute error – MAE, proportional to the average root mean square error) between the user and the DLC predicted labels. If the Euclidian error is not acceptable, and to provide a finer quantitative evaluation, the user can refine the network by training with additional labelled frames. Once the user is satisfied with the performance of the trained network, one can use 'analyze_video' function anytime to analyse, predict and label the body parts in unseen videos. This function will generate a .csv and .hdf file containing name of the body parts, pixel coordinates (x, y)

and likelihood for each frame per body part which then can be exported to a statistical software for analysis or stereo triangulated to get 3D coordinates in case of multiple cameras.

7.3 Method

7.3.1 Materials

Each trial was prepared by placing a wooden object at one of the two distances from the start position which was defined by a moulded grip and was close to the table edge and the participant prepared by holding the start position between the thumb and index finger. Participants were instructed to reach for and grasp an object that could be located at a distance of 200 or 400mm from the start position in the sagittal plane and can be reach with the simple extension of their arm. Two wooden objects of the same height and grasp surface size but of different widths (50 and 70mm) were used as shown in Figure 87. Grasping dowels of same size (height= 10mm, diameter= 10mm) were affixed on the sides and was set back 10 mm from the top of the object as shown in Figure 87. Participants were told to grip the object by its grasp surface with their thumb and index finger. Each participant performed 3 trials at each distance and object size combination, resulting in a total of 12 trials. Figure 86 shows unseen BIGKAT videos being analysed by DLC and plots on the right hand side shows extracted kinematic features throughout the video i.e., wrist velocity and maximum grip aperture.

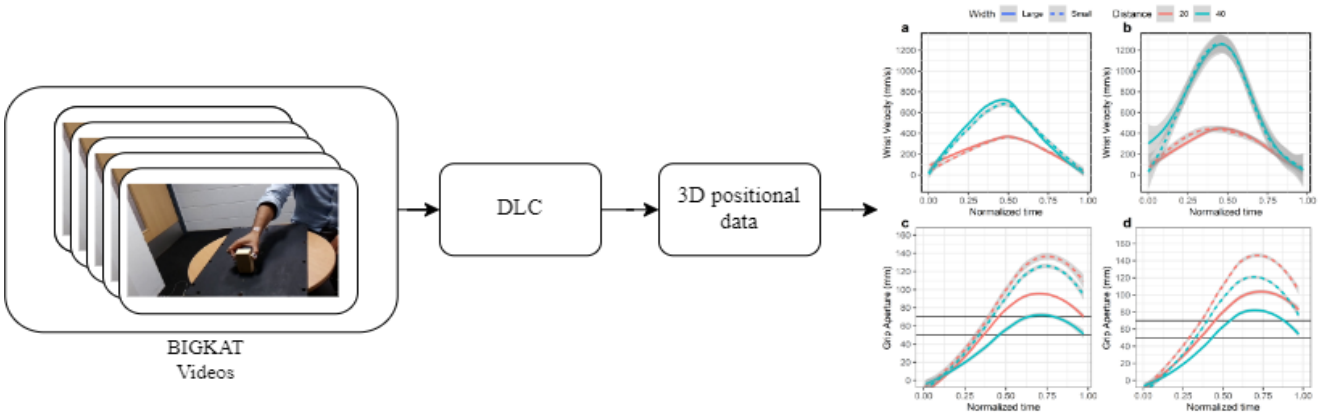

Figure 86: Schematic of DLC analysing unseen videos from BIGKAT and the plot showing the extracted kinematic properties.

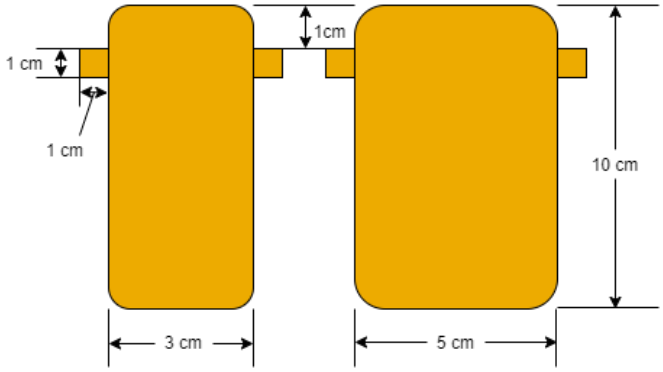

Figure 87: Two wooden objects reached and grasped by the participant at 20 and 40cm.

7.3.2 Procedure

Data acquisition was completed by BIGKAT and was initiated one second before the "go" in the experimenter's verbal start command "three, two, one, go" and the participant's task was to reach and grasp the object at the "go" signal. The basic ingredient for any deep pose estimation technique is recording movement via camera or multiple cameras resolving movement trajectory in 2D or 3D space, respectively. BIGKAT recorded reach-to-grasp movements at 60 Hz for 5 seconds via two cameras, simultaneously. With these videos, a network can be trained for each camera view, or one network can be trained across all camera views and in our case, we trained a separate network for each camera and then pixel coordinates were stereo triangulated to obtain 3D positional data. As this chapter aims to investigate DLC performance on human prehensile movements and in order to understand how large training data set is required by DLC for accurate and precise extraction of 3D positional data, therefore, DLC network training process was divided into three batches. In the first batch, the DLC network was trained on five trials (2 videos per trial per camera) from one participant only (referred to as batch-1 network) and then the same trained network was used to analyse unseen videos from two other participants and the remaining videos from the participant that the network was trained on. Following the DLC workflow described in the previous section, 20 frames per video were extracted based on k-means clustering, in total 200 $(\frac{frames}{trial} \times no.of\ trials \times no.of\ cameras \times no.of\ participants = 20 \times 5 \times 2 \times 1)$ frames were labelled. To reduce the time needed and human error while labelling, small micro-pore surgical tape was applied on the kinematic landmarks (dorsal wrist, distal joint of index finger and thumb) of participant's hand as shown in Figure 88. The training dataset was created using 95% of the labelled frame and then started training the network using the ResNet-50 architecture. The trained network was then used to analyse new unseen videos $(no.of\ trials \times no.of\ cameras \times no.of\ participants = 12 \times 2 \times 3 = 72\ videos)$, which labelled all the videos and output 2D pixel coordinates. Corresponding videos from the same trial were then stereo triangulated using the cameras' intrinsic and extrinsic properties as shown in Figure 89.

In the second batch, a new DLC network was trained on 5 participants (referred to as batch-2 network) in the same manner as the network was trained in the first batch. In this case, the training dataset was created by extracting frames from five participants at each combination of object distance and width (4 trials). Again, two cameras recorded the trials, simultaneously, therefore in total 800 frames ($(\frac{frames}{trial} \times no.of\ trials \times no.of\ cameras \times no.of\ participants = 20 \times 4 \times 2 \times 5)$ were extracted and labelled to train the network. The trained network was intended to analyse unseen videos from another 5 participants and the remaining trials from the five participants that network was trained on. However, due to the COVID-19 pandemic the study was paused and only managed to collect data from 3 other participants before lockdown. Similarly, it was impossible to carry out the planned study of batch 3, which was to train the network on ten participants and to analyse unseen videos from ten new participants. In both networks, DLC training dataset was not provided with any task constraints information like object size and distance as in our case. It is mainly due to the reason that trained network should be able to analyse videos from different experimental setups.

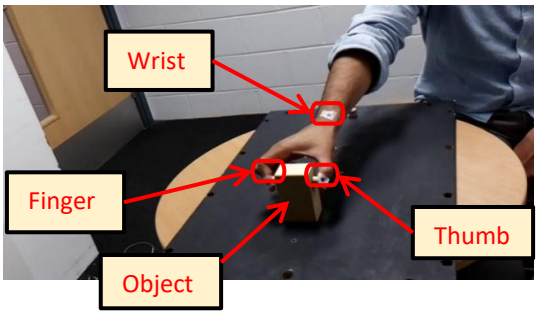

Figure 88: Wooden object being grasped. Distal end of index finger, thumb and wrist are clearly marked with micro-pore tape to ease labelling process

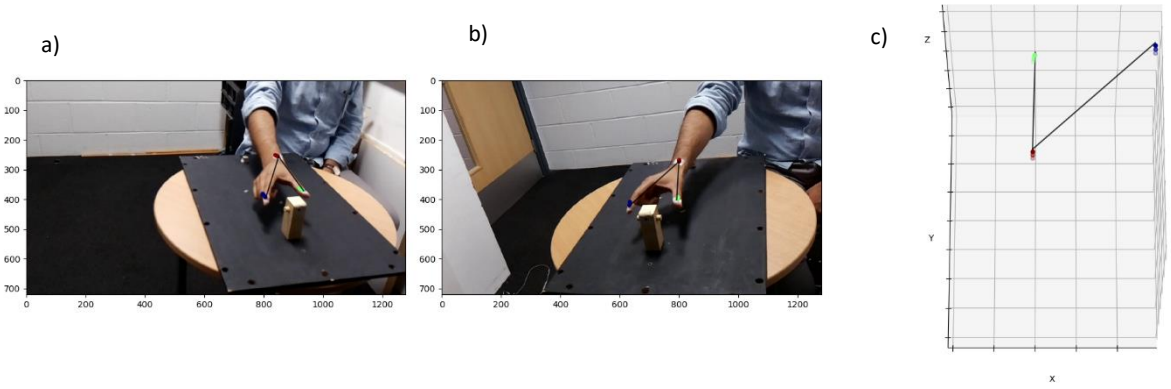

Figure 89: a) and b) multiple views from synchronized cameras with kinematic landmarks labelled by trained DLC network. c) stereo triangulation of labelled camera views to get 3D coordinates.

7.3.3 Data Analysis

Two synchronized videos of the same reach-to-grasp movement are treated and analysed separately by DLC, producing a file containing 2D pixel coordinates which are then stereo triangulated to output

3D spatial coordinates. The 2D pixel coordinates determined by DLC were first filtered by a low-pass butter-worth filter (4th order, $f_c = 5Hz$) shown in Figure 90 and then passed to the triangulation method to determine the 3D coordinates. As in previous chapters 4 & 6, prehensile kinematic measures, maximum grip aperture (MGA), peak velocity (PV), their time of occurrence (TMGA, TPV) and movement time (MT) were extracted.

The level of noise determines the spatial accuracy and precision of a tracking system and can be measured by the standard deviation (SD) of measured position of a tracked object (static measurement) over time [265], [266]. Noise levels are measured in each dimension, thus, the vector norm of the SDs for each dimension (alike to the root mean square (RMS) of distance from the mean position) was calculated. Higher values of SD indicate large variability between predicted data points of a static object. Similarly, average cumulative path length was determined by measuring the distance travelled by the object marker position as predicted by DLC. In our case, the object does not move therefore one should expect a lower cumulative path length, with large values of path length meaning a high noise level within the predicted object position.

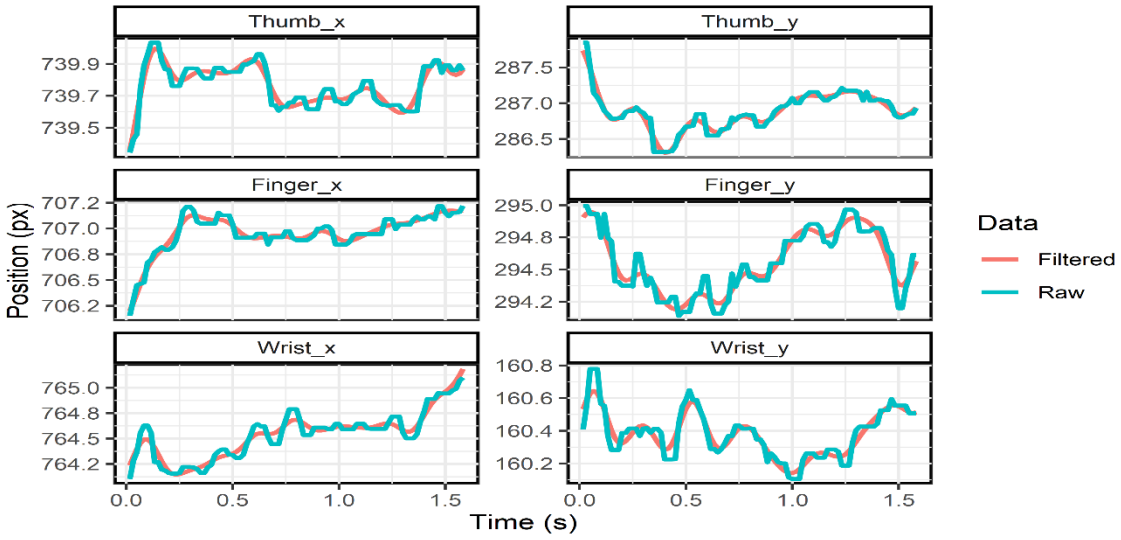

Figure 90: Raw data filtered by 4th order low-pass Butterworth filter at cut-ff frequency of 5Hz, plotted for time between 0 to 1.5s

7.3.4 Design

A 2x2 repeated measures analysis of variance with factors width (5 and 7cm) and movement amplitude (distance: 20 and 40cm) was used to evaluate the differences between all calculated kinematics. 2D pixel coordinates obtained through DLC for each video recording, were stereo triangulated to obtain 3D coordinates. Instead of using the triangulation method provided by DLC, the triangulation method already developed for BIGKAT to convert 2D into 3D coordinates was used because DLC outputs pixel coordinates instead of SI units. Five kinematic measures (Movement time

(MT), Maximum Grip Aperture (MGA), time to MGA (TMGA), Peak Velocity (PV) and time to PV (TPV)) were extracted from the filtered 3D positional data using a script developed in R.

7.4 Results

7.4.1 Spatial accuracy

To determine the spatial accuracy of DLC, the mean of the SD of the object position (static measurement) was determined across all subjects and task constraints and for each dimension. Table 12 presents the vector norm of SD for each dimension proportional to the RMS of the distance from mean position for both trained networks (batch-1 & batch-5). It can be seen from the Table 12 that large values of the vector norm of the SDs indicates higher noise level for the static object in turn increasing the variability and cumulative path length as well. Two trials with maximum and minimum variability in both trained networks were selected to illustrate the variability, and the normalized x and y position of the static object was plotted to determine the spatial range the predicted object position covered for the whole trial duration as shown in Figure 91**,** panel a and b shows trials analysed by network trained on 1 and 5 participants, respectively. One can deduce by looking at Figure 91 that the trial shown in blue has lower variability with lower spatial range $(\text{batch} - 1\ x\colon 0 \sim 1.554mm;\ y\colon 0 \sim 0.549mm, \text{batch} - 5\ x\colon 0 \sim 0.336mm;\ y\colon 0 \sim 0.658mm)$ than the trial with the maximum variability occupying a large spatial range for both networks $(\text{batch} - 1\ x\colon 0 \sim 5.316mm;\ y\colon 0 \sim 3.642mm, \text{batch} - 5\ x\colon 0 \sim 23.264mm;\ y\colon 0 \sim 15.011mm)$.

Table 12: Cumulative path length and norm vector of SDs in each dimension.

Network	Width	Distance	PL (mm)	$\lvert SD\ x\rvert$	$\lvert SD\ y\rvert$	$\lvert SD\ z\rvert$
batch-1	Large	20	23.397	4.208	1.941	8.172
		40	30.751	5.538	2.108	7.335
	Small	20	11.905	2.929	1.317	3.796
		40	18.008	2.891	1.755	3.672
batch-5	Large	20	7.386	1.916	2.168	5.112
		40	21.993	7.016	4.356	14.822
	Small	20	6.819	2.556	1.326	5.411
		40	25.259	8.331	5.729	21.598

After training the network for 1,030,000 iterations, the 'evaluate network' function provided by DLC evaluated the tracking accuracy by computing the MAE error within the training data set and also between the human and predicted labels. Training MAE error increased by increasing the size of training dataset (batch-2 five participants) but test MAE error decreased with sufficiently diverse training dataset – 800 annotated frames as presented in Table 13. It is suggested by the DLC authors that networks based on training dataset ranging from different individuals, backgrounds and postures would sufficiently generalize to an unseen dataset. But data presented in Table 12 reports a large mean cumulative path length and large mean vector norm of SDs for a static marker and also Figure 91 shows a large spatial range occupied by static marker, even though MAE (reported by DLC) is less

than 2.15 pixel. This indicates that the training dataset lacks diversity of the behaviour with respect to postures, luminous and background conditions and also needs to refine the labels by the function 'refine_labels' provided by DLC by which the user can delete wrongly predicted labels or move the predicted label to the actual position [203].

Table 13: Mean absolute error calculated by using the built-in function 'evaluate_network' of the trained network

Network	Train (px)	Test (px)	Iterations
1 participant	1.62	2.32	1,030,000
5 participants	2.04	2.15	1,030,000

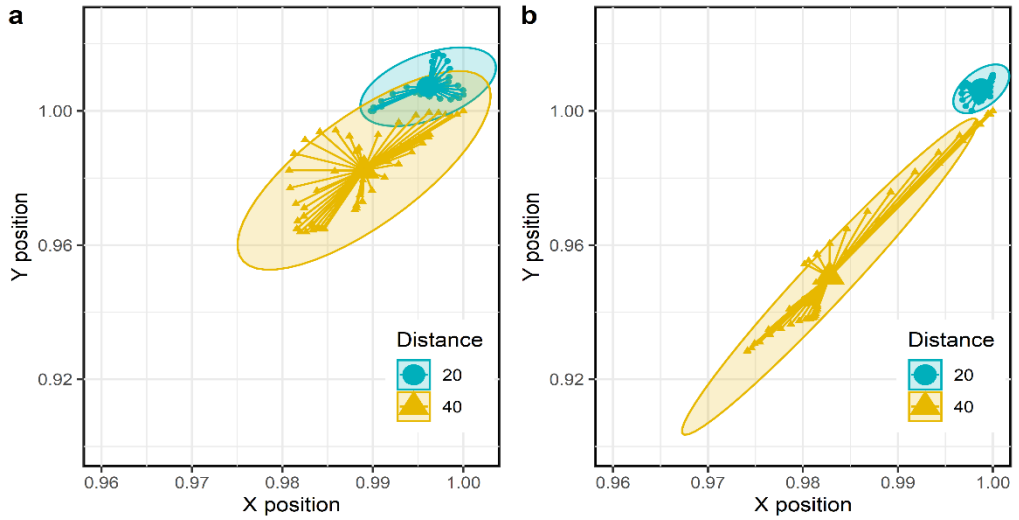

Figure 91 Illustration of the spatial range covered by static marker for two trials with max. and min. variability in each trained network a) batch-1 b) batch-2. Ellipse covered all the predicted position and centre point shows the mean position of the marker in mm.

7.4.2 DLC network performance

Successful grasping requires participants to match their grip aperture to the object width i.e., the distance between thumb and finger at the time of grasping should be the same as object width. Surprisingly, final grip size obtained for the farthest object was much larger than object width but matches object width for the nearest object as shown in Figure 93 (shaded grey area shows standard error – SE). Table 14 presents mean grip size and SE at movement offset. Such large grip size deviations for the farthest object but not for the nearest object might suggest that both networks are having difficulty in resolving movements of longer duration. It can be that longer distance trials had much greater variability on the final grip aperture size resulting in large overestimates which is also evident from the vector norm of SDs in each dimension (Table 12) i.e., spatial measures like grip aperture were largely effected by the amount of variability specifically during longer movements and has reduced the statistical power of the study. Figure 92 shows the movement frames at different stages of the movement and the estimated position of the wrist (red), finger (blue), and thumb (light green)

extracted by DLC for both cameras. Estimated kinematic landmark positions are then stereo triangulated for the 3D positional data as shown in the Figure 92.

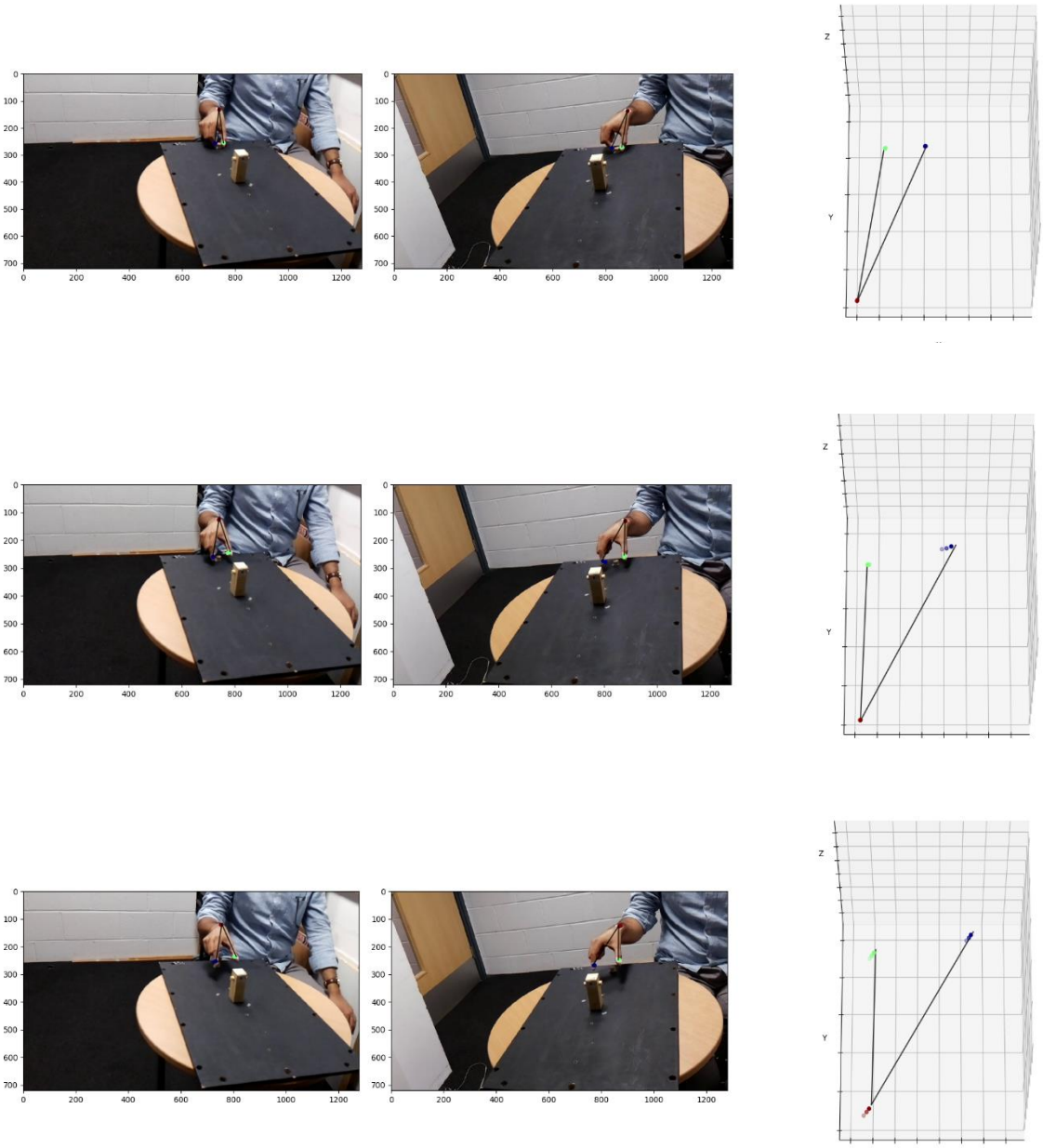

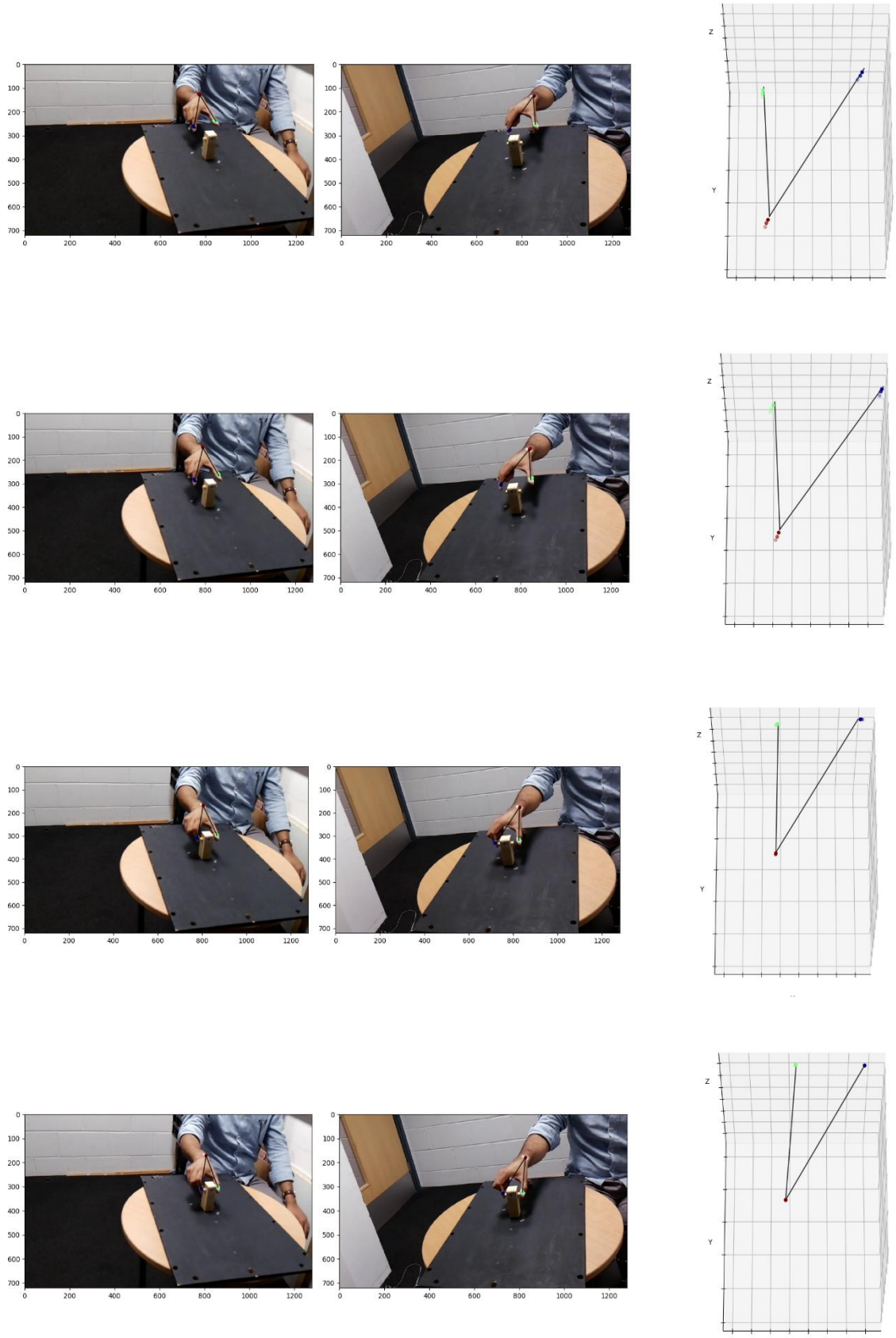

Figure 92: Movement frames at various timestamps of the movement and the dot shows the estimated kinematic landmarks position of wrist (red), finger (blue) and thumb (light green) in both cameras. Plot shows the trajectory of the estimated 3D position of each landmark.

Table 14 shows mean final grip size at the movement offset across all trials and it should be equal to object width, with deviations presented in overshoot column.

Network	Width	Distance	Mean final grip size	SE	Overshoot
batch-1	Large	20	70.177	9.141	0.177
		40	121.361	4.279	51.361
	Small	20	56.535	2.692	6.535
		40	98.224	6.351	48.225
batch-5	Large	20	84.407	5.962	14.407
		40	185.389	23.607	115.389
	Small	20	62.725	2.899	12.725
		40	131.504	15.831	81.504

Table 15 presents the kinematic measures obtained from both networks for all conditions across all participants and trials. shows wrist velocity and grip aperture profiles averaged across all participants and conditions exhibiting stereotypical nature of prehensile movement. Prehensile analysis in previous chapters also report that the time taken by the participant to reach for and grasp the object changes by changing its distance from the participant and spatiotemporal characteristics changes lawfully as well. MGA occurs relatively earlier for the nearest object than the farthest object and changes proportionally with object size.

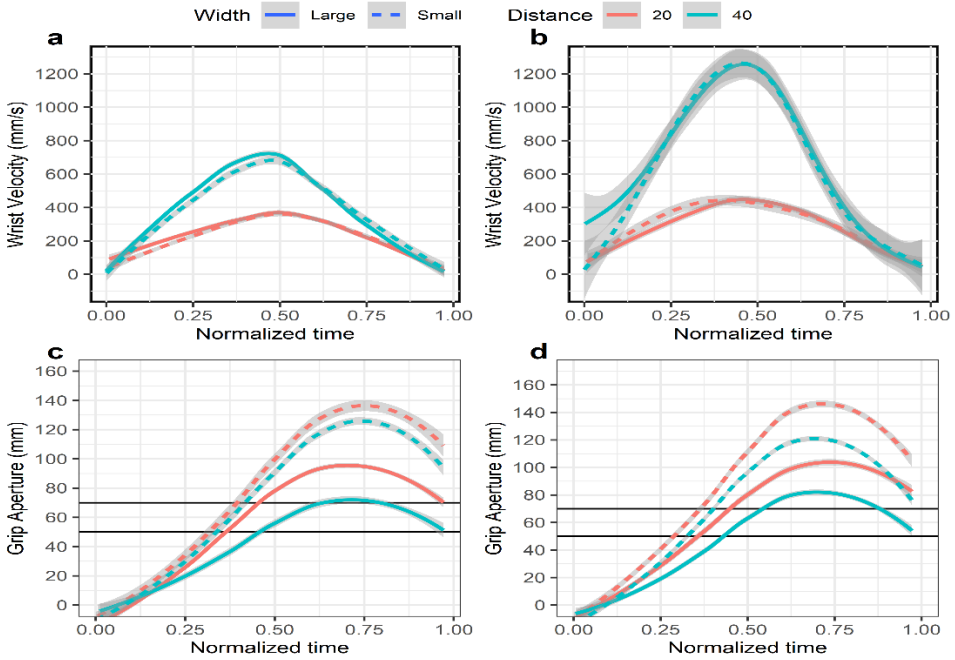

Figure 93: Mean wrist velocity and grip aperture profiles extracted from the resolved 3D position obtained by batch-1 (a &c) and batch-2 (b & d) network. Profiles are scaled with respect to object width and distance but with large standard error depicted by grey area, specifically for the batch-2 network when reaching for object at 40cm. Two horizontal lines in c& d represent object width, showing grip profiles at movement offset does not match object width placed at 40cm.

7.4.3 Movement Time

Figure 94 shows the effect of distance on MT, such that on average participant took longer to reach and grasp the farthest object $(batch-1: 0.931 \pm 0.141s;\ batch-2: 0.935 \pm 0.139s)$ than the nearest object $(batch-1;\ 0.702 \pm 0.096s;\ bacth-2;\ 0.692 \pm 0.094s)$. ANOVA found no significant differences for MT by both factors (distance & width) on batch-1 network but factor distance showed a significant effect for MT on batch-2 network $(F(1,7) = 54.719, p < 0.005, \mu_G^2 = 0.533)$ and object width had no significant effect. No significant interactions between factors were found for both networks and provided almost the same MT values. Low sample size analysed via batch-1 network prevented any statistically significant results.

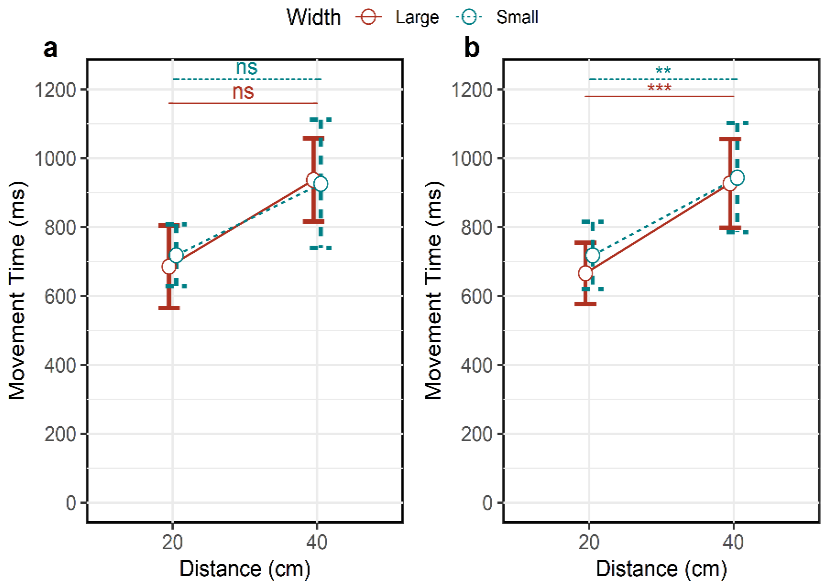

Figure 94: Effect of Object distance on movement Time (MT). Significant results found for batch-2 (b) & not for batch-1 (a)

7.4.4 MGA & Time to MGA

As reported in previous chapters and in literature, both independent variables related to grasping component, MGA and time taken to reach the maximum, are affected by changing dependent variables, object width and distance, respectively [5], [141], [273], [274]. ANOVA analysis showed that factor object width had a significant main effect on grasping $(bacth-1: (F(1,2) = 11.431, p < 0.01; bacth-2; F(1,7) = 34.419, p < 0.005)$ such that grip aperture scaled with respect to the object width and was wider for the large object $(\text{batch}-1: 109.99 \pm 21.309\ mm;\ \text{batch}-5: 132.875 \pm 67.272\ mm)$ than the smaller object$(\text{batch}-1: 92.186 \pm 19.154 mm;\ \text{batch}-5: 111.321 \pm 53.579 mm)$ and shown in Figure 95. In these results mean MGA is almost double the object width with large SD values, revealing large variability within dataset. Therefore, post-hoc test (Tukey-HSD) was performed which showed significant difference for the objects placed at 20cm in

batch-2 only Figure 95b, but no significant differences were found for batch-1 network as shown in the Figure 95a.

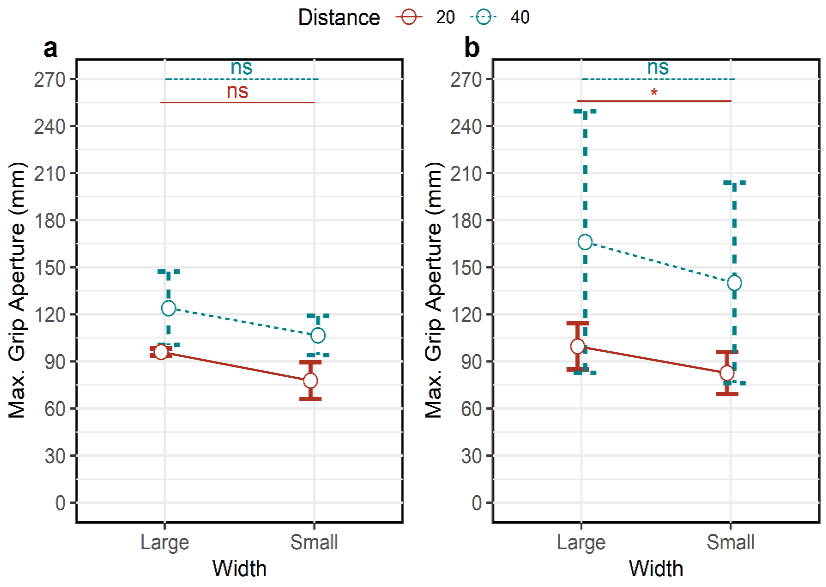

Figure 95: Maximum value of grip aperture varies with object width. a) batch-1 network show no significant difference due to low population size, and b) batch-2 show large variations in MGA for objects at distance 40cm.

TMGA extracted from the batch-1 and bacth-2 network showed no significant effect of object distance and width, as shown in Figure 96**,** contrary to the results reported in the literature that MGA occurs relatively later for the farthest object than the nearest one. No significant interaction was found between dependent variables for the grasping component.

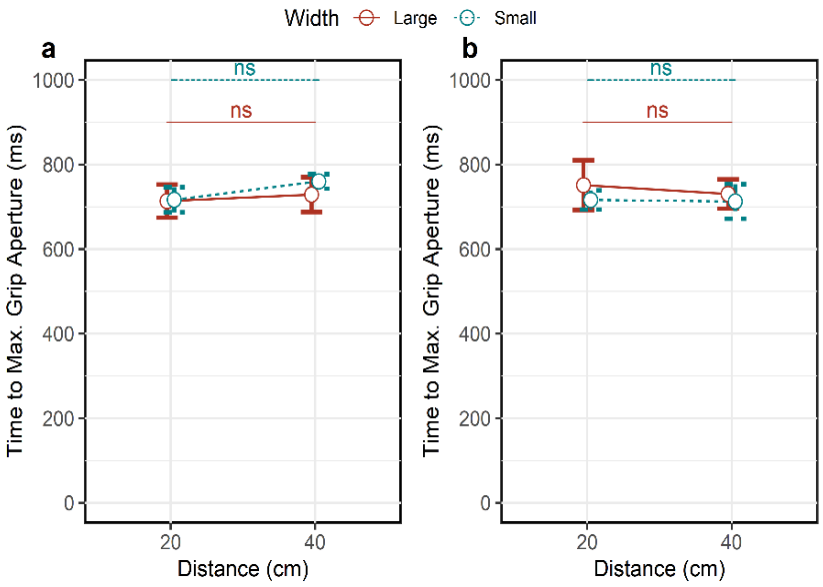

Figure 96: occurrence of MGA was not affected by the object distance from the participant.

7.4.5 Peak Velocity and time to Peak Velocity

Similarly, object distance forces participants to increase/decrease their speed accordingly and participants took longer to reach PV for the farthest object i.e. later in the movement than the nearest object [5], [145], [275]. In our datasets, we did find smaller PV for the nearest object ($batch-1: 227.312 \pm 43.860 mm/s$; $batch-2: 289.603 \pm 125.373 mm/s$) than the farthest object ($batch-1: 390.023 \pm 67.892 mm/s$; $batch-2: 653.537 \pm 400.033 mm/s$) with respect to the object distance but ANOVA showed no significant differences due to higher level of variability. Post-hoc analysis (Figure 97a) did reveal a significant difference between object distances such that adjusted p-value was 0.0218 and 0.0473 for large and small object, respectively. Similarly, post-hoc analysis of batch-2 network showed a significant effect for the nearest objects and no significant difference for farthest object, as shown in Figure 97b. Factor object width did not show any significant effect and no significant interaction was found between factors as well. Similarly, factors object width and distance showed no significant effect for TPV, shown in Figure 98, for both networks. However, literature reports increasing object distance from participant causes PV to occur later in the movement [4], [5], [145], [275], [276]. We found no significant interactions between both factors for the reaching component.

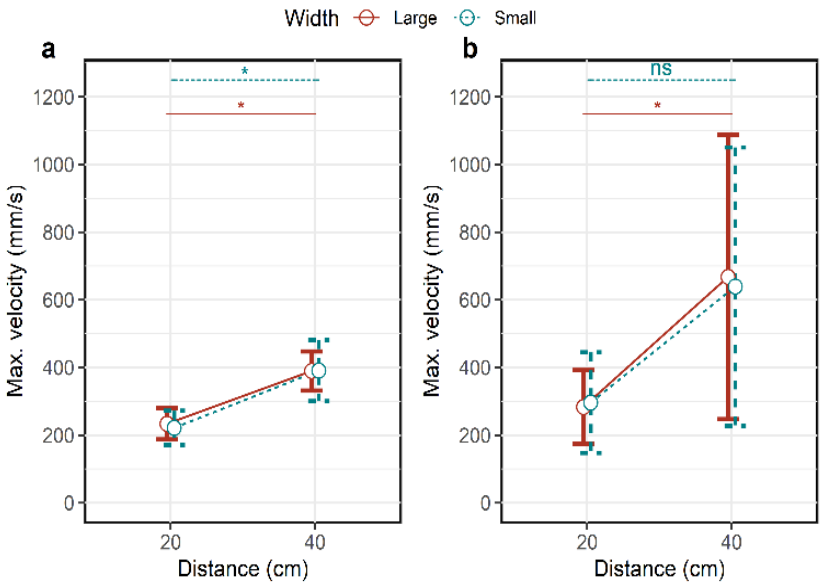

Figure 97: Factor distance showing small significant difference for PV extracted from a) batch-1 & b) batch-2 network. Error bars represent standard deviation across mean.

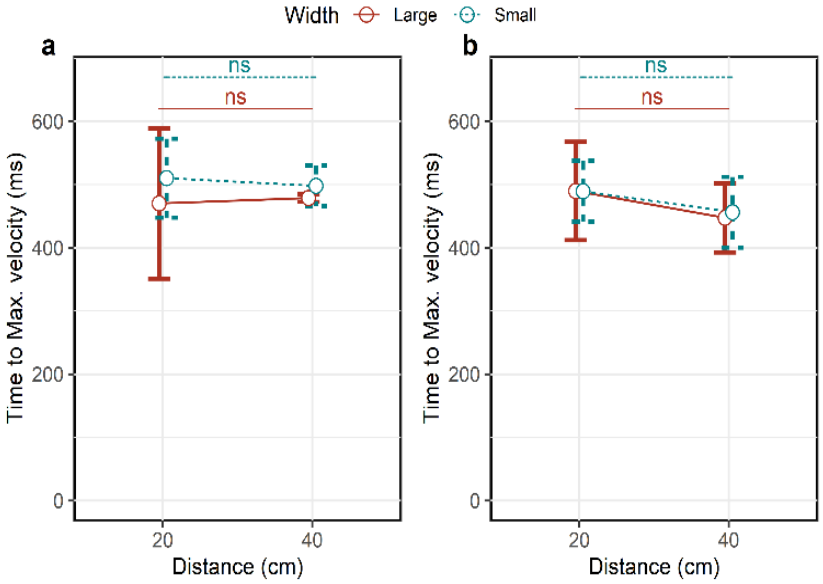

Figure 98: Effect of task constraints on time to PV.

Table 15: Reach-to-grasp kinematics extracted from both networks for all coditions across all particiapnts and trials.

DLC Network	Width	Distance	MT(s)	MGA (mm)	TMGA(s)	PV(mm/s)	TPV(s)
batch-1	Small	200	0.718 ± 0.089	77.781 ± 11.721	0.717 ± 0.029	221.233 ± 50.697	0.510 ± 0.062
		400	0.926 ± 0.186	106.591 ± 12.544	0.760 ± 0.017	390.558 ± 90.307	0.498 ± 0.032
	Large	200	0.685 ± 0.119	96.031 ± 2.193	0.713 ± 0.039	233.391 ± 46.133	0.470 ± 0.119
		400	0.937 ± 0.121	123.962 ± 23.353	0.729 ± 0.041	389.488 ± 58.026	0.479 ± 0.032

batch-2	Small	200	0.718 ± 0.118	82.592 ± 13.356	0.716 ± 0.023	295.984 ± 148.745	0.489 ± 0.048
		400	0.944 ± 0.175	140.049 ± 63.928	0.712 ± 0.041	639.242 ± 411.449	0.456 ± 0.056
	Large	200	0.666 ± 0.102	99.636 ± 14.753	0.751 ± 0.059	283.224 ± 108.795	0.489 ± 0.077
		400	0.927 ± 0.144	166.113 ± 83.395	0.730 ± 0.034	667.832 ± 420.663	0.447 ± 0.054

7.5 Discussion

This study has shown that this new motion capture toolkit, DLC, can identify and track kinematic landmarks in reach-to-grasp videos. The main goal of this study was to train a DLC network and investigate its performance in resolving the prehensile movement. Two networks trained with different datasets analysed unseen videos and showed that reaching and grasping profiles were scaled with respect to the object extrinsic and intrinsic properties as shown in Figure 93 but grasp size at movement offset does not match object width and also showed large variations specifically for the movements with longer duration i.e. object placed at 400mm away as shown in Table 14. And both networks also produced low spatial accuracy values measured by computing the cumulative path length and norm vector of SD of the static marker attached to the object as shown in Figure 91 and Table 12. Low spatial accuracy, large observed variations and moreover low sample size has significantly reduced the statistical power of this study indicating that trained DLC networks, in this study, were not capable of providing reliable kinematic measures and the network still needs training on large and diverse training dataset. So, the question arises: Do these kinematic measures obtained from these reaching and grasping profile significantly different from each other?

For the exact same purpose, repeated measures analysis of variance between task constraints for all the calculated kinematics measures were carried out and it showed significant differences between task constraints but not for all measures. It is due to a large amount of variability particularly in spatial measures (MGA, PV) and not for temporal measures (MT, TMGA, TPV) as presented in the Table 15. Variability in MGA and PV becomes more evident specifically when participants reached for and grasped the object placed 400mm away. It indicates an inaccurate and imprecise analysis of the movement of a longer duration by the DLC network. It can be attributed to a less diverse training dataset lacking multiple postures, different backgrounds and lightning conditions [202]–[204], suggesting refining the training dataset by manually moving the predicted label to the correct position or adding new frames until we have reasonable network performance and can generalize to a large collection of videos [200], [202]. Therefore, it intrigues us to further investigate the observed disparities in spatial and temporal kinematic measures by analysing the residual plots, as discussed in next section.

7.5.1 Spatial prehensile measures

Figure 99 shows the residuals plotted against fitted values for MGA and PV depicting non-linearity and large deviations due to the outliers present in the datasets. Literature reports the effect of object width on MGA [5], [141], [273], [274] and in this study, batch-2 network found a small significant difference between MGA values for the nearest objects of different widths and found no significant difference for the farthest objects and can be attributed to non-linearity observed in residual plot Figure 99c, which is due to large variability and large grasp size at movement offset. Similarly, residual plot for MGA of batch-1 network shows non-linearity Figure 99a, and thus, found no significant effect of object width for MGA.

Similarly, literature reports that object distance significantly effects reaching velocity [5], [145], [275]. Surprisingly, batch-1 network even with smaller population size (linear residual plot Figure 99c) found smaller significant difference for a large object (p-value = 0.0218) and smaller object (p-value = 0.0473) at either distance. Due to the non-linearity and large deviation in the residual plot of batch-2 network (Figure 99d), no significant difference was found.

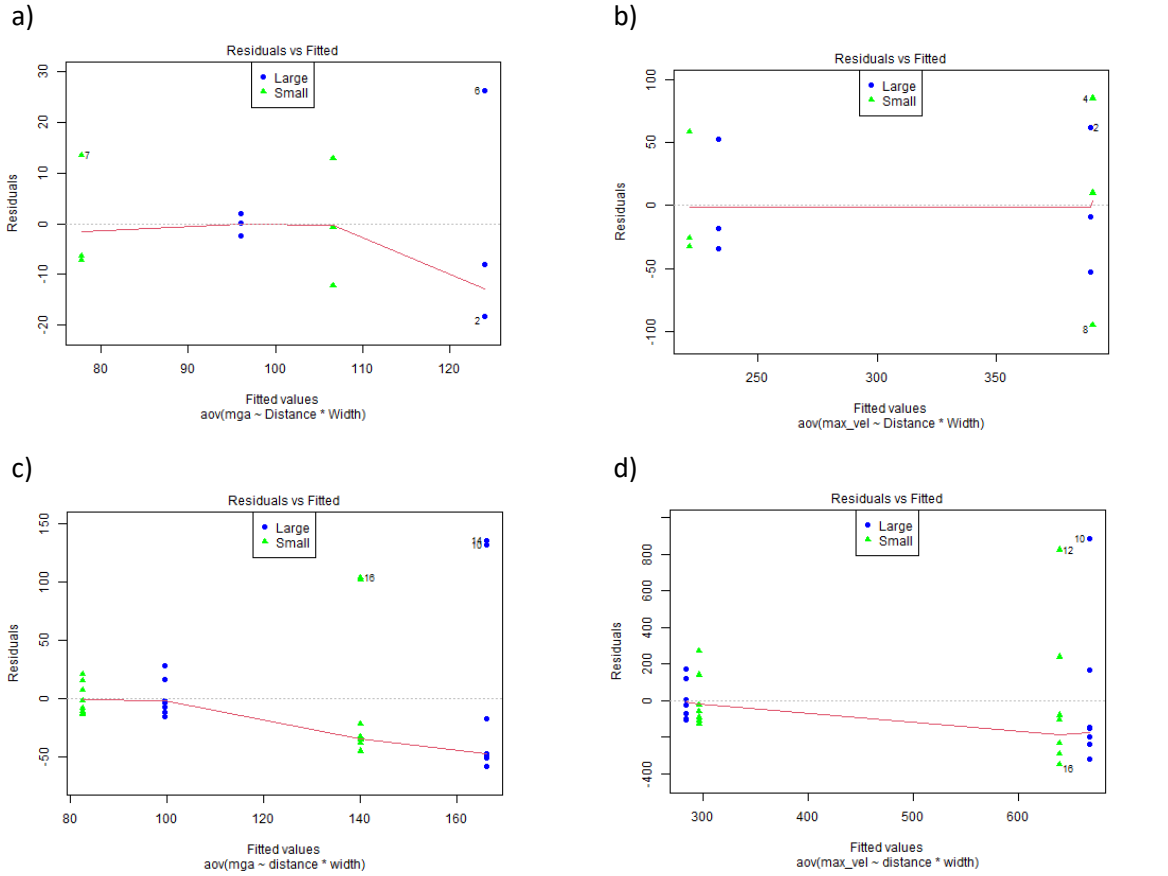

Figure 99: Residuals plot displaying non-linearity, changing variations and no-uniformity among spatial measures PV and MGA for a) & c) batch-1 b) & d) batch-2 networks.

7.5.2 Temporal prehensile measures

MT showed significant differences between object placement, placed nearest to the participants and further away but within participants' reach, as analysed by both networks and almost returning similar MT values, as well. But other temporal measures TMGA and TPV showed no statistically significant results as opposed to what is reported in literature [4], [5], [145], [275], [276] and in chapter 4 & 6, that increasing object distance causes MGA and PV to occur later in the movement.

7.5.3 Future Works

Measuring human behaviour helps psychologists and neurologists to understand the underlying connections, disease severity and progression, and provide objective measurements of clinical trial outcomes [277]. This deep-learning based marker-less motion capture tool (developed and deployed for studying animal behaviour) has the potential of being deployed in clinical neurology for measuring human movement disorder and recently one study has used DLC to quantify finger tapping movements made by PD patients [201]. However, in that study, the trained network was not used to analyse unseen videos but analysed those videos with which it was trained on i.e., the effectiveness with unseen videos remains to be seen. Similarly, the study presented in this chapter was meant to train a prehensile DLC network that can be used to analyse prehension videos from different cameras with multiple postures, changing backgrounds, different lightening conditions and environments [200], [202]. Unfortunately, it was not possible to get as far as training with a large number of trials due to the COVID-19 pandemic. Future work will be necessary to train an accurate and precise DLC network.

Computer vision algorithms for marker-less pose estimation using deep learning tools have been rapidly advanced and broadly adapted in a very short time, partly fuelled by sharing toolkits in public repositories on GitHub [278]–[282]. Current pose estimation methods require humans to annotate a training dataset with user-defined key-points on specific body parts which can get difficult to consistently label across images and can be laborious in case of multiple synchronized cameras to label key-points from every camera view [202], [283]. Recent advances in deep-learning techniques called inverse graphics model [284]–[286] do not need human-provided labels but use 3D volumetric models which are then optimized using information present in the 2D images.

7.6 Conclusions

This study has evaluated the DLC performance by training two networks with different training datasets. The results show that despite higher noise levels in the resolved 3D dataset, DLC was able to translate task constraints by scaling reaching and grasping components as also found in previous prehension chapters. Spatial measures were largely affected by the amount of variability specifically during longer movements and has reduced the statistical power of the study. Similarly, no significant

effect was found for temporal measures except for MT. But overall, it can be assumed that a network trained on a more diverse dataset might be able to statistically resolve kinematic differences and can be further utilized to discriminate patients from controls.

Chapter 8: A new tool for the temporal assessment of sequential 'Reach-to-Grasp-to-Transport' movement.

8.1 Introduction

Performance based tests to assess upper limb dysfunction generally involve reaching for and grasping an object and manipulating it depending on the task and instructional constraints. Motion capture systems (optical, mechanical, magnetic, inertial) provide useful objective information about impairment of upper limb movement during standardized tasks (finger tapping, reach-to-grasp) and they have been previously used as a measure of manual dexterity [15], [16], [287]. Before using an optical motion capture system for the comprehensive kinematic study of movement, time-based assessment can be used as a screening tool to evaluate upper limb performance quantitatively. And in clinical practice the Nine-Hole Peg Test (NHPT) is a widely used manual dexterity tool and as a 'gold-standard' in clinical research as well. NHPT provides a timed based outcome measure in seconds for completing the whole set of activity or alternatively pegs placed per second if experimenter instruct participants to place pegs in 50 or 100 seconds [288]. In essence, NHPT provides insight as to how long a participant took to complete a set of actions but not on how fast or slow the movement was. These outcome measure do not provide the detailed description of the movement such as how long did it took to reach and to grasp and to transport the peg into a hole. In other words, NHPT does not provide the time taken by a participant between different phases of the movement. Such detailed description of the movement would provide a useful insight into how manual dexterity improves in different phases of medication cycle and/or about the disease severity. Therefore, this chapter sought to design and develop a new tool capable of detecting occurrences of different phases of a sequential movement.

As reported in previous chapters and literature, reaching and grasping components of a sequential reach-to-grasp movement gets affected by covarying intrinsic (size) and extrinsic (location) properties of an object. Hence, this chapter set out to evaluate the performance of this new tool when participants are subjected to reach, grasp, and transport an object of different intrinsic properties to investigate if this tool is capable enough to detect subtle changes in the occurrence of different phases of movement due to task constraints. This tool hereafter will be referred as the Event Detection Tool (EDT) which can detect the occurrence of different phases of a sequential movement. For example, to reflect activities of daily living (ADL), a task may require a participant to reach, grasp and transport an object to a different location: this tool must be able detect when the participant initiated their movement, when he/she grasped the object, and when the object arrived at a new location. These events can then be used to calculate how long he/she took to complete each phase of the movement.

The next section describes design criteria that determine how EDT should function, and the hardware and software used to develop EDT.

8.2 Design & Development

The principal aim of developing EDT was to detect and record the start time and end time of different phases of reach-to-grasp-to-transport movements. To achieve this aim, we need to specify start and end-point of each phase i.e. the start position which participant should hold before reaching out to grasp an object placed at one of the three predetermined distances (200, 400 & 550mm) from the start position and then transporting the object again to a predetermined position that could be on either left or right side of the start position. Based on the above-stated aim, the following guidelines were considered while designing EDT.

- EDT must be capable of working in conjunction with BIGKAT and as a standalone system as well.
- Trial should be started when experimenter presses the start button.
- EDT should start recording as the start button is pressed and same for BIGKAT if both devices are being used together.
- EDT must calculate reaction time, hence, a random delay of between two seconds should be provided at the start of trial for triggering movement.
- EDT should record start and end timestamp of each phase of the movement i.e., when the participant leaves the start position, when the object get picked, and when was placed at the end location.
- EDT must accommodate for participants with either left or right dominant hand. In other words, a participant can place object on one of the two pegs on his left or right depending on his dominant hand.
- EDT should stop recording right after the object was placed
- EDT should transfer collected data on an external USB in a separate folder for every trial.
- EDT must be minimally distracting for the participants, only the key components should be affixed on top of the board.

8.2.1 Hardware

Prehension movements are performed within the participant's reach distance which is smaller or greater depending on whether a movement of the trunk is required/permitted. In this study, reaching movements involving the trunk were not required, therefore, the maximum distance that a participant can reach for is his/her upper-extremity workspace. Literature indicates that maximum distance at which the objects are placed in prehension studies is 600mm from the start position [234], [237], [289], [290] and based on anthropometric data available for British adults (age: 19 – 65) mean arm

length is $781 \pm 27mm$ [291], [292]. For this specific reason EDT dimension was taken as $650 \times 200 \times 50mm$ as shown in Figure 100. Design software SolidWorks was used to design EDT and as per the guidelines stated above three of its sides (left, right & top) were designed to support pegs, switches and buttons (see Figure 100). Black acrylic sheet of 5mm thickness was selected and was built using a laser cutting machine available in the prototyping lab in the school of Mechanical Engineering. Design of all three faces were uploaded into the laser cutting machine and then all faces were glued to make a rectangular EDT.

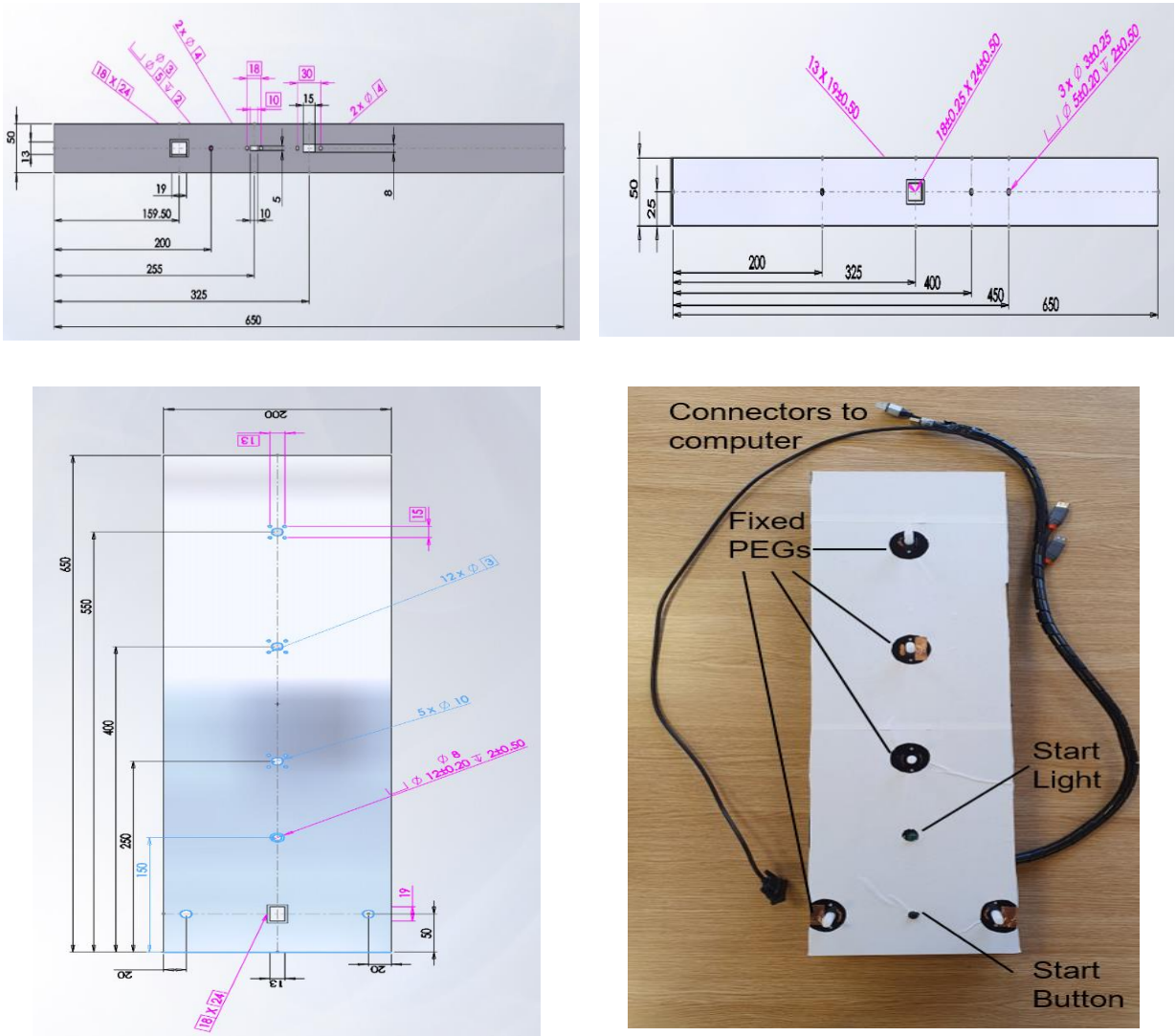

Figure 100: SolidWorks design for Event detection kit a) Right side b) Left side c) Top view d) EDT after fabrication. EDT allows movement across the board with either hand and can be connected to an external display.

As per the guidelines that top side must contain minimal components to mitigate against distraction and obstruction. Therefore, all necessary push buttons (power button, start trial button), all LEDs (power LED, object LED, trial LED, grip LED) and USB cables (A type to store data & B type for powering Pi) and HDMI cable to display the software were all located on the sides of EDT. And the top side of EDT contains the essential components needed such as grip button, move LED and five pegs (see

Figure 100d). A list of components used to develop EDT is shown in Table 16. Figure 101 shows the schematic of BIGKAT and EDT working as a single unit where wires from BIGKAT Raspberry Pi's are connected to the EDT Raspberry Pi such that both devices start recording simultaneously. Raspberry Pi was selected for EDT as BIGKAT was already using two Raspberry Pi's and it would be convenient to use same processor for interfacing two devices together.

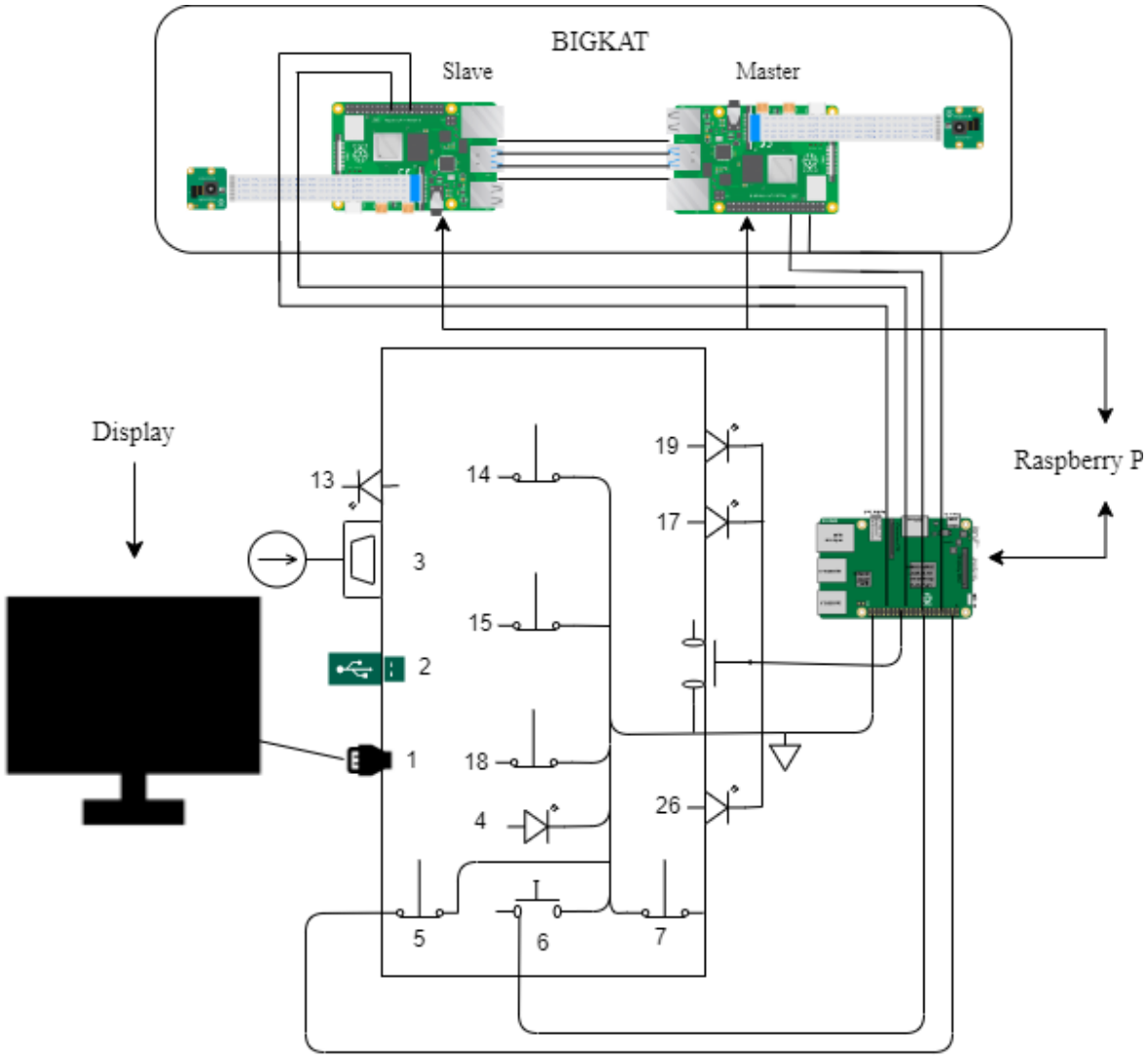

Figure 101: Schematic of BIGKAT and EDT functioning separately and simultaneously to collect spatiotemporal features of the trial. 13 power LED, 17 object LED, 19 trial LED, 26 grip LED, 4 move LED, 5 6 7 14 15 18 pegs for object placement, 1 HDMI, 2 USB A for data collection, 3 USB B for power supply

Table 16: List of components used to build EDT.

Items Name	**Quantity**
Raspberry Pi 3 Model A	1
LEDs	4
Panel mount SPST switch	2

Panel mount USB A male to A female	1
Panel mount micro USB B male to B female	1
10 mm through hole LED	1
4.2mm SPST miniature push button	1
Accessories (Resistors, jumper wires, double side copper tape, spiral wrap, cable gland)	

8.2.2 Objects

Four cylindrical objects were designed to resemble an electric toothbrush and to elicit actions that, in turn, reflect activities of daily living (ADL), such as reaching for, grabbing, and transporting a toothbrush. Each object has a 4 cm deep hole in the base that allows it to be inserted on a peg like a toothbrush on a charging station. The diameter of the base hole varies for these cylindrical objects (1 and 2 cm). Therefore, participants reached for the object, grabbed it from the peg and transported to be inserted onto the peg which is of fixed dimension (1 cm in diameter and 4 cm deep peg).

The object with the 2cm hole can be placed more easily on the peg. While the one with the 1cm hole in its base fits snuggly on the peg, such that, participants face difficulties while inserting the object, hence, forcing participants to insert the object with increased accuracy and precision. The objects also differed in terms of grasp surface size (1 and 3cm) such that smaller grasp size will cause participants to increase grasping aperture to avoid knocking down the object by increasing the safety margin thus making participants more cautious while reaching. Previous research also indicated that participants take longer to reach for smaller grasping surface size object as these force participants to grasp the more precisely and accurately [75], [293], [294].

a)

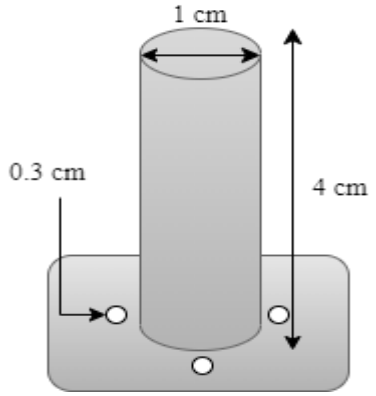

b)

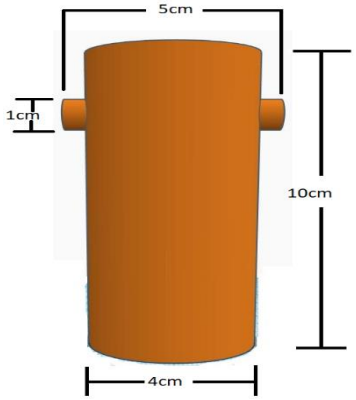

c)

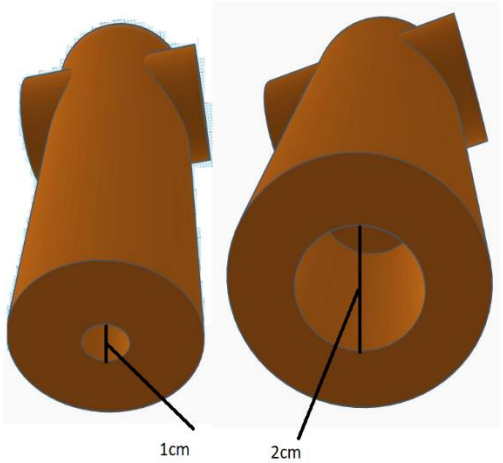

Figure 102 a) top panel shows peg design b) shows object design with different grasping surface size and hole diameter: 3D printed using Ultimaker.

8.2.3 Programming

As EDT was designed to be operated in conjunction with BIGKAT and BIGKAT employs two Raspberry Pi microcomputers, hence, EDT was also programmed using a Raspberry Pi microcomputer. Therefore, a Raspberry Pi microcomputer was used to control, communicate, and record temporal data for all trials performed on EDT. The following four scripts coded in Python, with all the necessary dependences installed, were developed for the effective and simultaneous working of EDT with BIGKAT such that both devices record trials separately and simultaneously as well. All scripts are provided in Appendix-C.

- Power Script: The Raspberry Pi microcomputer does not come with a built-in power on/off button. So, a power script was written to monitor the status of two GPIO pins and wait for a rising/falling edge to start/shut down the Pi, respectively.
- Boot Script: Once powered on and to make sure that relevant python script runs on boot, system fie '***rc.local***' was edited with the location of main python script. It turns on the boot LED and redirects the Pi to main python script.
- Main script: The main python script was developed according to the design criteria as shown in the flow chart (Figure 103). It first checks for whether the object has been placed on any of the predetermined positions on EDT or not and indicate its status via 'object_led'. EDT also checks whether the participant has gripped the button at the start position and similarly indicates its status via 'grip_led'. EDT then waits for the experimenter to press the trial start button to start the data collection session. EDT then records all the events and subsequently records the timestamp of each event, as they occur. EDT Main script then measures all the temporal measures i.e., reaction time (RT), reaching time (GT), transport time (TT), and movement time (MT). It also computes the samples between the start to the end of the trial

at 60Hz and labels the time instant of each event such that 3D data from BIGKAT and temporal data from EDT are synchronised.

Data Storage: Once all the relevant information has been extracted from the trial, the main script then calls the fourth script which transfers two files (.csv format) to an external storage device (USB, in our case). This script specifies methods by which it creates 'recorded_data' folder and a subdirectory folder for every recording made ('Record_0', 'Record_1' etc.) in the USB.

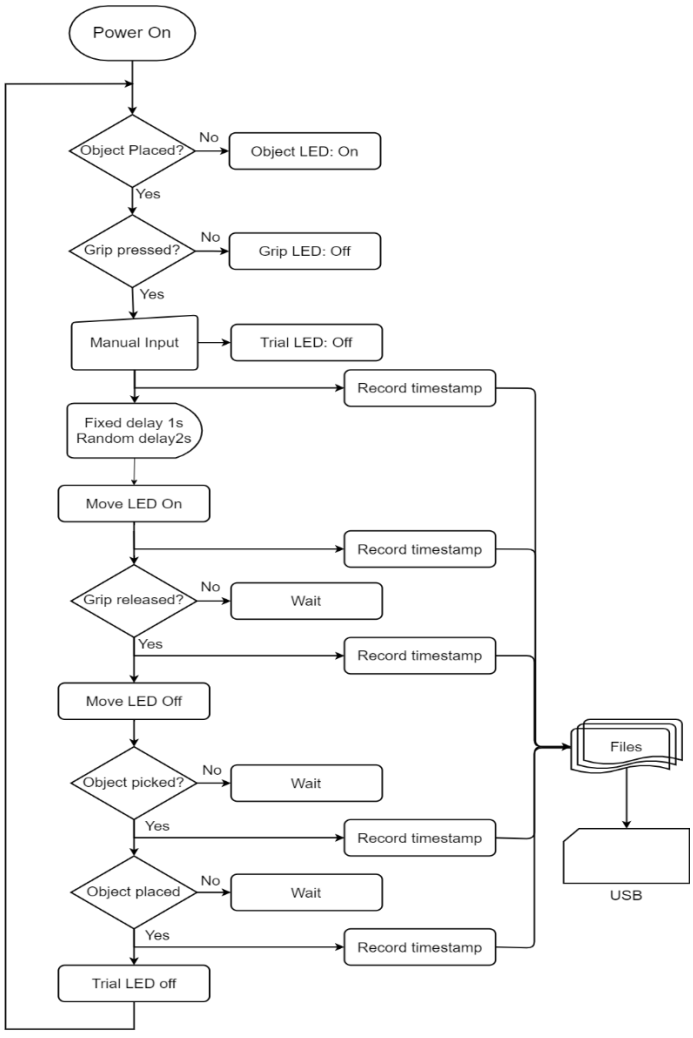

Figure 103: Flow chart describing the operations of EDT by which main script was developed on.

Once the EDT design was finalized, it was uploaded to the laser cutter machine (prototype lab; School of Mechanical Engineering) to cut the acrylic sheet according to the design. Four objects and five pegs were 3D printed using an Ultimaker 3D printer. EDT was assembled with all the necessary switches and LEDs, soldered, and wired to the GPIO of the Raspberry Pi, and pegs were screwed to the board at their predefined positions.

8.3 Method

Each trial was prepared by placing a 3d printed object at a predetermined distance of 350mm from the start position which was defined by a miniature SPST switch (grip button) and the participant prepared by holding and pressing the grip button. It will power on 'grip led' letting experimenter know of that participant is ready. Participants were instructed to reach for and grasp an object by its grasping surface between the thumb and index finger with the simple extension of their arm. Four cylindrical objects of same diameter and height but different grasping surface size (10mm & 30mm) with a hole in its base of diameter (10mm & 20mm) were used. Participants were told to reach for and grasp the object and lift it from the peg and then insert it on another peg at end point to finish the trial. Each participant performed 5 trials for each grasping size and base-hole combination by both preferred and non-preferred hand, resulting in a total of 40 trials.

Only three unpaid participants of age 25-35 could be recruited for this study before the start of the COVID-19 pandemic and had to face further delays therefore the study was paused. And the aim was to perform a pilot test before going into studies with MS population. All participants were right-handed, gave their informed consent prior to participating and were naive as to the purpose of the experiment. None had any history of neurological deficit, and all had normal or corrected to normal vision. The study was approved by national research ethics committee and from the Health Research Authority. This study also received ethical approval from the local research and innovation department of Leeds Teaching Hospital NHS Trust. This study was conducted on the clinical premises of the Leeds Teaching Hospitals Trust in conjunction with the University of Leeds and performed in accordance with the ethical standards laid down in the Declaration of Helsinki.

Data acquisition was completed by both EDT and BIGKAT and was initiated one second before the 'move LED' turns on and the participant's task was to reach, grasp and transport the object when the 'move LED' lit up, in turn enabling us to measure reaction time. Reach responses were recorded by attaching infra-red emitting diodes (IREDs) on the participant's wrist to measure its positional change over time. Similarly, grasping responses were recorded by attaching infra-red emitting diodes to the distal joint of the index finger and thumb and measuring the distance between them.

Movement time is defined as the temporal difference between movement onset, when the participant left the start button, and movement offset, when object base touches the board. We also separated the movement into phases to obtain more nuanced data: reaching time is measured as the temporal difference between object lift time and when the movement was initiated. Transport time reflects the time between when the object was lifted and when it was placed onto the peg.

8.4 Results

A 2 x 2 x2 repeated measures analysis of variance with factors grasp surface size (10mm, 30mm), base (hole diameter of 10mm, 20mm), and hand (left, right) was used to evaluate the differences between all temporal measures. For reaching time (time taken by the participant to reach and grasp object) there was a significant effect of factor grasp surface size ($F_{(1,2)} = 35.273, p < 0.05, \eta_G^2 = 0.251$) but post-hoc analysis showed significant differences for the large grasp surface size and only for the right hand as shown in Figure 104. Participants took longer to reach and grasp objects with smaller grasping surface size (Left: $0.727 \pm 0.102s$; Right: $0.796 \pm 0.088s$) than the larger grasp size (Left: $0.654 \pm 0.147s$; Right: $0.738 \pm 0.103s$). No significant differences were found for base hole. The ANOVA also revealed significant interaction between factors grasp size and base ($F_{(1,2)} = 63.227, p < 0.05 \eta_G^2, = 0.175$) and post-hoc test revealed significant difference for large base hole as shown in Figure 105.

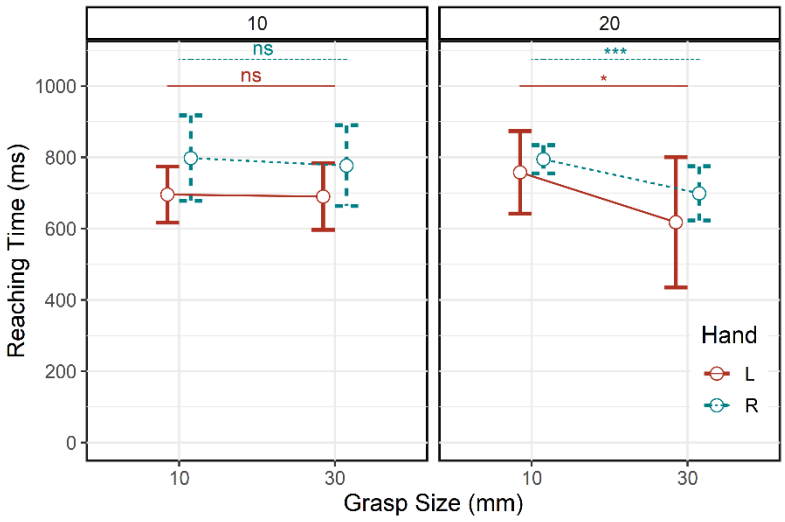

Figure 104: Effect of grasp size for reaching time at each level of base-hole diameter.

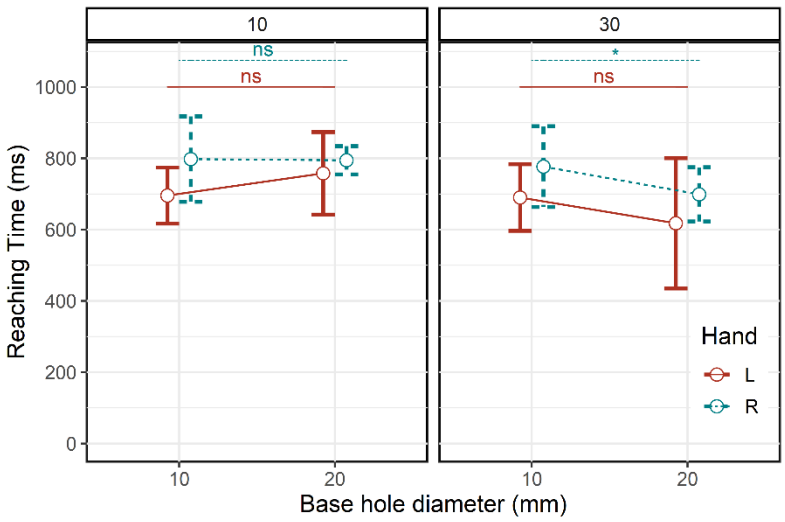

Figure 105: Effect of base-hole diameter for reaching time at each level of grasp surface size.

Factor base hole diameter revealed a significant effect for transport time ($F_{(1,2)} = 177.829, p < 0.05, \eta_G^2 = 0.937$) such that small hole forced participant to take longer (Left: $1.755 \pm 0.269s$; Right: 1.853 ± 0.283s) than larger hole (Left: $1.237 \pm 0.253s$; Right: 1.320 ± 0.223s) as shown in Figure 106. Grasp size showed no significant effect for transport time, and similarly, no interaction was found between grasp size and base hole. ANOVA showed no significant effect of any of the factors on reaction time.

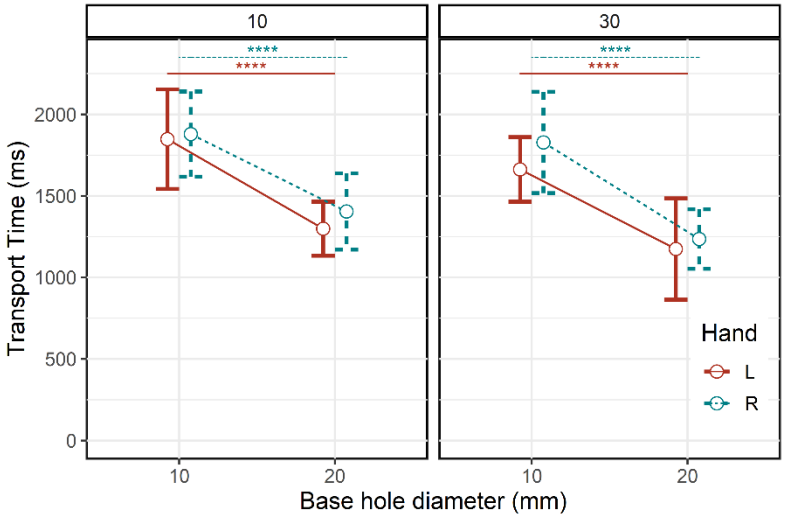

Figure 106: Transport Time for healthy controls being affected by base-hole diameter at each level of grasp surface size

8.5 Discussion

EDT has been robust in determining the time duration taken by the participant during reaching and transport phase of the movement. Currently, pilot testing of EDT was limited to three healthy controls due to the COVID-19 pandemic otherwise should have been tested for minimum of ten participants. And in future it is suggested that it should be tested with a larger data set to access its ability in discriminating MS patients from healthy controls and against current clinical standards, and track disease progression over time. Linford Constantino Fernandes is now conducting research at the Leeds Institute for Clinical Trials Research, School of Medicine, to ascertain the application of the EDT in clinical settings for his project, "Kinematic Assessment of Upper Limb Function in Progressive Multiple Sclerosis." Using BIGKAT in conjunction with EDT and validating EDT its performance against the Nine-Hole PEG test (NHPT), Expanded Disability Status Scale (EDSS), and other qualitative measures. Linford seeks to examine the level and evolution of upper limb disability in progressive MS patients. Results from this pilot study suggest that grasp size affected the reach component as shown in Figure 105, while base hole diameter was responsible for longer transport time as shown in Figure 106. This increase in transport time is due to the fact that the smaller hole in the base fits snuggly onto the peg

and trial would not end until object fits properly. This increases the demands of eye-hand coordination by the participant such that he/she must insert the object perpendicular to the peg to end the trial. No significant differences were found for the reaction time for any task constraints which is mainly because of the low sample size.

In this pilot study, temporal measures from EDT were analysed but it still remains to be validated against the temporal measures from BIGKAT. Both EDT and BIGKAT recorded movements until the participant completely placed the object onto the peg. In this pilot study, only EDT's temporal data was analysed, as BIGKAT's data has already been analysed and validated in chapter 3, 4 and 5. But it remains to be validated how the temporal measures from EDT correlate with the corresponding temporal measures from BIGKAT, which is planned for the near future with large dataset. BIGKAT itself can provide rich temporal measures as obtained from EDT but it requires sub-setting dataset based on threshold to determine movement onset and offset (if reaching velocity exceeds by and drops by 50mm/s). BIGKAT together with EDT can overcome this limitation by sub-setting positional data from BIGKAT into reaching and transport phase by the timestamps provided by EDT. Other than that, BIGKAT and EDT data can be used to determine the time taken by the participant when the object was being lifted from the peg (object manipulation time) and the time taken when the object was being inserted into the peg at the end of trial (object insertion time). Hence, quantifying such important temporal measures while manipulating objects can provide a useful insight into disease progression and severity of movement disorders.

Chapter 9: Conclusions & Future Works

9.1 Summary of Findings

This thesis aimed to explore the opportunities for objectively measuring and studying sequential 'reach-to-grasp' and repetitive 'finger-tapping' movement of upper limb using low-cost portable motion capture tools i.e., optoelectronics, virtual-reality, and deep-learning. The goal was to test the feasibility of using a portable and affordable motion capture tool to quantify hand kinematics and manual dexterity outside of a laboratory environment and to explore alternatives to opto-electronic marker tracking for quantifying sequential and repetitive actions. Each of the key objectives will be reviewed in turn and were as follows.

1) Evaluate the suitability of the PSAT optoelectronic marker tracking system for use in measuring hand kinematics by:

1.1 Extending the existing PSAT system into a Boxed Infrared Gross Kinematic Assessment Tool (BIGKAT) capable of capturing and analysing kinematic data related to hand and arm movements;

1.2 Benchmarking the new BIGKAT system against an existing gold standard for motion capture (Optotrak) to determine the working volume in which BIGKAT provides an acceptable level of precision and accuracy; and

1.3 Validating the new BIGKAT system by comparing it with an existing gold standard for motion capture (Optotrak) when measuring reach-to-grasp and finger-tapping activities.

The Boxed Infrared Kinematic Assessment Tool (BIGKAT), which was developed from the existing PSAT, was used in this thesis to investigate the possibilities for objectively evaluating reach-to-grasp actions utilising a low-cost, portable optical motion capture system. It was intended to find out if spatiotemporal characteristics could be accurately and precisely measured by determining BIGKAT's working volume and benchmarking its strength against the research-grade Optotrak system. The conclusions drawn from this research are as follows:

The findings from Chapter 3 revealed the spatial accuracy and precision levels associated with the PSAT system, consequently locating the source (hardware & software) of error while tracking IREDs and provided solutions to overcome them. The modifications were made to the existing PSAT system, such as replacing bespoke IREDs with opto-markers due to the measurement noise generated by glares from bespoke IREDs. The PSAT system was developed to track two IREDs only and when the number of IREDs being tracked was increased, PSAT would mix up the IREDs seen from the different cameras, resulting in false triangulation and inaccurate 3D positional data. This was resolved by

changing the tracking algorithm to correctly label markers based on minimum distance between IREDs in successive frames and throughout the video. With this in place, the PSAT system had been adapted into the proposed BIGKAT system that could reliably track the multiple markers required for prehension experiments.

The investigation of spatial accuracy and precision in Chapter 3 demonstrated that BIGKAT can accurately determine IRED positions when compared with the positional data of Optotrak. Several subsets of tracking area, with a MAE less than 5mm, were found in the horizontal plane ranging from as large as $720 \times 648\ mm^2$ to $72 \times 72\ mm^2$ (centered around the middle FOV). The vertical resolution was also determined at three different distances (700, 1400 & 2100mm) from BIGKAT to determine how far the BIGKAT can accurately resolve IRED position. It was found the tracking accuracy significantly decreases by increasing the distance between the BIGKAT and experimental setup, and tracking accuracy is sufficient when movements are carried out within a distance of 700mm to 1400mm from BIGKAT. It was found that in order to accurately and precisely estimate the IRED position, movements should be made within a tracking volume of $720 \times 648 \times 576\ mm^3$ which was acquired via horizontal and vertical resolution experiments. This tracking volume has a mean absolute error of less than 5mm and a root mean square error of less than 0.001mm in each dimension. This tracking volume is suitable for conducting reach-to-grasp studies, with variations in tracking area depending on the experimental setup.

Chapter 4 and 5 further investigated and validated the performance of BIGKAT by comparing the spatiotemporal characteristics of reach-to-grasp and finger tapping movements against the research-grade Optotrak system. The results of regression analysis between kinematic measures obtained from BIGKAT and Optotrak showed a linear relationship between both devices with large R-squared values and low-intercept values. The results showed a strong correlation between BIGKAT and Optotrak, indicating that BIGKAT is capable of capturing the kinematic features associated with fine and gross motor abilities. This validates the applicability of BIGKAT in objectively analysing motor tasks and provides insights into motor development and identification of individuals at risk.

The second objective of the project was to investigate alternatives to opto-electronic marker tracking for quantifying prehension actions, which were as follows:

2) Investigate three alternatives to opto-electronic marker tracking for quantifying prehension actions:

2.1 Leap Motion: hand tracking technology used to perform prehension tasks in virtual reality.

2.2 DeepLabCut: a machine learning algorithm for marker-less motion tracking from recorded video by using sample videos as a training set; and

2.3 An Event Detection Kit designed and developed as part of this thesis that detects the timing of different phases of prehension activities based on an object being grasped and moved.

Chapter 6 evaluated the potential of using VR and finger tracking, specifically Leap Motion, for studying prehensile behaviour. This study aimed to compare prehensile performance in two virtual environments (VEs) with alternative sensory feedback and compared it to performance in the real world. It was found that the hand visual feedback in VR environments strongly affected the kinematics of the reaching component, with the "HV" environment (hand visual feedback but no haptics condition) showing stronger correlation with real-world reaching than "Hap" (haptics but no hand visual feedback condition). Grasping profiles in VR environments showed strong correlation with real-world grasping, indicating that grip aperture scaled according to object size, but when hand visual feedback was absent, participants exhibited a larger grip aperture and safety margin compared to real-world movements. Strong correlation was found between wrist velocity and grip aperture profiles in real and virtual environments indicating that participants used similar reach-to-grasp strategies, preserving the coordination between reach and grasp components. Comparing real and VR environments, participants moved slower in VR with longer movement and deceleration times, and differences in movement time (MT) were significant between Real and VEs. The absence of haptic or visual feedback in VR did not significantly affect MT but VR itself was responsible for the slowness of movements, compared to real-world prehensile movements. Participants achieved maximum wrist velocity later in the movement in VR compared to real-world movements, suggesting participants moved slower with a longer deceleration phase achieving maximum wrist velocity relatively later in the movement showing significant differences to the real-world prehensile movements. The findings highlighted the importance of sensory feedback, such as hand visual information, in guiding reach-to-grasp actions in virtual environments.

The findings of this study have important implications for the use of virtual reality (VR) and finger tracking in motor studies. While VR can serve as an alternative to optical motion capture systems, it is essential to consider certain factors for effective utilization. Firstly, the study highlights the significance of hand visual feedback in guiding prehensile movements in VR. The absence of hand visual information during the initial and final phases of the movement trajectory led to systematic biases and affected the coordination and timing of reaching actions. Therefore, incorporating hand visual feedback in VR setups is crucial to ensure accurate and natural movement patterns. Additionally, the study suggests that haptic feedback may not be necessary for successful completion

of the grasping action. Information about finger position and object contact points was found to be sufficient. This implies that while haptics can enhance the realism of the VR experience, it may not be essential for studying basic kinematic aspects of prehension.

Chapter 7 aimed to evaluate the suitability of DeepLabCut (DLC) for studying prehensile tasks by training a deep neural network model by the images from the videos recorded by BIGKAT. However, due to the limitations imposed by the COVID-19 pandemic and the lack of diversity in the training dataset, the study could not proceed further, and the trained network was not able to determine statistically significant differences. Inferential statistics showed that spatial measures were largely affected by the large amount of variability in the resolved 3D positional data specifically during longer movements and this effectively reduced the statistical power of the study. But DLC was still able to translate task constraints by scaling reaching and grasping trajectories. Further training with a more diverse dataset could enable the DLC network to resolve kinematic differences and facilitate the discrimination of patients from controls.

Chapter 8 focused on the development and pilot study of the Event Detection Kit (EDK). It further contributed by providing a tool specifically designed to detect and analyse different phases of reach-to-grasp-to-lift-to-transport actions. The EDK, used in conjunction with BIGKAT, offers a comprehensive approach to capturing and analysing both spatial and temporal aspects of prehension movements, providing valuable insights into upper limb dysfunction and functional independence.

9.2 Discussion

Motor dysfunction in neurodegenerative diseases like Parkinson's disease (PD) and multiple sclerosis (MS) significantly impacts quality of life and functional independence. Current clinical assessment methods for motor performance in PD and MS rely on subjective observations and visual interpretation, leading to variability and limitations in diagnosing and quantifying symptoms. Bradykinesia, a primary symptom of PD, is currently assessed subjectively through visual observations, highlighting the need for more objective and quantitative assessment methods. Multiple sclerosis affects young adults and causes upper-limb motor dysfunction, impacting activities of daily living, making objective measurements crucial for assessing the progression of the disease and designing interventions. Laboratory-based motion capture systems and wearable sensors have shown potential in tracking kinematic landmarks and assessing upper limb function in MS [20], [100], [295]–[297]. Regarding the importance of low-cost, portable, and easy-to-use motion capture systems, there are several research gaps and limitations in the field that highlight the need for such systems. There are challenges in implementing these technologies in clinical practice, some of these include:

Cost: Research-grade optoelectronic motion capture systems can be expensive, limiting their accessibility to researchers, small-scale projects, or individuals with limited resources. Low-cost alternatives are needed to make motion capture technology more widely available.

Portability: Many motion capture systems require a controlled environment with specialized equipment, making them less suitable for fieldwork or real-world applications. Portable systems are necessary to enable motion capture in diverse settings.

Ease of use: Current motion capture systems often require technical expertise to set up, calibrate, and operate. Simplifying the process and making it more user-friendly would enable a wider range of users to utilize motion capture technology effectively.

The development of low-cost, portable, and accessible technologies could improve early diagnosis, monitoring, and intervention for motor disorders. Various sensing technologies, including inertial sensors, sensor-engineered gloves, EMG, and optoelectronic motion capture systems, are being used to study upper limb motor dysfunction in laboratory settings [20], [97], [98], [102], [175], [218], [296]–[301]. By addressing these limitations and developing low-cost, portable, and easy-to-use motion capture systems, researchers can advance the field in several ways:

Accessibility: Making motion capture technology more affordable and user-friendly would allow researchers, educators, and practitioners from various fields to incorporate motion capture into their work, promoting interdisciplinary collaborations and expanding the applications of motion analysis.

Versatility: Portable systems would enable motion capture in real-world scenarios, such as sports training, healthcare, entertainment, and virtual reality, providing researchers and professionals with valuable data in more naturalistic settings.

Innovation: Low-cost and user-friendly systems can encourage innovation and experimentation, as they lower the barrier to entry for individuals and organizations interested in exploring new applications and techniques.

Objective measurement and analysis of reaching and grasping movements can provide insights into movement patterns and their implications for activities of daily living. Despite the potential benefits, the practical implementation of objective assessments remains a challenge, requiring further research and development in the field. Such as to address the limitations of motion capture research, low-cost motion capture systems should be compared with research-grade optoelectronic system (such as Optotrak) to evaluate their accuracy and reliability across different movement tasks and conditions. And conducting studies in specific domains, such as sports, healthcare, or rehabilitation, can provide

insights into the practical utility and limitations of low-cost motion capture systems in various contexts. The research presented in this thesis helps to advance this in a number of ways.

Chapter 3 contributes to advancing the field of motion capture by evaluating the spatial accuracy and precision of the BIGKAT system. It provides valuable information on the system's performance, identifying subsets of accurate tracking and offering guidelines for optimal usage in prehension studies.

BIGKAT offers potential solution for overcoming cost and space limitations of traditional motion capture systems. The research builds upon existing literature that explored motion capture systems and their application in prehension studies. The comparison with the Optotrak system served as a benchmark for evaluating the performance of BIGKAT and provided a basis for assessing its suitability for clinical applications. The performance of BIGKAT in capturing reach-to-grasp movements, particularly concerning object size and location, had significant implications for clinical practice. The system was found to be reliable and accurate in capturing and analysing these movements, making it a valuable tool in clinical assessments. Objective measurements and insights into motor control and coordination could be obtained through its use.

The exploration of BIGKAT as an assessment tool in clinical routine, which involved kinematic analysis of Finger Tapping movements performed by PD patients and healthy controls, expanded the scope of motion capture systems in clinical settings. In chapters 3, 4, and 5, the advantages of using low-cost and portable optical motion capture systems like BIGKAT were highlighted. The findings demonstrated the potential of these systems to enhance clinical assessments and interventions for a range of motor-related conditions. Further research in this area may involve investigating reach-to-grasp movements in specific clinical populations or assessing the system's performance under different experimental conditions. Additionally, the integration of BIGKAT with other assessment tools or modalities could be explored to provide a more comprehensive evaluation of motor performance and facilitate interdisciplinary approaches in clinical practice. Optical motion capture systems are not the only way of capturing kinematics. Hence, other low-cost alternatives to optical motion capture systems were investigated.

Technological advancements in virtual reality (VR) systems offer opportunities for novel strategies in difficult-to-reach populations to support treatment and enhance functional improvements. Investigation was made to determine the kinematic similarity between reach-to-grasp movements in virtual environments and real-world movements. Profiles of reaching and grasping over normalized time showed invariant movement patterns across environments, with variations in maximum grip aperture (MGA) and peak velocity (PV) values and their timing [112], [117], [118], [228], [302]. Despite

absolute landmark changes, the correlations between conditions were preserved, indicating that participants used similar reach-to-grasp actions and maintained coordination between reaching and grasping components. Participants took longer to reach for and grasp the object in VEs, suggesting participants moved slower with a longer deceleration phase achieving maximum wrist velocity relatively later in the movement showing significant differences to the real-world prehensile movements. Visual guidance played a crucial role in achieving an appropriate grip aperture, while the absence of haptic feedback increased grip aperture as a safety measure. Kinematic similarities between reach-to-grasp movements in VR with visual or haptic guidance were observed, but critical differences existed, and combined visuo-haptic guidance (real-world movements) optimized movement by reducing grip aperture and speeding up the reaching component. Overall, the findings suggest that VR combined with finger tracking technology can be a valuable tool for studying changes in motor behaviour. Although some differences were observed between VR and real-world movements, the study demonstrates that prehensile movements made in VR still produced statistically significant kinematic measures and showed kinematic similarities to real-world movements. This indicates that VR can provide a close approximation of real-world scenarios and can be used to investigate motor changes in a controlled and immersive environment.

However, it is important for researchers to acknowledge the potential differences introduced by VR and account for them in their experimental design and interpretation of results. Adjustments may need to be made to account for factors such as slower reaching velocity in VR or the influence of hand visual feedback on grasping actions. By considering these implications, VR and finger tracking can be effectively utilized in motor studies, offering new possibilities for understanding and evaluating motor function and rehabilitation approaches.

Computer vision techniques, using smartphones or cameras, are employed to extract movement information from images or videos. Marker-less human pose estimation using machine learning techniques such as DeepLabCut (DLC) is another approach to motion capture. It eliminates the need for markers and uses computer vision algorithms to estimate body pose from images or videos [303], [304]. These methods have been used to assess bradykinesia in Parkinson's patients and extract finger tapping information. However, they may have limitations in capturing 2D movement and absolute hand measurements [182], [305]. By leveraging machine learning techniques, marker-less human pose estimation models can accurately track and reconstruct the human body's movements without the requirement of attaching markers to the subject's body. Two networks trained with different datasets were used to analyse unseen videos. Repeated measures analysis of variance showed significant differences between task constraints for some kinematic measures, primarily the spatial measures and no significant differences were found for temporal measures. The observed disparities in spatial

and temporal measures were further analysed through residual plots, which showed non-linearity and large deviations due to outliers. The study suggests that refining the training dataset and improving network performance could help resolve kinematic differences more reliably. Despite limitations, DLC has the potential to measure human movement disorders and provide objective clinical trial outcomes. Future work should focus on training an accurate and precise DLC network using a larger and more diverse dataset. Overall, marker-less human pose estimation using machine learning techniques offers a promising and versatile approach to motion capture, enabling more natural and immersive interactions between humans and digital environments. As technology continues to advance, we can expect further progress in this field and the development of more sophisticated and accurate pose estimation methods.

The Event Detection Tool (EDT) has shown effectiveness in determining the duration of reaching and transport phases in movements. However, due to the COVID-19 pandemic, its pilot testing was limited to three healthy controls. The pilot study revealed that grasp size influences the reach component, while base hole diameter affects transport time. However, no significant differences in reaction time were found, likely due to the small sample size. The combination of data from BIGKAT and EDT can provide valuable insights into object manipulation time and object insertion time, which can contribute to understanding disease progression and the severity of movement disorders. The pilot study did not find significant differences, likely due to the small sample size. The temporal measures obtained from EDT need to be validated against the corresponding measures from BIGKAT in future studies. Combining the data from BIGKAT and EDT can provide insights into object manipulation time and object insertion time, which can be useful for understanding disease progression and severity of movement disorders.

9.3 Contributions of this research

This research contributes to the development of low-cost, portable, and easy-to-use solutions for the quantitative assessment of sequential 'reach-to-grasp' and repetitive 'finger-tapping' movements produced by neurologically deficit and/or intact populations in clinical and/or non-clinical settings. The contributions are summarized as below:

BIGKAT's spatial and temporal resolution was established and validated against high-end Optotrak to determine maximum and minimum positional errors (accuracy) and RMS error (precision) it produces while tracking markers. Results showed that the tracking volume of $720 \times 648 \times 576\ mm^3$ produces maximum average error less than 5mm and RMS error less than 0.001mm in each dimension. Such tracking volume is sufficient for capturing and analysing kinematic data related to hand and arm movements. Hence, BIGKAT can reliably be deployed for undertaking reach-to-grasp studies and its performance was then evaluated by concurrently recording reach-to-grasp movements with Optotrak.

Five kinematic measures (two spatial and three temporal) were extracted from 3D positional coordinates of both devices. ANOVA and linear regression analysis between all measures was carried out to determine if BIGKAT can find statistically significant results in similar to Optotrak and how these measures are related to Optotrak. Results showed that low-cost, portable BIGKAT found similar statistically significant results as obtained by expensive Optotrak. Similarly, regression analysis depicted strong relationship between BIGKAT and Optotrak with nearly unity slope, low y-intercept values, large R-squared value with significant p-value. For instance, Parkinson's disease patients often experience impairments in motor control, leading to difficulties in performing fine motor tasks like reaching and grasping. BIGKAT allows for detailed analysis of kinematic data during reach-to-grasp movements, providing information on movement smoothness, accuracy, and coordination between finger and thumb. This information can aid in understanding the specific motor control deficits in Parkinson's patients and guide rehabilitation strategies. Longitudinal kinematic analysis using BIGKAT can help monitor disease progression in Parkinson's patients over time. By regularly assessing kinematic parameters of upper limb movements, clinicians can track changes in motor function, identify deterioration trends, and adjust treatment plans accordingly to optimize patient care.

Similarly, BIGKAT was deployed for the quantitative assessment of bradykinesia (Finger Tapping movement – conventional clinical examination) by attaching two infrared markers: one at the distal end of the finger and other at distal end of the thumb. Finger-tapping is analogous to the grasping component of prehension, requiring co-ordination between finger and thumb and provides a test of BIGKAT's ability to reliably record the aperture between the two digits. BIGKAT and Optotrak simultaneously recorded finger tapping (FT) movements made by PD patient and a healthy control to determine if BIGKAT can find statistically significant differences between the subjects as by Optotrak. Three kinematic measures related to bradykinesia (average speed, amplitude variance and rhythm regularity) were extracted from the 3D positional data to quantify FT movement. Results from BIGKAT and Optotrak found significant differences between PD patients and healthy controls for all three kinematic measures and for each hand and found strong correlations between the corresponding objective measures as well. The results proved that the low-cost motion capture system BIGKAT can compute the principal characteristics of bradykinesia and have paved the way for its potential usage in clinical settings. Thus, BIGKAT measures exhibit convergent validity with Optotrak measures, demonstrating the applicability of BIGKAT to be deployed in clinical and laboratory settings. Motion capture systems like BIGKAT, enable precise and objective measurement of bradykinesia, which is a common motor symptom in Parkinson's disease characterized by slow and reduced movements. By quantifying the kinematic parameters of finger-tapping movements, such as average speed, amplitude

variance, and rhythm regularity, these methods can provide valuable insights into the severity and progression of bradykinesia in Parkinson's patients.

Characterising kinematic differences produced in three different environments (based on available sensory information) can help understand what trade-offs have to be taken care of while using VR approaches to study prehension skills, to guide future clinical inquiry and upper limb rehabilitation that is transferable into real-world functional independence. Our study shows that reach and grasp components were strongly correlated in both environments and showed properly coordinated reaching and grasping kinematic profiles. Instead of similarities, we also found significant differences in kinematic landmarks demonstrating key role of hand vision and haptic feedback during initial and final phase of movement trajectory. In conclusion, these findings suggest that in the absence of sensory information, prehensile movement show systematic biases, signifying the importance of online sensory information to guide the hand until it makes contact with the object. And in order for the grasping action to be completed successfully, information about fingers position and object contact points is sufficient.

Computer vision algorithms for marker-less pose estimation using deep learning tools have been rapidly advanced and broadly adapted in a very short time, partly fuelled by sharing toolkits in public repositories on GitHub. Open source DeepLabCut (DLC) was used for marker-less tracking of reach-to-grasp movements and evaluated its performance by training two networks with different training dataset. Due to the COVID-19 pandemic and before lockdown was imposed, this study managed to collect reach-to-grasp videos from 8 participants only and therefore, was paused for further data collection. However, results show that despite higher noise levels in the resolved 3D dataset, DLC was able to translate task constraints by scaling reaching and grasping components but grasp size at the end of the movement does not match object size being grasped due to the higher noise levels in the resolved 3D dataset. And inferential statistics showed that spatial measures were largely affected by the large amount of variability in the resolved 3D positional data specifically during longer movements and this effectively reduced the statistical power of the study. Similarly, no significant effect was found for temporal measures except for movement time. But overall, a DLC network trained on a more diverse dataset might be able to statistically resolve kinematic differences and can be further utilized to discriminate patients from controls.

An Event Detection Tool (EDT) was designed using off the shelf products that detects the timing of different phases of prehension activities based on an object being grasped and moved. EDT provides temporal measures like reaction time, reaching time, transport time and movement time. A pilot study was conducted using EDT in which healthy controls were instructed to reach for, grasp, lift and transport four cylindrical object varied by grasp surface size (10 & 30mm) and diameter of the hole

(10 & 20mm). Due to the COVID-19 pandemic, this study managed to collect data from three participants only and was unable to find significant difference between outcome measures for different objects. Due to low sample size, data from EDT was analysed only and it remains to be validated that how the temporal measures from EDT correlates with the corresponding temporal measures from BIGKAT, which is planned for near future with large dataset. Hence, quantifying such important temporal measures while manipulating object can provide a useful insight into disease progression and severity of movement disorder.

9.4 Conclusions

In conclusion, this thesis successfully evaluated the suitability of a low-cost motion capture system for measuring hand kinematics and explored alternatives to opto-electronic marker tracking for quantifying prehension actions. The findings validated the performance of the developed BIGKAT system, demonstrated the importance of sensory feedback in prehensile behaviour, and proposed the use of the EDK for assessing prehension movements. These contributions enhance our understanding of prehensile actions and provide valuable tools for objectively measuring and analysing hand kinematics in various contexts. This thesis has demonstrated the feasibility and effectiveness of using low-cost optical motion capture systems, such as BIGKAT, for objective measurement of hand kinematics in prehension studies. The integration of alternative tracking methods, such as Virtual Reality, DeepLabCut and Event Detection Kit expands the possibilities for studying prehension actions in various contexts. These methods provide researchers with additional tools to analyse hand movements, particularly in virtual reality environments and marker-less scenarios. The combination of BIGKAT with these alternative methods allows for a more comprehensive analysis of both spatial and temporal aspects of prehension movements, enhancing our understanding of motor skills and functional independence.

Furthermore, the findings from this research have implications beyond the academic realm. The development of low-cost and portable motion capture systems opens opportunities for applications in clinical settings, rehabilitation centres, and even home-based assessments. With BIGKAT, healthcare professionals can objectively evaluate motor impairments, track the progress of rehabilitation programs, and tailor interventions to individuals' specific needs. This technology has the potential to improve the quality of care and enhance the functional outcomes of patients with hand-related conditions,

In summary, this thesis has demonstrated the value of low-cost optical motion capture systems, such as BIGKAT, in objectively measuring hand kinematics during prehension actions. The integration of alternative tracking methods, such as Leap Motion and DeepLabCut, expands the capabilities and applications of motion capture technology. These advancements have the potential to benefit both

the research and clinical communities. As technology continues to advance, we can expect further innovations in motion capture systems, leading to even more accurate, accessible, and versatile tools for studying and enhancing human movement.

9.5 Future Works

To enhance the tracking accuracy of BIGKAT, it is suggested to update the tracking algorithm to communicate with the active markers used by the BIGKAT system. This communication would reduce the chances of mislabelling markers in consecutive frames captured by the cameras. The use of active opto-markers provides low spatial noise values, characterized by high glare, and their integration with the tracking algorithm would improve the overall tracking accuracy of BIGKAT.

BIGKAT has demonstrated its effectiveness in studying sequential prehensile movements in healthy individuals. However, further research is needed to determine whether it can accurately identify subtle differences between individuals with neurological deficits and healthy controls. In the context of Parkinson's disease (PD), BIGKAT has been utilized to differentiate PD patients from healthy controls by kinematically analysing repetitive finger tapping movements. To fully assess BIGKAT's potential in clinical settings, it is recommended to evaluate its ability to discriminate PD patients from healthy controls and monitor disease progression. Deploying BIGKAT in clinical settings can provide valuable insights into the motor impairments associated with PD and aid in tracking the progression of the disease. Similarly, the use of virtual reality (VR) setups for studying prehensile movements in individuals with neurological deficits has not been extensively explored. Future research should focus on evaluating the capability and usability of VR in clinical settings for assessing and analysing prehensile movements in individuals with neurological impairments. By incorporating VR technology, clinicians and researchers can potentially gain valuable insights into the motor deficits and functional limitations experienced by these individuals. VR-based assessments may offer a novel and engaging approach to rehabilitation and intervention strategies for neurological conditions.

Future works in marker-less human pose estimation using machine learning techniques such as DeepLabCut (DLC) can focus on several aspects:

Dataset Improvement: Future research should aim to refine and expand the training dataset used for marker-less tracking of reach-to-grasp movements. Increasing the size and diversity of the dataset can help improve the accuracy and generalizability of the models.

Network Performance Enhancement: Efforts should be made to enhance the performance of the trained network. This can involve optimizing the architecture, fine-tuning hyperparameters, or exploring advanced deep learning techniques to achieve more reliable and precise results.

Clinical Applications: Future work should explore the application of DLC in assessing and measuring movement disorders in clinical settings. This can involve conducting studies to evaluate the reliability and validity of these techniques compared to traditional motion capture methods. Additionally, the use of marker-less pose estimation in clinical trials can provide objective and quantitative outcomes for assessing treatment effectiveness.

Larger and Diverse Datasets: Training the marker-less human pose estimation models on larger and more diverse datasets can help improve their accuracy and robustness. Including a wider range of subjects with varying demographics, body types, and movement patterns can enhance the generalizability and applicability of the models.

Advancements in Technology: As technology continues to advance, there is the potential for the development of more sophisticated and accurate pose estimation methods. This includes leveraging advancements in computer vision, machine learning, and hardware capabilities to enhance the precision, speed, and usability of marker-less pose estimation systems.

Overall, future work in marker-less human pose estimation should focus on refining the models, expanding the datasets, validating the techniques in clinical settings, and leveraging advancements in technology to further improve the accuracy and applicability of these methods.

The Event detection tool (EDT) has not been tested with large datasets involving MS patients and healthy controls. It is recommended to conduct future testing with a larger dataset to assess its ability to differentiate multiple sclerosis (MS) patients from healthy controls and track disease progression. Researcher Linford Constantino Fernandes is currently conducting a study to evaluate the application of EDT in clinical settings for assessing upper limb function in progressive MS patients. The study aims to validate EDT by comparing it with the Nine-Hole PEG test, Expanded Disability Status Scale, and other qualitative measures [306], [307]. It is recommended to validate the temporal measures obtained from EDT against corresponding measures from BIGKAT in future studies.

9.6 Research Publications

Journal article was submitted and published in Journal of the Neurological Sciences: **'The discerning eye of computer vision: Can it measure Parkinson's finger tap bradykinesia?'**
https://doi.org/10.1016/j.jns.2020.117003

Two conferences posters covering results from BIGKAT and EDT were presented at European Committee for Treatment and Research in Multiple Sclerosis (ECTRIMS) and are as follows

- Fernandes,d L., Hafeez, A., Coats, R., Mon-Williams, M. and Ford, H., 2020, December. Kinematic assessment of upper limb function in progressive multiple sclerosis. In *MULTIPLE*

SCLEROSIS JOURNAL (Vol. 26, No. 3_ SUPPL, pp. 167-168). 1 OLIVERS YARD, 55 CITY ROAD, LONDON EC1Y 1SP, ENGLAND: SAGE PUBLICATIONS LTD.

- Fernandes, L., Hafeez, A., Coats, R.O., Mon-Williams, M. and Ford, H.L., 2021, October. Evaluation of upper limb impairment in progressive multiple sclerosis using kinematic techniques. In *MULTIPLE SCLEROSIS JOURNAL* (Vol. 27, No. 2_ SUPPL, pp. 276-277). 1 OLIVERS YARD, 55 CITY ROAD, LONDON EC1Y 1SP, ENGLAND: SAGE PUBLICATIONS LTD.

References

[1] R. O. Coats, A. J. Fath, S. L. Astill, and J. P. Wann, “Eye and hand movement strategies in older adults during a complex reaching task,” *Exp Brain Res*, vol. 234, no. 2, pp. 533–547, Feb. 2016, doi: 10.1007/s00221-015-4474-7.

[2] R. K. Raw, G. K. Kountouriotis, M. Mon-Williams, and R. M. Wilkie, “Movement control in older adults: does old age mean middle of the road?,” *Journal of Experimental Psychology*, p. 26, 2011.

[3] R. Coats, G. P. Bingham, and M. Mon-Williams, “Calibrating grasp size and reach distance: interactions reveal integral organization of reaching-to-grasp movements,” *Exp Brain Res*, vol. 189, no. 2, pp. 211–220, Aug. 2008, doi: 10.1007/s00221-008-1418-5.

[4] R. O. Coats, R. J. Holt, G. P. Bingham, and M. A. Mon-Williams, “Predicting the duration of reach-to-grasp movements to objects with asymmetric contact surfaces,” *PLoS ONE*, vol. 13, no. 2, p. e0193185, Feb. 2018, doi: 10.1371/journal.pone.0193185.

[5] R. G. Marteniuk, J. L. Leavitt, C. L. MacKenzie, and S. Athenes, “Functional relationships between grasp and transport components in a prehension task,” *Human Movement Science*, vol. 9, no. 2, pp. 149–176, Apr. 1990, doi: 10.1016/0167-9457(90)90025-9.

[6] M. Mon-Williams and G. P. Bingham, “Discovering affordances that determine the spatial structure of reach-to-grasp movements,” *Exp Brain Res*, vol. 211, no. 1, pp. 145–160, May 2011, doi: 10.1007/s00221-011-2659-2.

[7] R. G. Marteniuk, C. L. Mackenzie, M. Jeannerod, S. Athenes, and C. Dugas, “Constraints on human arm movement trajectories.,” *Canadian Journal of Psychology/Revue canadienne de psychologie*, vol. 41, no. 3, pp. 365–378, 1987, doi: 10.1037/h0084157.

[8] K. Libertus, K. A. Sheperd, S. W. Ross, and R. J. Landa, “Limited Fine Motor and Grasping Skills in 6-Month-Old Infants at High Risk for Autism,” *Child Dev*, p. n/a-n/a, Jun. 2014, doi: 10.1111/cdev.12262.

[9] S. Ozonoff *et al.*, “Gross Motor Development, Movement Abnormalities, and Early Identification of Autism,” *J Autism Dev Disord*, vol. 38, no. 4, pp. 644–656, Apr. 2008, doi: 10.1007/s10803-007-0430-0.

[10] B. Wright *et al.*, “Systematic approach to school-based assessments for autism spectrum disorders to reduce inequalities: a feasibility study in 10 primary schools,” *BMJ Open*, vol. 11, no. 1, p. e041960, Jan. 2021, doi: 10.1136/bmjopen-2020-041960.

[11] J. S. R. Leversen, M. Haga, and H. Sigmundsson, “From Children to Adults: Motor Performance across the Life-Span,” *PLoS ONE*, vol. 7, no. 6, p. e38830, Jun. 2012, doi: 10.1371/journal.pone.0038830.

[12] C. Voelcker-Rehage, “Motor-skill learning in older adults—a review of studies on age-related differences,” *Eur Rev Aging Phys Act*, vol. 5, no. 1, pp. 5–16, Apr. 2008, doi: 10.1007/s11556-008-0030-9.

[13] C. H. Adler *et al.*, “Low clinical diagnostic accuracy of early vs advanced Parkinson disease: Clinicopathologic study,” *Neurology*, vol. 83, no. 5, pp. 406–412, Jul. 2014, doi: 10.1212/WNL.0000000000000641.

[14] C. G. Goetz *et al.*, “Movement Disorder Society-sponsored revision of the Unified Parkinson’s Disease Rating Scale (MDS-UPDRS): Scale presentation and clinimetric testing results: MDS-UPDRS: Clinimetric Assessment,” *Mov. Disord.*, vol. 23, no. 15, pp. 2129–2170, Nov. 2008, doi: 10.1002/mds.22340.

[15] C. G. Goetz and G. T. Stebbins, “Assuring interrater reliability for the UPDRS motor section: Utility of the UPDRS teaching tape,” *Mov Disord.*, vol. 19, no. 12, pp. 1453–1456, Dec. 2004, doi: 10.1002/mds.20220.

[16] L. Bonzano *et al.*, “Quantitative Assessment of Finger Motor Impairment in Multiple Sclerosis,” *PLOS ONE*, vol. 8, no. 5, p. 7, 2013.

[17] B. Brandauer *et al.*, “Impairments of prehension kinematics and grasping forces in patients with cerebellar degeneration and the relationship to cerebellar atrophy,” *Clinical*

Neurophysiology, vol. 119, no. 11, pp. 2528–2537, Nov. 2008, doi: 10.1016/j.clinph.2008.07.280.
[18] S. R. Simon, "Quantification of human motion: gait analysis—benefits and limitations to its application to clinical problems," *Journal of Biomechanics*, vol. 37, no. 12, pp. 1869–1880, Dec. 2004, doi: 10.1016/j.jbiomech.2004.02.047.
[19] A. Pfister, A. M. West, S. Bronner, and J. A. Noah, "Comparative abilities of Microsoft Kinect and Vicon 3D motion capture for gait analysis," *Journal of Medical Engineering & Technology*, vol. 38, no. 5, pp. 274–280, Jul. 2014, doi: 10.3109/03091902.2014.909540.
[20] M. A. Wirth, G. Fischer, J. Verdú, L. Reissner, S. Balocco, and M. Calcagni, "Comparison of a New Inertial Sensor Based System with an Optoelectronic Motion Capture System for Motion Analysis of Healthy Human Wrist Joints," *Sensors*, vol. 19, no. 23, p. 5297, Dec. 2019, doi: 10.3390/s19235297.
[21] D. J. Geerse, B. H. Coolen, and M. Roerdink, "Kinematic Validation of a Multi-Kinect v2 Instrumented 10-Meter Walkway for Quantitative Gait Assessments," *PLoS ONE*, vol. 10, no. 10, p. e0139913, Oct. 2015, doi: 10.1371/journal.pone.0139913.
[22] L. C. Benson, C. A. Clermont, E. Bošnjak, and R. Ferber, "The use of wearable devices for walking and running gait analysis outside of the lab: A systematic review," *Gait & Posture*, vol. 63, pp. 124–138, Jun. 2018, doi: 10.1016/j.gaitpost.2018.04.047.
[23] M. Mon-Williams, J. R. Tresilian, V. E. Bell, V. L. Coppard, A. Jobling, and R. G. Carson, "The preparation of reach to grasp movements in adults with Down syndrome," *Human Movement Science*, vol. 20, no. 4–5, pp. 587–602, Nov. 2001, doi: 10.1016/S0167-9457(01)00069-0.
[24] J. Tresilian, *Sensorimotor control and learning: An introduction to the behavioral neuroscience of action*. in Sensorimotor control and learning: An introduction to the behavioral neuroscience of action. New York, NY: Palgrave Macmillan, 2012, pp. xxxii, 879.
[25] "Lifespan Development: A Psychological Perspective - Second Edition," *Open Textbook Library*. https://open.umn.edu/opentextbooks/textbooks/540 (accessed Apr. 06, 2021).
[26] S. Vieluf, G. Aschersleben, and S. Panzer, "Lifespan development of the bilateral deficit in a simple reaction time task," *Exp Brain Res*, vol. 235, no. 4, pp. 985–992, Apr. 2017, doi: 10.1007/s00221-016-4856-5.
[27] J. P. Piek, L. Dawson, L. M. Smith, and N. Gasson, "The role of early fine and gross motor development on later motor and cognitive ability," *Human Movement Science*, vol. 27, no. 5, pp. 668–681, Oct. 2008, doi: 10.1016/j.humov.2007.11.002.
[28] I. Flatters *et al.*, "Children's head movements and postural stability as a function of task," *Exp Brain Res*, vol. 232, no. 6, pp. 1953–1970, Jun. 2014, doi: 10.1007/s00221-014-3886-0.
[29] E. W. Bushnell and J. P. Boudreau, "Motor Development and the Mind: The Potential Role of Motor Abilities as a Determinant of Aspects of Perceptual Development," *Child Development*, vol. 64, no. 4, pp. 1005–1021, 1993, doi: 10.2307/1131323.
[30] L. Wijnroks and N. van Veldhoven, "Individual differences in postural control and cognitive development in preterm infants," *Infant Behavior and Development*, vol. 26, no. 1, pp. 14–26, Feb. 2003, doi: 10.1016/S0163-6383(02)00166-2.
[31] S. Schneiberg, H. Sveistrup, B. McFadyen, P. McKinley, and M. F. Levin, "The development of coordination for reach-to-grasp movements in children," *Exp Brain Res*, vol. 146, no. 2, pp. 142–154, Sep. 2002, doi: 10.1007/s00221-002-1156-z.
[32] A. H. Mason, J. L. Bruyn, and J.-A. C. Lazarus, "Bimanual coordination in children: manipulation of object distance," *Exp Brain Res*, vol. 231, no. 2, pp. 153–164, Nov. 2013, doi: 10.1007/s00221-013-3678-y.
[33] K. Grandez, G. Solas, P. Bustamante, and B. Sedano, "Sensor device for testing activities in Parkinson and ALS patients," in *Proceedings of the 4th International ICST Conference on Pervasive Computing Technologies for Healthcare*, Munchen, Germany: IEEE, 2010. doi: 10.4108/ICST.PERVASIVEHEALTH2010.8867.

[34] J. Tresilian, “Stability of reach-to-grasp movement patterns in Parkinson’s disease,” *Brain*, vol. 120, no. 11, pp. 2093–2111, Nov. 1997, doi: 10.1093/brain/120.11.2093.
[35] A. A. Faisal, L. P. J. Selen, and D. M. Wolpert, “Noise in the nervous system,” *Nat Rev Neurosci*, vol. 9, no. 4, pp. 292–303, Apr. 2008, doi: 10.1038/nrn2258.
[36] P. Neri, “How inherently noisy is human sensory processing?,” *Psychon Bull Rev*, vol. 17, no. 6, pp. 802–808, Dec. 2010, doi: 10.3758/PBR.17.6.802.
[37] P. L. Weir, B. J. Mallat, J. L. Leavitt, E. A. Roy, and J. R. Macdonald, “Age-Related Differences in Prehension: The Influence of Task Goals,” *Journal of Motor Behavior*, vol. 30, no. 1, pp. 79–89, Mar. 1998, doi: 10.1080/00222899809601324.
[38] R. O. Coats and J. P. Wann, “The reliance on visual feedback control by older adults is highlighted in tasks requiring precise endpoint placement and precision grip,” *Exp Brain Res*, vol. 214, no. 1, pp. 139–150, Sep. 2011, doi: 10.1007/s00221-011-2813-x.
[39] E. Boisseau, P. Scherzer, and H. Cohen, “Eye-Hand Coordination in Aging and in Parkinson’s Disease,” *Aging, Neuropsychology, and Cognition*, vol. 9, no. 4, pp. 266–275, Dec. 2002, doi: 10.1076/anec.9.4.266.8769.
[40] Y.-X. Wang *et al.*, “Associations between cognitive impairment and motor dysfunction in Parkinson’s disease,” *Brain and Behavior*, vol. 7, no. 6, p. e00719, 2017, doi: https://doi.org/10.1002/brb3.719.
[41] I. Flatters, P. Culmer, R. J. Holt, R. M. Wilkie, and M. Mon-Williams, “A new tool for assessing head movements and postural sway in children,” *Behav Res*, vol. 46, no. 4, pp. 950–959, Dec. 2014, doi: 10.3758/s13428-013-0419-x.
[42] J. P. Piek, G. B. Baynam, and N. C. Barrett, “The relationship between fine and gross motor ability, self-perceptions and self-worth in children and adolescents,” *Human Movement Science*, vol. 25, no. 1, pp. 65–75, Feb. 2006, doi: 10.1016/j.humov.2005.10.011.
[43] I. J. Flatters, “Posture and Visuomotor Performance in Children,” p. 172.
[44] I. Flatters, F. Mushtaq, L. J. B. Hill, R. J. Holt, R. M. Wilkie, and M. Mon-Williams, “The relationship between a child’s postural stability and manual dexterity,” *Exp Brain Res*, vol. 232, no. 9, pp. 2907–2917, Sep. 2014, doi: 10.1007/s00221-014-3947-4.
[45] P. R. Culmer, M. C. Levesley, M. Mon-Williams, and J. H. G. Williams, “A new tool for assessing human movement: The Kinematic Assessment Tool,” *Journal of Neuroscience Methods*, vol. 184, no. 1, pp. 184–192, Oct. 2009, doi: 10.1016/j.jneumeth.2009.07.025.
[46] E. J. Smits *et al.*, “Standardized Handwriting to Assess Bradykinesia, Micrographia and Tremor in Parkinson’s Disease,” *PLoS ONE*, vol. 9, no. 5, p. e97614, May 2014, doi: 10.1371/journal.pone.0097614.
[47] P. Feys *et al.*, “The Nine-Hole Peg Test as a manual dexterity performance measure for multiple sclerosis,” *Mult Scler*, vol. 23, no. 5, pp. 711–720, Apr. 2017, doi: 10.1177/1352458517690824.
[48] M. M. Schoemaker, A. S. Niemeijer, B. C. T. Flapper, and B. C. M. Smits-Engelsman, “Validity and reliability of the Movement Assessment Battery for Children-2 Checklist for children with and without motor impairments,” *Developmental Medicine & Child Neurology*, vol. 54, no. 4, pp. 368–375, 2012, doi: https://doi.org/10.1111/j.1469-8749.2012.04226.x.
[49] L. H. Eddy *et al.*, “The validity and reliability of observational assessment tools available to measure fundamental movement skills in school-age children: A systematic review,” *PLoS ONE*, vol. 15, no. 8, p. e0237919, Aug. 2020, doi: 10.1371/journal.pone.0237919.
[50] W. Cools, K. D. Martelaer, C. Samaey, and C. Andries, “Movement Skill Assessment of Typically Developing Preschool Children: A Review of Seven Movement Skill Assessment Tools,” *J Sports Sci Med*, vol. 8, no. 2, pp. 154–168, Jun. 2009.
[51] T. Brown and A. Lalor, “The Movement Assessment Battery for Children—Second Edition (MABC-2): A Review and Critique,” *Physical & Occupational Therapy In Pediatrics*, vol. 29, no. 1, pp. 86–103, Jan. 2009, doi: 10.1080/01942630802574908.

[52] S. Williams *et al.*, “The discerning eye of computer vision: Can it measure Parkinson’s finger tap bradykinesia?,” *Journal of the Neurological Sciences*, vol. 416, p. 117003, Sep. 2020, doi: 10.1016/j.jns.2020.117003.
[53] J. Parkinson, “An Essay on the Shaking Palsy,” *J Neuropsychiatry Clin Neurosci*, p. 14, 2002.
[54] V. L. Feigin *et al.*, “Global, regional, and national burden of neurological disorders during 1990–2015: a systematic analysis for the Global Burden of Disease Study 2015,” *The Lancet Neurology*, vol. 16, no. 11, pp. 877–897, Nov. 2017, doi: 10.1016/S1474-4422(17)30299-5.
[55] E. R. Dorsey and B. R. Bloem, “The Parkinson Pandemic—A Call to Action,” *JAMA Neurol*, vol. 75, no. 1, p. 9, Jan. 2018, doi: 10.1001/jamaneurol.2017.3299.
[56] E. R. Dorsey, T. Sherer, M. S. Okun, and B. R. Bloem, “The Emerging Evidence of the Parkinson Pandemic,” *JPD*, vol. 8, no. s1, pp. S3–S8, Dec. 2018, doi: 10.3233/JPD-181474.
[57] T. Pringsheim, N. Jette, and A. Frolkis, “The prevalence of Parkinson’s disease A systematic review and meta-analysis.pdf.”
[58] A. J. Hughes, S. E. Daniel, Y. Ben-Shlomo, and A. J. Lees, “The accuracy of diagnosis of parkinsonian syndromes in a specialist movement disorder service,” *Brain*, vol. 125, no. 4, pp. 861–870, Apr. 2002, doi: 10.1093/brain/awf080.
[59] M. Delenclos, D. R. Jones, P. J. McLean, and R. J. Uitti, “Biomarkers in Parkinson’s disease: Advances and strategies,” *Parkinsonism & Related Disorders*, vol. 22, pp. S106–S110, Jan. 2016, doi: 10.1016/j.parkreldis.2015.09.048.
[60] S. Yagi *et al.*, “Progression from Unilateral to Bilateral Parkinsonism in Early Parkinson Disease: Implication of Mesocortical Dopamine Dysfunction by PET,” *Journal of Nuclear Medicine*, vol. 51, no. 8, pp. 1250–1257, Aug. 2010, doi: 10.2967/jnumed.110.076802.
[61] A. Kishore *et al.*, “Unilateral versus bilateral tasks in early asymmetric Parkinson’s disease: Differential effects on bradykinesia,” *Mov Disord.*, vol. 22, no. 3, pp. 328–333, Feb. 2007, doi: 10.1002/mds.21238.
[62] R. B. Postuma *et al.*, “MDS clinical diagnostic criteria for Parkinson’s disease: MDS-PD Clinical Diagnostic Criteria,” *Mov Disord.*, vol. 30, no. 12, pp. 1591–1601, Oct. 2015, doi: 10.1002/mds.26424.
[63] C. Walton *et al.*, “Rising prevalence of multiple sclerosis worldwide: Insights from the Atlas of MS, third edition,” *Multiple Sclerosis Journal*, p. 6.
[64] A. I. Spooren, A. A. Timmermans, and H. A. Seelen, “Motor training programs of arm and hand in patients with MS according to different levels of the ICF: a systematic review,” p. 11, 2012.
[65] L. Holper, M. Coenen, A. Weise, G. Stucki, A. Cieza, and J. Kesselring, “Characterization of functioning in multiple sclerosis using the ICF,” *J Neurol*, vol. 257, no. 1, pp. 103–113, Jan. 2010, doi: 10.1007/s00415-009-5282-4.
[66] S. Johansson *et al.*, “High concurrent presence of disability in multiple sclerosis: Associations with perceived health,” *J Neurol*, vol. 254, no. 6, pp. 767–773, Jun. 2007, doi: 10.1007/s00415-006-0431-5.
[67] C. G. Goetz *et al.*, “Movement Disorder Society-sponsored revision of the Unified Parkinson’s Disease Rating Scale (MDS-UPDRS): Scale presentation and clinimetric testing results: MDS-UPDRS: Clinimetric Assessment,” *Mov. Disord.*, vol. 23, no. 15, pp. 2129–2170, Nov. 2008, doi: 10.1002/mds.22340.
[68] C. H. Adler *et al.*, “Low clinical diagnostic accuracy of early vs advanced Parkinson disease: Clinicopathologic study,” *Neurology*, vol. 83, no. 5, pp. 406–412, Jul. 2014, doi: 10.1212/WNL.0000000000000641.
[69] C. G. Goetz and G. T. Stebbins, “Assuring interrater reliability for the UPDRS motor section: Utility of the UPDRS teaching tape,” *Mov Disord.*, vol. 19, no. 12, pp. 1453–1456, Dec. 2004, doi: 10.1002/mds.20220.
[70] G. Ebersbach, H. Baas, I. Csoti, M. Müngersdorf, and G. Deuschl, “Scales in Parkinson’s disease,” *J Neurol*, vol. 253, no. S4, pp. iv32–iv35, Sep. 2006, doi: 10.1007/s00415-006-4008-0.

[71] N. Yozbat, “Motor assessment of upper extremity function and its relation with fatigue, cognitive function and quality of life in multiple sclerosis patients,” *Journal of the Neurological Sciences*, p. 6, 2006.
[72] L. Barrett, S. Cano, J. Zajicek, and J. Hobart, “Can the ABILHAND handle manual ability in MS?,” *Multiple Sclerosis Journal*, p. 10.
[73] M. A. Luijten, I. Eekhout, M. D’Hooghe, B. M. Uitdehaag, and L. B. Mokkink, “Development of the Arm Function in Multiple Sclerosis Questionnaire-Short Form (AMSQ-SF): A static 10-item version,” *Multiple Sclerosis Journal*, p. 10.
[74] I. Lamers and P. Feys, “Assessing upper limb function in multiple sclerosis,” *Mult Scler*, vol. 20, no. 7, pp. 775–784, Jun. 2014, doi: 10.1177/1352458514525677.
[75] I. Lamers, S. Kelchtermans, I. Baert, and P. Feys, “Upper Limb Assessment in Multiple Sclerosis: A Systematic Review of Outcome Measures and their Psychometric Properties,” *Archives of Physical Medicine and Rehabilitation*, vol. 95, no. 6, pp. 1184–1200, Jun. 2014, doi: 10.1016/j.apmr.2014.02.023.
[76] J. T. Hinkle and G. M. Pontone, “Psychomotor processing and functional decline in Parkinson’s disease predicted by the Purdue Pegboard test,” *International Journal of Geriatric Psychiatry*, vol. n/a, no. n/a, doi: https://doi.org/10.1002/gps.5492.
[77] A. Ranjan, L. E. Raj, D. Kumar, P. Sandhya, and D. Danda, “Reliability of Box and Block Test for manual dexterity in patients with rheumatoid arthritis: a pilot study,” *International Journal of Rheumatic Diseases*, vol. 19, no. 12, pp. 1272–1277, 2016, doi: https://doi.org/10.1111/1756-185X.12655.
[78] J. F. Kurtzke, “Rating neurologic impairment in multiple sclerosis: An expanded disability status scale (EDSS),” *Neurology*, vol. 33, no. 11, pp. 1444–1444, Nov. 1983, doi: 10.1212/WNL.33.11.1444.
[79] D. S. Goodin, *Multiple sclerosis and related disorders*. in Handbook of clinical neurology ; volume 122, 3rd series. Edinburgh ; Elsevier, 2014.
[80] D. GOODKIN *et al.*, “INTERRATER AND INTRARATER SCORING AGREEMENT USING GRADES 1.0 TO 3.5 OF THE KURTZKE EXPANDED DISABILITY STATUS SCALE (EDSS),” *Neurology*, vol. 42, no. 4, pp. 859–863, 1992, doi: 10.1212/WNL.42.4.859.
[81] J. H. NOSEWORTHY, M. K. VANDERVOORT, C. J. WONG, and G. C. EBERS, “Interrater variability with the expanded disability status scale (EDSS) and functional systems(FS) in a multiple sclerosis clinical trial,” *Neurology*, vol. 40, no. 6, pp. 971–975, 1990, doi: 10.1212/WNL.40.6.971.
[82] J. A. Cohen, S. C. Reingold, C. H. Polman, and J. S. Wolinsky, “Disability outcome measures in multiple sclerosis clinical trials: current status and future prospects,” *The Lancet Neurology*, vol. 11, no. 5, pp. 467–476, May 2012, doi: 10.1016/S1474-4422(12)70059-5.
[83] R. Okuno, M. Yokoe, K. Akazawa, K. Abe, and S. Sakoda, “Finger taps movement acceleration measurement system for quantitative diagnosis of Parkinson’s disease,” in *2006 International Conference of the IEEE Engineering in Medicine and Biology Society*, New York, NY: IEEE, 2006, pp. 6623–6626. doi: 10.1109/IEMBS.2006.260904.
[84] R. J. W. Dunnewold, C. E. Jacobi, and J. J. van Hilten, “Quantitative assessment of bradykinesia in patients with parkinson’s disease,” *Journal of Neuroscience Methods*, vol. 74, no. 1, pp. 107–112, Jun. 1997, doi: 10.1016/S0165-0270(97)02254-1.
[85] J. Stamatakis *et al.*, “Finger Tapping Clinimetric Score Prediction in Parkinson’s Disease Using Low-Cost Accelerometers,” *Computational Intelligence and Neuroscience*, vol. 2013, pp. 1–13, 2013, doi: 10.1155/2013/717853.
[86] A. Salarian, H. Russmann, C. Wider, P. R. Burkhard, F. J. G. Vingerhoets, and K. Aminian, “Quantification of Tremor and Bradykinesia in Parkinson’s Disease Using a Novel Ambulatory Monitoring System,” *IEEE Trans. Biomed. Eng.*, vol. 54, no. 2, pp. 313–322, Feb. 2007, doi: 10.1109/TBME.2006.886670.

[87] J.-W. Kim *et al.*, "Quantification of bradykinesia during clinical finger taps using a gyrosensor in patients with Parkinson's disease," *Med Biol Eng Comput*, vol. 49, no. 3, pp. 365–371, Mar. 2011, doi: 10.1007/s11517-010-0697-8.
[88] D. A. Heldman *et al.*, "The modified bradykinesia rating scale for Parkinson's disease: Reliability and comparison with kinematic measures," *Mov. Disord.*, vol. 26, no. 10, pp. 1859–1863, Aug. 2011, doi: 10.1002/mds.23740.
[89] E. Rovini, C. Maremmani, and F. Cavallo, "How Wearable Sensors Can Support Parkinson's Disease Diagnosis and Treatment: A Systematic Review," *Front. Neurosci.*, vol. 11, p. 555, Oct. 2017, doi: 10.3389/fnins.2017.00555.
[90] R. Krupicka, Z. Szabo, S. Viteckova, and E. Ruzicka, "Motion Capture System for Finger Movement Measurement in Parkinson Disease," vol. 23, no. 2, p. 6, 2014.
[91] E. Růžička, R. Krupička, K. Zárubová, J. Rusz, R. Jech, and Z. Szabó, "Tests of manual dexterity and speed in Parkinson's disease: Not all measure the same," *Parkinsonism & Related Disorders*, vol. 28, pp. 118–123, Jul. 2016, doi: 10.1016/j.parkreldis.2016.05.009.
[92] I. Carpinella, D. Cattaneo, and M. Ferrarin, "Quantitative assessment of upper limb motor function in Multiple Sclerosis using an instrumented Action Research Arm Test," *J NeuroEngineering Rehabil*, vol. 11, no. 1, p. 67, 2014, doi: 10.1186/1743-0003-11-67.
[93] L. Bonzano *et al.*, "Quantitative Assessment of Finger Motor Impairment in Multiple Sclerosis," *PLoS ONE*, vol. 8, no. 5, p. e65225, May 2013, doi: 10.1371/journal.pone.0065225.
[94] A. Signori, M. P. Sormani, C. Lapucci, A. Uccelli, M. Bove, and L. Bonzano, "Effects of aging on finger movements in multiple sclerosis," *Multiple Sclerosis and Related Disorders*, vol. 37, p. 101449, Jan. 2020, doi: 10.1016/j.msard.2019.101449.
[95] I. Carpinella, D. Cattaneo, S. Abuarqub, and M. Ferrarin, "Robot-based rehabilitation of the upper limbs in multiple sclerosis: Feasibility and preliminary results," *J Rehabil Med*, vol. 41, no. 12, pp. 966–970, 2009, doi: 10.2340/16501977-0401.
[96] L. Padua *et al.*, "Reply to 'Motor assessment of upper extremity function and its relation with fatigue, cognitive function and quality of life in multiple sclerosis patients,'" *Journal of the Neurological Sciences*, vol. 253, no. 1–2, p. 106, Feb. 2007, doi: 10.1016/j.jns.2006.11.016.
[97] L. Pellegrino, M. Coscia, M. Muller, C. Solaro, and M. Casadio, "Evaluating upper limb impairments in multiple sclerosis by exposure to different mechanical environments," *Sci Rep*, vol. 8, no. 1, p. 2110, Dec. 2018, doi: 10.1038/s41598-018-20343-y.
[98] C. Pierella *et al.*, "Upper Limb Sensory-Motor Control During Exposure to Different Mechanical Environments in Multiple Sclerosis Subjects With No Clinical Disability," *Front. Neurorobot.*, vol. 16, p. 920118, Jul. 2022, doi: 10.3389/fnbot.2022.920118.
[99] E. Vergaro *et al.*, "Adaptive robot training for the treatment of incoordination in Multiple Sclerosis," *J NeuroEngineering Rehabil*, vol. 7, no. 1, p. 37, Dec. 2010, doi: 10.1186/1743-0003-7-37.
[100] R. O. Coats, A. J. Fath, S. L. Astill, and J. P. Wann, "Eye and hand movement strategies in older adults during a complex reaching task," *Exp Brain Res*, vol. 234, no. 2, pp. 533–547, Feb. 2016, doi: 10.1007/s00221-015-4474-7.
[101] V. L. Coppard, J. R. Tresilian, M. Mon-Williams, and R. G. Carson, "The effect of obstacle position on reach-to-grasp movements," *Experimental Brain Research*, vol. 137, no. 3–4, pp. 497–501, Apr. 2001, doi: 10.1007/s002210100684.
[102] R. J. Holt *et al.*, "Grasping the Changes Seen in Older Adults When Reaching for Objects of Varied Texture," *PLoS ONE*, vol. 8, no. 7, p. e69040, Jul. 2013, doi: 10.1371/journal.pone.0069040.
[103] R. K. Raw, "The Effect of Old Age on Motor Control: Performance and Learning," p. 249.
[104] K. M. B. Bennett and U. Castiello, "Reach to Grasp: Changes With Age," *Journal of Gerontology*, vol. 49, no. 1, pp. P1–P7, Jan. 1994, doi: 10.1093/geronj/49.1.P1.

[105] A. Rossiter *et al.*, “Manual tracking impairs postural stability in older adults,” *British Journal of Occupational Therapy*, vol. 80, no. 9, pp. 539–548, Sep. 2017, doi: 10.1177/0308022617712206.
[106] M. Thomas, A. Lenka, and P. Kumar Pal, “Handwriting Analysis in Parkinson’s Disease: Current Status and Future Directions,” *Mov Disord Clin Pract*, vol. 4, no. 6, pp. 806–818, Nov. 2017, doi: 10.1002/mdc3.12552.
[107] K. K. Maitra and A. K. Dasgupta, “Incoordination of a sequential motor task in Parkinson’s disease,” *Occup. Ther. Int.*, vol. 12, no. 4, pp. 218–233, Dec. 2005, doi: 10.1002/oti.7.
[108] M. K. Rand, A. W. A. Van Gemmert, A. B. M. I. Hossain, and G. E. Stelmach, “Coordination deficits during trunk-assisted reach-to-grasp movements in Parkinson’s disease,” *Exp Brain Res*, vol. 232, no. 1, pp. 61–74, Jan. 2014, doi: 10.1007/s00221-013-3720-0.
[109] R. D. Seidler, J. L. Alberts, and G. E. Stelmach, “Changes in multi-joint performance with age,” *Motor Control*, vol. 6, no. 1, pp. 19–31, Jan. 2002, doi: 10.1123/mcj.6.1.19.
[110] E. Solesio-Jofre, L. Serbruyns, D. G. Woolley, D. Mantini, I. A. M. Beets, and S. P. Swinnen, “Aging effects on the resting state motor network and interlimb coordination,” *Hum. Brain Mapp.*, vol. 35, no. 8, pp. 3945–3961, Aug. 2014, doi: 10.1002/hbm.22450.
[111] F. T. J. M. Zaal, R. J. Bootsma, and P. C. W. van Wieringen, “Coordination in prehension,” *Experimental Brain Research*, vol. 119, no. 4, pp. 427–435, Apr. 1998, doi: 10.1007/s002210050358.
[112] O. Lambercy, M.-C. Fluet, I. Lamers, L. Kerkhofs, P. Feys, and R. Gassert, “Assessment of upper limb motor function in patients with multiple sclerosis using the Virtual Peg Insertion Test: A pilot study,” in *2013 IEEE 13th International Conference on Rehabilitation Robotics (ICORR)*, Seattle, WA: IEEE, Jun. 2013, pp. 1–6. doi: 10.1109/ICORR.2013.6650494.
[113] C. Solaro *et al.*, “Subtle upper limb impairment in asymptomatic multiple sclerosis subjects,” *Mult Scler*, vol. 13, no. 3, pp. 428–432, Apr. 2007, doi: 10.1177/1352458506069926.
[114] R. Bove *et al.*, “Evaluating more naturalistic outcome measures: A 1-year smartphone study in multiple sclerosis,” *Neurol Neuroimmunol Neuroinflamm*, vol. 2, no. 6, p. e162, Dec. 2015, doi: 10.1212/NXI.0000000000000162.
[115] K. S. Messan *et al.*, “Assessment of Smartphone-Based Spiral Tracing in Multiple Sclerosis Reveals Intra-Individual Reproducibility as a Major Determinant of the Clinical Utility of the Digital Test,” *Front. Med. Technol.*, vol. 3, p. 714682, Feb. 2022, doi: 10.3389/fmedt.2021.714682.
[116] I. Carpinella, D. Cattaneo, R. Bertoni, and M. Ferrarin, “Robot Training of Upper Limb in Multiple Sclerosis: Comparing Protocols With or WithoutManipulative Task Components,” *IEEE Trans. Neural Syst. Rehabil. Eng.*, vol. 20, no. 3, pp. 351–360, May 2012, doi: 10.1109/TNSRE.2012.2187462.
[117] N. Hussain, K. S. Sunnerhagen, and M. Alt Murphy, “End-point kinematics using virtual reality explaining upper limb impairment and activity capacity in stroke,” *J NeuroEngineering Rehabil*, vol. 16, no. 1, p. 82, Dec. 2019, doi: 10.1186/s12984-019-0551-7.
[118] C. M. Kanzler, R. Sylvester, R. Gassert, J. Kool, O. Lambercy, and R. Gonzenbach, “Goal-directed upper limb movement patterns and hand grip forces in multiple sclerosis,” *Multiple Sclerosis Journal - Experimental, Translational and Clinical*, vol. 8, no. 3, p. 205521732211162, Jul. 2022, doi: 10.1177/20552173221116272.
[119] L. E. Cofré Lizama, F. Khan, P. V. Lee, and M. P. Galea, “The use of laboratory gait analysis for understanding gait deterioration in people with multiple sclerosis,” *Mult Scler*, vol. 22, no. 14, pp. 1768–1776, Dec. 2016, doi: 10.1177/1352458516658137.
[120] M. De Angelis *et al.*, “Digital Technology in Clinical Trials for Multiple Sclerosis: Systematic Review,” *JCM*, vol. 10, no. 11, p. 2328, May 2021, doi: 10.3390/jcm10112328.
[121] A. Pfister, A. M. West, S. Bronner, and J. A. Noah, “Comparative abilities of Microsoft Kinect and Vicon 3D motion capture for gait analysis,” *Journal of Medical Engineering & Technology*, vol. 38, no. 5, pp. 274–280, Jul. 2014, doi: 10.3109/03091902.2014.909540.

[122] V. Cimolin *et al.*, "3D analysis of upper limb movements during gait in healthy subjects and in patients with diplegia," *Gait & Posture*, vol. 24, pp. S19–S20, Nov. 2006, doi: 10.1016/j.gaitpost.2006.09.036.
[123] G. Coghe *et al.*, "Is There Any Relationship between Upper and Lower Limb Impairments in People with Multiple Sclerosis? A Kinematic Quantitative Analysis," *Multiple Sclerosis International*, vol. 2019, pp. 1–6, Oct. 2019, doi: 10.1155/2019/9149201.
[124] C. Elsworth-Edelsten *et al.*, "Upper limb movement analysis during gait in multiple sclerosis patients," *Human Movement Science*, vol. 54, pp. 248–252, Aug. 2017, doi: 10.1016/j.humov.2017.05.014.
[125] C. T. F. Menegoni, "Kinematic analysis of upper limb movement in multiple sclerosis," vol. 22, no. 14, pp. 1768–1766, 2016.
[126] J. Quintern, I. Immisch, H. Albrecht, W. Pöllmann, S. Glasauer, and A. Straube, "Influence of visual and proprioceptive afferences on upper limb ataxia in patients with multiple sclerosis," *Journal of the Neurological Sciences*, vol. 163, no. 1, pp. 61–69, Feb. 1999, doi: 10.1016/S0022-510X(99)00006-4.
[127] G. Rab, K. Petuskey, and A. Bagley, "A method for determination of upper extremity kinematics," *Gait & Posture*, vol. 15, no. 2, pp. 113–119, Apr. 2002, doi: 10.1016/S0966-6362(01)00155-2.
[128] R. Di Giovanni *et al.*, "A comparison of upper limb function in subjects with multiple sclerosis and healthy controls using an inertial measurement unit," *Multiple Sclerosis and Related Disorders*, vol. 53, p. 103036, Aug. 2021, doi: 10.1016/j.msard.2021.103036.
[129] B. R. Greene, M. Healy, S. Rutledge, B. Caulfield, and N. Tubridy, "Quantitative assessment of multiple sclerosis using inertial sensors and the TUG test," in *2014 36th Annual International Conference of the IEEE Engineering in Medicine and Biology Society*, Chicago, IL: IEEE, Aug. 2014, pp. 2977–2980. doi: 10.1109/EMBC.2014.6944248.
[130] L. Pellegrino *et al.*, "Analysis of upper limb movement in Multiple Sclerosis subjects during common daily actions," in *2015 37th Annual International Conference of the IEEE Engineering in Medicine and Biology Society (EMBC)*, Milan: IEEE, Aug. 2015, pp. 6967–6970. doi: 10.1109/EMBC.2015.7319995.
[131] M. Jeannerod, "The Timing of Natural Prehension Movements," *Journal of Motor Behavior*, vol. 16, no. 3, pp. 235–254, Sep. 1984, doi: 10.1080/00222895.1984.10735319.
[132] C. Bozzacchi, R. Volcic, and F. Domini, "Effect of visual and haptic feedback on grasping movements," *Journal of Neurophysiology*, vol. 112, no. 12, pp. 3189–3196, Dec. 2014, doi: 10.1152/jn.00439.2014.
[133] M. A. Goodale, L. S. Jakobson, and J. M. Keillor, "Differences in the visual control of pantomimed and natural grasping movements," *Neuropsychologia*, vol. 32, no. 10, pp. 1159–1178, Oct. 1994, doi: 10.1016/0028-3932(94)90100-7.
[134] J. B. J. Smeets, J. J. van den Dobbelsteen, D. D. J. de Grave, R. J. van Beers, and E. Brenner, "Sensory integration does not lead to sensory calibration," *Proceedings of the National Academy of Sciences*, vol. 103, no. 49, pp. 18781–18786, Dec. 2006, doi: 10.1073/pnas.0607687103.
[135] G. Bingham, R. Coats, and M. Mon-Williams, "Natural prehension in trials without haptic feedback but only when calibration is allowed," *Neuropsychologia*, vol. 45, no. 2, pp. 288–294, 2007, doi: 10.1016/j.neuropsychologia.2006.07.011.
[136] M. F. Bradshaw, A. D. Parton, and A. Glennerster, "The task-dependent use of binocular disparity and motion parallax information," *Vision Research*, vol. 40, no. 27, pp. 3725–3734, Dec. 2000, doi: 10.1016/S0042-6989(00)00214-5.
[137] A. Ma-Wyatt and S. P. McKee, "Visual information throughout a reach determines endpoint precision," *Exp Brain Res*, vol. 179, no. 1, pp. 55–64, Apr. 2007, doi: 10.1007/s00221-006-0767-1.

[138] M. Jeannerod, “The formation of finger grip during prehension. A cortically mediated visuomotor pattern,” *Behavioural Brain Research*, vol. 19, no. 2, pp. 99–116, Feb. 1986, doi: 10.1016/0166-4328(86)90008-2.
[139] L. S. Jakobson and M. A. Goodale, “Factors affecting higher-order movement planning: a kinematic analysis of human prehension,” *Exp Brain Res*, vol. 86, no. 1, Aug. 1991, doi: 10.1007/BF00231054.
[140] ReinoudJ. Bootsma, RonaldG. Marteniuk, ChristineL. MacKenzie, and FrankT. J. M. Zaal, “The speed-accuracy trade-off in manual prehension: effects of movement amplitude, object size and object width on kinematic characteristics,” *Exp Brain Res*, vol. 98, no. 3, Apr. 1994, doi: 10.1007/BF00233990.
[141] C. van de Kamp, R. M. Bongers, and F. T. J. M. Zaal, “Effects of Changing Object Size During Prehension,” *Journal of Motor Behavior*, vol. 41, no. 5, pp. 427–435, Oct. 2009, doi: 10.3200/35-08-033.
[142] F. T. J. M. Zaal and R. M. Bongers, “Movements of Individual Digits in Bimanual Prehension Are Coupled into a Grasping Component,” *PLoS ONE*, vol. 9, no. 5, p. e97790, May 2014, doi: 10.1371/journal.pone.0097790.
[143] C. van de Kamp and F. T. J. M. Zaal, “Prehension is really reaching and grasping,” *Exp Brain Res*, vol. 182, no. 1, pp. 27–34, Sep. 2007, doi: 10.1007/s00221-007-0968-2.
[144] J. B. J. Smeets and E. Brenner, “A New View on Grasping,” *Motor Control*, vol. 3, no. 3, pp. 237–271, Jul. 1999, doi: 10.1123/mcj.3.3.237.
[145] M. Mon-Williams and G. P. Bingham, “Task constraints alter prehension movements qualitatively and quantitatively,” *Journal of Vision*, vol. 5, no. 8, pp. 124–124, Mar. 2010, doi: 10.1167/5.8.124.
[146] M. Gentilucci, U. Castiello, M. L. Corradini, M. Scarpa, C. Umiltà, and G. Rizzolatti, “Influence of different types of grasping on the transport component of prehension movements,” *Neuropsychologia*, vol. 29, no. 5, pp. 361–378, Jan. 1991, doi: 10.1016/0028-3932(91)90025-4.
[147] U. Castiello, K. M. B. Bennett, and Y. Paulignan, “Does the type of prehension influence the kinematics of reaching,” *Behavioural Brain Research*, vol. 50, no. 1–2, pp. 7–15, Sep. 1992, doi: 10.1016/S0166-4328(05)80283-9.
[148] U. Castiello, K. M. B. Bennett, and G. E. Stelmach, “Reach to grasp: the natural response to perturbation of object size,” *Exp Brain Res*, vol. 94, no. 1, May 1993, doi: 10.1007/BF00230479.
[149] Y. Paulignan, C. MacKenzie, R. Marteniuk, and M. Jeannerod, “Selective perturbation of visual input during prehension movements,” p. 11.
[150] I. J. Flatters *et al.*, “Predicting the Effect of Surface Texture on the Qualitative Form of Prehension,” *PLoS ONE*, vol. 7, no. 3, p. e32770, Mar. 2012, doi: 10.1371/journal.pone.0032770.
[151] E. van Bergen, L. M. van Swieten, J. H. G. Williams, and M. Mon-Williams, “The effect of orientation on prehension movement time,” *Exp Brain Res*, vol. 178, no. 2, pp. 180–193, Apr. 2007, doi: 10.1007/s00221-006-0722-1.
[152] U. Castiello, G. E. Stelmach, and A. N. Lieberman, “Temporal dissociation of the prehension pattern in Parkinson’s disease,” *Neuropsychologia*, vol. 31, no. 4, pp. 395–402, Apr. 1993, doi: 10.1016/0028-3932(93)90162-S.
[153] K. M. Zackowski, W. T. Thach, and A. J. Bastian, “Cerebellar subjects show impaired coupling of reach and grasp movements,” *Exp Brain Res*, vol. 146, no. 4, pp. 511–522, Oct. 2002, doi: 10.1007/s00221-002-1191-9.
[154] C. Lu, A. Bharmal, Z. H. Kiss, O. Suchowersky, and A. M. Haffenden, “Attention and reach-to-grasp movements in Parkinson’s disease,” *Exp Brain Res*, vol. 205, no. 1, pp. 69–80, Aug. 2010, doi: 10.1007/s00221-010-2341-0.
[155] L. F. Schettino, V. Rajaraman, D. Jack, S. V. Adamovich, J. Sage, and H. Poizner, “Deficits in the evolution of hand preshaping in Parkinson’s disease,” *Neuropsychologia*, vol. 42, no. 1, pp. 82–94, 2004, doi: 10.1016/S0028-3932(03)00150-7.

[156] M. K. Rand, A. L. Smiley-Oyen, Y. P. Shimansky, J. R. Bloedel, and G. E. Stelmach, “Control of aperture closure during reach-to-grasp movements in parkinson’s disease,” *Exp Brain Res*, vol. 168, no. 1–2, pp. 131–142, Jan. 2006, doi: 10.1007/s00221-005-0073-3.
[157] J. L. Alberts, M. Saling, C. H. Adler, and G. E. Stelmach, “Disruptions in the reach-to-grasp actions of Parkinson’s patients,” *Exp Brain Res*, vol. 134, no. 3, pp. 353–362, Oct. 2000, doi: 10.1007/s002210000468.
[158] M. P. Furmanek, L. F. Schettino, M. Yarossi, S. Kirkman, S. V. Adamovich, and E. Tunik, “Coordination of reach-to-grasp in physical and haptic-free virtual environments,” *J NeuroEngineering Rehabil*, vol. 16, no. 1, p. 78, Dec. 2019, doi: 10.1186/s12984-019-0525-9.
[159] E. C. Magdalon, S. M. Michaelsen, A. A. Quevedo, and M. F. Levin, “Comparison of grasping movements made by healthy subjects in a 3-dimensional immersive virtual versus physical environment,” *Acta Psychologica*, vol. 138, no. 1, pp. 126–134, Sep. 2011, doi: 10.1016/j.actpsy.2011.05.015.
[160] M. Delrobaei, S. Memar, M. Pieterman, T. W. Stratton, K. McIsaac, and M. Jog, “Towards remote monitoring of Parkinson’s disease tremor using wearable motion capture systems,” *Journal of the Neurological Sciences*, vol. 384, pp. 38–45, Jan. 2018, doi: 10.1016/j.jns.2017.11.004.
[161] “Validity of an inertial measurement unit to assess pelvic orientation angles during gait, sit-stand transfers and step-up transfers: Comparison with an optoelectronic motion capture system*,” *Medical Engineering and Physics*, p. 7, 2016.
[162] C. Bregler, “Motion Capture Technology for Entertainment [In the Spotlight],” *IEEE Signal Process. Mag.*, vol. 24, no. 6, pp. 160–158, Nov. 2007, doi: 10.1109/MSP.2007.906023.
[163] E. van der Kruk and M. M. Reijne, “Accuracy of human motion capture systems for sport applications; state-of-the-art review,” *European Journal of Sport Science*, vol. 18, no. 6, pp. 806–819, Jul. 2018, doi: 10.1080/17461391.2018.1463397.
[164] S. Sharma, S. Verma, M. Kumar, and L. Sharma, “Use of Motion Capture in 3D Animation: Motion Capture Systems, Challenges, and Recent Trends,” in *2019 International Conference on Machine Learning, Big Data, Cloud and Parallel Computing (COMITCon)*, Faridabad, India: IEEE, Feb. 2019, pp. 289–294. doi: 10.1109/COMITCon.2019.8862448.
[165] J. C. P. Chan, H. Leung, J. K. T. Tang, and T. Komura, “A Virtual Reality Dance Training System Using Motion Capture Technology,” *IEEE Trans. Learning Technol.*, vol. 4, no. 2, pp. 187–195, Apr. 2011, doi: 10.1109/TLT.2010.27.
[166] N. Eichler, H. Hel-Or, I. Shimshoni, D. Itah, B. Gross, and S. Raz, “3D motion capture system for assessing patient motion during Fugl-Meyer stroke rehabilitation testing,” *IET Computer Vision*, vol. 12, no. 7, pp. 963–975, Oct. 2018, doi: 10.1049/iet-cvi.2018.5274.
[167] D. Buongiorno, I. Bortone, G. D. Cascarano, G. F. Trotta, A. Brunetti, and V. Bevilacqua, “A low-cost vision system based on the analysis of motor features for recognition and severity rating of Parkinson’s Disease,” *BMC Med Inform Decis Mak*, vol. 19, no. S9, p. 243, Dec. 2019, doi: 10.1186/s12911-019-0987-5.
[168] C. M. N. Brigante, N. Abbate, A. Basile, A. C. Faulisi, and S. Sessa, “Towards Miniaturization of a MEMS-Based Wearable Motion Capture System,” *IEEE Trans. Ind. Electron.*, vol. 58, no. 8, pp. 3234–3241, Aug. 2011, doi: 10.1109/TIE.2011.2148671.
[169] B. Fang, F. Sun, H. Liu, and D. Guo, “Development of a Wearable Device for Motion Capturing Based on Magnetic and Inertial Measurement Units,” *Scientific Programming*, vol. 2017, pp. 1–11, 2017, doi: 10.1155/2017/7594763.
[170] R. Mergl, P. Tigges, A. Schröter, H.-J. Möller, and U. Hegerl, “Digitized analysis of handwriting and drawing movements in healthy subjects: methods, results and perspectives,” *Journal of Neuroscience Methods*, vol. 90, no. 2, pp. 157–169, Aug. 1999, doi: 10.1016/S0165-0270(99)00080-1.
[171] M. Thomas, A. Lenka, and P. K. Pal, “Handwriting Analysis in Parkinson’s Disease: Current Status and Future Directions,” p. 13.

[172] N. Preston, A. Weightman, P. Culmer, M. Levesley, B. Bhakta, and M. Mon-Williams, “The Cerebral Palsy Kinematic Assessment Tool (CPKAT): feasibility testing of a new portable tool for the objective evaluation of upper limb kinematics in children with cerebral palsy in the non-laboratory setting,” *Disability and Rehabilitation: Assistive Technology*, pp. 1–6, Aug. 2014, doi: 10.3109/17483107.2014.951974.
[173] V. Bobić, M. Djurić-Jovičić, N. Dragašević, M. B. Popović, V. S. Kostić, and G. Kvaščev, “An Expert System for Quantification of Bradykinesia Based on Wearable Inertial Sensors,” p. 17, 2019.
[174] P. Y. Chan and Z. M. Ripin, “Development of wearable inertial sensors for measurement of hand arm tremors,” in *2013 IEEE International Conference on Smart Instrumentation, Measurement and Applications (ICSIMA)*, Kuala Lumpur, Malaysia: IEEE, Nov. 2013, pp. 1–6. doi: 10.1109/ICSIMA.2013.6717926.
[175] I. Flatters *et al.*, “Children’s head movements and postural stability as a function of task,” *Exp Brain Res*, vol. 232, no. 6, pp. 1953–1970, Jun. 2014, doi: 10.1007/s00221-014-3886-0.
[176] J. C. van den Noort *et al.*, “Quantification of Hand Motor Symptoms in Parkinson’s Disease: A Proof-of-Principle Study Using Inertial and Force Sensors,” *Ann Biomed Eng*, vol. 45, no. 10, pp. 2423–2436, Oct. 2017, doi: 10.1007/s10439-017-1881-x.
[177] C. Duc, P. Salvia, A. Lubansu, V. Feipel, and K. Aminian, “A wearable inertial system to assess the cervical spine mobility: Comparison with an optoelectronic-based motion capture evaluation,” *Medical Engineering & Physics*, vol. 36, no. 1, pp. 49–56, Jan. 2014, doi: 10.1016/j.medengphy.2013.09.002.
[178] I. Poitras *et al.*, “Validity and Reliability of Wearable Sensors for Joint Angle Estimation: A Systematic Review,” *Sensors*, vol. 19, no. 7, p. 1555, Mar. 2019, doi: 10.3390/s19071555.
[179] V. N. Iliukhin, K. B. Mitkovskii, D. A. Bizyanova, and A. A. Akopyan, “The Development of Motion Capture System Based on Kinect Sensor and Bluetooth-Gloves,” *Procedia Engineering*, vol. 176, pp. 506–513, 2017, doi: 10.1016/j.proeng.2017.02.350.
[180] N. Yadav and C. Bleakley, “Accurate Orientation Estimation Using AHRS under Conditions of Magnetic Distortion,” p. 17, 2014.
[181] M. Kok and T. B. Schon, “Magnetometer Calibration Using Inertial Sensors,” *IEEE Sensors J.*, vol. 16, no. 14, pp. 5679–5689, Jul. 2016, doi: 10.1109/JSEN.2016.2569160.
[182] S. Williams *et al.*, “Supervised classification of bradykinesia in Parkinson’s disease from smartphone videos,” *Artificial Intelligence in Medicine*, vol. 110, p. 101966, Nov. 2020, doi: 10.1016/j.artmed.2020.101966.
[183] S. Williams *et al.*, “Supervised classification of bradykinesia in Parkinson’s disease from smartphone videos,” *Artificial Intelligence in Medicine*, vol. 110, p. 101966, Nov. 2020, doi: 10.1016/j.artmed.2020.101966.
[184] T. Khan, D. Nyholm, J. Westin, and M. Dougherty, “A computer vision framework for finger-tapping evaluation in Parkinson’s disease,” *Artificial Intelligence in Medicine*, vol. 60, no. 1, pp. 27–40, Jan. 2014, doi: 10.1016/j.artmed.2013.11.004.
[185] S. Das *et al.*, “Quantitative measurement of motor symptoms in Parkinson’s disease: A study with full-body motion capture data,” in *2011 Annual International Conference of the IEEE Engineering in Medicine and Biology Society*, Boston, MA: IEEE, Aug. 2011, pp. 6789–6792. doi: 10.1109/IEMBS.2011.6091674.
[186] “A comparison of currently available optoelectronic motion capture systems | Elsevier Enhanced Reader.” https://reader.elsevier.com/reader/sd/pii/S0021929020302438?token=94DD8FA25DF6FFBAF3A246A6005359A214A6D4FB9EB28C7AA40D103B50BF6D70FDBE7B67E70E0DD147F5BC2FAB9777FC&originRegion=eu-west-1&originCreation=20210407150719 (accessed Apr. 07, 2021).
[187] J. Schmidt, D. R. Berg, H.-L. Ploeg, and L. Ploeg, “Precision, repeatability and accuracy of Optotrak® optical motion tracking systems,” p. 14.

[188] S. De Amici, A. Sanna, F. Lamberti, and B. Pralio, “A Wii remote-based infrared-optical tracking system,” *Entertainment Computing*, vol. 1, no. 3–4, pp. 119–124, Dec. 2010, doi: 10.1016/j.entcom.2010.08.001.
[189] S. Hay, J. Newman, and R. Harle, “Optical tracking using commodity hardware,” in *2008 7th IEEE/ACM International Symposium on Mixed and Augmented Reality*, Cambridge, UK: IEEE, Sep. 2008, pp. 159–160. doi: 10.1109/ISMAR.2008.4637345.
[190] T. Pintaric and H. Kaufmann, “Affordable Infrared-Optical Pose-Tracking for Virtual and Augmented Reality,” p. 8.
[191] C. Modroño *et al.*, “A low cost fMRI-compatible tracking system using the Nintendo Wii remote,” *Journal of Neuroscience Methods*, vol. 202, no. 2, pp. 173–181, Nov. 2011, doi: 10.1016/j.jneumeth.2011.05.014.
[192] D. Scherfgen and R. Herpers, “3D tracking using multiple Nintendo Wii Remotes: a simple consumer hardware tracking approach,” in *Proceedings of the 2009 Conference on Future Play on @ GDC Canada - FuturePlay ’09*, Vancouver, British Columbia, Canada: ACM Press, 2009, p. 31. doi: 10.1145/1639601.1639620.
[193] “Camera Module.” https://www.raspberrypi.org/documentation/hardware/camera/
[194] A. I. Dell *et al.*, “Automated image-based tracking and its application in ecology,” *Trends in Ecology & Evolution*, vol. 29, no. 7, pp. 417–428, Jul. 2014, doi: 10.1016/j.tree.2014.05.004.
[195] G. Alarcón-Nieto, J. M. Graving, J. A. Klarevas-Irby, A. A. Maldonado-Chaparro, I. Mueller, and D. R. Farine, “An automated barcode tracking system for behavioural studies in birds,” *Methods Ecol Evol*, vol. 9, no. 6, pp. 1536–1547, Jun. 2018, doi: 10.1111/2041-210X.13005.
[196] A. Pérez-Escudero, J. Vicente-Page, R. C. Hinz, S. Arganda, and G. G. de Polavieja, “idTracker: tracking individuals in a group by automatic identification of unmarked animals,” p. 9, 2014.
[197] F. Romero-Ferrero, “idtracker.ai: tracking all individuals in small or large collectives of unmarked animals,” *Nature Methods*, vol. 16, p. 9, 2019.
[198] J. M. Graving *et al.*, “DeepPoseKit, a software toolkit for fast and robust animal pose estimation using deep learning,” *eLife*, vol. 8, p. e47994, Oct. 2019, doi: 10.7554/eLife.47994.
[199] T. D. Pereira, “Fast animal pose estimation using deep neural networks,” *Nature Methods*, vol. 16, p. 13, 2019.
[200] A. Mathis *et al.*, “DeepLabCut: markerless pose estimation of user-defined body parts with deep learning,” *Nat Neurosci*, vol. 21, no. 9, pp. 1281–1289, Sep. 2018, doi: 10.1038/s41593-018-0209-y.
[201] S. Williams *et al.*, “The discerning eye of computer vision: Can it measure Parkinson’s finger tap bradykinesia?,” *Journal of the Neurological Sciences*, vol. 416, p. 117003, Sep. 2020, doi: 10.1016/j.jns.2020.117003.
[202] T. Nath, A. Mathis, A. C. Chen, A. Patel, M. Bethge, and M. W. Mathis, “Using DeepLabCut for 3D markerless pose estimation across species and behaviors,” *Nat Protoc*, vol. 14, no. 7, pp. 2152–2176, Jul. 2019, doi: 10.1038/s41596-019-0176-0.
[203] A. Mathis, S. Schneider, J. Lauer, and M. W. Mathis, “A Primer on Motion Capture with Deep Learning: Principles, Pitfalls, and Perspectives,” *Neuron*, vol. 108, no. 1, pp. 44–65, Oct. 2020, doi: 10.1016/j.neuron.2020.09.017.
[204] M. W. Mathis and A. Mathis, “Deep learning tools for the measurement of animal behavior in neuroscience,” *Current Opinion in Neurobiology*, vol. 60, pp. 1–11, Feb. 2020, doi: 10.1016/j.conb.2019.10.008.
[205] G. Huang, Z. Liu, L. Van Der Maaten, and K. Q. Weinberger, “Densely Connected Convolutional Networks,” in *2017 IEEE Conference on Computer Vision and Pattern Recognition (CVPR)*, Honolulu, HI: IEEE, Jul. 2017, pp. 2261–2269. doi: 10.1109/CVPR.2017.243.
[206] J. Brookes, M. Warburton, M. Alghadier, M. Mon-Williams, and F. Mushtaq, “Studying human behavior with virtual reality: The Unity Experiment Framework,” *Behav Res*, Apr. 2019, doi: 10.3758/s13428-019-01242-0.

[207] M. Warburton *et al.*, “Getting stuck in a rut as an emergent feature of a dynamic decision-making system,” Neuroscience, preprint, Jun. 2020. doi: 10.1101/2020.06.02.127860.
[208] H. G. Hoffman, A. Garcia-Palacios, D. R. Patterson, M. Jensen, T. Furness, and W. F. Ammons, “The Effectiveness of Virtual Reality for Dental Pain Control: A Case Study,” *CyberPsychology & Behavior*, vol. 4, no. 4, pp. 527–535, Aug. 2001, doi: 10.1089/109493101750527088.
[209] G. S. Ruthenbeck and K. J. Reynolds, “Virtual reality for medical training: the state-of-the-art,” *Journal of Simulation*, vol. 9, no. 1, pp. 16–26, Feb. 2015, doi: 10.1057/jos.2014.14.
[210] R. Coats, G. P. Bingham, and M. Mon-Williams, “Calibrating grasp size and reach distance: interactions reveal integral organization of reaching-to-grasp movements,” *Exp Brain Res*, vol. 189, no. 2, pp. 211–220, Aug. 2008, doi: 10.1007/s00221-008-1418-5.
[211] M. Gentilucci, E. Daprati, and M. Gangitano, “Haptic information differentially interferes with visual analysis in reaching-grasping control and in perceptual processes:,” *NeuroReport*, vol. 9, no. 5, pp. 887–891, Mar. 1998, doi: 10.1097/00001756-199803300-00023.
[212] M. F. Levin, E. C. Magdalon, S. M. Michaelsen, and A. A. F. Quevedo, “Quality of Grasping and the Role of Haptics in a 3-D Immersive Virtual Reality Environment in Individuals With Stroke,” *IEEE Transactions on Neural Systems and Rehabilitation Engineering*, vol. 23, no. 6, pp. 1047–1055, Nov. 2015, doi: 10.1109/TNSRE.2014.2387412.
[213] L. A. Knaut, S. K. Subramanian, B. J. McFadyen, D. Bourbonnais, and M. F. Levin, “Kinematics of Pointing Movements Made in a Virtual Versus a Physical 3-Dimensional Environment in Healthy and Stroke Subjects,” *Archives of Physical Medicine and Rehabilitation*, vol. 90, no. 5, pp. 793–802, May 2009, doi: 10.1016/j.apmr.2008.10.030.
[214] C. Bozzacchi, R. Volcic, and F. Domini, “Grasping in absence of feedback: systematic biases endure extensive training,” *Exp Brain Res*, vol. 234, no. 1, pp. 255–265, Jan. 2016, doi: 10.1007/s00221-015-4456-9.
[215] G. Bingham, R. Coats, and M. Mon-Williams, “Natural prehension in trials without haptic feedback but only when calibration is allowed,” *Neuropsychologia*, vol. 45, no. 2, pp. 288–294, 2007, doi: 10.1016/j.neuropsychologia.2006.07.011.
[216] N. Papatheodorou, A. Pino, G. TH. Kouroupetroglou, V. Constantinides, E. Andreadou, and C. C. Papageorgiou, “Upper Limb Motor Skills Performance Evaluation Based on Point-and-Click Cursor Trajectory Analysis: Application in Early Multiple Sclerosis Detection,” *IEEE Access*, vol. 7, pp. 28999–29013, 2019, doi: 10.1109/ACCESS.2019.2901926.
[217] J. Stamatakis *et al.*, “Finger Tapping Clinimetric Score Prediction in Parkinson’s Disease Using Low-Cost Accelerometers,” *Computational Intelligence and Neuroscience*, vol. 2013, pp. 1–13, 2013, doi: 10.1155/2013/717853.
[218] I. Flatters, P. Culmer, R. J. Holt, R. M. Wilkie, and M. Mon-Williams, “A new tool for assessing head movements and postural sway in children,” *Behav Res*, vol. 46, no. 4, pp. 950–959, Dec. 2014, doi: 10.3758/s13428-013-0419-x.
[219] D. Buongiorno, I. Bortone, G. D. Cascarano, G. F. Trotta, A. Brunetti, and V. Bevilacqua, “A low-cost vision system based on the analysis of motor features for recognition and severity rating of Parkinson’s Disease,” *BMC Med Inform Decis Mak*, vol. 19, no. S9, p. 243, Dec. 2019, doi: 10.1186/s12911-019-0987-5.
[220] I. Flatters, F. Mushtaq, L. J. B. Hill, R. J. Holt, R. M. Wilkie, and M. Mon-Williams, “The relationship between a child’s postural stability and manual dexterity,” *Exp Brain Res*, vol. 232, no. 9, pp. 2907–2917, Sep. 2014, doi: 10.1007/s00221-014-3947-4.
[221] “Raspberry Pi Documentation - Camera.” https://www.raspberrypi.com/documentation/accessories/camera.html (accessed Oct. 28, 2022).
[222] M.-H. Song and R. I. Godøy, “How Fast Is Your Body Motion? Determining a Sufficient Frame Rate for an Optical Motion Tracking System Using Passive Markers,” *PLoS ONE*, vol. 11, no. 3, p. e0150993, Mar. 2016, doi: 10.1371/journal.pone.0150993.

[223] S. Hay, J. Newman, and R. Harle, “Optical tracking using commodity hardware,” in *2008 7th IEEE/ACM International Symposium on Mixed and Augmented Reality*, Cambridge, UK: IEEE, Sep. 2008, pp. 159–160. doi: 10.1109/ISMAR.2008.4637345.
[224] G. W. Jensen, P. van der Smagt, E. Heiss, H. Straka, and T. Kohl, “SnakeStrike: A Low-Cost Open-Source High-Speed Multi-Camera Motion Capture System,” *Front. Behav. Neurosci.*, vol. 14, p. 116, Aug. 2020, doi: 10.3389/fnbeh.2020.00116.
[225] “Raspberry Pi Documentation - Raspberry Pi Hardware.” https://www.raspberrypi.com/documentation/computers/raspberry-pi.html (accessed Oct. 28, 2022).
[226] “Raspberry Pi Documentation - Display.” https://www.raspberrypi.com/documentation/accessories/display.html (accessed Oct. 28, 2022).
[227] Z. Zhang, “Flexible camera calibration by viewing a plane from unknown orientations,” in *Proceedings of the Seventh IEEE International Conference on Computer Vision*, Sep. 1999, pp. 666–673 vol.1. doi: 10.1109/ICCV.1999.791289.
[228] T. Pintaric and H. Kaufmann, “Affordable Infrared-Optical Pose-Tracking for Virtual and Augmented Reality,” p. 8.
[229] S. Roy, J. L. Bryant, Y. Cao, and D. H. Heck, “High-Precision, Three-Dimensional Tracking of Mouse Whisker Movements with Optical Motion Capture Technology,” *Front. Behav. Neurosci.*, vol. 5, 2011, doi: 10.3389/fnbeh.2011.00027.
[230] “Accuracy map of an optical motion capture system with 42 or 21 cameras in a large measurement volume,” *Journal of Biomechanics*, vol. 58, pp. 237–240, Jun. 2017, doi: 10.1016/j.jbiomech.2017.05.006.
[231] A. Myronenko and X. Song, “Point Set Registration: Coherent Point Drift,” *IEEE Transactions on Pattern Analysis and Machine Intelligence*, vol. 32, no. 12, pp. 2262–2275, Dec. 2010, doi: 10.1109/TPAMI.2010.46.
[232] R. Khadem *et al.*, “Comparative Tracking Error Analysis of Five Different Optical Tracking Systems,” *Computer Aided Surgery*, vol. 5, no. 2, pp. 98–107, Jan. 2000, doi: 10.3109/10929080009148876.
[233] D. C. Niehorster, L. Li, and M. Lappe, “The Accuracy and Precision of Position and Orientation Tracking in the HTC Vive Virtual Reality System for Scientific Research,” *i-Perception*, vol. 8, no. 3, p. 204166951770820, Jun. 2017, doi: 10.1177/2041669517708205.
[234] R. Coats, G. P. Bingham, and M. Mon-Williams, “Calibrating grasp size and reach distance: interactions reveal integral organization of reaching-to-grasp movements,” *Exp Brain Res*, vol. 189, no. 2, pp. 211–220, Aug. 2008, doi: 10.1007/s00221-008-1418-5.
[235] M. Gentilucci, U. Castiello, M. L. Corradini, M. Scarpa, C. Umiltà, and G. Rizzolatti, “Influence of different types of grasping on the transport component of prehension movements,” *Neuropsychologia*, vol. 29, no. 5, pp. 361–378, Jan. 1991, doi: 10.1016/0028-3932(91)90025-4.
[236] Y. Paulignan, V. G. Frak, I. Toni, and M. Jeannerod, “Influence of object position and size on human prehension movements:,” *Exp Brain Res*, vol. 114, no. 2, pp. 226–234, Apr. 1997, doi: 10.1007/PL00005631.
[237] M. Jeannerod, “The Timing of Natural Prehension Movements,” *Journal of Motor Behavior*, vol. 16, no. 3, pp. 235–254, Sep. 1984, doi: 10.1080/00222895.1984.10735319.
[238] C. van de Kamp, R. M. Bongers, and F. T. J. M. Zaal, “Effects of Changing Object Size During Prehension,” *Journal of Motor Behavior*, vol. 41, no. 5, pp. 427–435, Oct. 2009, doi: 10.3200/35-08-033.
[239] M. Mon-Williams and G. P. Bingham, “Discovering affordances that determine the spatial structure of reach-to-grasp movements,” *Exp Brain Res*, vol. 211, no. 1, pp. 145–160, May 2011, doi: 10.1007/s00221-011-2659-2.
[240] *Set of tool for managing files from Optotrak 3020*. [Online]. Available: https://github.com/immersivecognition/optotools

[241] R. G. Marteniuk, J. L. Leavitt, C. L. MacKenzie, and S. Athenes, “Functional relationships between grasp and transport components in a prehension task,” *Human Movement Science*, vol. 9, no. 2, pp. 149–176, Apr. 1990, doi: 10.1016/0167-9457(90)90025-9.
[242] E. R. Dorsey and B. R. Bloem, “The Parkinson Pandemic—A Call to Action,” *JAMA Neurol*, vol. 75, no. 1, p. 9, Jan. 2018, doi: 10.1001/jamaneurol.2017.3299.
[243] E. R. Dorsey, T. Sherer, M. S. Okun, and B. R. Bloem, “The Emerging Evidence of the Parkinson Pandemic,” *JPD*, vol. 8, no. s1, pp. S3–S8, Dec. 2018, doi: 10.3233/JPD-181474.
[244] T. Pringsheim, N. Jette, A. Frolkis, and T. D. L. Steeves, “The prevalence of Parkinson’s disease: A systematic review and meta-analysis,” *Movement Disorders*, vol. 29, no. 13, pp. 1583–1590, 2014, doi: 10.1002/mds.25945.
[245] D. A. Heldman *et al.*, “The modified bradykinesia rating scale for Parkinson’s disease: Reliability and comparison with kinematic measures,” *Mov. Disord.*, vol. 26, no. 10, pp. 1859–1863, Aug. 2011, doi: 10.1002/mds.23740.
[246] C. H. Adler *et al.*, “Low clinical diagnostic accuracy of early vs advanced Parkinson disease: Clinicopathologic study,” *Neurology*, vol. 83, no. 5, pp. 406–412, Jul. 2014, doi: 10.1212/WNL.0000000000000641.
[247] S. Lemeshow and World Health Organization, Eds., *Adequacy of sample size in health studies*. Chichester [England] ; New York : New York, NY, USA: Published on behalf of the World Health Organization by Wiley ; Distributed in the U.S.A., Canada, and Japan by Liss, 1990.
[248] V. Bobić, M. Djurić-Jovičić, N. Dragašević, M. B. Popović, V. S. Kostić, and G. Kvaščev, “An Expert System for Quantification of Bradykinesia Based on Wearable Inertial Sensors,” *Sensors*, vol. 19, no. 11, p. 2644, Jun. 2019, doi: 10.3390/s19112644.
[249] A. Letanneux, J. Danna, J.-L. Velay, F. Viallet, and S. Pinto, “From micrographia to Parkinson’s disease dysgraphia: Parkinson’s Disease Dysgraphia,” *Mov Disord.*, vol. 29, no. 12, pp. 1467–1475, Oct. 2014, doi: 10.1002/mds.25990.
[250] P. Zham *et al.*, “Effect of levodopa on handwriting tasks of different complexity in Parkinson’s disease: a kinematic study,” *J Neurol*, vol. 266, no. 6, pp. 1376–1382, Jun. 2019, doi: 10.1007/s00415-019-09268-2.
[251] E. L. Stegemöller, A. Zaman, and J. Uzochukwu, “Repetitive finger movement and circle drawing in persons with Parkinson’s disease,” *PLoS ONE*, vol. 14, no. 9, p. e0222862, Sep. 2019, doi: 10.1371/journal.pone.0222862.
[252] S. Williams, “Supervised classification of bradykinesia in Parkinson?s disease from smartphone videos,” *Artificial Intelligence In Medicine*, p. 9, 2020.
[253] Á. Sánchez-Ferro *et al.*, “New methods for the assessment of Parkinson’s disease (2005 to 2015): A systematic review: New Methods for PD Assessment,” *Mov Disord.*, vol. 31, no. 9, pp. 1283–1292, Sep. 2016, doi: 10.1002/mds.26723.
[254] T. Khan, D. Nyholm, J. Westin, and M. Dougherty, “A computer vision framework for finger-tapping evaluation in Parkinson’s disease,” *Artificial Intelligence in Medicine*, vol. 60, no. 1, pp. 27–40, Jan. 2014, doi: 10.1016/j.artmed.2013.11.004.
[255] D. Buongiorno, I. Bortone, G. D. Cascarano, G. F. Trotta, A. Brunetti, and V. Bevilacqua, “A low-cost vision system based on the analysis of motor features for recognition and severity rating of Parkinson’s Disease,” *BMC Med Inform Decis Mak*, vol. 19, no. S9, p. 243, Dec. 2019, doi: 10.1186/s12911-019-0987-5.
[256] M. Li, “Objective Vision-Based Assessment of Parkinsonism and Levodopa-Induced Dyskinesia in Persons with Parkinson’s Disease,” p. 132.
[257] M. Tayag, B. Ronie, and R. Marvin, “Leap Motion Controller Enabled Simulations of Personal Computer Assembly Programs,” in *2021 The 4th International Conference on Software Engineering and Information Management*, Yokohama Japan: ACM, Jan. 2021, pp. 17–21. doi: 10.1145/3451471.3451474.
[258] Á. Aguilera-Rubio, I. M. Alguacil-Diego, A. Mallo-López, and A. Cuesta-Gómez, “Use of the Leap Motion Controller® System in the Rehabilitation of the Upper Limb in Stroke. A Systematic

Review," *Journal of Stroke and Cerebrovascular Diseases*, vol. 31, no. 1, p. 106174, Jan. 2022, doi: 10.1016/j.jstrokecerebrovasdis.2021.106174.
[259] "How Hand Tracking Works | Ultraleap." https://www.ultraleap.com/company/news/blog/how-hand-tracking-works/ (accessed Dec. 23, 2022).
[260] J. Brookes, M. Warburton, M. Alghadier, M. Mon-Williams, and F. Mushtaq, "Studying human behavior with virtual reality: The Unity Experiment Framework," *Behav Res*, Apr. 2019, doi: 10.3758/s13428-019-01242-0.
[261] I. Camponogara and R. Volcic, "Grasping movements toward seen and handheld objects," *Sci Rep*, vol. 9, no. 1, p. 3665, Dec. 2019, doi: 10.1038/s41598-018-38277-w.
[262] P. Archambault, P. Pigeon, A. G. Feldman, and M. F. Levin, "Recruitment and sequencing of different degrees of freedom during pointing movements involving the trunk in healthy and hemiparetic subjects," *Experimental Brain Research*, vol. 126, no. 1, pp. 55–67, Apr. 1999, doi: 10.1007/s002210050716.
[263] J. J. Burkitt, L. E. M. Grierson, V. Staite, D. Elliott, and J. Lyons, "The Impact of Prior Knowledge about Visual Feedback on Motor Performance and Learning," *APE*, vol. 03, no. 01, pp. 1–9, 2013, doi: 10.4236/ape.2013.31001.
[264] S. Chieffi and M. Gentilucci, "Coordination between the transport and the grasp components during prehension movements," *Exp Brain Res*, vol. 94, no. 3, Jun. 1993, doi: 10.1007/BF00230205.
[265] L. P. Maletsky, J. Sun, and N. A. Morton, "Accuracy of an optical active-marker system to track the relative motion of rigid bodies," *Journal of Biomechanics*, p. 4, 2007.
[266] "Proceedings of the 9th Sound and Music Computing Conference, Copenhagen, Denmark, 11-14 July, 2012," p. 6, 2012.
[267] E. Insafutdinov, L. Pishchulin, B. Andres, M. Andriluka, and B. Schiele, "DeeperCut: A Deeper, Stronger, and Faster Multi-Person Pose Estimation Model," *arXiv:1605.03170 [cs]*, Nov. 2016, Accessed: Mar. 24, 2021. [Online]. Available: http://arxiv.org/abs/1605.03170
[268] J. Deng, W. Dong, R. Socher, L.-J. Li, Kai Li, and Li Fei-Fei, "ImageNet: A large-scale hierarchical image database," in *2009 IEEE Conference on Computer Vision and Pattern Recognition*, Miami, FL: IEEE, Jun. 2009, pp. 248–255. doi: 10.1109/CVPR.2009.5206848.
[269] A. Mathis and R. Warren, "On the inference speed and video-compression robustness of DeepLabCut," Animal Behavior and Cognition, preprint, Oct. 2018. doi: 10.1101/457242.
[270] A. Toshev and C. Szegedy, "DeepPose: Human Pose Estimation via Deep Neural Networks," *arXiv:1312.4659 [cs]*, Aug. 2014, doi: 10.1109/CVPR.2014.214.
[271] E. Insafutdinov *et al.*, "ArtTrack: Articulated Multi-person Tracking in the Wild," *arXiv:1612.01465 [cs]*, May 2017, Accessed: Mar. 24, 2021. [Online]. Available: http://arxiv.org/abs/1612.01465
[272] M. Andriluka, L. Pishchulin, P. Gehler, and B. Schiele, "2D Human Pose Estimation: New Benchmark and State of the Art Analysis," in *2014 IEEE Conference on Computer Vision and Pattern Recognition*, Columbus, OH, USA: IEEE, Jun. 2014, pp. 3686–3693. doi: 10.1109/CVPR.2014.471.
[273] R. J. Holt *et al.*, "Grasping the Changes Seen in Older Adults When Reaching for Objects of Varied Texture," *PLoS ONE*, vol. 8, no. 7, p. e69040, Jul. 2013, doi: 10.1371/journal.pone.0069040.
[274] F. T. J. M. Zaal, R. J. Bootsma, and P. C. W. van Wieringen, "Coordination in prehension," *Experimental Brain Research*, vol. 119, no. 4, pp. 427–435, Apr. 1998, doi: 10.1007/s002210050358.
[275] R. Coats, G. P. Bingham, and M. Mon-Williams, "Calibrating grasp size and reach distance: interactions reveal integral organization of reaching-to-grasp movements," *Exp Brain Res*, vol. 189, no. 2, pp. 211–220, Aug. 2008, doi: 10.1007/s00221-008-1418-5.

[276] R. D. McIntosh, M. Mon-Williams, and J. R. Tresilian, “Grasping at laws: Speed-accuracy trade-offs in manual prehension.,” *Journal of Experimental Psychology: Human Perception and Performance*, vol. 44, no. 7, pp. 1022–1037, Jul. 2018, doi: 10.1037/xhp0000512.
[277] J. W. Krakauer, A. A. Ghazanfar, A. Gomez-Marin, M. A. MacIver, and D. Poeppel, “Neuroscience Needs Behavior: Correcting a Reductionist Bias,” *Neuron*, vol. 93, no. 3, pp. 480–490, Feb. 2017, doi: 10.1016/j.neuron.2016.12.041.
[278] “DeepLabCut.” https://github.com/DeepLabCut/DeepLabCut
[279] “DeepPoseKit.” https://github.com/jgraving/DeepPoseKit
[280] “AniPose.” https://github.com/lambdaloop/anipose
[281] “sleap.” https://github.com/murthylab/sleap
[282] “OptiFlex.” https://github.com/saptera/OptiFlex
[283] S. Günel, H. Rhodin, D. Morales, J. Campagnolo, and P. Fua, “1 DeepFly3D: A deep learning-based 2 approach for 3D limb and appendage 3 tracking in tethered, adult Drosophila,” p. 20.
[284] S. Zuffi, A. Kanazawa, D. W. Jacobs, and M. J. Black, “3D Menagerie: Modeling the 3D Shape and Pose of Animals,” in *2017 IEEE Conference on Computer Vision and Pattern Recognition (CVPR)*, Honolulu, HI: IEEE, Jul. 2017, pp. 5524–5532. doi: 10.1109/CVPR.2017.586.
[285] S. Zuffi, A. Kanazawa, T. Berger-Wolf, and M. Black, “Three-D Safari: Learning to Estimate Zebra Pose, Shape, and Texture From Images ‘In the Wild,’” in *2019 IEEE/CVF International Conference on Computer Vision (ICCV)*, Seoul, Korea (South): IEEE, Oct. 2019, pp. 5358–5367. doi: 10.1109/ICCV.2019.00546.
[286] N. Hesse, S. Pujades, M. J. Black, M. Arens, U. G. Hofmann, and A. S. Schroeder, “Learning and Tracking the 3D Body Shape of Freely Moving Infants from RGB-D sequences,” *IEEE Trans. Pattern Anal. Mach. Intell.*, vol. 42, no. 10, pp. 2540–2551, Oct. 2020, doi: 10.1109/TPAMI.2019.2917908.
[287] M. Omori *et al.*, “Hand Dexterity Impairment in Patients with Cervical Myelopathy: A New Quantitative Assessment Using a Natural Prehension Movement,” *Behavioural Neurology*, vol. 2018, pp. 1–10, Jul. 2018, doi: 10.1155/2018/5138234.
[288] S. H. Alusi, J. Worthington, S. Glickman, L. J. Findley, and P. G. Bain, “Evaluation of three diVerent ways of assessing tremor in multiple sclerosis,” p. 5.
[289] U. Castiello, K. M. B. Bennett, and Y. Paulignan, “Does the type of prehension influence the kinematics of reaching,” *Behavioural Brain Research*, vol. 50, no. 1–2, pp. 7–15, Sep. 1992, doi: 10.1016/S0166-4328(05)80283-9.
[290] R. O. Coats, R. J. Holt, G. P. Bingham, and M. A. Mon-Williams, “Predicting the duration of reach-to-grasp movements to objects with asymmetric contact surfaces,” *PLoS ONE*, vol. 13, no. 2, p. e0193185, Feb. 2018, doi: 10.1371/journal.pone.0193185.
[291] S. T. Pheasant, “Anthropometric estimates for British civilian adults,” *Ergonomics*, vol. 25, no. 11, pp. 993–1001, Nov. 1982, doi: 10.1080/00140138208925060.
[292] “Anthropometrics Notes,” *Roymech*. https://www.roymech.co.uk/Useful_Tables/Human/Human_sizes.html (accessed Dec. 26, 2022).
[293] “Analyzing finger interdependencies during the Purdue Pegboard Test and comparative activities of daily living | Elsevier Enhanced Reader.” https://reader.elsevier.com/reader/sd/pii/S0894113016300400?token=C9E0EFC0C80F1FB8EAA79208FCF4363DA344257DFCA3B1CA0DFA5A730CD4B8662A5FDC52C822FC9EE15CCA60912E8A19&originRegion=eu-west-1&originCreation=20210424081919 (accessed Apr. 24, 2021).
[294] J. E. Mendoza, G. T. Apostolos, J. D. Humphreys, B. Hanna-Pladdy, and S. E. O’Bryant, “Coin Rotation Task (CRT): A New Test of Motor Dexterity,” *Archives of Clinical Neuropsychology*, vol. 24, no. 3, pp. 287–292, May 2009, doi: 10.1093/arclin/acp030.
[295] R. O. Coats and J. P. Wann, “The reliance on visual feedback control by older adults is highlighted in tasks requiring precise endpoint placement and precision grip,” *Exp Brain Res*, vol. 214, no. 1, pp. 139–150, Sep. 2011, doi: 10.1007/s00221-011-2813-x.

[296] V. Bobić, M. Djurić-Jovičić, N. Dragašević, M. B. Popović, V. S. Kostić, and G. Kvaščev, “An Expert System for Quantification of Bradykinesia Based on Wearable Inertial Sensors,” *Sensors*, vol. 19, no. 11, p. 2644, Jun. 2019, doi: 10.3390/s19112644.
[297] E. Rovini, C. Maremmani, and F. Cavallo, “How Wearable Sensors Can Support Parkinson’s Disease Diagnosis and Treatment: A Systematic Review,” *Front. Neurosci.*, vol. 11, p. 555, Oct. 2017, doi: 10.3389/fnins.2017.00555.
[298] P. Y. Chan and Z. M. Ripin, “Development of wearable inertial sensors for measurement of hand arm tremors,” in *2013 IEEE International Conference on Smart Instrumentation, Measurement and Applications (ICSIMA)*, Kuala Lumpur, Malaysia: IEEE, Nov. 2013, pp. 1–6. doi: 10.1109/ICSIMA.2013.6717926.
[299] J.-W. Kim *et al.*, “Quantification of bradykinesia during clinical finger taps using a gyrosensor in patients with Parkinson’s disease,” *Med Biol Eng Comput*, vol. 49, no. 3, pp. 365–371, Mar. 2011, doi: 10.1007/s11517-010-0697-8.
[300] A. Salarian, H. Russmann, C. Wider, P. R. Burkhard, F. J. G. Vingerhoets, and K. Aminian, “Quantification of Tremor and Bradykinesia in Parkinson’s Disease Using a Novel Ambulatory Monitoring System,” *IEEE Trans. Biomed. Eng.*, vol. 54, no. 2, pp. 313–322, Feb. 2007, doi: 10.1109/TBME.2006.886670.
[301] I. J. Flatters *et al.*, “Predicting the Effect of Surface Texture on the Qualitative Form of Prehension,” *PLoS ONE*, vol. 7, no. 3, p. e32770, Mar. 2012, doi: 10.1371/journal.pone.0032770.
[302] M. Demers, “Reaching, thinking, moving: virtual reality for upper limb rehabilitation,” p. 215.
[303] A. Mathis *et al.*, “DeepLabCut: markerless pose estimation of user-defined body parts with deep learning,” *Nat Neurosci*, vol. 21, no. 9, pp. 1281–1289, Sep. 2018, doi: 10.1038/s41593-018-0209-y.
[304] T. Nath, A. Mathis, A. C. Chen, A. Patel, M. Bethge, and M. W. Mathis, “Using DeepLabCut for 3D markerless pose estimation across species and behaviors,” *Nat Protoc*, vol. 14, no. 7, pp. 2152–2176, Jul. 2019, doi: 10.1038/s41596-019-0176-0.
[305] S. Williams *et al.*, “The discerning eye of computer vision: Can it measure Parkinson’s finger tap bradykinesia?,” *Journal of the Neurological Sciences*, vol. 416, p. 117003, Sep. 2020, doi: 10.1016/j.jns.2020.117003.
[306] L. C. Fernandes, “Kinematic assessment of upper limb function in progressive multiple sclerosis,” md, University of Leeds, 2022. Accessed: May 13, 2023. [Online]. Available: https://etheses.whiterose.ac.uk/32677/
[307] “119 A novel kinematic tool to assess upper limb dysfunction in multiple sclerosis - ProQuest.” https://www.proquest.com/openview/e5bbd581a5d00c43479c1b8e335ec6d2/1?pq-origsite=gscholar&cbl=2041879 (accessed May 13, 2023).

Appendix A – Spatial Resolution

Horizontal Resolution

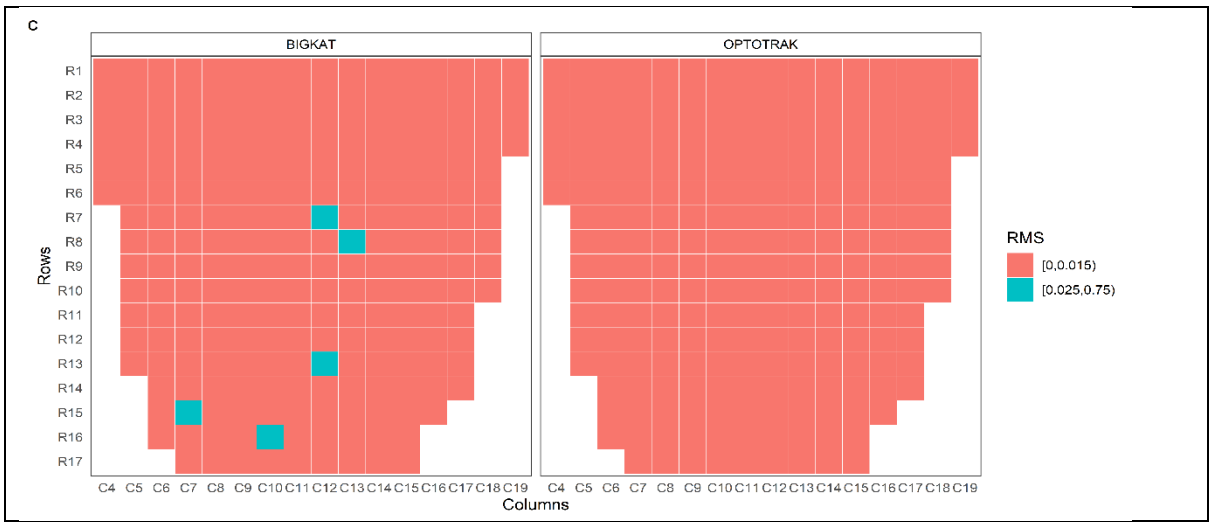

Vertical Resolution – 700mm

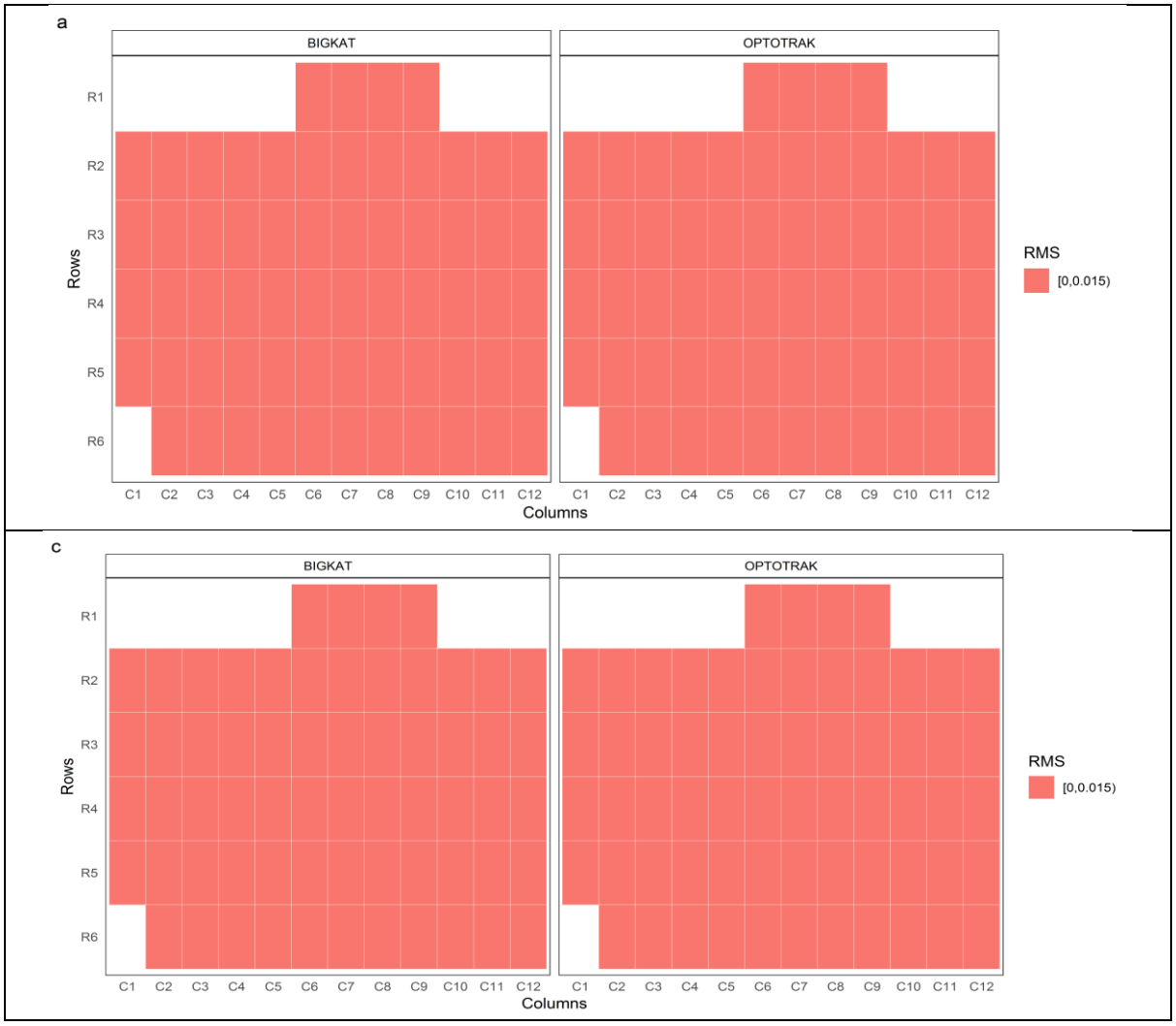

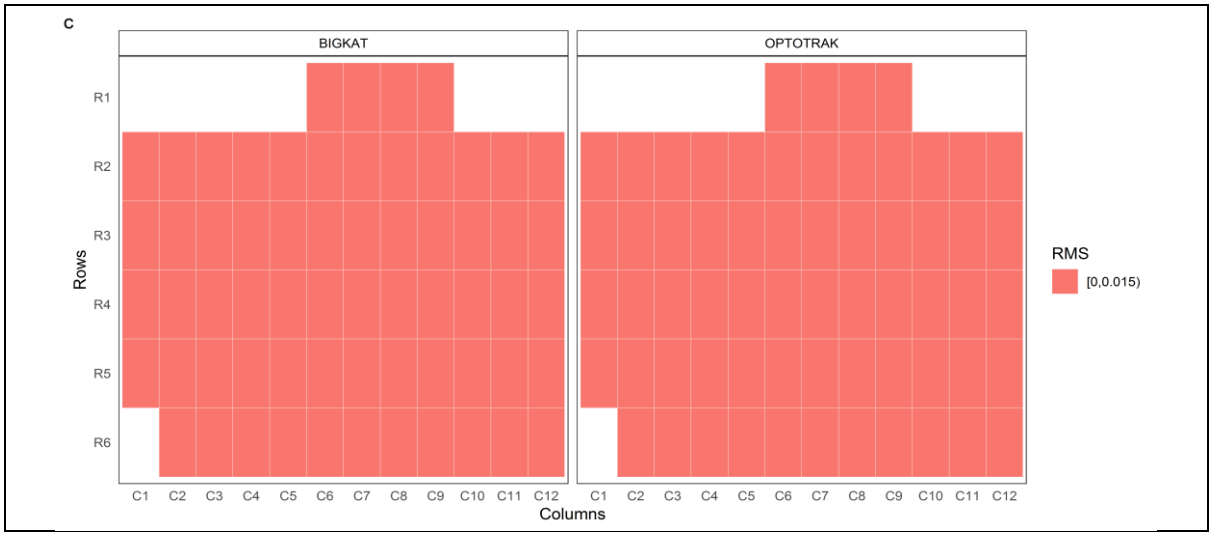

Vertical Resolution – 1400mm

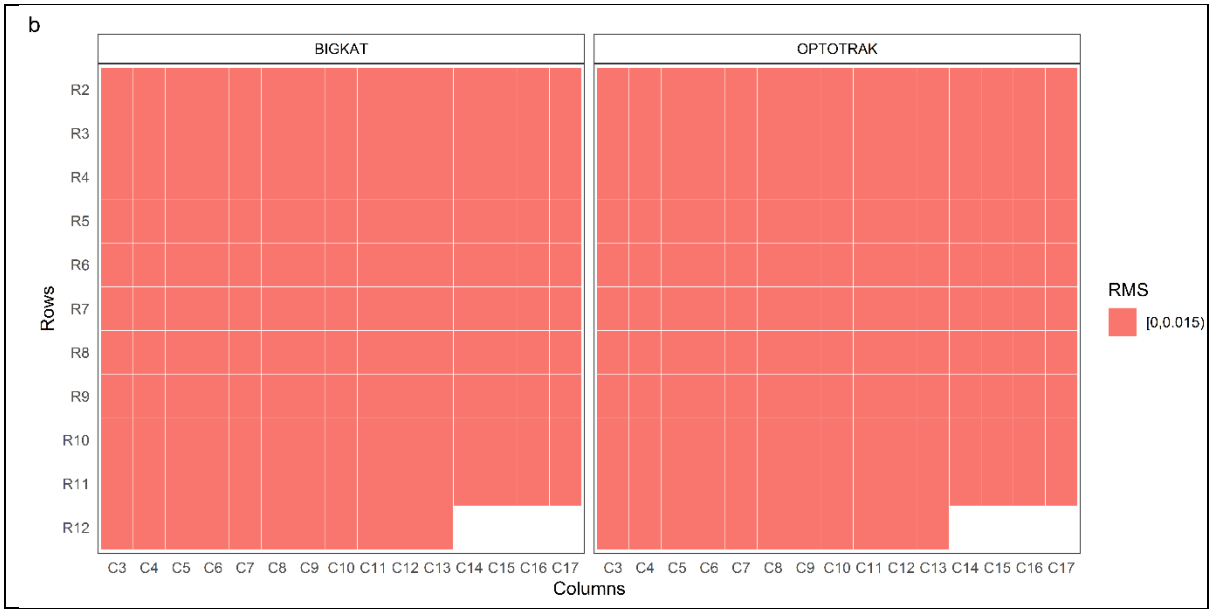

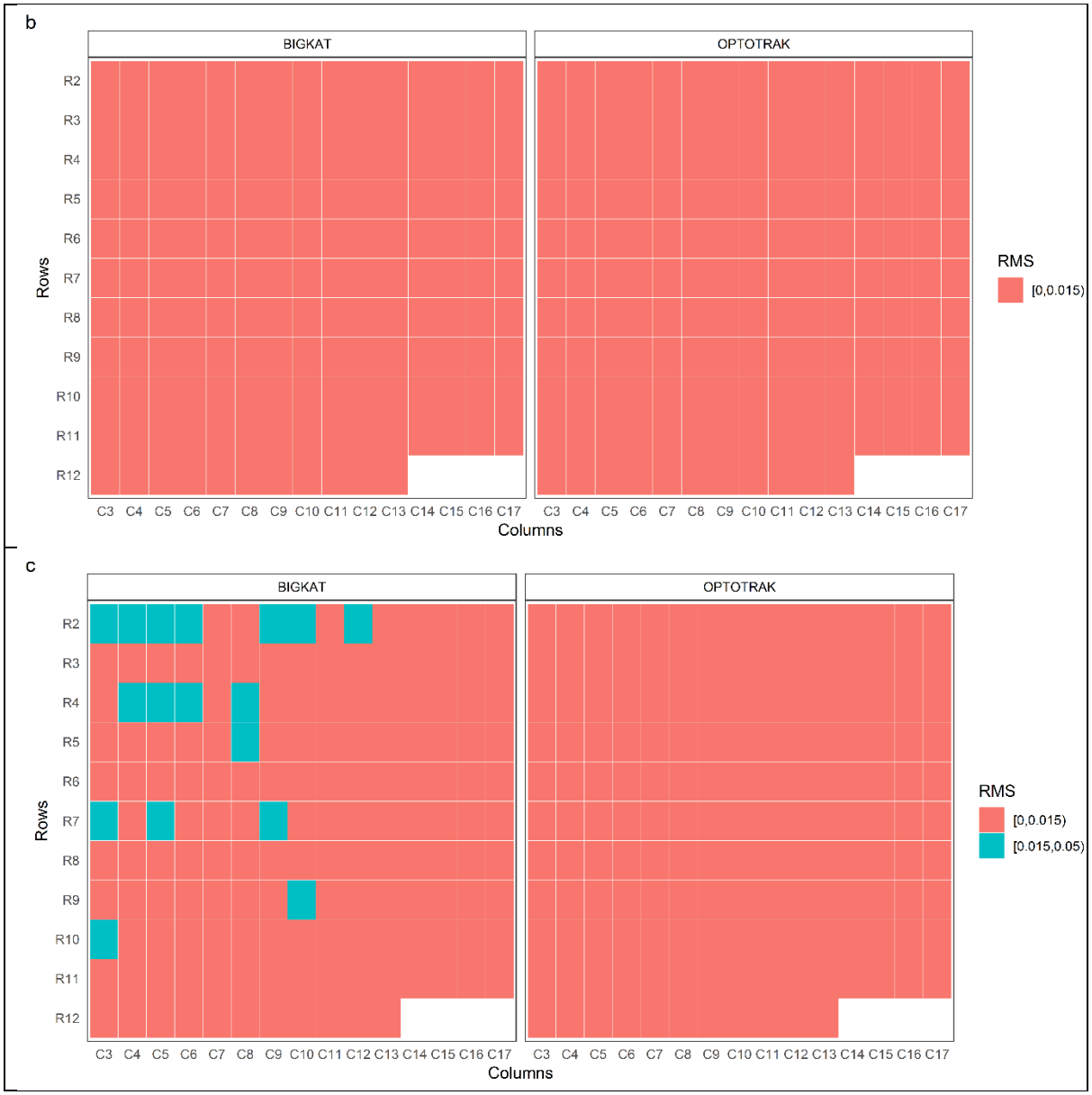

Vertical Resolution – 2100mm

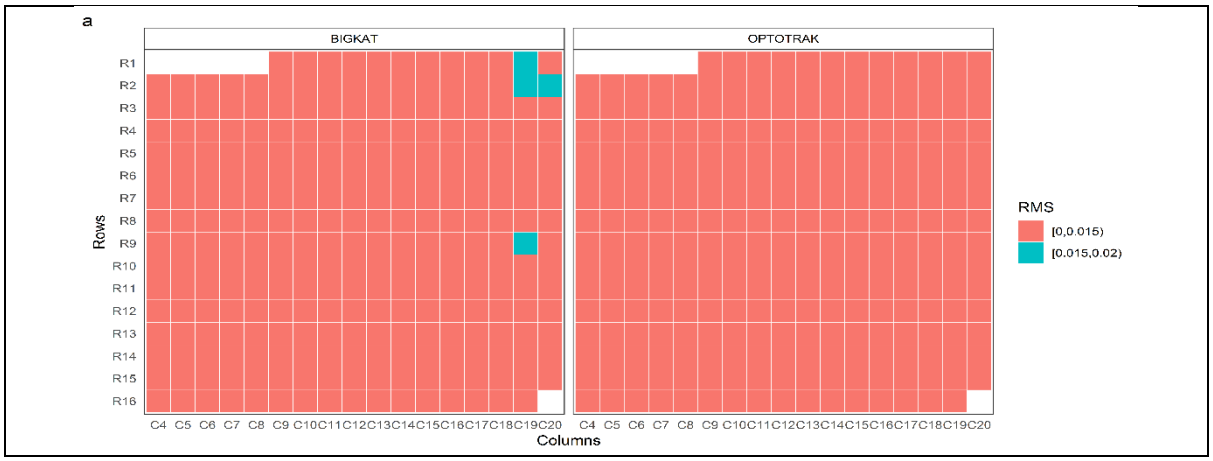

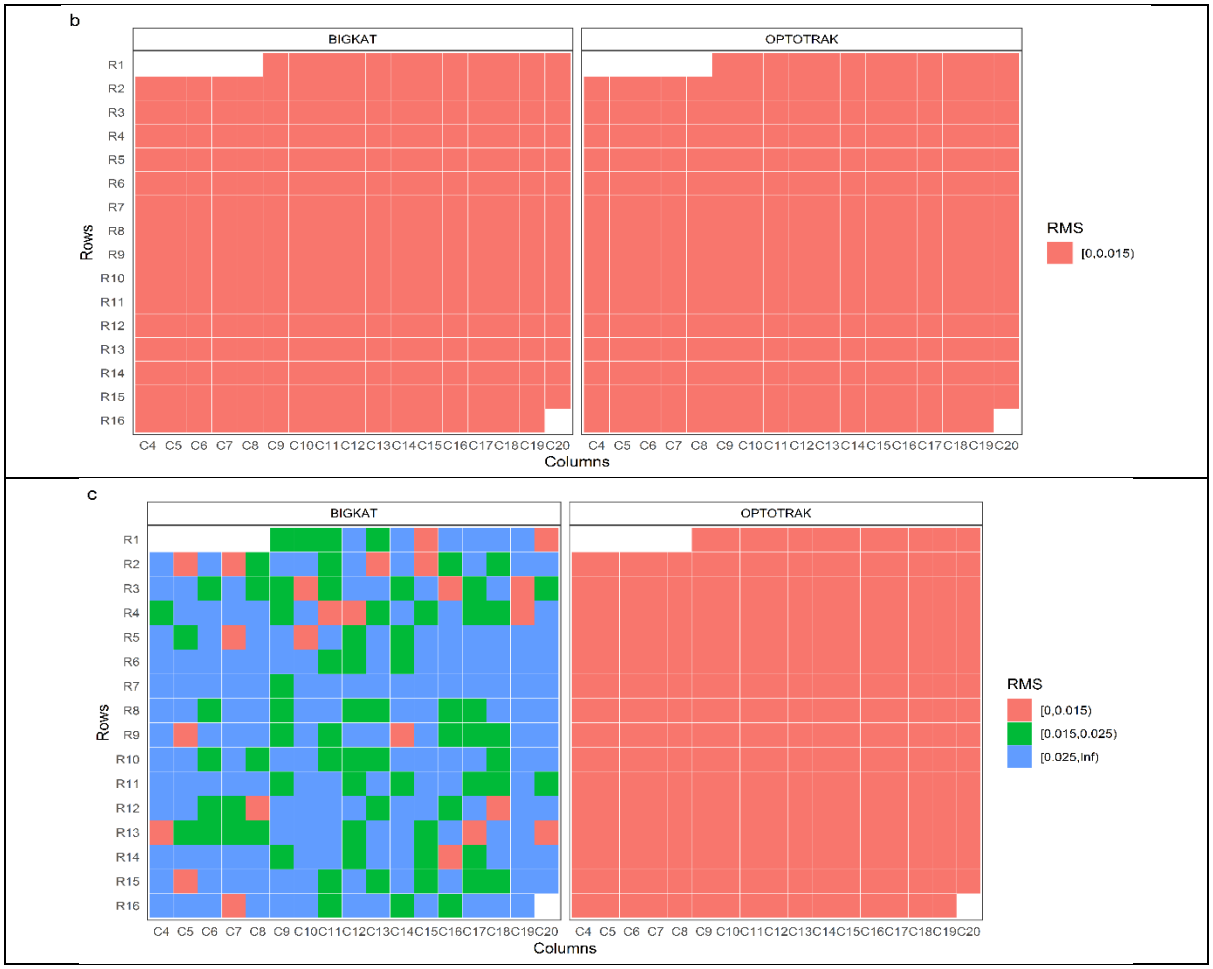

Appendix B – Reconstructed Grids

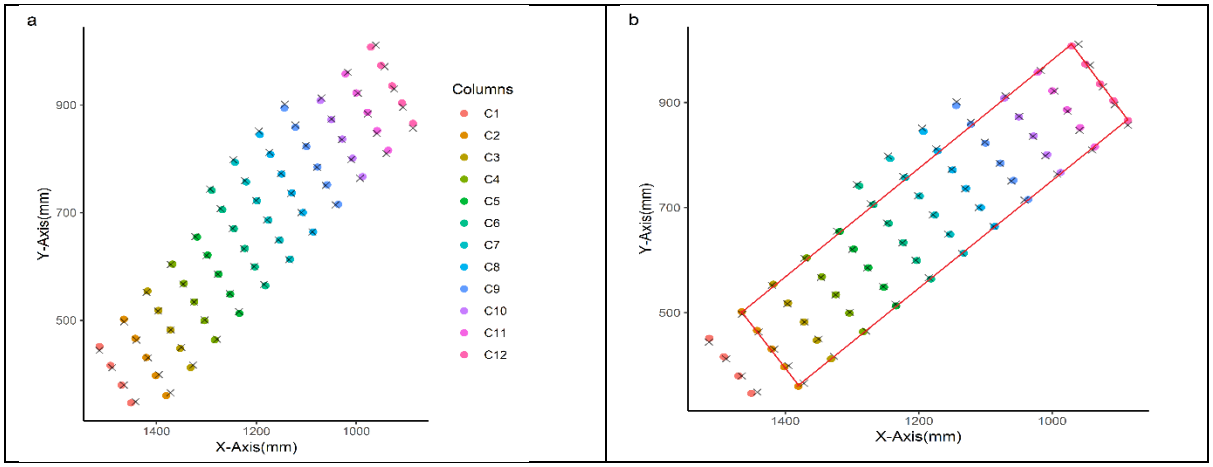

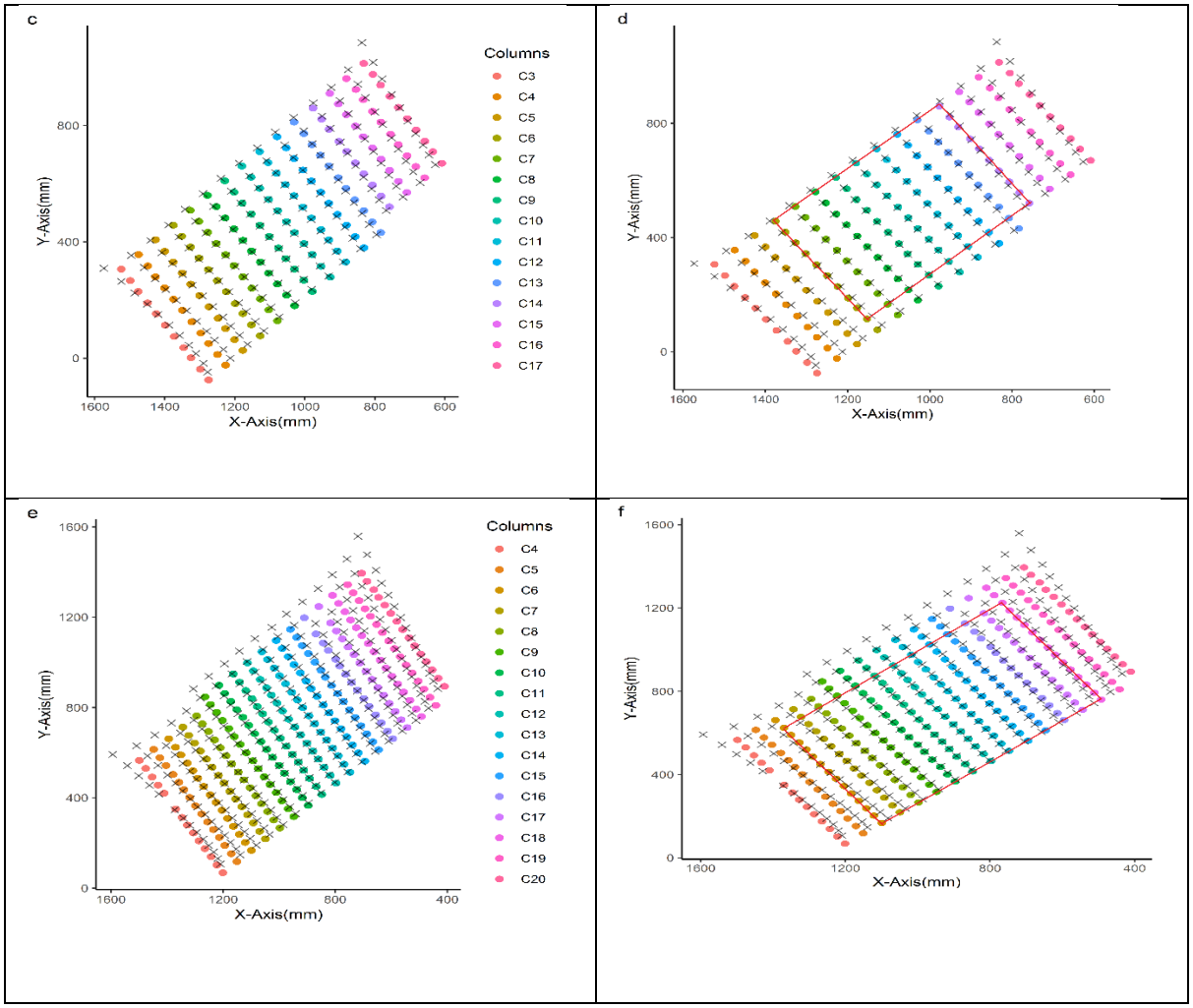

Appendix C - Event Detection Tool

Boot Script

```
GPIO.setmode(GPIO.BCM)
GPIO.setwarnings(False)
GPIO.setup(13,GPIO.OUT) # boot LED
GPIO_switch = 6 # select pin to connect button
GPIO.setup(GPIO_switch, GPIO.IN, pull_up_down=GPIO.PUD_UP)

try:
    while True:
        GPIO.output(13,GPIO.HIGH)
        rpistr = "/home/pi/butt_prehensionv2.py"
        p=subprocess.Popen(rpistr, shell=True, preexec_fn=os.setsid)
        p.wait()
        if GPIO.input(GPIO_switch)==0:
            GPIO.output(13,GPIO.LOW)


except KeyboardInterrupt:

    GPIO.cleanup()

finally:
    GPIO.cleanup()
```

Main Script

```
#!/usr/bin/env python3
```
```
Author : Awais Hafeez
```
```
import RPi.GPIO as GPIO
import time
import csv
import sys, os
import glob
import shutil
from kit_test import kit
import random
if getattr(sys, 'frozen', False):
  base_path = sys._MEIPASS
  print(base_path)
else:
  base_path = os.path.dirname(os.path.realpath(sys.argv[0]))
  print('el' + '' + base_path )
GPIO.setmode(GPIO.BCM)
GPIO.setwarnings(False)
start_switch = 24 # select pin to start
GPIO.setup(start_switch, GPIO.IN, pull_up_down=GPIO.PUD_UP)
object = [14,15,18]
GPIO.setup(object,GPIO.IN,pull_up_down=GPIO.PUD_UP)
# grip button
grip_btn = 23
GPIO.setup(grip_btn,GPIO.IN,pull_up_down=GPIO.PUD_UP)
#move LED
move_led=4
GPIO.setup(move_led,GPIO.OUT)
# start trial LED
st_trial_led=26
GPIO.setup(st_trial_led,GPIO.OUT)
# object LED
obj_led=19
GPIO.setup(obj_led,GPIO.OUT)
grip_led=17
GPIO.setup(grip_led,GPIO.OUT)
# GPIO 8 stop btn, connected to 3V3 on button press
stop_btn=8
GPIO.setup(stop_btn, GPIO.IN,pull_up_down=GPIO.PUD_UP)
def any_number_range(a,b,s=1):
   if (a == b):
      return a
   else:
      mx = max(a,b)
      mn = min(a,b)
      result = []
   # inclusive upper limit. If not needed, delete '+1' in the line below
      while(mn < mx):
```

```
        # if step is positive we go from min to max
            if s > 0:
                result.append(mn)
                mn += s
        # if step is negative we go from max to min
            if s < 0:
                result.append(mx)
                mx += s
        return result
try:
    run = 0
    ob=0
    grip = 0
    while True:
        if GPIO.input(grip_btn)==0 and grip == 0:
            GPIO.output(grip_led,GPIO.HIGH)
            grip = 1
        if GPIO.input(grip_btn)==1 and grip == 1:
            GPIO.output(grip_led,GPIO.LOW)
            grip = 0
        any_b = [GPIO.input(pin) for pin in object]
        if sum(i ==1 for i in any_b)==3 and ob==0:
            GPIO.output(obj_led,GPIO.HIGH)
            ob=1
        if sum(i ==1 for i in any_b)==2 and ob==1:
            GPIO.output(obj_led,GPIO.LOW)
            ob=0
        if GPIO.input(start_switch)==0 and run == 0:
            any_A = [GPIO.input(pin) for pin in object]
            print(any_A)
            if sum(i ==1 for i in any_A)==3:
                GPIO.output(obj_led,GPIO.HIGH)
            elif sum(i ==1 for i in any_A)==2:
                GPIO.output(obj_led,GPIO.LOW)
            else:
                break
            g=(i for i, e in enumerate(any_A) if e ==0)
            t=next(g)
            y=object[t]
            dist = [50,35,20]
            dist_cm = dist[t]
            GPIO.output(st_trial_led,GPIO.HIGH)
            trial_start_time = time.strftime("%M.%S")
            trial_start_time_ms = int(round(time.time()*1000))

            with open('/home/pi/record.csv', 'w', newline='') as file:
                data_writer = csv.writer(file)
                data_writer.writerow(["Event", "Time(M:S)" , "Time(ms)"])
                file.write("trial_start_time: " +  "," + trial_start_time + "," + str(trial_start_time_ms) + "\n")
            n=random.randrange(1,3)
            print("random time" + str(n))
```

```
    time.sleep(n)
    print ("LED on")
    GPIO.output(move_led,GPIO.HIGH)
    LED_time = time.strftime("%M.%S")
    LED_time_ms = int(round(time.time()*1000))
    with open('/home/pi/record.csv', 'a', newline='') as file:
        file.write("led_ON_time: " +"," + LED_time + "," + str(LED_time_ms)+ "\n" )
    print ("Waiting for rising edge on grib btn 23")
    GPIO.wait_for_edge(grip_btn, GPIO.RISING)
    GPIO.output(move_led,GPIO.LOW)
    grip_rel_time = time.strftime("%M.%S")
    grip_rel_time_ms = int(round(time.time()*1000))
    with open('/home/pi/record.csv', 'a', newline='') as file:
        file.write("grip_rel_time: " +"," + grip_rel_time + "," + str(grip_rel_time_ms) + "\n" )
    print ("Waiting for rising edge on object btns")
    GPIO.wait_for_edge(y, GPIO.RISING)
    obj_time = time.strftime("%M.%S")
    obj_time_ms = int(round(time.time()*1000))
    print("obj_lift_time: " + obj_time)
    with open('/home/pi/record.csv', 'a', newline='') as file:
        file.write("obj_lift_time: " + "," + obj_time + "," + str(obj_time_ms) + "\n" )
    run=1
    print('object Lifted - next phase started')
if GPIO.input(stop_btn)==0 and run == 1:
    end_time = time.strftime("%M.%S")
    end_time_ms = int(round(time.time()*1000))
    with open('/home/pi/record.csv', 'a', newline='') as file:
        file.write("obj_placed_time: " + "," + end_time + "," + str(end_time_ms) + "\n"  )
    #trial_end_time = time.strftime("%M.%S")
    #trial_end_time_ms = int(round(time.time()*1000))
    RT = grip_rel_time_ms - LED_time_ms
    MT_to_obj =  obj_time_ms - grip_rel_time_ms
    wrist_speed = (dist_cm / MT_to_obj)*1000
    MT_obj_to_tar = end_time_ms - obj_time_ms
    total_MT = end_time_ms - grip_rel_time_ms
    trial_time = end_time_ms - trial_start_time_ms
    with open('/home/pi/record.csv', 'a', newline='') as file:
        #file.write("trial_end_time: " + "," + trial_end_time + "," + str(trial_end_time_ms) + "\n")
        file.write("RT" + "," + "NA" + "," + str(RT) +"\n")
        file.write("MT_to_obj" + "," + "NA" + "," + str(MT_to_obj) +"\n")
        file.write("MT_obj_to_tar" + "," + "NA" + "," + str(MT_obj_to_tar) +"\n")
        file.write("total_MT" + "," + "NA" + "," + str(total_MT) +"\n")
        file.write("trial_time" + "," + "NA" + "," + str(trial_time) +"\n")
        file.write("wrist_speed(cm/s)" + "," + "NA" + "," + str(wrist_speed) +"\n")
        file.write("object gripped" + "," + "NA" + "," + str(dist_cm) +"\n")
    run = 0
  #  it+=1
    start_time_init = 0
    t=any_number_range(start_time_init,trial_time+16.667,s=16.667)
    t[:]=[i/1000 for i in t]
    led=[]
```

```
        led[:]=[i/1000 for i in (any_number_range(trial_start_time_ms,LED_time_ms,s=16.667))]
        print(len(led))
        g=[]
        g[:]=[i/1000 for i in (any_number_range(trial_start_time_ms,grip_rel_time_ms,s=16.667))]
        print(len(g))
        o=[]
        o[:]=[i/1000 for i in (any_number_range(trial_start_time_ms,obj_time_ms,s=16.667))]
        print(len(o))
        p=[]
        p[:]=[i/1000 for i in any_number_range(trial_start_time_ms,end_time_ms,s=16.667)]
        print(len(p))
        idx_list = [len(led),len(g),len(o),len(p)]
        print(idx_list)
        test_copy = t.copy()
        any_idx = [idx for idx in idx_list]
        for n,i in enumerate(t):
        if n in any_idx:
          test_copy[n] = 1
        if n not in any_idx:
          test_copy[n] = 0

        with open('/home/pi/timestamps.csv', 'w', newline='') as csvfile:
           wr=csv.writer(csvfile)
           wr.writerow(["time", "Events"])
           rcount=0
           for row in t:
              wr.writerow((t[rcount],test_copy[rcount]))
              rcount+=1
        fos=kit('/media/pi/LCF1')
        fos.find_participant_recording()
        fos.move_files_to_record()
        GPIO.output(st_trial_led,GPIO.LOW)
except KeyboardInterrupt:
   GPIO.cleanup()
finally:
   GPIO.cleanup()
```